Modeling of Creep in Hot-cured Concrete Used in Prestressed, Precast Bridge Girders

Kristján Steinn Magnússon

A thesis

Submitted in partial fulfillment of the

requirements of the degree of

Master of Science in Civil Engineering

University of Washington

2016

Committee:

John F. Stanton

Marc O. Eberhard

Don Janssen

Richard Wiebe

Program Authorized to Offer Degree:

Civil and Environmental Engineering

Abstract

Concrete fabricators, contractors and designers need accurate predictions of time-dependent deformations of concrete, such as creep and shrinkage. This is especially true for fabricators of precast, prestressed bridge girders, for which large differences in camber between adjacent girders can lead to significant contractual difficulties, increased cost, and legal consequences. In order to improve predictions of these deformations, good quality data and computationally convenient and well-calibrated models are needed.

Fabricators often use accelerated curing regimes to make the concrete gain strength faster and thus increase girder production rates. Little data currently exist on the creep and shrinkage characteristics of concrete for such a curing regime, and current models have not been calibrated using concrete of this type. In this research, an experiment was conducted to obtain data on the creep and shrinkage of high-strength concrete with an accelerated curing regime.

Current prediction models of creep and shrinkage all assume a constant stress history and deal with changes in stress by applying the principle of superposition, originally proposed in 1943. The validity of the application of the principle of superposition to creep strains has been greatly debated, and the experimental program was partly designed to test this assumption. Dealing with variable stresses through the use of superposition is not computationally convenient. A new one-dimensional rate-type model based on visco-elastic behavior was designed and calibrated using data from the experiments. This new model can deal with variable stresses without the need for superposition. Several configurations of the model were calibrated, and a good fit was achieved to creep data from concrete with a diverse set of loading and unloading histories.

TABLE OF CONTENTS

List of Figures

List of Tables

Acknowledgments

Dedication

To my loving wife, Petrea, and my family. Thank you for your endless love and support.

CHAPTER 1

INTRODUCTION

1.1 Deflections in Precast, Pretensioned Girders

For many years, it has been popular to build bridges from precast, prestressed girders. This method is economically viable and allows for longer spans and quicker construction than using traditional cast-in-place concrete girders. Prestressing the concrete reduces the risk of tension cracking and the problems that arise from it, such as corrosion and excessive deflections and vibrations. The prestressing in bridge girders and in many other structural applications of prestressed concrete is commonly applied using prestressing strands made from high-strength steel. These strands are highly stressed, either before the concrete is cast (pretensioned prestressing) or after the concrete has hardened (post-tensioned prestressing).

The prestressing force is often applied eccentrically, so the girder usually cambers upwards immediately as the prestressing force is applied to girder, and for long girders this camber is visible to the naked eye. The girder then undergoes time-dependent deformations due to relaxation of the strands, as well as creep and shrinkage of the concrete. Shrinkage is the time-dependent deformation of the concrete in the absence of applied loads. It is caused by hydration of the cement and loss of water. Additional long-term deformations of the concrete due to loading is referred to as creep.

Both shrinkage and creep of the concrete contribute to the long-term deformations of the fabricated girders. To avoid construction problems, especially with ever increasing girder spans, accurate and reliable predictions of these time-dependent deformations are of utmost importance. Inaccurate predictions can result in either too much or too little camber, both of which can have functional, economic and even legal ramifications. If the camber is too high, the girder may interfere with the deck reinforcement. If the camber is too low, additional concrete may be needed to bring the roadway up to the target elevation.

1.2 Challenges to Estimating Girder Deflections

To help engineers estimate girder deflections, it is necessary to account for the time-dependent deformations. The American Concrete Institute (ACI) guidance document (ACI Committee 209, 2008) lists four models that account for shrinkage and for creep under constant loads. In practice, however, the stresses in the prestressed girders are not constant, because the stress in the prestressing strands changes due to creep and shrinkage in the concrete, and relaxation (reduction in stress under constant strain) in the strands. In addition the girder loading varies during construction (e.g., placement of bridge deck) and in

service. To handle these changes in loading, it is generally assumed that the effects of the numerous changes in loading can be superimposed. The validity of this assumption has been debated for decades but is today generally accepted for stresses below 40% of the concrete compressive strength. (ACI Committee 209, 2008). Chapter 2 contains references to some of the research done on the subject in the past, and the assumption itself is tested in this project.

A key difference between precast girders and conventional RC construction is that the concrete in the precast girders is cured using an accelerated curing regime whereby the concrete is heated to just over 70 degrees Celsius only a few hours after casting and kept at that temperature until 14-16 hours after casting. This curing regime allows the concrete to develop strength much faster than it would otherwise. This rapid strength gain allows the precaster to release the prestressing strands at an earlier time and increase the turnover rate for the girders.

The accuracy of current models used to predict creep and shrinkage depends heavily on the characteristics of the concretes used to calibrate those models. At this time, little data exists on the creep and shrinkage of high-strength, hot cured concrete, making it difficult to calibrate new or existing models.

1.3 Scope of Thesis

The objective of this project was to conduct an experiment in which hot-cured, high-strength concrete provided by a commercial precaster was put under load, and measured for creep and shrinkage. Some of the concrete specimens were subjected to monotonic loading, i.e. put under a certain load and kept that way indefinitely. Other specimens had the load reduced or removed completely at various times to observe the creep recovery and test the validity of the principle of superposition.

Another objective was to develop a new model to predict creep strains in concrete with a variable stress time history. The model was then calibrated using data from the conducted experiment.

The thesis is organized as follows:

- Chapter 2 provides an overview of previous research conducted in this field and contains references to papers and other documents on previously conducted experiments and previously developed models on creep and shrinkage.
- In Chapter 3 the experimental program is outlined. An overview of the test matrix is provided and the test setup, instrumentation and procedure is described.
- Chapter 4 describes the processing of the data obtained from the experiment. It contains a description of any technical or practical difficulties experienced during the tests and explains how the datasets later used to calibrate the new model were obtained.

- In Chapter 5 the strength and elastic modulus data from the experiment is analyzed and modeled.
- In Chapter 6 the shrinkage data from the experiment is analyzed and modeled.
- In Chapter 7 the creep data from the experiment is analyzed and modeled. The validity of the principle of superposition applied to creep strains is evaluated.
- Chapter 8 looks at the validity of the principle of superposition for creep strains.
- Chapter 9 describes the new model, its governing equations are outlined, and solution procedures are described. An attempt is also made to relate different model parameters to certain material characteristics of concrete.
- In Chapter 10 the model is calibrated using data from the experiment. Four configurations of the model are calibrated and evaluated.
- Chapter 11 contains a discussion on some of the topics covered in this thesis.
- Chapter 12 contains a summary, conclusions, and recommendations for implementation and further research.

CHAPTER 2
PREVIOUS WORK

A large body of work exists on the experimental measurements and numerical modeling of shrinkage and creep of concrete. This chapter reviews some of the key experimental findings and models.

2.1 Experimental Work

Numerous experiments on the shrinkage and creep of concrete have been performed in the past. The RILEM databank (Bazant and Panula 1978; Hillsdorf and Carreira 1980; Kuttner 1997; Muller et al. 1999) documents the results of 1827 shrinkage tests and 1433 creep tests, all under constant load. This databank is useful for calibrating conventional models of shrinkage and creep, but some key characteristics of the databank limit its usefulness in evaluating models of concrete in precast, prestressed girders.

- All of the creep tests were conducted with a near-constant axial load, which is not the case for precast, prestressed girders
- Many of the tests measured shrinkage and creep over relatively short durations, which reduces the usefulness of the data to predict long-term effects. (ACI Committee 209, 2008).
- The databank lacks data on hot-cured, high-strength concretes, loaded at an early age, such as is the case in precast, prestressed girders.

Most authorities consider two main sources for shrinkage, autogenous and drying, and two main sources for creep, basic and drying. Autogenous shrinkage and basic creep are caused by hydration of the cement, and drying shrinkage, and drying creep are caused by moisture loss of the concrete.

Brooks (2005) reports the results of a landmark, long-term study on the shrinkage and creep of concrete. Brooks reported the results of 30 years of monitoring of shrinkage and creep for 18 types of concrete. Mixes with two types of normal-weight coarse aggregates were tested, each tested for five levels of water/cement ratios. Mixes with two types of lightweight coarse aggregates were tested too, for four levels of water/cement ratios. During the tests, cylinders were loaded after 14 days, stored in air or water, and monitored for 30 years.

Brooks found that that shrinkage strains at 30 years ranged from 280 to 1460$\mu\varepsilon$, and the creep coefficient ranged from 1.2 to 9.2, depending on the particular mix. The rate of creep of wet-stored concrete started to increase after approximately ten years contrary to the rate of creep of dry-stored concrete, which became steady or reduced with time. An implication of that observation is that the long-term creep of wet-stored concrete may not be the same as basic creep of sealed or mass concrete in which there is no

moisture exchange with the environment. The data was compared to predictions from the four models in the ACI-209 report. For normal-weight aggregate concrete, all methods underestimated strains, with the best estimates being given by the ACI method (40% for basic creep) and the GL2000 method (33% for total strain). It must be kept in mind however, that this study was conducted on concretes of much higher w/c ratio and lower strength than the concrete usually used in precast, prestressed applications.

Pan et al. (2011) studied the applicability of three of the four creep models in the ACI 209 report, all of which are discussed in the modeling section of this chapter, for creep and shrinkage in high-strength concrete. The three models are the ACI 209 model, the B3 model and the GL2000 model. They found that all three models overestimated both shrinkage strains and creep coefficients, but the accuracy of the predictions could be increased greatly by conducting short-term creep and shrinkage measurements and modifying the prediction model parameters accordingly. This finding supports the notion that there is reason to modify existing models or come up with new ones to predict creep in high-strength concrete.

2.2   Superposition

The concrete in precast, prestressed girders undergoes a complex loading history, resulting from relaxation of the prestressing strands, creep and shrinkage in the concrete (which creates secondary effects that depend on the boundary conditions) and changes in loading. McHenry (1943) originally suggested that these loading histories could be accounted for by treating each load increment as a separate constant-load, load case, and then superimposing all of the load cases. Since then, this approach has been used for lack of a better alternative, but the assumption has none the less been debated (ACI Committee 209, 2008).

Gardner and Tsuruta (2004) did an experimental investigation to study the validity of superposition of creep strains for specimens subjected to (1) drying before loading, (2) loading before drying and (3) sealed specimens, all subjected to uniaxial compression and then unloaded. In all three conditions, creep recovery was found to be only 70-80% of the creep of previously unloaded concrete for loads applied at the same age as the recovery, suggesting that the principle of superposition is not entirely valid for creep strains. Further, they found that, for increasing loads, the validity of the principle of superposition depended upon whether or not the concrete was sealed or subjected to drying. For specimens subjected to drying, measured incremental creep strains were 10-20% larger than creep strains for late loaded specimens. For sealed concrete, the creep strain due to an incremental increase in load was effectively identical to the creep strain of sealed, late-loaded concrete, suggesting that basic creep can be recovered whereas drying creep cannot.

Brown (2005) did an experimental investigation into superposition of creep strains for concrete and found indications that the principle of superposition is valid for basic creep but less so for drying creep. Three series of 100x100x400 mm prisms were made; one series was moist cured for four days and then sealed, and the other two series were moist cured for three and four days respectively and then transferred to a 50% relative humidity room. For the sealed series, a good approximation of the experimental results was achieved with the principle of superposition, both for increasing loads and creep recovery. For the other two series, both subjected to drying, superposition underestimated strains under increasing loads by 5-10% and overestimated creep recovery by 10-12%.

2.3 Modeling

Numerous models of shrinkage and creep have been proposed. This section describes only the four that are documented in the ACI 209 report, as well as model recently developed by Davison (2013).

2.3.1 *ACI 209-R92 Model*

The ACI 209 model was developed by Branson and Christianson (1971). It was initially developed for the precast-prestressing industry (Branson and Ozell 1961; Branson 1963, 1964, 1968; Branson et al. 1970; Meyers et al. 1970; Branson and Kripanayanan 1971; Branson and Chen 1972) and has been used in design for many years. However, the concretes used in the industry have changed significantly in the intervening years. In its basic form, the model requires the following input parameters:

- Age of concrete when drying starts
- Age of concrete at loading
- Curing method
- Relative humidity
- Volume-to-surface ratio
- Cement type

The shrinkage strain at any given time after the start of drying is given as a time ratio multiplied by a value given for the ultimate shrinkage strain. In absence of the necessary data, an average value of the ultimate shrinkage strain of 780 x 10^{-6} in./in. is suggested. That value can be modified with factors taking into account different curing regimes, relative humidity, volume-surface ratios, slump, aggregate, cement content and air content. Comparison with data from the RILEM databank shows that the model overestimates measured shrinkage at low shrinkage values and underestimates measured shrinkage at high shrinkage values. (Gardner 2004).

The creep coefficient at any given time after the time of loading is given with a similar method, a time ratio multiplied by a value given for the ultimate creep coefficient. The average value of the ultimate creep coefficient is given as 2.35, but it can be modified with correction factors like the ultimate shrinkage value. The compliance is taken as one plus the creep coefficient divided by the elastic modulus at the time of loading which is calculated based on the unit weight, cement type, curing regime and 28-day mean compressive strength of the concrete. This may introduce problems as the variation of the elastic modulus with time is not taken into account. The comparison with data from the RILEM databank shows that the model tends to underestimate measured values of compliance (Gardner 2004).The model is described in detail in the ACI 209 report (ACI Committee 209, 2008).

2.3.2   *Bazant-Baweja B3 Model*

The B3 model is the culmination of work done by Bazant and his colleagues at Northwestern University over several decades. It is based on a mathematical description of approximately 10 physical phenomena affecting creep and shrinkage. This model uses a compliance function instead of predicting a creep coefficient like the ACI model and thus reduces the risk of errors due to inaccurate values of the elastic modulus. The model distinguishes between basic and drying creep. The model requires the following input parameters:

- Age of concrete when drying starts
- Age of concrete at loading
- Aggregate content in concrete
- Cement content in concrete
- Cement type
- Concrete mean compressive strength at 28 days
- Modulus of elasticity of concrete at 28 days
- Curing method
- Relative humidity
- Shape of specimen
- Volume-to-surface ratio
- Water content in concrete

The shrinkage strain at any given time after drying starts is given as a multiple of a value for ultimate shrinkage strain, a humidity factor and a so-called time curve. The value for ultimate shrinkage strain is a function of the water content of the concrete, the compressive strength at 28 days, the elastic modulus at 28 days, the cement type and curing method. The humidity factor is a function of the relative humidity as

7

the name suggests. The time curve is function of the compressive strength at 28 days, the shape of the specimen and the volume/surface ratio.

The compliance at any given time after loading is divided up into three terms. First there is the instantaneous strain do to unit stress, then a term for basic creep and finally a term for drying creep. The basic creep itself is made up of three terms, an aging viscoelastic term, a nonaging viscoelastic term and an aging flow term. The drying creep term accounts for drying before loading and is the only term that does so. The model is described in detail in the ACI 209 report (ACI Committee 209, 2008).

2.3.3   *CEB MC90-99 Model*

The CEB MC90-99 model, originally presented in 1990, was developed by Muller and Hilsdorf (1990) and revised in 1999 (CEB 1999) to include normal- and high-strength concretes and to separate the total shrinkage into its autogenous and drying components. This model does not require any information regarding the duration of curing or curing condition. It requires the following input parameters:

- Age of concrete when drying starts
- Age of concrete at loading
- Concrete mean compressive strength at 28 days
- Relative humidity
- Volume-surface ratio
- Cement type

The shrinkage strain at any given time is divided up into an autogenous shrinkage term and a drying shrinkage term. The autogenous shrinkage term is a function of the mean compressive strength at 28 days and the cement type. The drying shrinkage term is a function of the mean compressive strength at 28 days, the cement type, the relative humidity and the volume-surface ratio.

The compliance at any given time is divided up into an instantaneous strain term and a creep coefficient term. The instantaneous strain term is a function of the elastic modulus at the time of loading which itself is a function of the elastic modulus at 28 days and the cement type. The creep coefficient term is a function of relative humidity, volume-surface ratio, the mean compressive strength at 28 days and the age of concrete at loading. Correction factors are available to correct for elevated or reduced temperatures and the effect of high stresses. The model is described in detail in the ACI 209 report (ACI Committee 209, 2008).

Comparison with data suggests that this model generally underestimates the shrinkage of North American concretes and substantially underestimates the shrinkage of concretes containing basalt aggregates found

in Hawaii, Australia and New Zealand. (McDonald 1990; McDonald and Roper 1993; Robertson 2000). The main reason is that European concretes, which generally have lower cement content and use other cement types than North American concretes, were considered when the model was optimized. (ACI Committee 209, 2008).

2.3.4   GL2000 Model

The GL2000 model was developed by Gardner and Lockman (2001), with minor modifications introduced by Gardner (2004). Except for the mean concrete compressive strength, the model only requires input data that are typically available to the engineer at the time of design. The following input parameters are needed:

- Age of concrete when drying starts
- Age of concrete at loading
- Relative humidity
- Volume-surface ratio
- Cement type
- Concrete mean compressive strength at 28 days

The shrinkage strain at any given time is a product of a value of the ultimate shrinkage strain, which is a function of cement type and the concrete mean compressive strength at 28 days, a correction factor for humidity and a correction factor for the effect of the time of drying, which is a function of the age of concrete when drying starts and the volume-surface ratio.

The compliance at any given time is divided up into an instantaneous strain term and a creep coefficient term. The instantaneous strain term is a function of the elastic modulus at the time of loading which can be derived using the mean compressive strength at 28 days and the cement type. The creep coefficient term has three terms within itself: two terms for basic creep and a third for drying creep. These are functions of the age at loading, relative humidity and volume-surface ratio. The model is described in detail in the ACI 209 report (ACI Committee 209, 2008).

2.3.5   Davison (2013)

All four of the previously described models were calibrated by their developers using the results of constant stress creep tests. To implement these models for complex loading histories, it is necessary to repeatedly superimpose the creep results for every change in load.

Bill Davison (2013) proposed another approach to predict camber in precast, prestressed concrete girders. For his creep predictions, Davison used a rheological time-stepping model upon which the model put forth in this thesis is based.

One of Davison's conclusions was that a more thorough calibration was needed for the creep model. Davison's camber program is modular so an improved and calibrated creep model from this thesis could be used to improve his model.

CHAPTER 3
EXPERIMENTAL PROGRAM

In the study described here, elastic, creep and shrinkage data were generated for a concrete mix that is normally used for prestressed concrete bridge girders. The experimental program provided data on the creep and shrinkage behavior of hot-cured concrete, which demonstrate the behavioral trends of such concrete. This data were also used for the calibration of the analytical model described in Chapter 10.

Each creep rig was loaded with one sealed and one unsealed cylinder, and unloaded companion cylinders from the same batch of concrete were monitored to measure shrinkage. The goal was to obtain data for basic creep alone (from the sealed cylinders) and total creep from the unsealed ones. Similarly, the sealed and unsealed shrinkage cylinders were intended to provide data for autogenous and total shrinkage respectively. Drying shrinkage can then be obtained by subtracting the autogenous shrinkage from the total shrinkage. Similarly, drying creep can be obtained by subtracting the basic creep from the total creep.

3.1 Test Program Overview

Creep tests were conducted on 11 sets of specimens to measure the elastic, creep and shrinkage strains under various curing and loading conditions. Companion, unloaded cylinders, provided shrinkage strains. The elastic and creep strains were obtained from the difference between the two sets of data. All tests were conducted on sealed and unsealed 4 x 8 in. cylinders. This size was chosen because most of the cylinders were hot-cured using a temperature-controlled regime that required special cylinder molds, which were available only at the 4 x 8 in. size.

The 11 sets of specimens were designed to generate a versatile set of data with which to calibrate the model and to test different parameters that affect creep, such as age at loading and unloading, load level and curing regimes. Table 3.1 shows an overview of these 11 specimen and their different characteristics.

Curing Regime. Specimens A, B and C were compared in an attempt to compare creep behavior of concrete with different curing regimes. It is sometimes accepted in practice that a day of hot curing has the same effect on strength as a week of moist curing at ambient temperature. Specimens A, B and C were designed to provide insight into the validity of that view. With more creep rigs available, more ambient- and weekend-cured specimens would have been made and loaded at different times, to permit more detailed comparisons.

Age at Loading. Specimen A, D, F, H and J were all loaded to the same value of 2.7 ksi but at different times to see the effect of different times of loading on the creep characteristics of the concrete.

Loading History and Creep Recovery. Specimens A were loaded continuously to a stress of 2.7 ksi. Specimens E, G and I were also loaded to 2.7 ksi but were then unloaded at different times to investigate creep recovery. Specimens E and G were fully unloaded after 3.8 and 7.8 days respectively but I was unloaded in three steps, each reducing the load by a third of the original value at 3.8, 7.8 and 14.8 days.

Table 3.1 Overview of Test Program

Specimen Set	Curing method	Age at loading	Stress history
A	Hot	0.7 days	Loaded to 2.7 ksi and load sustained
B	Weekend	2.8 days	Loaded to 2.7 ksi and load sustained
C	Ambient	3.8 days	Loaded to 2.7 ksi and load sustained
D	Hot	3.8 days	Loaded to 2.7 ksi and load sustained
E	Hot	0.7 days	Loaded to 2.7 ksi and unloaded at 3.8 days
F	Hot	7.8 days	Loaded to 2.7 ksi and load sustained
G	Hot	0.7 days	Loaded to 2.7 ksi and unloaded at 7.8 days
H	Hot	12.8 days	Loaded to 2.7 ksi and load sustained
I	Hot	0.8 days	Loaded to 2.7 ksi, load reduced to 1.8 ksi at 3.8 days, to 0.9 ksi at 7.8 days and unloaded at 14.8 days
J	Hot	57.7 days	Loaded to 2.7 ksi and load sustained
K	Hot	0.7 days	Loaded to 4.5 ksi and load sustained

Load Superposition. With data from specimens loaded and unloaded at different times it is possible to test the principle of superposition in a variety of ways. The data from Specimen E can thus be compared to a curve made by taking the data from specimen A and subtracting from it the data from Specimen D, which was loaded at the same time as E was unloaded. The same thing can be done by comparing data from specimen F to a curve made by subtracting data from specimen G from data from specimen A. The partial unloadings of specimen I can be utilized in this way as well, by comparing data from specimen I up until the second unloading with a curve made by subtracting a third of the data from specimen D from the data from specimen A for that same time period. Finally, data from specimen I up until the third unloading can be compared to a curve made by subtracting a third of the data from specimen F from the previously made A-0.33D curve. If superposition was perfectly valid and data could be acquired without errors the curves in all these cases would be identical. Figure 3.1 explains the principle of superposition.

12
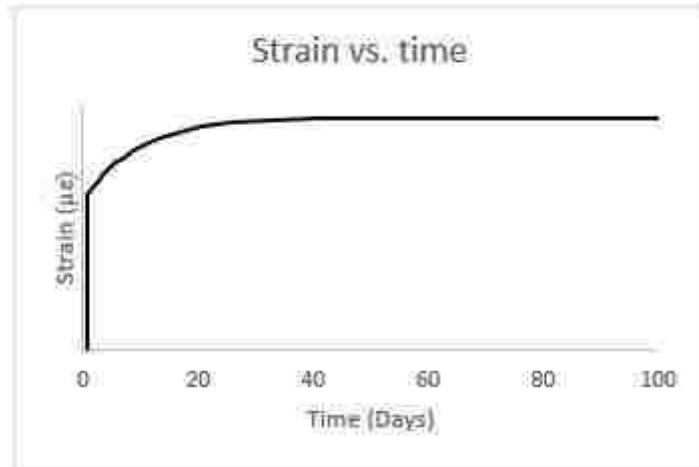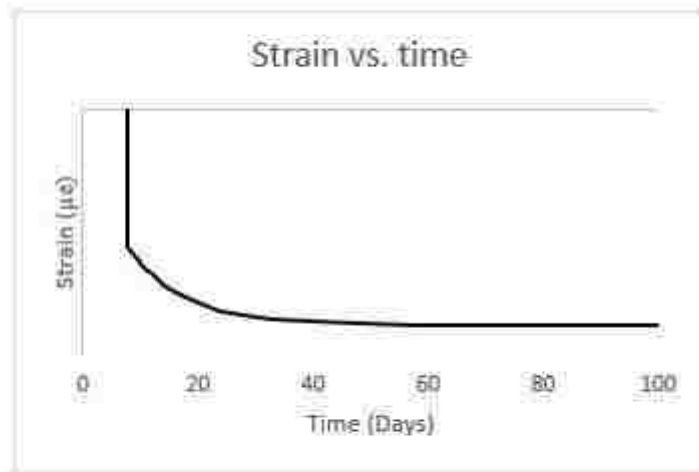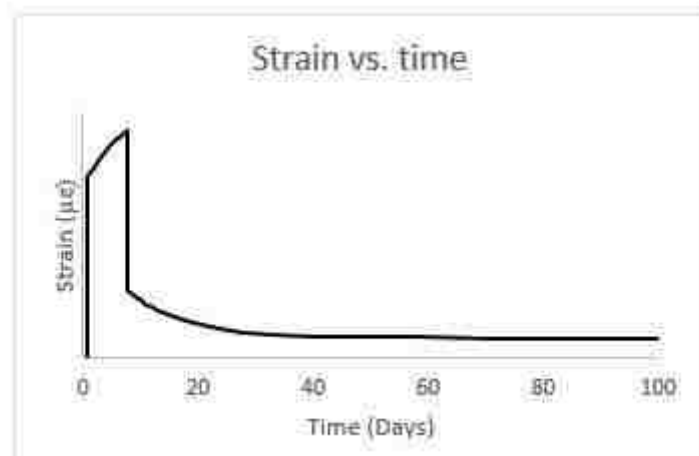
Figure 3.1 The Principle of Superposition

13

Stress Amplitude. Superposition can also be tested by comparing data from specimen A and K. Both were loaded at 0.7 days, A to 2.7 ksi and K to 4.5 ksi. If superposition was perfectly valid, the strains would be proportional to the applied stresses. Superposition is valid only for linear processes, so, for it to be true in this case, the stresses should remain in the linear part of the stress-strain curve. Specimen K was loaded to approximately 45% of the strength at the time, which is just over the generally accepted 40% limit of proportionality for concrete (Wight 2016).

- Specimens A, B and C could be compared directly to evaluate the effect of three curing methods: Hot (for girders cast on a one-day cycle), Weekend (for girders heated to a lower temperature as they cured over a weekend) and Ambient (unheated, except for their own hydration, providing a reference to conventional curing conditions).
- Specimens A, D, F, H and J provided data to evaluate the effects of the age at loading, ranging from 0.7 days to 58 days.
- Specimens A, E, G and I provided data on the effect of decreasing the load after a period of time.
- Data from specimens A and K could be compared to evaluate the effect of the stress level.

3.2   Concrete Properties

3.2.1   Concrete Mix Design

The concrete mix used for all of the tests was a standard mix used by Concrete Technology Corporation (CTC) for precast bridge girders. It had the following mix proportions:

- Cement Type III: 752 pcy
- Water: 234 pcy
- Coarse aggregate (AASHTO #67): 1950 pcy
- Fine aggregate: 1197 pcy
- Water-reducing admixture: 3.0 oz pr. cwt of cement
- High range water-reducing admixture: 8.0 oz pr. cwt of cement
- Air-entrainment: none

3.2.2   Curing Regimes

Cylinders using the same concrete mix were cured in three ways, as shown in Table 3.1 as "hot", "weekend" and "ambient". These descriptions refer to the different early age temperature histories for the different concretes. The reason for choosing this concrete and these curing regimes was that the primary use envisioned for the model was to embed it in a program to predict camber and prestress loss in pretensioned bridge girders.

This project focused on the creep and shrinkage of hot-cured concrete. Hot refers to cylinders cast and cured in "Sure-cure" molds, which were heated to follow a prescribed temperature history, as shown in Figure 3.2. This history is the standard one used by the precaster, CTC, which cast and cured the cylinders. Such concrete is typically cured hot to gain high early strength for the timely release of the prestressing strands. The hot curing method allows the concrete to gain strength faster and leads to efficient use of forms, because one girder can be produced every 24 hours out of each form. This loading occurs much earlier than the 7 days that is common in conventional creep testing.

Sets of weekend and ambient cured specimens, made from the same batch of concrete as the hot-cured cylinders, were also cast to allow comparisons to be made. Weekend curing refers to concrete that is cast on a Friday and not demolded until the next Monday. The temperature curve for that type of curing is lower than that of the hot-cured one but is designed to make the concrete reach the same maturity as the hot-cured concrete over the course of a weekend instead of in one day. Ambient refers to a cylinder cast in a plastic mold that is not externally heated, but that still shows a modest temperature gain due to the heat of hydration. Figure 3.2 shows the temperature of the concrete for the first 16-20 hours after casting for the ambient (plastic) and hot (Sure Cure) cured concretes.
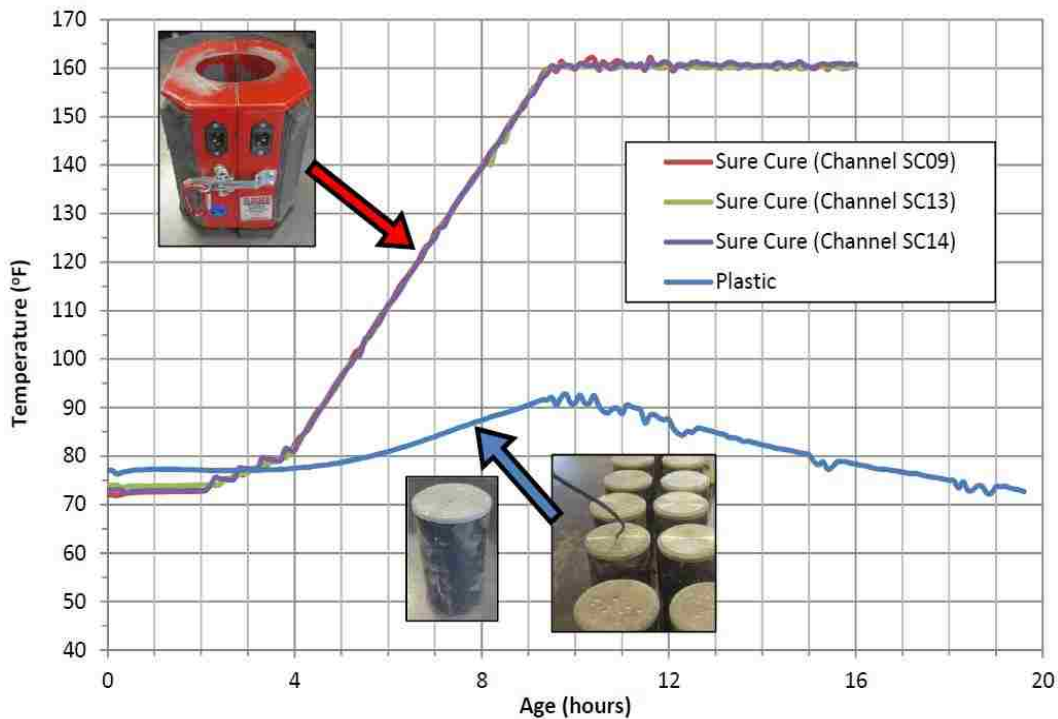
Figure 3.2 Curing Temperature Histories for Ambient- and Hot-cured Concrete (Courtesy David Chapman, CTC)

Figure 3.3 shows the temperature history for weekend cured concrete cast on a Friday.
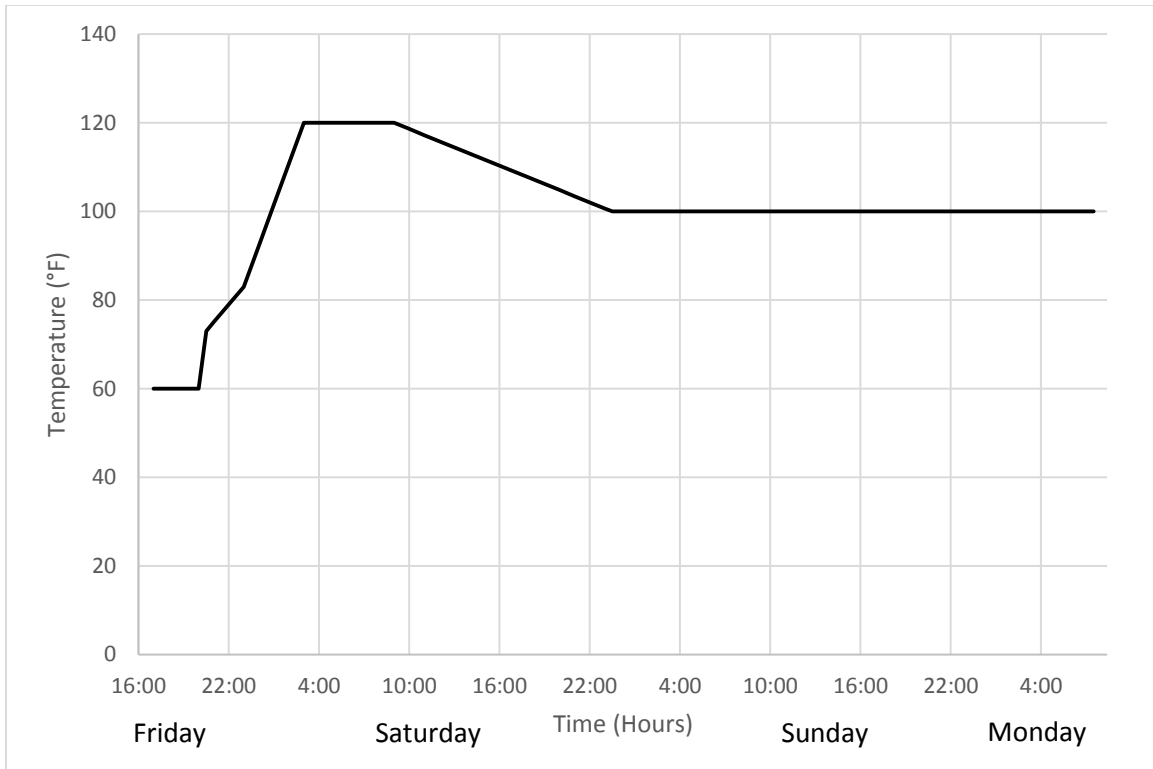
Figure 3.3 Curing Temperature History for Weekend-cured Concrete (Courtesy David Chapman, CTC)

The cylinders used in the experiment were cast from two nominally identical batches made by CTC during a six-day period in early July 2016. The reason for not using a single batch was that CTC was only able to make 16 Sure Cure cylinders per batch. In addition, having two batches made it more practical to transport all the cylinders to the test location at the University of Washington, where they needed to be capped, sealed, gaged and loaded within the shortest time possible. A third, nominally identical batch was made separately by CTC and used to conduct the strength and elastic modulus tests described in Chapter 3.6.

3.3   Creep Rigs

Eight creep rigs were set up in a small room in the Structural Research Lab at the University of Washington. The number of tests conducted was largely constrained by the number of creep rigs available. Before any data could be collected, a considerable effort had to be put into preparing the creep rigs. Aside from the brute force labor required to disassemble the rigs where they had previously been used, move them to the room where the experiments took place and re-assemble them there it was necessary to design the rig configuration in such a way that the capacity of each rig was sufficient not

16

only for this experimental program but for others potentially conducted in the future. A description of those design calculations can be found in Appendix A.

Figure 3.4 explains what the creep rigs look like and Figure 3.5 is a picture of one from the lab. Each rig consists of 2 steel plates (A and B) with four sets of springs, a set consisting of a spring with an outside diameter of 4.5 inches inside a spring with an outside diameter of 8 inches, in between them. The measured stiffness of a set of springs is 18.42 kips/in. The lower plate (A) is attached to four legs. Through these two plates go 4 threaded steel rods. The smallest diameter of these rods is 0.9755 inches and the smallest cross-sectional area is therefore 0.747 in^2. The elastic modulus of steel is approximately 29000 ksi and the length of the rod that is in tension in the creep rig assembly is 43 inches. The stiffness of each rod is therefore AE/L = 504.1 kips/in. Mounted on these steel rods is a slightly smaller steel plate (C) above the two bigger plates. High-strength steel nuts hold this assembly together. The sealed and unsealed concrete cylinders (F) are placed between the small top plate (C) and the upper big plate (B). Two smaller cylinders (G) are placed on the top and the bottom of the stack, which sits on a rotating swivel head (D). The elastic modulus of the concrete varies with time (and curing regime) but an average value of 6500 ksi can be used to approximate the stiffness of the cylinder stack. The cross-sectional area of the stack is 4π and it is 24 inches long. The stiffness of the concrete stack is therefore AE/L = 3403.4 kips/in. Beneath plates A and B is another steel plate (E) upon which the hydraulic loading ram sits during application of loads.

The total stiffness of the rig and cylinder stack are therefore 71.1 and 3403 kip/in. respectively. Thus a strain change in the concrete of 500με would lead to a change in load of approximately 0.85 kips, or 68 psi. Since all specimens were loaded to at least 2700 psi, this value is about 2.5% of the total load and that was considered small enough to obviate the need for re-jacking during the test in order to keep the load constant.
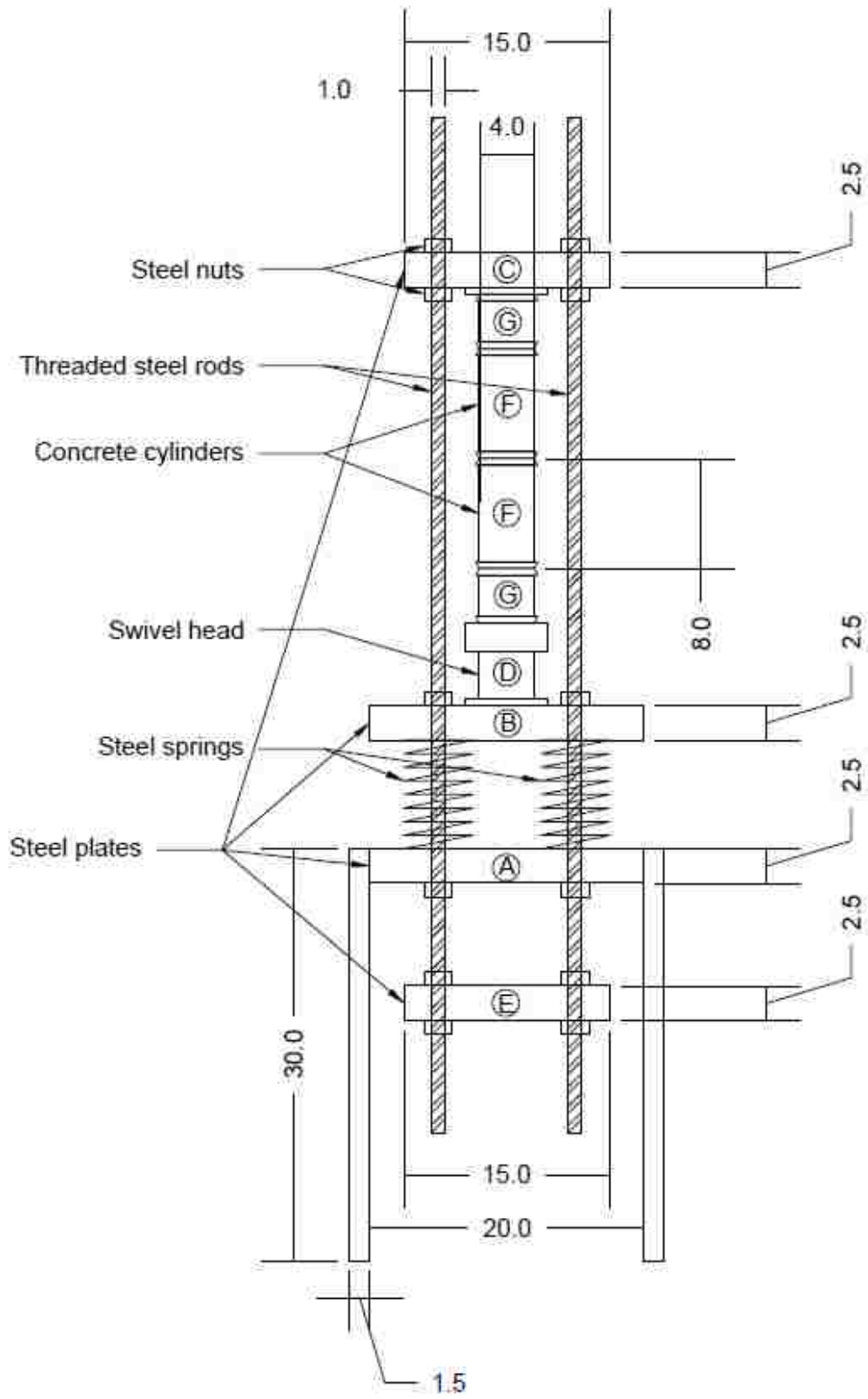
Figure 3.4 Creep Rig Diagram (All dimensions in inches)

Figure 3.5 A Loaded Creep Rig in the Lab

3.4 Test Procedure

Concrete for the hot-cured cylinders was placed in Sure Cure cylinder molds (such as the one seen on the top left corner of Figure 3.2) and consolidated with a vibrating table. The concrete for the ambient-cured cylinders was placed in conventional plastic cylinder molds and consolidated by rodding. All cylinders were 4" x 8".

After the curing period of approximately 16 hours, the hot-cured cylinders were picked up from the precaster and driven up to the UW campus where testing took place. The cylinders were demolded, capped with sulfur caps and the sealed ones were sealed with a 1/8th inch thick, self-adhesive rubber sleeve, cut to size from sheets manufactured by McMaster-Carr Corp. The strain gages were glued to the cylinders using superglue and any exposed concrete surfaces around the free edges of the rubber sheet were sealed with silicone. Several adhesives were tried during trial runs, including fast-setting epoxies, but superglue was found to be the most satisfactory because it required no mixing and it set faster than any other adhesive. Time was critical during the process of capping, sealing and attaching gages, in order to adhere as closely as possible to the curing regime and concrete maturity that would be used in the production plant. A team of five people was necessary to complete the work, and a dry-run was conducted a few days before the real cylinders were processed.

The cylinders were then placed in the creep rig room and loaded in the rigs according to the loading schedule in Table 3.1 with a hydraulic ram connected to a hand pump fitted with a pressure gage. To get rid of potential end effects some 4" by 4" cylinders were made alongside the test specimens, capped with sulfur caps and placed on the top and bottom of the cylinder stack in every creep rig. In the absence of these half-cylinders, the friction from the creep rig plates might provide unwanted radial confinement at the ends of the test cylinders. To try to minimize the risk of eccentric loading and to get as close to a uniaxial load as possible the cylinder stack was placed on top of a swivel head for easy adjustment of the vertical alignment of the stack with the rig. A diagram of a loaded creep rig can be seen in Figure 3.4 and a picture of one can be seen in Figure 3.5.

3.5 Instrumentation and Data Acquisition

To record the strains, a data acquisition system was set up alongside the creep rigs to which 90 vibrating wire (VW) strain gages were connected via multiplexers through a datalogger and to a computer. The VW gages were model 4000 strain gages made by Geokon Inc. They had a 6.5 inch gage length and consist of an encased steel wire mounted between two blocks that are superglued to the concrete cylinders. The steel

wire is under tension which changes as the mounting blocks move relative to one another. The tension in the wire is measured by plucking the wire and measuring its natural frequency of vibration by means of an electromagnetic coil positioned next to the wire (Geokon 2016). From the change in tension in the wire, the relative movement of the two blocks and thus the deformation of the concrete cylinder can be calculated.

A single measurement from every gage was automatically registered into a text file on the computer every four minutes. This rate of measurement illustrates the huge advantage of using VW gages as opposed to manual gages as the data acquisition is completely automatic and free from potential errors caused by human hands and eyes. A dense set of data points is necessary only during a period of time shortly after loading or unloading but the software did not allow variable spacing between the readings. Thus the data file was post-processed to select only data points taken every eight minutes for the first day after loading, every hour for the next two weeks and once every day from that point onwards. This reduced the file to a manageable size. The dataset was further reduced when fitting the model to it, as described in Chapter 10.

Some preliminary tests were required to determine things like the best adhesive for gluing the mounting blocks to the concrete, the number of gages to put on each cylinder, the effects of temperature changes on gage readings etc. These tests are outlined in detail in Appendix A.

From each batch of concrete made, two sets of hot cured shrinkage cylinders (one sealed and one unsealed) were cast. The data acquisition system had a limited number (96) of channels so, for the weekend and ambient cured specimens, only one set of shrinkage cylinders was cast for each. Each shrinkage cylinder was instrumented with two VW gages. Each hot cured specimen therefore has four different measurements for shrinkage of unsealed cylinders and four different measurements for shrinkage of sealed cylinders. The weekend and ambient cured specimens have two of each. All creep cylinders were instrumented with three VW gages each.

3.6   Strength and Elastic Modulus Test Program

Strength and stiffness values obtained from cylinders were used to characterize the properties of the cylinders tested in the creep rigs at the University of Washington. Parallel to the experiments conducted at the UW, lab technicians at CTC's plant in Tacoma conducted strength and elastic modulus tests on a separate batch of nominally identical concrete. A sample from the batch was tested for slump, unit weight and air content. 24 cylinders were made and cured in Sure Cure molds, and 24 cylinders were made and ambient-cured in plastic molds.

The Sure Cure cylinders were consolidated with a vibrating table and the ambient cured ones were consolidated by rodding. Sure-Cure cylinders tested within 15 hours of casting remained in their molds until their test time but Sure Cure cylinders tested later were removed from their molds at approximately 15 hours and immersed in CTC's lime-saturated water curing tank. Ambient-cured cylinders tested within 24 hours of casting remained in their molds until their test time but ambient-cured cylinders tested later were removed from their molds at approximately 23 hours and immersed in CTC's lime-saturated water curing tank. The cylinders were tested for strength and elastic modulus at 9, 12, 15 and 18 hours within the first day after casting and then at 1, 2, 5, 7, 14, 28 and 56 days thereafter.

The tests were performed with CTC's fully automatic Forney 400k VFD compression testing machines.

3.7   Potential Sources of Error in the Test Program

The usefulness of the findings from the study depend on the accuracy of the test data. This particularly true for the creep data, because it can be isolated only by subtracting from the total stain the elastic and shrinkage components. All three strain components inevitably have some level of error in them. In this section the different sources of error are considered.

Loading error. Several behaviors contributed to possible inaccuracy in the load. First, the load on the cylinder stack was found to be somewhat eccentric, despite the best efforts to avoid it. Whether this was caused by poor centering, or by side sway of the rig during loading, is not known. Second, the load was applied by a ram driven by a hand pump and was measured by the oil pressure. It was not possible to use a load cell, because that would have required an additional (non VW) data acquisition system. The pressure gage was calibrated prior to testing, but it was possible to set the load only within about 0.32 kips due to bleed-down of the pressure while the nuts on the rig's rods were tightened. The ram force is also somewhat open to question, because there is inevitably some friction on the piston. This was minimized by arranging for the smallest possible piston extension, and the ram was calibrated using the same extension as was used in the creep rigs, but some error is nonetheless inevitable. It is estimated to be less than 1 kip.

Strain gages. The manufacturer of the strain gages claims that their accuracy is within ±0.5%. The gages are claimed to be able to correct for strains induced by temperature changes. This was tested and the test is described in Appendix A.5. The thermal coefficient obtained in that test was around 10% of the thermal coefficient for stainless steel, of which the gages are made, and thus the self-compensation for temperature was deemed good enough.

Concrete cylinders. The variability of the concrete between cylinders is a potential source for error. This error is assumed to be small since the concrete in the cylinder is from only two nominally identical batches made under controlled conditions by a commercial precaster. Another potential source for errors is if some of the sealed cylinders were not sealed properly and are therefore losing moisture. Again, this error is assumed to be small as great care was taken to seal the cylinder using self-adhering sleeves made from a 1/8" thick rubber sheet.

Laboratory conditions. If the temperature and relative humidity where the creep rigs are located vary by a large amount over the test period, that can be a potential source for error. The temperature and relative humidity of the room where the creep rigs in this project were located were recorded for a part of the duration of the tests. These data are shown in Figure A.4 in Appendix A.6.

CHAPTER 4
DATA PROCESSING

This chapter documents the data processing procedures used to convert the raw data from the Vibrating-Wire (VW) gages into the key components of strain, including the elastic strain, autogenous shrinkage, drying shrinkage, basic creep and drying creep. A single specimen series (K) is discussed in this chapter as an example, but the same general procedure applies to all of them. Raw data for all specimens, to which the procedure outlined in this chapter was applied, are provided in Appendix B. A naming convention was established so every curve presented could be traced to each respective gage, cylinder, specimen etc. An illustration of the convention is shown in Figure 4.1.

Figure 4.1 Illustration of Gage Naming Convention

4.1 Shrinkage Data

For both batches of hot-cured concrete used in testing, two unsealed and two sealed shrinkage cylinders were instrumented with two gages each. Batch #1 was used for creep series tests A, D, E, F, G and I, and batch #2 was used in creep series H, J and K. Thus four sets of shrinkage measurements were available for the hot-cured batches of concrete. For the weekend and ambient-cured specimens, only one unsealed and one sealed shrinkage cylinder were monitored to optimize the use of the available channels on the data acquisition system. Thus only two curves are available for total and autogenous shrinkage respectively.

Figure 4.2 shows raw data for the two unsealed hot-cured shrinkage cylinders from the same batch (#2) as creep specimen K, from the time of loading of creep specimen K. Positive strain indicates shortening.

24
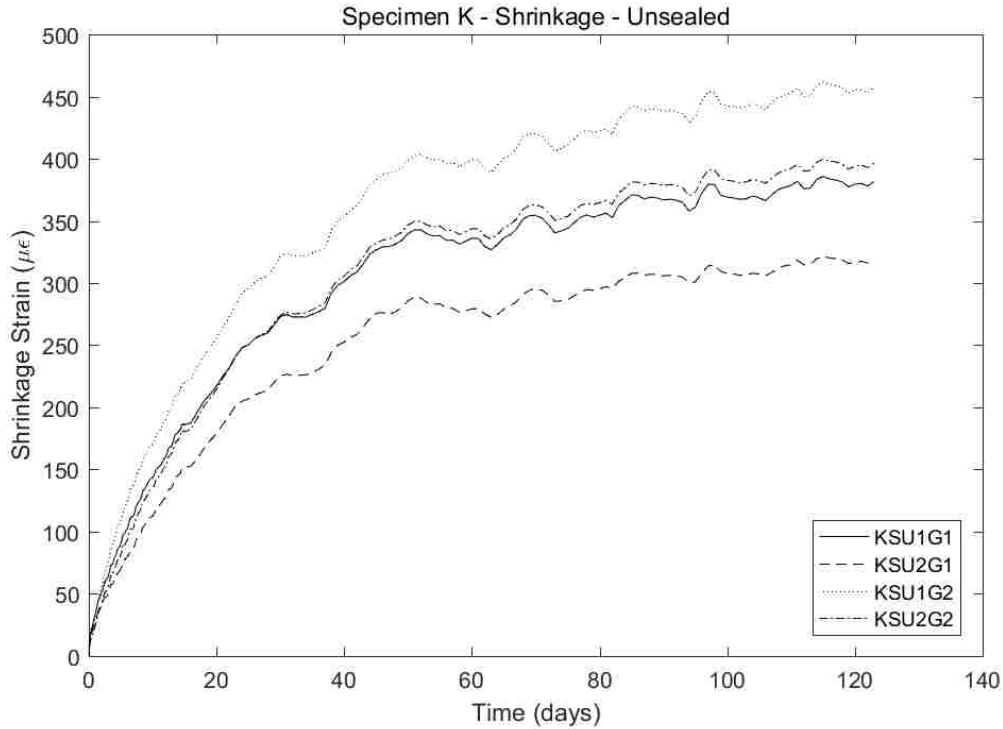
Figure 4.2 Raw Data for Unsealed Shrinkage Cylinders for Specimen K

The four curves track each other fairly well, and no gage failure is apparent in the data. Note that, on each cylinder, the two gages differ by about $75\mu\varepsilon$ after 100 days. Whether this represents gage error or a difference in real strain on the two sides is not known. The average strain in the two cylinders differs by about $60\mu\varepsilon$. At 90 days the average measured shrinkage strain for the four gages was $374\mu\varepsilon$ with a coefficient of variation of 12.6%. The average of the four curves was taken as the total shrinkage for the specimen. The internal consistency between the four gages suggests that the VW gages are reliable and provides confidence in the data yielded by them.

Figure 4.3 shows raw data for the two sealed, shrinkage cylinders from the same batch (#2) as creep specimen K. As was the case for the unsealed cylinders, good internal consistency is observed for three of the four gages. After a few days, gage KSS2G2 shifted down by about 200 microstrain. After that jump, the four gages all measured similar changes in strain. Since this good internal consistency between the gages is apparent, the failed gage was dropped from further calculations, and the single curve for autogenous shrinkage for specimen K were taken as the average of the other three curves. At 90 days the average measured shrinkage strain for the sealed cylinders was $171\mu\varepsilon$ with a coefficient of variation of 12.6%.

25
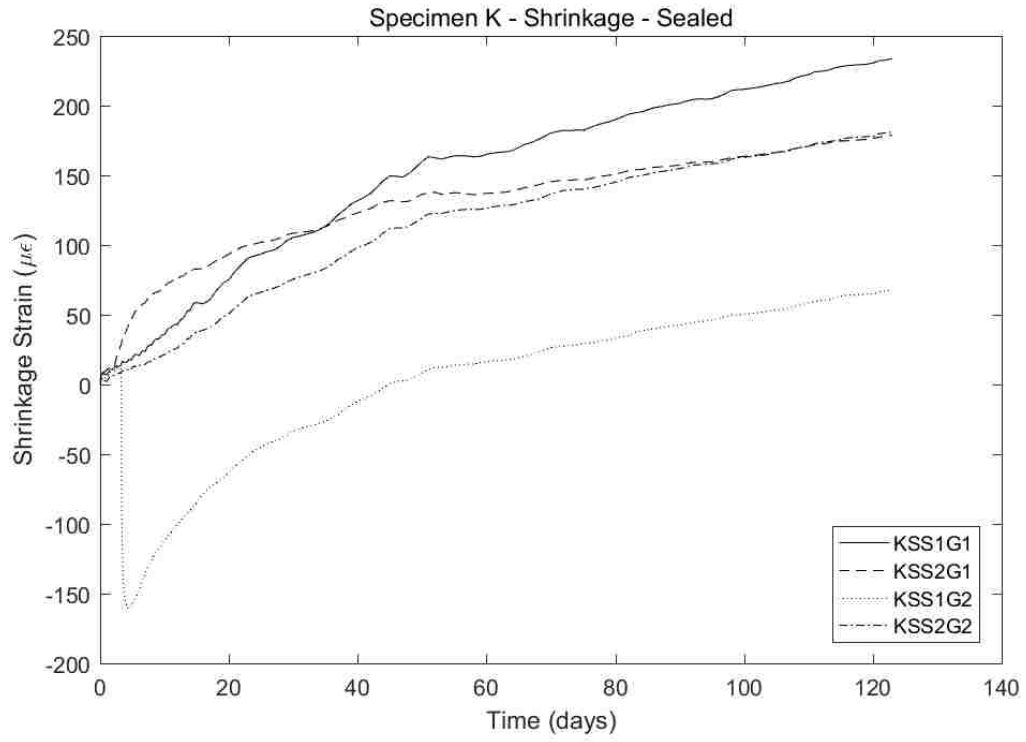
Figure 4.3 Raw Data for Sealed Shrinkage Cylinders for Specimen K

4.2   Creep Data

Figure 4.4 shows raw data for the unsealed, loaded cylinders of Specimen series K.
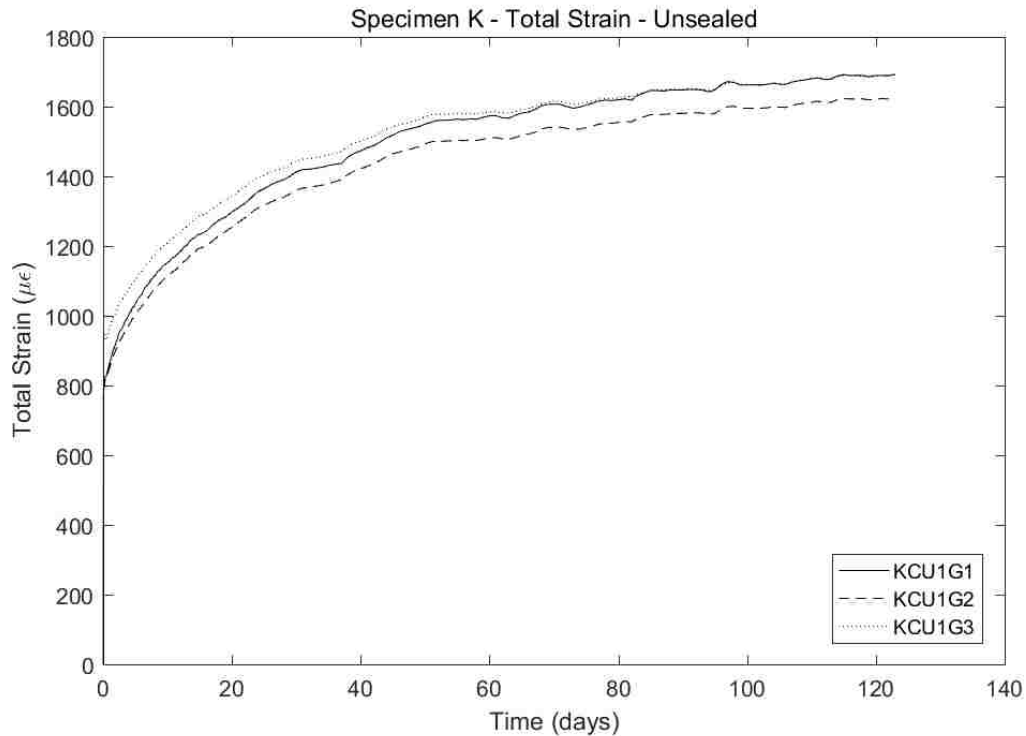
Figure 4.4 Raw Data for Unsealed Creep Cylinders for Specimen K

The gages measuring strain in the creep cylinders were subject to the same sources of error as in the shrinkage cylinders, with an additional one as well: in practice it is impossible to achieve completely concentric loading on the stack of creep cylinders and thus some eccentricity will always be present. This causes gages on different sides of the cylinders to register different values of strain. An effort was made to minimize this eccentricity by placing the cylinder stack on a rotating swivel head for ease of alignment with the plates in the rig. This eccentricity problem is particularly unfortunate in cases of gage failure, because in order to get the correct axial strain in the cylinder, an average of all three gages is needed. For these cylinders, a failed gage cannot be dropped without compromising the dataset. A larger number of gages on each cylinder would have been preferable, but this was impossible because the data acquisition system had only 96 channels. A list of all gage failures can be found in Table B.1 in Appendix B.

The unsealed, loaded cylinder of specimen K, whose data is shown in Figure 4.4, is an example of a cylinder for which these problems were minimal. The eccentricity was low, and none of the gages seem to have failed. To obtain a single curve for elastic + total creep + total shrinkage strain, the average of the three gages was used.

Figure 4.5 shows raw data for the sealed, loaded cylinder of specimen K. A greater eccentricity problem is apparent for this cylinder than the corresponding unsealed one. Also, gage KCS1G2 seems to have malfunctioned shortly after loading.
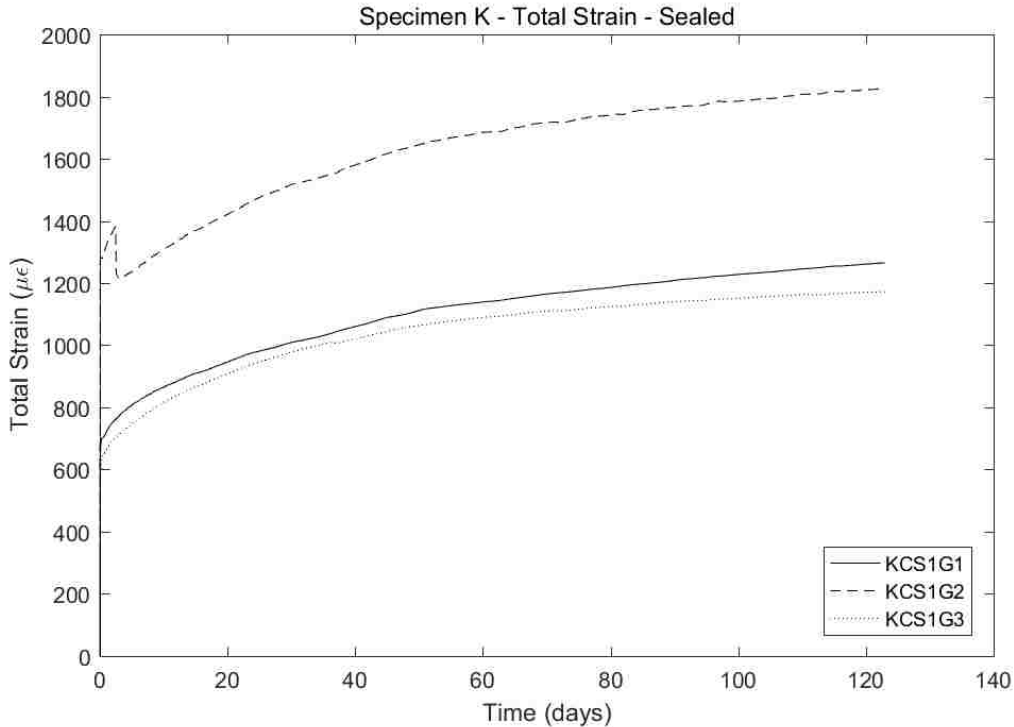
Figure 4.5 Raw Data for Sealed Creep Cylinders for Specimen K

This problem was also observed with one gage on the sealed, loaded cylinders of specimens D and G, as well as for two gages on the sealed, loaded cylinder of specimen C. When two out of the three gages on a loaded cylinder fail, the data from that cylinder is effectively useless. This is unfortunate, because specimen C was the only ambient-cured specimen in the experiment. It should however be noted that data from the unsealed, loaded cylinder for specimen C was consistent across the three gages monitoring it. To salvage some data from sealed, ambient-cured concrete cylinder tests, data from the single working gage on the cylinder was used, since both its elastic value and creep rate seemed plausible on the assumption that the eccentricity was the same under elastic and creep conditions.

For the other three specimens for which only one gage failed per cylinder, various techniques were tried to fix the problem, such as dropping the faulty gage and taking weighted averages of the other two based on their relative elastic strains. However, no technique proved successful because, for each one tried, some aspect of the outcome proved implausible, such as strains in the sealed cylinder exceeding strains in the unsealed cylinder. At the cost of compromising the quality of the data, it was eventually decided to

keep those faulty gages in when processing the data and use the average of the three gages. This resulted in some implausible bumps in the curves for the sealed cylinders, but in all three cases the drops were relatively small, and soon after the gages appeared to work normally again and to show a strain rate similar to those of the other two. A single curve for the elastic + basic creep + autogenous shrinkage for specimen K was therefore obtained by taking the average of the three gages in Figure 4.5. Since one of the gages jumped shortly after loading, there is a possibility that the average elastic strain in the three gages is therefore too high.

4.3   Identification of Strain Components

In processing the data, the values for the gages on each cylinder were averaged, unless one or more had to be discarded due to faulty behavior as described above. This left the following average curves.

- A single curve for elastic + total creep + total shrinkage from the unsealed, loaded cylinder,
- A single curve for elastic + basic creep + autogenous shrinkage from the sealed, loaded cylinder,
- A single curve for total shrinkage from the unsealed, unloaded cylinder(s), and
- A single curve for autogenous shrinkage from the sealed, unloaded cylinder(s).

Keeping all the data points for all the curves led to large datasets. In order to reduce the amount of data but to weight the points towards the early parts of the curves, it was decided to retain and use points of equal intervals of 0.1 in log time, that is points taken at times $10^{0.1}$ days, $10^{0.2}$ days, and so on, as well as two points on each side of a stress change event, to capture elastic strains as well. The curves obtained by this procedure were used to produce the plot shown in Figure 4.6 for Specimen K. It shows the breakdown of the measured strains into different phenomena. The smaller number of data points also sped up the model fitting described in Chapter 10.
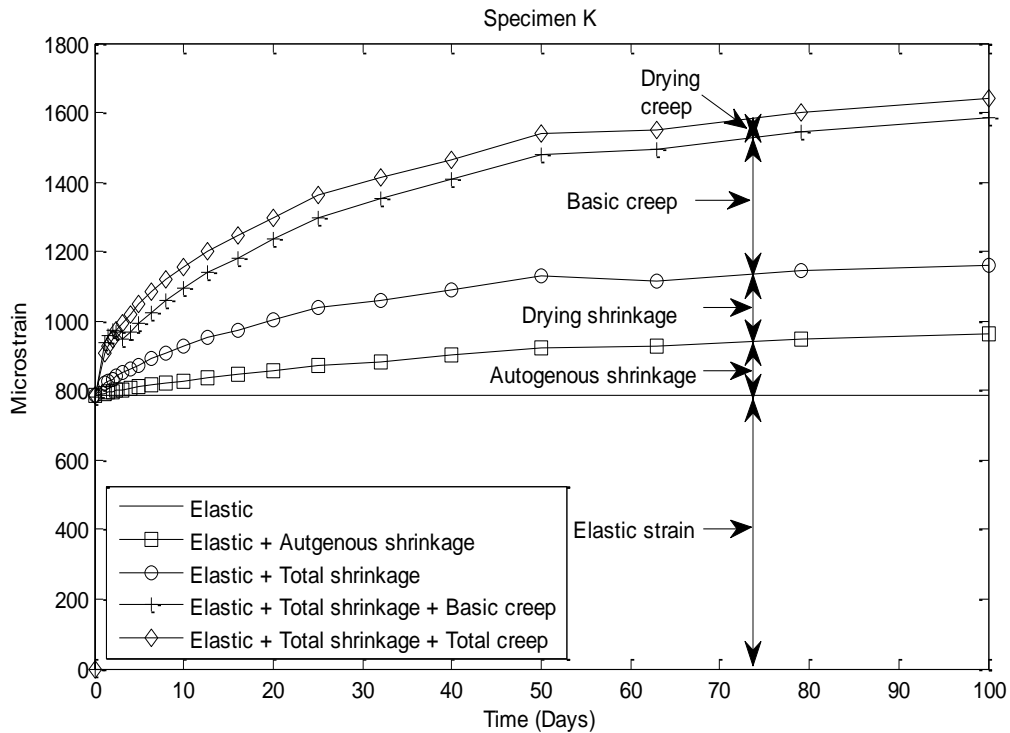
Figure 4.6 Breakdown of Total Strain into Components

In Figure 4.6 the total strain is broken down in the following way:

- The top curve is the total measured strain in the unsealed, loaded cylinder.
- The curve second from top is the total measured strain in the sealed, loaded cylinder plus the drying shrinkage obtained by subtracting the sealed, unloaded curve from the unsealed, unloaded curve. This represents the elastic plus total shrinkage plus basic creep strains.
- The curve third from top is the elastic strain from the unsealed, loaded cylinder plus the measured strain from the unsealed, unloaded cylinder. This represents the elastic plus total shrinkage strains.
- The curve second from bottom is the elastic strain from the unsealed, loaded cylinder plus the measured strain from the sealed, unloaded cylinder. This represents the elastic plus autogenous shrinkage strains.

The bottom horizontal line represents the elastic strain from the unsealed, loaded cylinder.

CHAPTER 5

ANALYSIS OF STRENGTH AND ELASTIC MODULUS DATA

In this chapter, the measured data from the compressive strength and elastic modulus tests are analyzed. The strength and elastic modulus of concrete (nominally identical to the concrete used in the creep tests but from a different batch) were measured at regular intervals by CTC at ages up to 56 days. Additional data on the elastic modulus was obtained from the specimens in the creep rigs by dividing the force applied to them by the cylinder cross-sectional area and measured elastic strain.

5.1 Measured Compressive Strength

Figure 5.1 shows the compressive strengths measured by CTC for both the hot- and ambient-cured concrete.
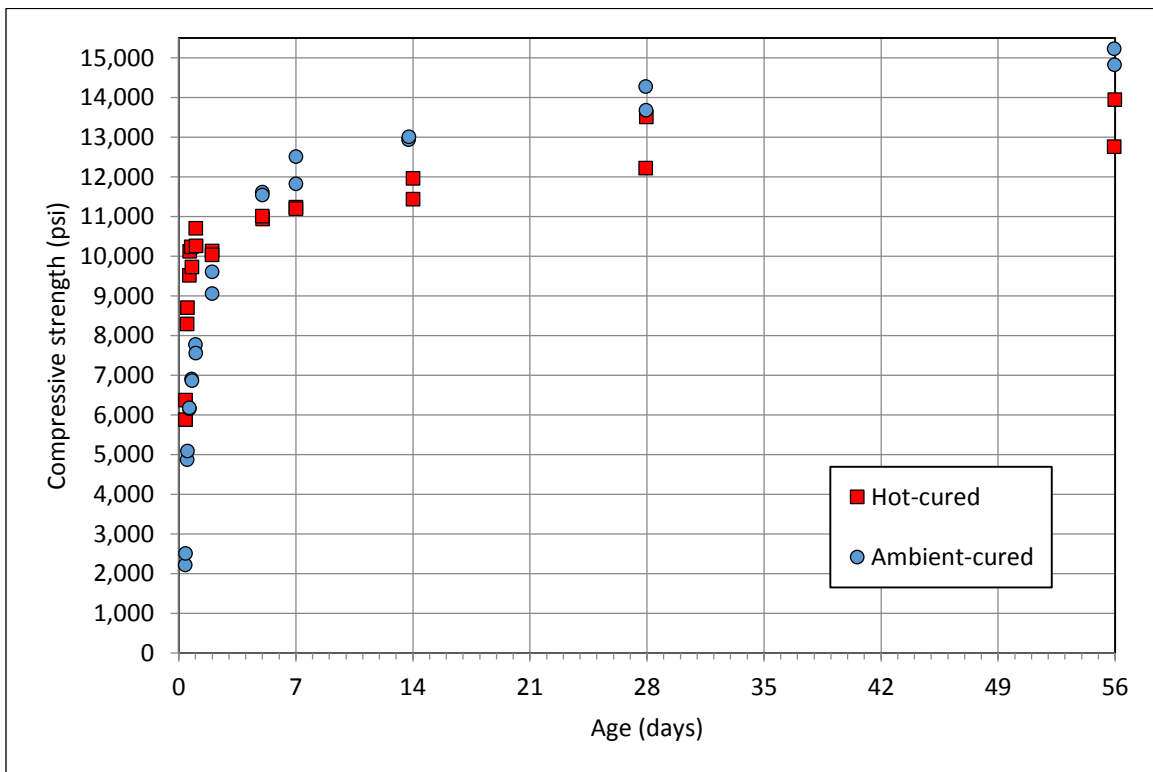
Figure 5.1 Measured Compressive Strength for Ambient- and Hot-cured Concretes

Figure 5.2 shows the same data as Figure 5.1 but zoomed in on the first 7 days of monitoring. The hot-cured concrete initially gained strength faster than the ambient-cured concrete. For example at an age of one day, the compressive strength of the hot-cured concrete was 10,482 psi, which was 37% higher than that of the ambient-cured concrete.

31

That strength gain then slowed, and after about 4 days, the ambient-cured concrete had a higher strength. At 56 days, the mean concrete compressive strength of the ambient-cured concrete, taken as the average of the two measured values, was 15,203 psi. That strength is 14% higher than the mean concrete compressive strength of the hot-cured concrete at 56 days, which was 13,351 psi.
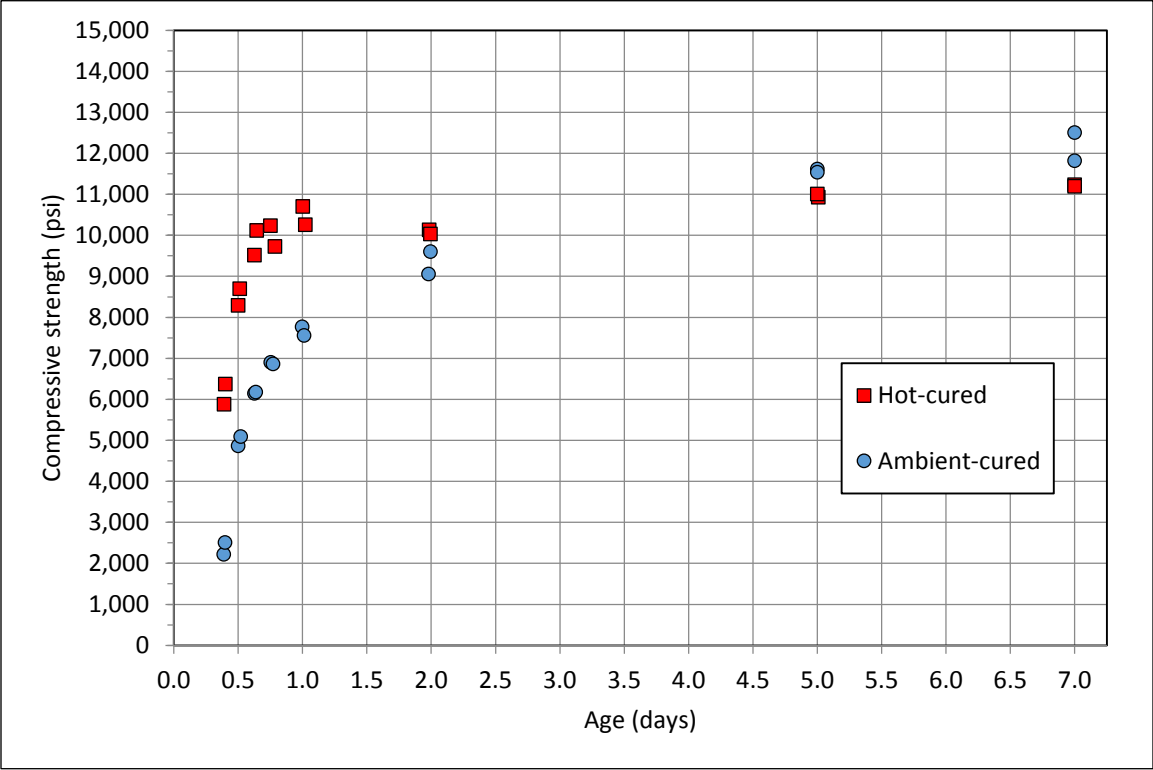
Figure 5.2 Measured Compressive Strength for Ambient- and Hot-cured Concretes - First 7 Days

5.2   Modeling of Compressive Strength Gain

The ACI 209R-92 model and the GL2000 model have two expressions for modeling the development of compressive strength with time (ACI Committee 209, 2008). The ACI function form is as follows:

$$\bar{f}_c(t) = \left[\frac{t}{a + bt}\right] * \bar{f}_c(28)$$

$$5.1$$

where $\bar{f}_c(28)$ is the compressive strength at 28 days, t is the time in days since the mixing of the concrete, and a and b are constants that depend on the cement type and the curing regime of the concrete. Typical recommended values for the parameters are given in Table 5.1. Note that, because the time function must have the value 1.0 at t = 28, a and b are not independent, and $b = 1 - {}^a/_{28}$. The time function is

therefore a one-parameter function, which dictates that the strength at infinite time is $1/b$, or $\frac{28}{28-a}$, times the 28-day strength. That ratio is computed and given in Table 5.1.

Table 5.1 Values of the Constants a and b for the ACI 209R-92 Model

Type of cement	Moist-cured concrete			Steam-cured concrete		
	a	b	$\frac{\bar{f}_c(\infty)}{\bar{f}_c(28)}$	a	b	$\frac{\bar{f}_c(\infty)}{\bar{f}_c(28)}$
I	4.0	0.85	1.17	1.0	0.95	1.05
III	2.3	0.92	1.09	0.70	0.98	1.02

The GL2000 function form, which is a modification of the strength-development relationship used in the CEB MC90-99 model (CEB 1999), is as follows:

$$\bar{f}_c(t) = \beta^2(t) * \bar{f}_c(28) \qquad 5.2$$

where

$$\beta(t) = exp\left[\frac{s}{2}\left(1 - \sqrt{\frac{28}{t}}\right)\right] \qquad 5.3$$

The variable s is a strength-development parameter that depends on cement type. Recommended values for s are given in Table 5.2. This function $\beta(t)$, also has the value 1.0 at 28 days, as it should. The strength at infinite time is exp(s) times the 28-day strength. That ratio is given in Table 5.2 for three values of s. This is also a one-parameter model, so the strength ratio at infinite time and the initial value of strength gain are directly related.

Table 5.2 Parameter s as a Function of Cement Type for the GL2000 Model

Cement type	s	$\frac{\bar{f}_c(\infty)}{\bar{f}_c(28)}$
Type I	0.335	1.40
Type II	0.4	1.49
Type III	0.13	1.14

Neither of these strength-development functions was developed for the accelerated curing regime used in this experiment. Minor modifications to these models, such as changing the speed of the development in the GL2000 model by varying the exponent for the 28/t term, yielded some implausible behaviors. For

example the curvature of some versions of the model were positive, indicating that the rate of strength gain increased with time.

Instead, a time-dependent function was developed to fit to the data for both the hot- and the ambient-cured concrete. The function form is:

$$\bar{f}_c(t) = \kappa(t) * \bar{f}_c(28) \qquad\qquad 5.4$$

where

$$\kappa(t) = \frac{a}{(a-1) * \left(\dfrac{28 - t_0}{t - t_0}\right)^{1/n} + 1} \qquad\qquad 5.5$$

In Eq. 5.4, $\bar{f}_c(28)$ is the strength at 28 days. In Eq. 5.5, a is the ratio between the ultimate strength (i.e., at infinite time) and the strength at 28 days, n is a parameter that controls the rate of strength gain, t is the time in days since mixing the concrete, and t_0 is a time offset parameter that reflects the time taken for the initial set to take place. For any dataset, parameters a, n, and t_0 can be adjusted. Regardless of the values of the parameters, $\kappa(28) = 1.0$, $d\kappa/dt$ is always positive and, for $n > 1.0$, $d^2\kappa/dt^2$ is always negative (indicating a strength gain rate that decreases continuously). Figure 5.3 shows the values of κ with time for the arbitrarily chosen a value of 1.44, $t_0 = 0$ and four different values of n: 1, 2, 5, and 10.
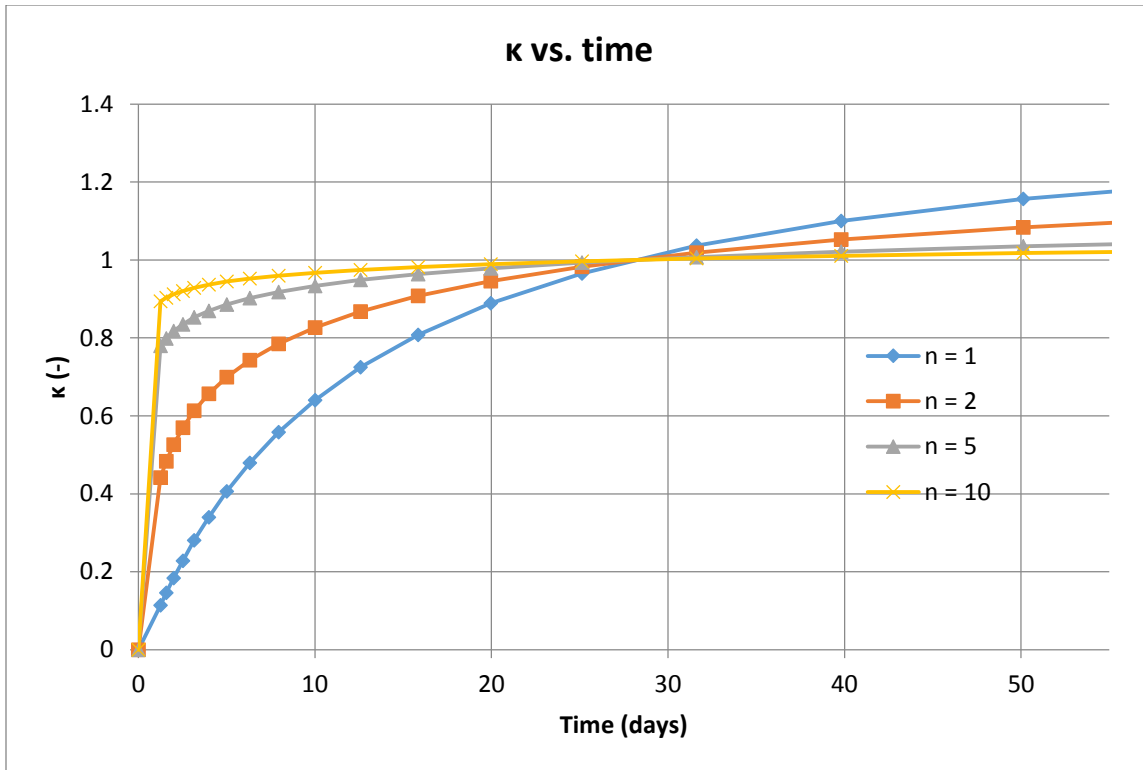
Figure 5.3 The Time-dependent Function, κ, with Time.

By roughly estimating how the two datasets trace back down to the x-axis and thus where they start gaining strength it was decided to make t_0 equal to 5 hours or 5/24 days. The strength was tested on two cylinders at 28 days, and the 28 day value was simply taken as the average of the two measured values at that age.

By doing a least squares fit to the strength data, both for hot-cured and ambient-cured concretes, with a and n being the free parameters, the following optimal results were obtained:

Table 5.3 Optimized Values for Parameters a, 1/n and t_0

	Hot	Ambient
a	1.114	1.075
n	2.44	1.35
t_0	0.2083	0.2083

The fact that the exponent n is larger for the hot concrete is consistent with the expectation that the hot-cured concrete gains strength faster at early ages.

Figure 5.4 compares the measured and fitted strength gains for the hot-cured concrete up to an age of 56 days, and Figure 5.5 shows the same comparison for the first 7 days. The fitted curve approximates the measured values well overall, however it considerably under predicts the strength during ages of 0.5-1 days and slightly over predicts the strength during ages of 2-14 days. The fit is influenced by the fact that the time function increases continuously with time but the strength, surprisingly, drops between 1 and 2 days. [CTC has found a similar drop with other hot-cured mixes, so the drop may be a consequence of heat-curing rather than testing errors].
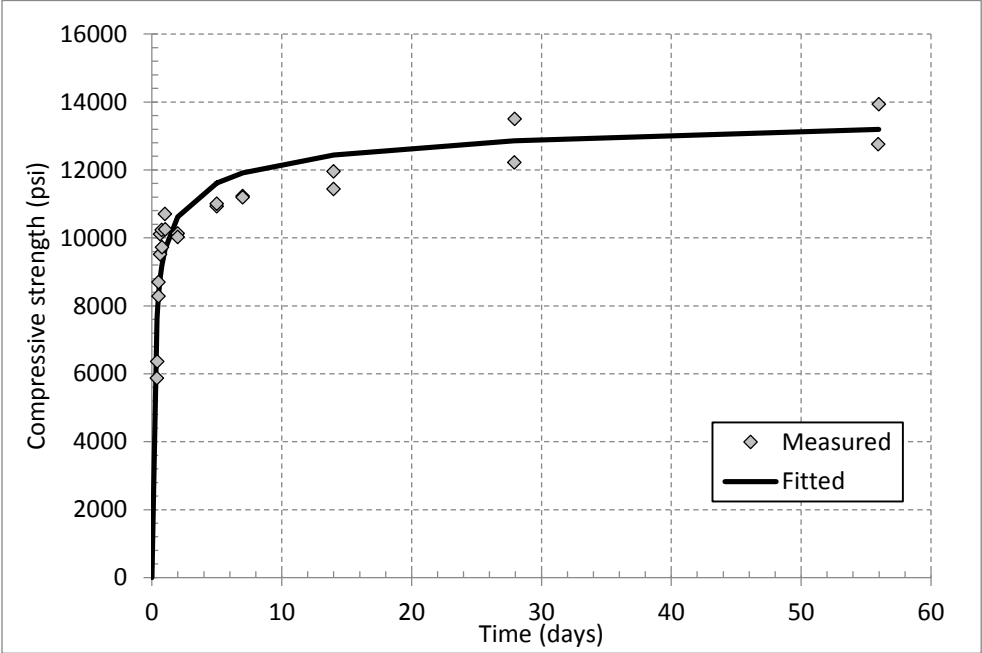
Figure 5.4 Compressive Strength vs. Time for Hot-cured Concrete
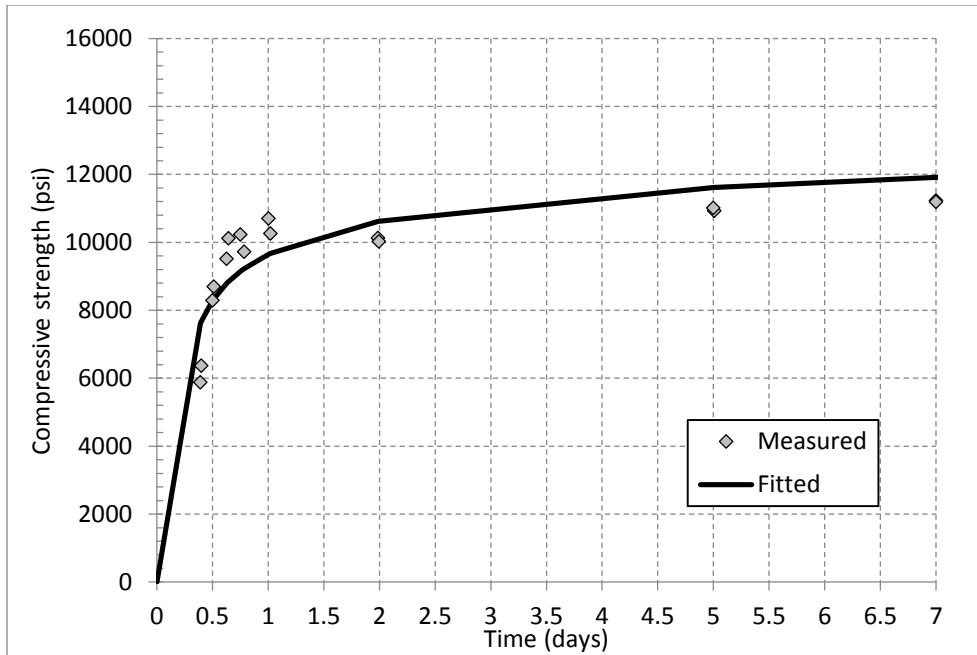
Figure 5.5 Compressive Strength vs. Time for Hot-cured Concrete, First 7 Days

Figure 5.6 compares the measured and fitted strength gains for the ambient-cured concrete up to an age of 56 days, and Figure 5.7 shows the same comparison for the first 7 days. The fit of the data is good at all ages, with slight under predictions at 56 days. The measured strength rises continuously at all ages.
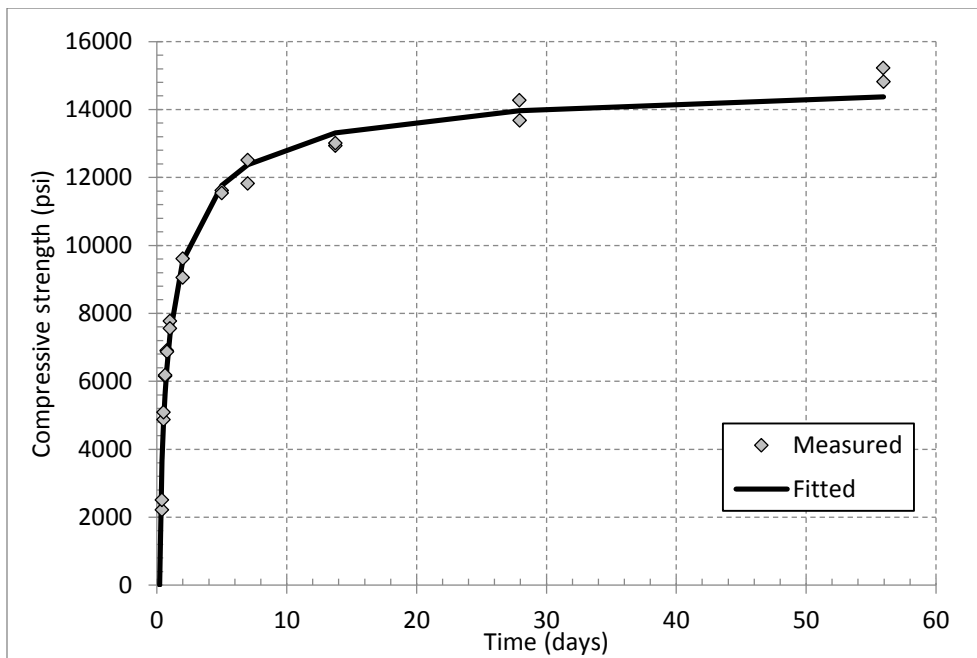
Figure 5.6 Compressive Strength vs. Time for the Ambient-cured Concrete
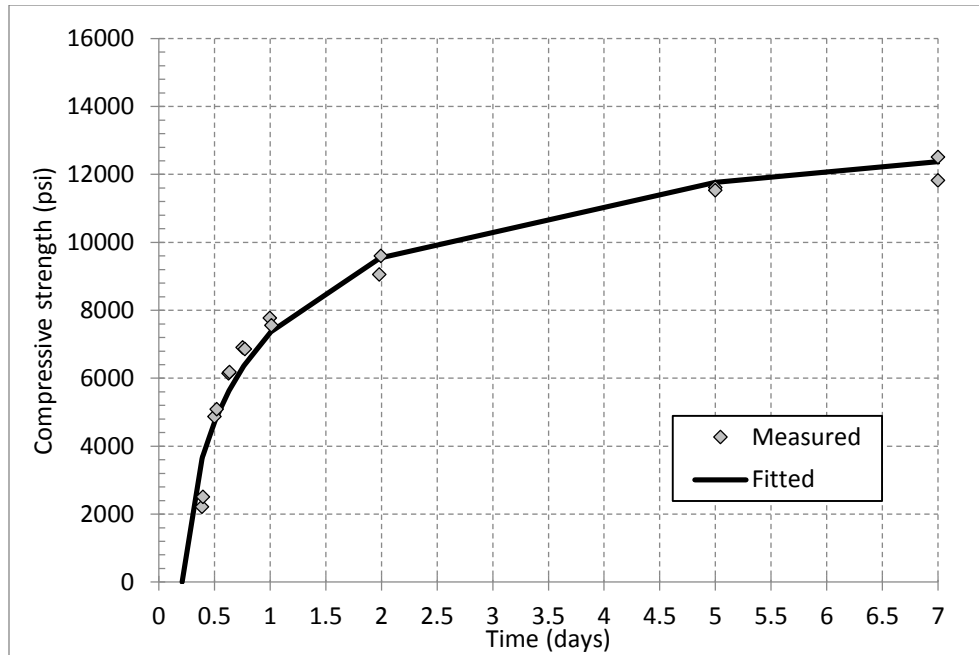
Figure 5.7 Compressive Strength vs. Time for the Ambient-cured Concrete, First 7 Days

5.3   Measured Elastic Modulus

Figure 5.8 shows the results of the elastic modulus tests conducted by CTC for both the hot-cured and the ambient-cured concrete up to an age of 56 days. Figure 5.9 shows the same comparison for the first 7 days.
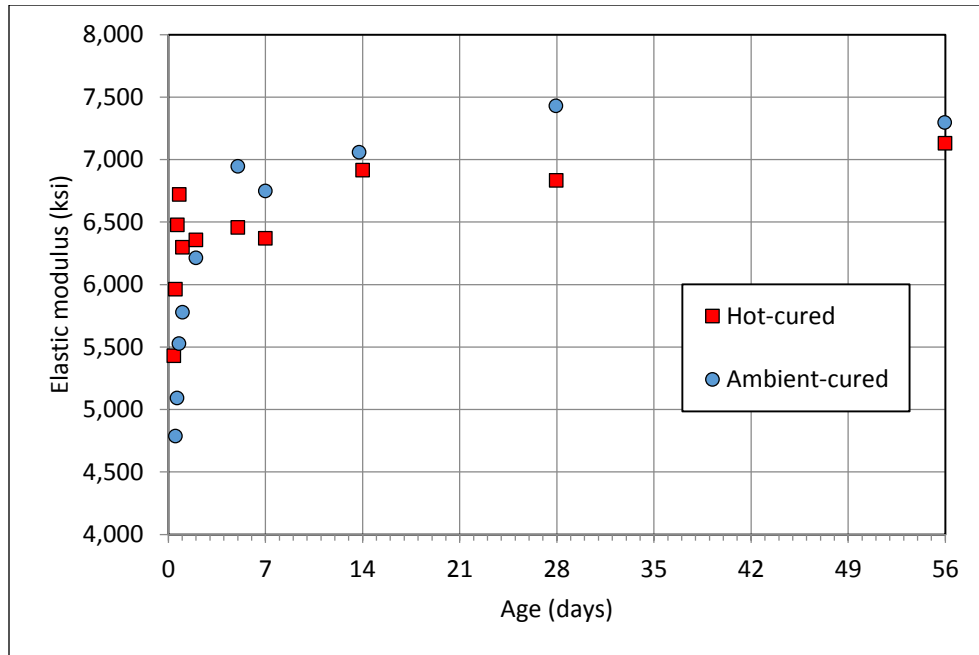
Figure 5.8 Measured Elastic Moduli for Ambient- and Hot-cured Concrete
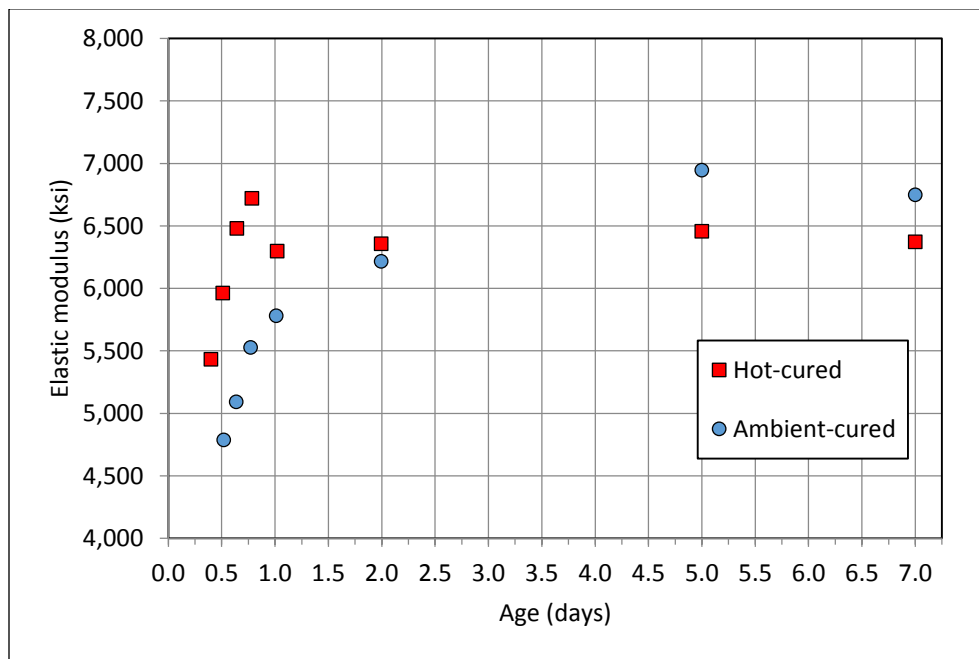
Figure 5.9 Measured Elastic Moduli for Ambient- and Hot-cured Concrete, First 7 Days

As was the case for the compressive strength, the values of elastic modulus for the hot-cured concrete were higher for the first few days, but at five days, the values for the ambient-cured concrete were higher

39

and remained higher out to 56 days. A curious result from these tests is that between 0.8 and 1 days, 5 and 7 days and 14 and 28 days for the hot-cured concrete, the measured elastic modulus value dropped. This was also the case for the ambient-cured concrete between 5 and 7 days and 28 and 56 days. This drop is contrary to the fundamental assumption of the model which assumes that the elastic modulus always increases with time.

Values of the elastic modulus could also be inferred from the initial elastic deformation in the creep rigs. One measure of the quality of the data yielded by the creep rigs is to compare elastic modulus values calculated by dividing the stress on each specimen for the sealed and unsealed cylinders. Because the cylinders were loaded shortly after being sealed, any differences in strength and stiffness due to differences in moisture during that time should be negligible. Table 5.4 shows values for elastic moduli for the sealed and unsealed cylinders for each specimen. The mean ratio of the elastic modulus for the unsealed and sealed cylinders was 0.99 with a coefficient of variation of 4.8%. With the exception of specimen J the difference between the sealed and the unsealed elastic strains is within 6%. The unsealed and sealed cylinder in the same rig and therefore under the same stress should be expected to experience the same elastic (and creep) strains and thus this small variation of strains between them is a testament to the reliability of the gages and the consistency of the concrete in the different cylinders.

Table 5.4 Elastic Moduli Based on Measured Elastic Strains

Speci-men	Batch no.	Curing regime	Load change	Age at loading	Cylinder type	Elastic strain	Elastic modulus (ksi)	Unsealed /Sealed ratio
A	3	Hot	+ 2.7 ksi	0.7 days	Unsealed	434.5	6214	1.03
					Sealed	446.9	6041	
E	3	Hot	+ 2.7 ksi	0.7 days	Unsealed	437.8	6186	0.99
					Sealed	434.2	6238	
			- 2.7 ksi	3.8 days	Unsealed	399.4	6782	1.04
					Sealed	416.7	6501	
G	3	Hot	+ 2.7 ksi	0.7 days	Unsealed	435.3	6172	1.04
					Sealed	454.8	5908	
			- 2.7 ksi	7.8 days	Unsealed	377.0	7126	1.02
					Sealed	383.7	7002	
K	2	Hot	+ 4.5 ksi	0.7 days	Unsealed	785.8	5726	1.00
					Sealed	782.1	5754	
I	3	Hot	+ 2.7 ksi	0.8 days	Unsealed	442.6	6070	0.95
					Sealed	421.5	6374	
			- 0.9 ksi	3.8 days	Unsealed	104.4	8577	1.05
					Sealed	109.7	8165	
			- 0.9 ksi	7.8 days	Unsealed	136.1	6581	1.02
					Sealed	139.4	6424	
			- 0.9 ksi	14.8 days	Unsealed	149.2	6004	0.94
					Sealed	139.5	6421	
B	1	Weekend	+ 2.7 ksi	2.8 days	Unsealed	413.7	6412	0.99
					Sealed	411.4	6449	
C	3	Ambient	+ 2.7 ksi	3.8 days	Unsealed	414.2	6518	1.00
					Sealed	413.1	6536	
D	3	Hot	+ 2.7 ksi	3.8 days	Unsealed	433.9	6222	0.94
					Sealed	406.2	6646	
F	3	Hot	+ 2.7 ksi	7.8 days	Unsealed	411.1	6561	1.02
					Sealed	418.8	6440	
H	2	Hot	+ 2.7 ksi	12.8 days	Unsealed	378.0	7130	1.01
					Sealed	380.4	7085	
J	2	Hot	+ 2.7 ksi	57.7 days	Unsealed	420.4	6392	0.87
					Sealed	363.8	7385	
							Mean	0.99
							CoV	4.8%

The elastic moduli inferred from the elastic deformations can also be compared with the elastic modulus values measured by CTC. The two would be expected to be roughly the same because they are for the same age, same concrete and under the same stress. Figure 5.10 shows the development of the elastic modulus with time for the concrete in the rigs, along with the CTC measurements. Figure 5.11 shows the same data for the first 7 days.
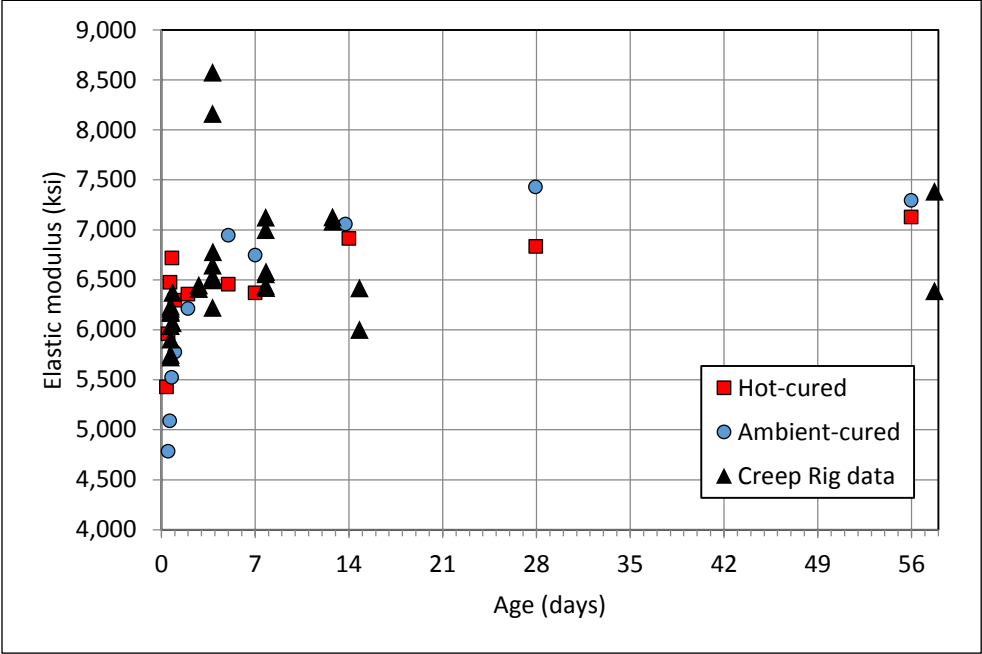
Figure 5.10 Elastic Moduli from Measured Elastic Strains
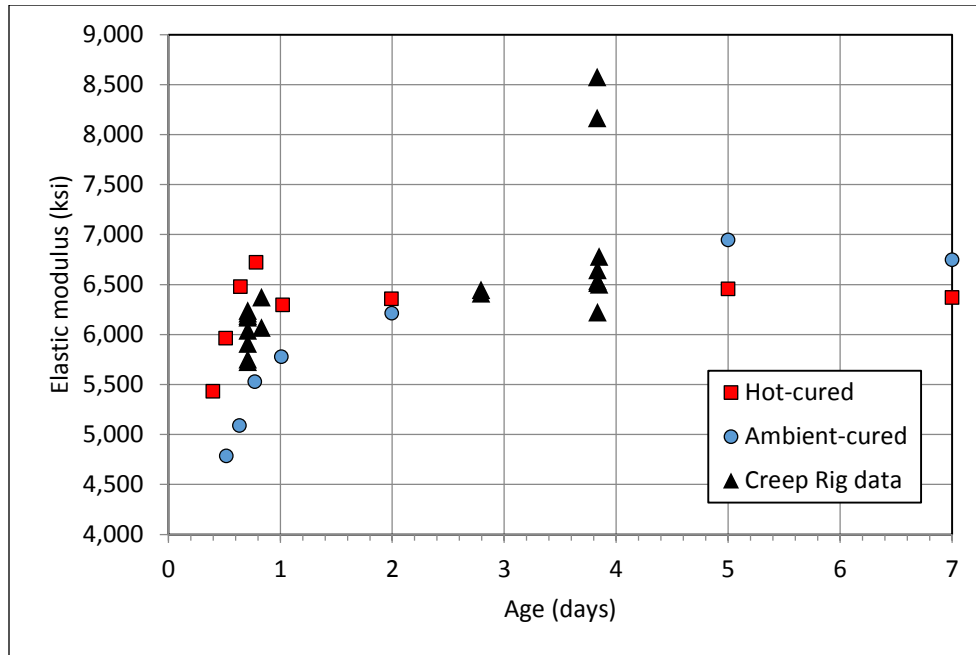
Figure 5.11 Elastic Moduli from Measured Elastic strains, First 7 Days

Apart from a few outliers, the creep rig data agree with CTC's data quite well. The outliers above 8000 ksi at 3.8 days and below 6500 ksi at 14.8 days are from partial unloadings of Specimen I. In both cases, the stress change was 0.9 ksi, rather than the 2.7 or 4.5 ksi used for the other cylinders, and it is likely that the smaller stress range affected the accuracy of the readings. For example, as described in Appendix A, friction in the ram piston introduced a small error into the load readings, and this would cause a larger relative error in the smaller load increments of Specimen I. Furthermore, the readings were taken during unloading rather than loading.

5.4   Relationships between Elastic Modulus and Compressive Strength

A generalized form of the equation used by ACI (2014) and AASHTO (2014) was used to make a best fit to the combined dataset from both the hot- and ambient-cured concretes. The equation is as follows:

$$E_c(t) = c * w^{n_w} * \bar{f_c}(t)^{n_f} \qquad\qquad 5.6$$

where c, n_w and n_f are free parameters determined by a least squares fit to data, w is the unit weight of the concrete in pounds per cubic foot, and $\bar{f_c}$ is the concrete strength. ACI and AASHTO use this same form with different values for c, n_w and n_f. In the ACI version of this equation, the unit weight is expressed in pounds per cubic foot and the concrete strength is expressed in pounds per square inch. In the AASHTO version of this equation the unit weight should be in kips per cubic foot and the concrete strength in kips per square inch. For clarity, the fitted constants are given for both sets of units for the AASHTO equation.

43

Table 5.5 shows the parameters yielded by the best fit to the data as well as the standard values used by ACI and AASHTO.

Table 5.5 Parameters for Elastic Modulus Equation

Parameter	Fitted Data (lb units)	ACI (lb units)	AASHTO (lb units)	AASHTO (kip units)
c	0.012	0.033	0.0121	121000
n_w	1.890	1.5	2.0	2.0
n_f	0.4	0.5	0.33	0.33

Figure 5.12 compares ACI's predictions and the measured data. All of the data fall within +/-10% of the predicted values. For measured values of the elastic modulus below 6,000 ksi, the ACI model under predicts the measured elastic moduli. Above measured values of about 6,700 ksi, the ACI equation slightly overestimates the measured values. The root mean square (rms) values for the ambient- and the hot-cured concretes are 246 and 307, respectively, meaning that the ambient-cured values have less scatter.
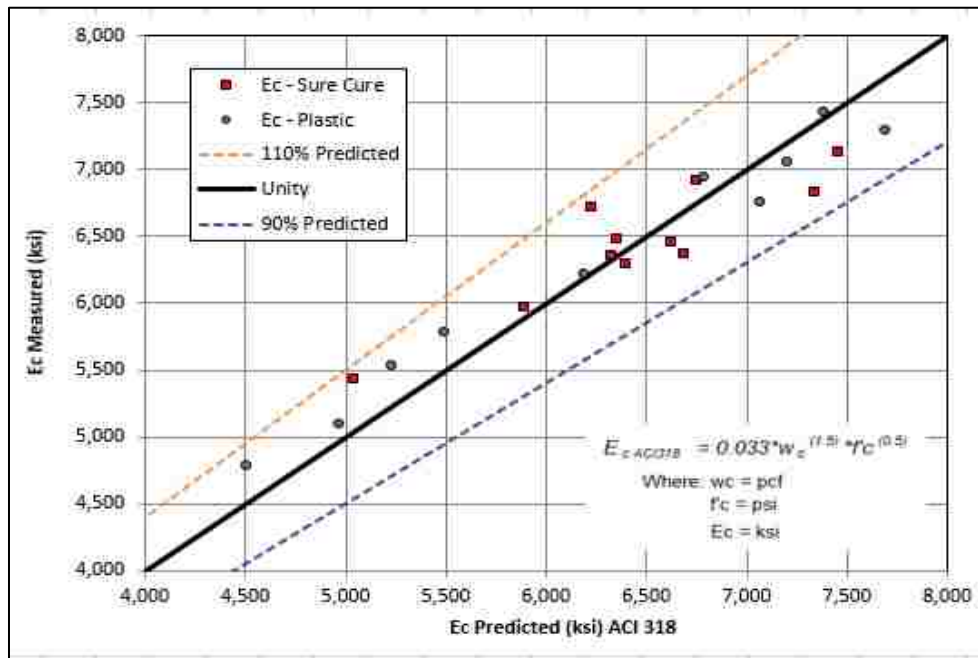
Figure 5.12 ACI318 Predictions vs. Measured Values of Elastic Moduli

Figure 5.13 compares AASHTO's predictions and the measured data. As was the case for the ACI model, all of the data fall within +/-10% of the predicted values, but the tendency to overestimate or underestimate the elastic modulus is different from that observed for the ACI equation. For measured values of the elastic modulus below 6,000 ksi, the AASHTO model predicts the measured values well. Above measured values of about 6,000 ksi, the AASHTO equation slightly overestimates the elastic moduli the measured values. The rms values for the ambient- and the hot-cured concretes are 273 and 250, respectively, meaning that the hot-cured values have less scatter.
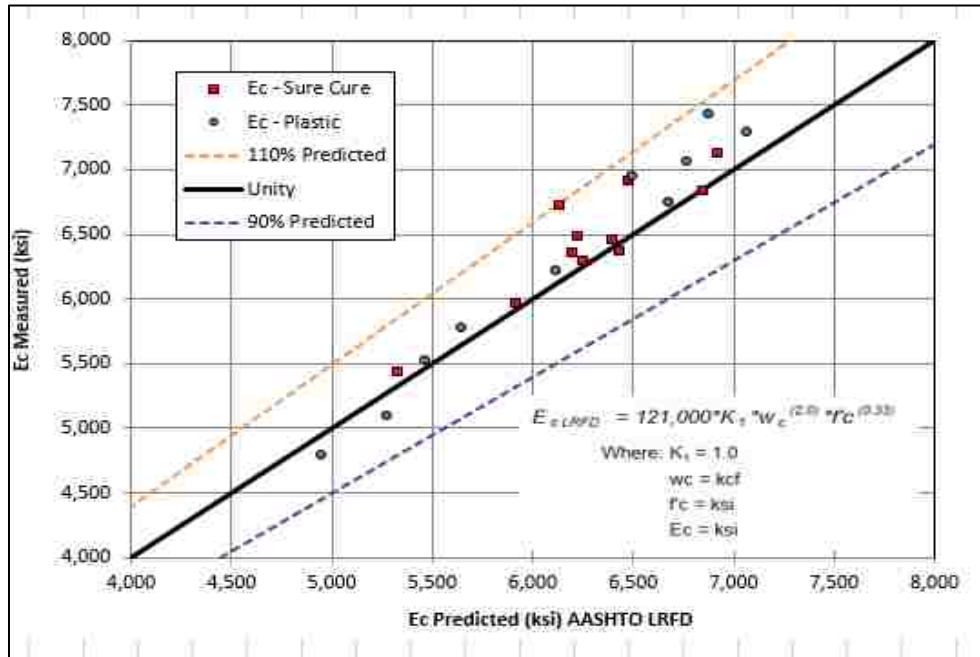
Figure 5.13 AASHTO Predictions vs. Measured Values of Elastic Moduli

Figure 5.14 compares the fitted model (Eq. 5.6) and the measured data. The value of the exponent for this model (0.407, rounded to 0.4) is between the value used in the ACI model (0.5) and the AASHTO model (0.33), resulting in a better fit of the data over the full range of measured values. The rms values for the ambient- and the hot-cured concretes are 143 and 212, respectively, meaning that the ambient-cured values have less scatter.
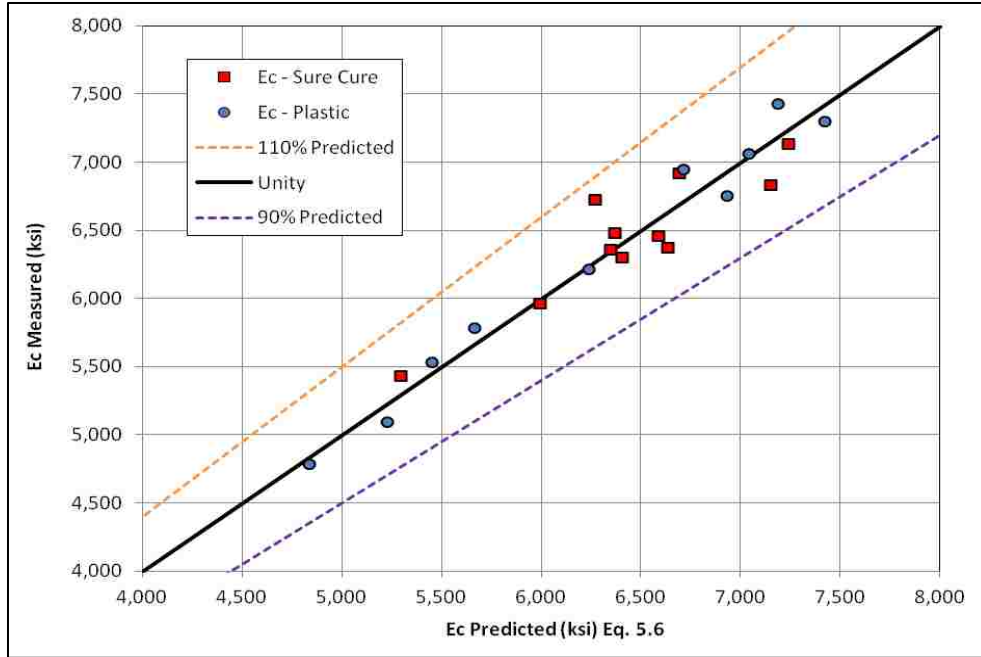
Figure 5.14 New Model Predictions vs. Measured Values of Elastic Moduli

5.5 Measured Elastic Strains

5.5.1 Elastic Strains of Loading with Time

The mean compressive strength of concrete and the elastic modulus both increase with time. Therefore it would be expected that for two concrete specimen loaded to the same stress value but at different times, the specimen loaded at a later age would deform less, both elastically and via creep. Figure 5.15 shows a comparison between elastic values from both unsealed and sealed cylinders for Specimens A, D, F, H and J which were loaded to the same stress of 2.7 ksi at different ages in increasing order. The third bar for each specimen shows a value predicted by the best fit curve to the elastic modulus measurements made by CTC as derived in Chapter 5.4.
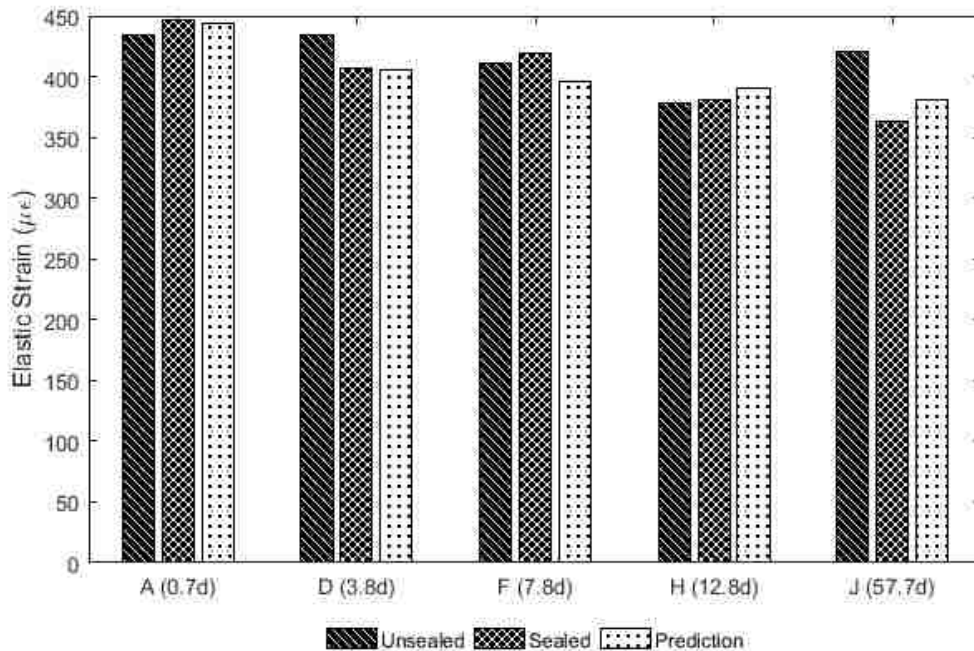
Figure 5.15 Elastic Strain Values for Specimens with Monotonic Loading

The unsealed J and D cylinders and the sealed F cylinder seem to be anomalies in the expected trend of decreasing elastic strain with greater age at loading. The unsealed J cylinder showed higher elastic and creep strains than expected, so it is possible that the cylinder itself was in some way defective (e.g. internal air voids). The unexpectedly high strain in the sealed F cylinder is harder to explain. Apart from these three anomalous results, the data show that the strains decrease with increased age of loading.

5.5.2 *Elastic Strains of Unloaded Specimens*

Figure 5.16 shows the relative differences between the elastic strains for the unsealed and sealed cylinders of Specimen E loaded at 0.7 days and unloaded at 3.8 days. These differences should be minimal since the two cylinders are in the same rig and thus loaded to the same value. The state of cure of the sealed and unsealed cylinders might be expected to be identical at the time of loading (shortly after sealing), but perhaps to differ slightly by the time of unloading because of the difference in retained humidity. The elastic strains during unloading for the two cylinders differ by less than 5% for both the loading and the unloading. The unloading strains are smaller than the loading strains, which was expected, because the elastic modulus likely increased between these two times.
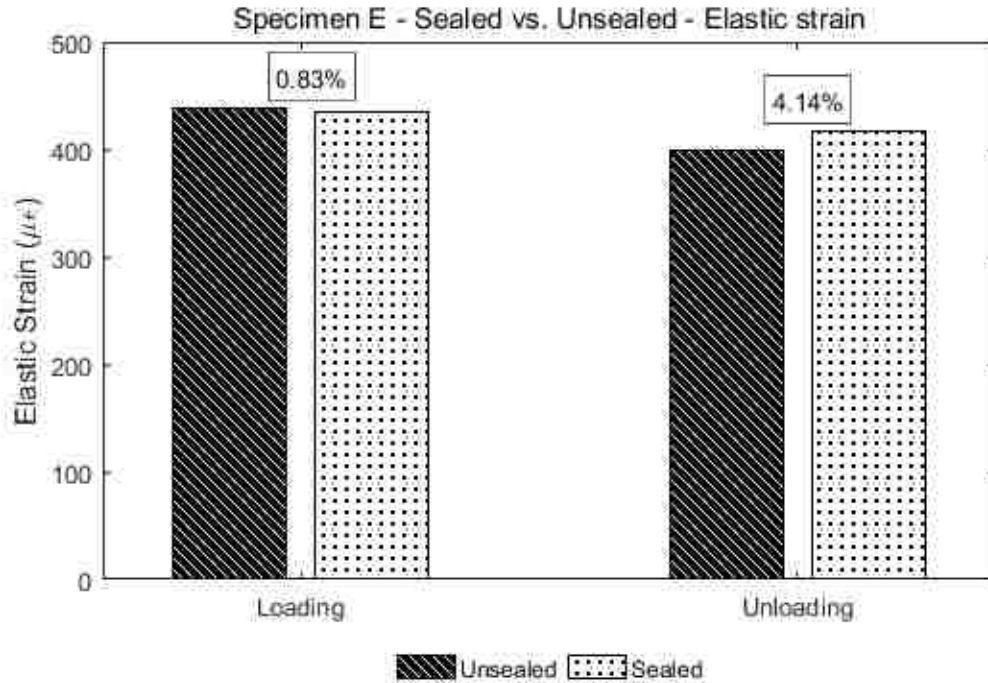
Figure 5.16 Elastic Strains for Stress Change Events of Specimen E

Figure 5.17 shows the relative differences between the elastic strains for Specimen G, which was loaded at 0.7 days and unloaded at 7.8 days. These differences should be minimal since the two cylinders are in the same rig and thus loaded to the same value. The two cylinders differ by less than 5% for both the loading and the unloading.
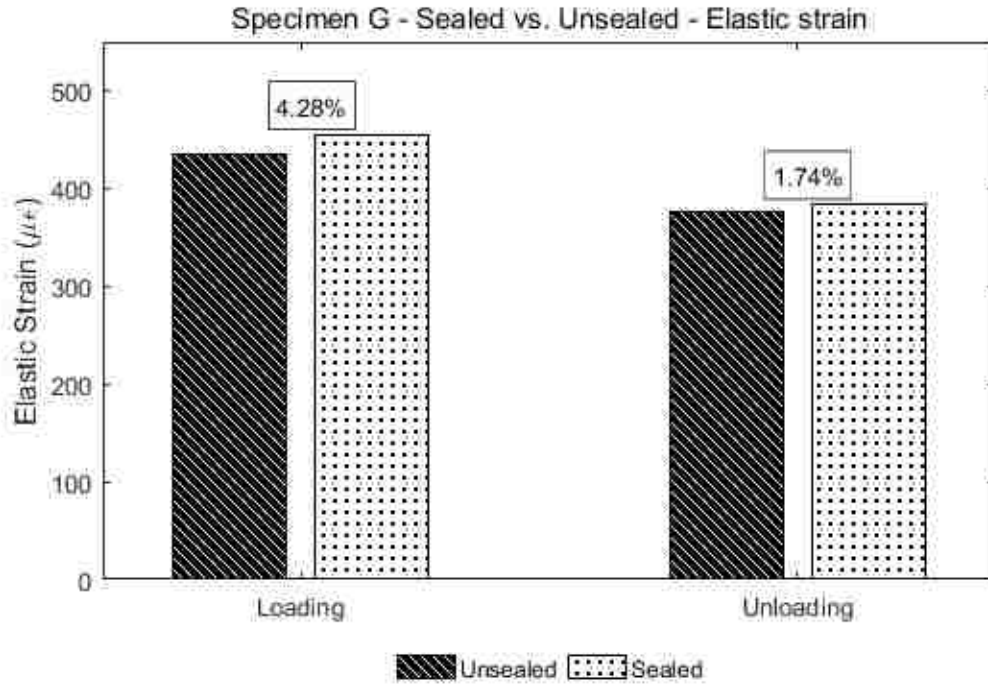
Figure 5.17 Elastic Strains for Stress Change Events of Specimen G

Figure 5.18 shows the relative differences between the elastic strains for the unsealed and the sealed cylinder for Specimen I loaded at 0.8 days, unloaded to 2/3 of the original value at 3.8 days, unloaded to 1/3 of the original value at 7.8 days and unloaded completely at 14.8 days.. These differences should be minimal since the two cylinders are in the same rig and thus loaded to the same value.
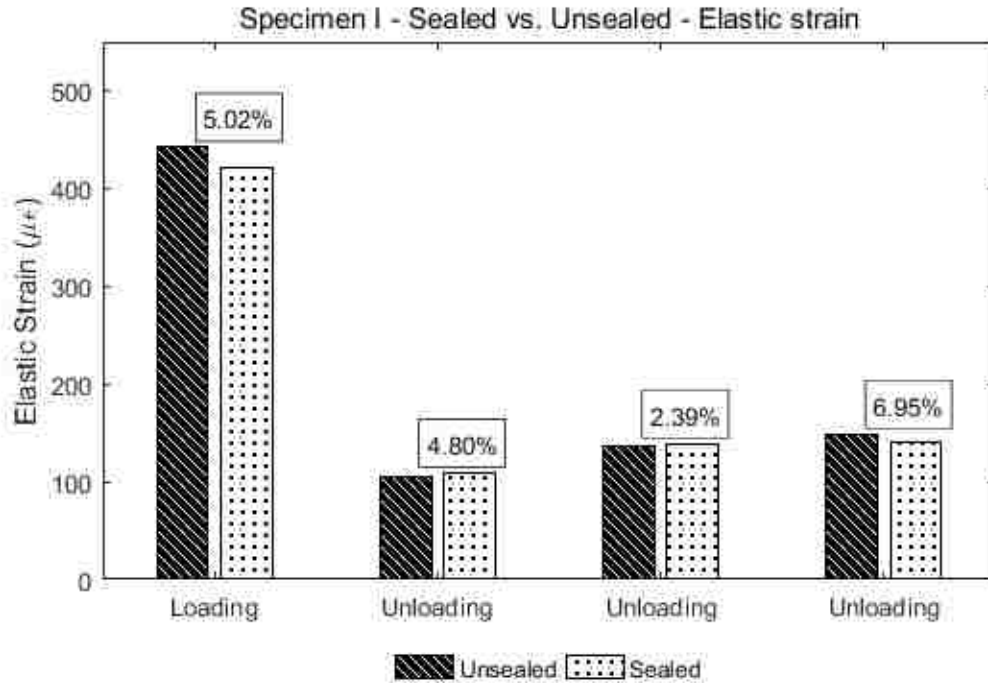
Figure 5.18 Elastic Strains for Stress Change Events of Specimen I

The elastic strain measured for the two cylinders differed by less than 7% for all stress change events. For Specimen I, one would expect the increments in the elastic strains to go down with time but they go up with time. This can likely be attributed to inaccuracies in the partial unloading procedure.

5.5.3 Discussion

The following trends were observed:

- Values for sealed and unsealed cylinders in the same rig match closely. This implies that the cylinders were consistent and the gages are reliable.
- The increase with time in the elastic modulus is reflected in the elastic strain data, except for Specimen I where inaccuracies in the partial unloading procedure are a likely cause for that anomalous behavior.
- No real trend can be observed between elastic strain values for sealed and unsealed cylinders.

CHAPTER 6

ANALYSIS OF SHRINKAGE DATA

Data from the four sets of unloaded cylinders provided data on the total (unsealed cylinders), autogenous (sealed cylinders) and drying shrinkage strains (difference between unsealed and sealed cylinders).

6.1   Measured Shrinkage Strains

Figure 6.1 and Figure 6.2 show the shrinkage strain histories for the two batches (#1 and #2) of hot-cured concrete. At 100 days, the total shrinkage was 395με for Batch 1 and 376με for Batch 2, a difference of only 5%. The autogenous shrinkage accounted for 62% of the total for Batch 1 and 48% for Batch 2. The consistency between the two sets of measurements (each the result of averaging the strains from two gages) suggests that the data are reproducible.

Figure 6.3 shows shrinkage strain histories for the weekend-cured concrete. At 100 days the total shrinkage was 344με, which was 11% lower than the average total strain for the hot-cured concrete. At this age, the autogenous shrinkage accounted for 59% of the total shrinkage, approximately the same as for hot-concrete batch #1.

Figure 6.4 shows shrinkage strain histories for the ambient-cured concrete which was taken from the same batch as the hot-cured concrete batch #1. At 100 days the total shrinkage was 316με, which was 18% lower than the average total strain for the hot-cured concrete. The autogenous shrinkage accounted for 58% of the total shrinkage.

The measured shrinkage strains were roughly similar for the four batches. In all cases:

- The shrinkage strains ranged from 316 to 395με.
- The basic strains accounted for 48% to 62% of the total shrinkage strains

The drying shrinkage, with 4"x8" cylinders (effective thickness = 2"), occured much faster than the autogenous shrinkage. The drying shrinkage occurred mainly during the first 20 to 30 days and was nearly constant after approximately 40 to 50 days. In contrast, the basic and total shrinkage continued to increase with time throughout the 100 days of monitoring.

6.2   Parametrization of Measured Shrinkage Strains

For each case, a time-dependent relationship, similar to the one used for the time development of the concrete strength, was fitted to measured strains. The functional form of the relationship was:

$$\varepsilon(t) = \kappa(t) * \varepsilon(28) \qquad\qquad 6.1$$

where

$$\kappa(t) = \frac{a}{(a-1) * \left(\frac{28}{t}\right)^{1/n} + 1}$$ 6.2

In this expression, ε is the shrinkage, $\varepsilon(28)$ is the shrinkage strain at 28 days, a is the ratio between the ultimate strain value and the strain value at 28 days, and n is a parameter that controls the rate of strain gain with time. For this model, the time taken to reach half of the ultimate strain, t_{50}, can be calculated as follows:

$$t_{50} = 28 * (a-1)^n$$ 6.3
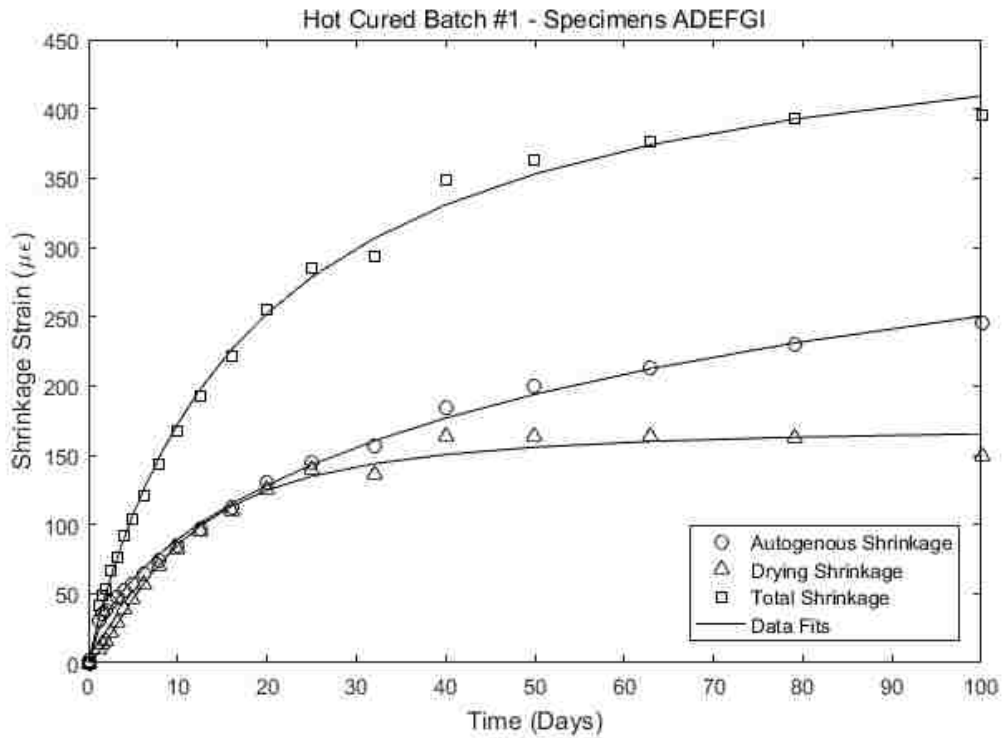
Figure 6.1 Drying, Autogenous, Total and Predicted Shrinkage Strains for Hot-cured Concrete Batch #1
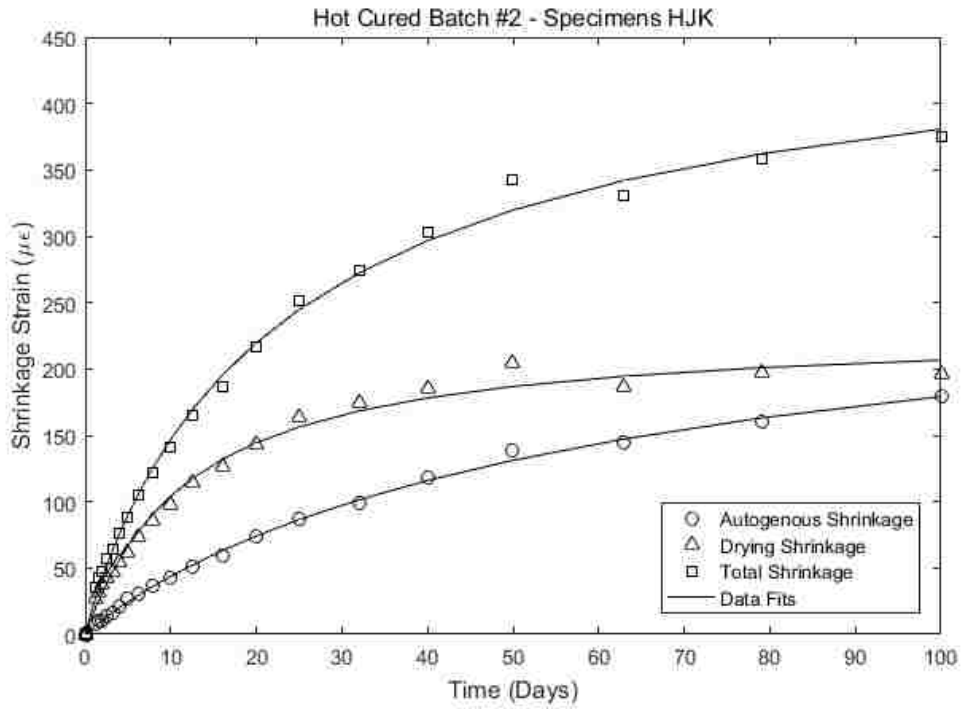
Figure 6.2 Drying, Autogenous, Total and Predicted Shrinkage Strains for Hot-cured Concrete Batch #2
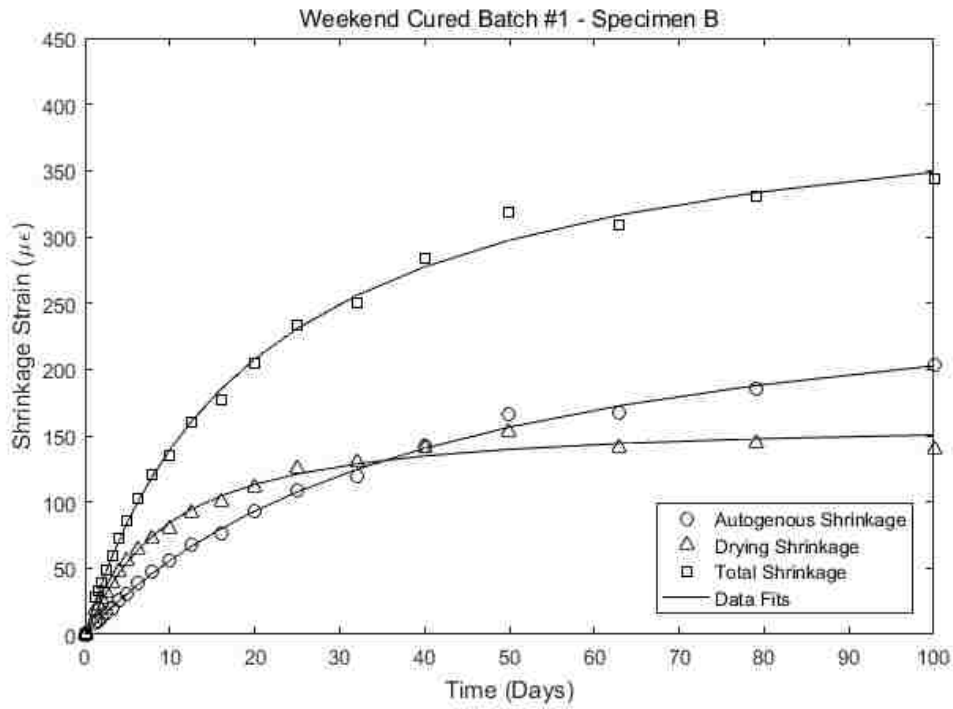
Figure 6.3 Drying, Autogenous, Total and Predicted Shrinkage Strains for Weekend-cured Concrete Batch #1

53
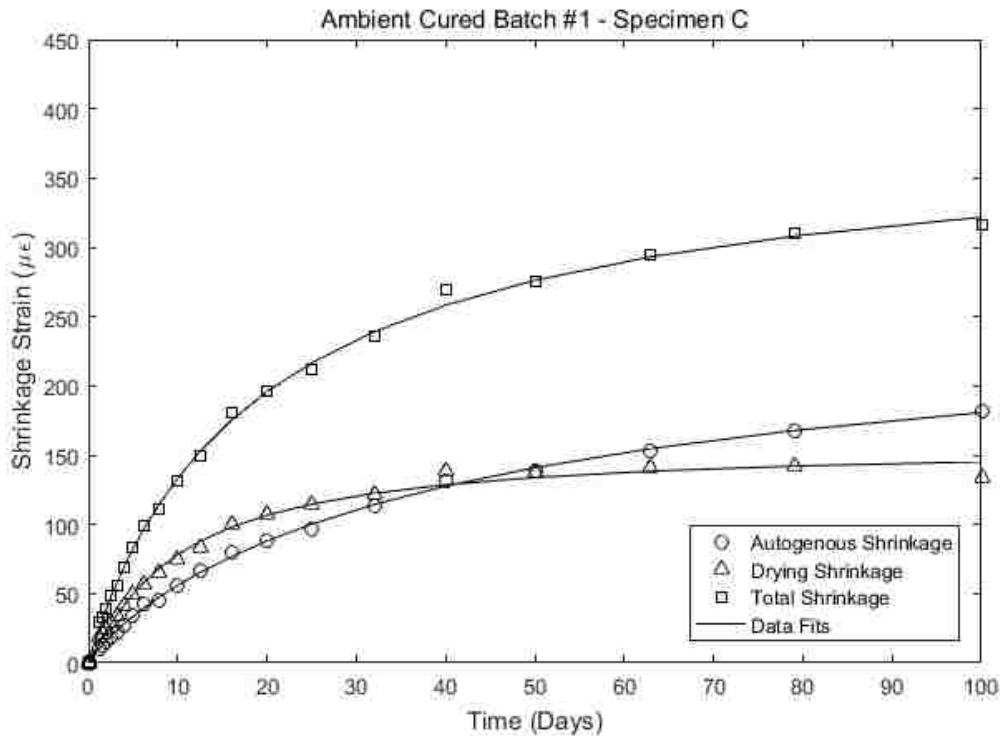
Figure 6.4 Drying, Autogenous, Total and Predicted Shrinkage Strains for Ambient-cured Concrete Batch #1

Table 6.1 shows the parameters yielded from least-squares fit to the data for all four sets of specimens.

Table 6.1 Curve Fit Parameters for Drying, Autogenous and Total Shrinkage

	Total Shrinkage			Autogenous Shrinkage			Drying Shrinkage		
	ε(28)	a	1/n	ε(28)	a	1/n	ε(28)	a	1/n
Hot-Cured 1 - ADEFGI	292	1.69	0.96	151	3.28	0.67	139	1.23	1.43
Hot-Cured 2 - HJK	258	1.87	0.93	93	3.17	0.95	162	1.42	1.03
Weekend-Cured	242	1.75	0.97	115	2.51	0.99	125	1.30	1.09
Ambient-Cured	227	1.72	0.96	107	2.54	0.89	118	1.33	1.10

There is a fair agreement between the parameters for the two hot-cured batches. The contrast between a values between autogenous and drying shrinkage reflects the fact that most of the drying shrinkage seems to have taken place in the first 28 days, whereas the autogenous shrinkage seems to have continued.

For all four specimens, Table 6.2 shows the ultimate strain and t_{50}, which were derived from the fitted curves.

Table 6.2 Predicted Ultimate Strain and t_{50} Values for Drying, Autogenous and Total Shrinkage

	Total Shrinkage		Autogenous Shrinkage		Drying Shrinkage		Autogenous + Drying
	ε_{ult}	t_{50} (days)	ε_{ult}	t_{50} (days)	ε_{ult}	t_{50} (days)	ε_{ult}
Hot Cured 1 - ADEFGI	492	19	494	96	172	10	666
Hot Cured 2 - HJK	481	24	296	64	230	12	526
Weekend Cured	425	21	289	42	162	9	451
Ambient	390	20	271	46	157	10	427

The ultimate strain value predicted for the autogenous shrinkage of hot cured batch #1 is higher than the ultimate strain value predicted for the total shrinkage. This might change if this fit was done with a dataset that covered a longer duration of monitoring. If this anomaly is overlooked, there is a fair agreement between the two hot cured batches for both ε_{ult} and t_{50} values. This suggests that the total shrinkage for this type of hot-cured concrete is around 500$\mu\varepsilon$.

The fitted parameters helped identify trends in the shrinkage behavior. The major trends are:

- The parameters $\varepsilon(28)$, a and n are surprisingly similar for the total shrinkage of all four of the batches.
- In particular, the values of total shrinkage for the two hot cured batches were nearly identical.
- In each case t_{50}, the estimated time it takes to get to 50% of the ultimate shrinkage, for drying shrinkage was roughly half that for total shrinkage. The t_{50} does not vary much among the four batches. For the total shrinkage, t_{50} varied from 19 to 24 days. For drying shrinkage, it varied from 9 to 12 days.
- The total shrinkage predicted is considerably less for the ambient and weekend cured concretes than for the hot cured ones.

There were also some anomalies:

- The hot-cured batch #1 cylinder results are anomalous in several ways. First, the curves predict ε_{ult} values for which the total is less than the autogenous component alone, even though they also predict significant drying shrinkage. This is not rational. Second, the autogenous ε_{ult} value (494$\mu\varepsilon$) is much larger than any of the other three autogenous ε_{ult} values. The autogenous $1/n$ value, and the associated t_{50}, also differ markedly from the other three.
- If the hot-cured batch #1 results are disregarded, the total autogenous shrinkage appears to be about the same for all three curing regimes. This is surprising, because hot curing speeds up the

hydration reaction, as can be seen by the early strength gain. Autogenous shrinkage is by definition directly related to hydration, so the different curing regimes were expected to lead to different autogenous shrinkage results.

- ε_{ult} values for the two nominally identical hot cured batches differ by a lot for both autogenous and drying shrinkage. For the drying shrinkage, the value for the first batch is only 75% of the value for the second batch and for the autogenous shrinkage, the value for the second batch is only 60% of the value for the first batch.

- In all four cases the combined autogenous and drying shrinkages exceed the value predicted for the total shrinkage.

Experimental error is unlikely to be the cause of these anomalies, because both gages on each cylinder gave similar results. One possible explanation, at least for the ε_{ult} findings, is that, while the fitted curves provide an excellent fit for the three-month duration of the readings, they would not fit well if the readings were carried on for much longer.

There is also the possibility, despite the great care taken in sealing the sealed cylinders, that they could be slowly losing moisture. The concrete is exposed in small areas around where the gages were stuck to the cylinders and while those areas were sealed with silicone that might not provide a perfect seal.

CHAPTER 7 ANALYSIS OF CREEP DATA

This chapter discusses the creep strains that were measured in the unsealed and sealed cylinders. The procedure followed to convert the raw data into the processed creep data is described in Chapter 4.

7.1 Contributions of Basic Creep to Total Creep

Total creep strains are often divided into two categories: basic creep and drying creep. Basic creep is the creep that occurs in the absence of drying, and drying creep is the additional creep that occurs when the concrete is allowed to dry.

The ratio of the basic creep strain at 7 days (sealed cylinders) to the total creep strains (unsealed cylinders) are plotted in Figure 7.1 for all specimens with constant loading. If the sealing of the sealed cylinders in the experiment work sufficiently well to prevent moisture loss, it can be assumed that only basic creep occurred in those cylinders, and drying creep was negligible. It can therefore be helpful to calculate the measured basic creep as a ratio of the total creep measured in the unsealed cylinders
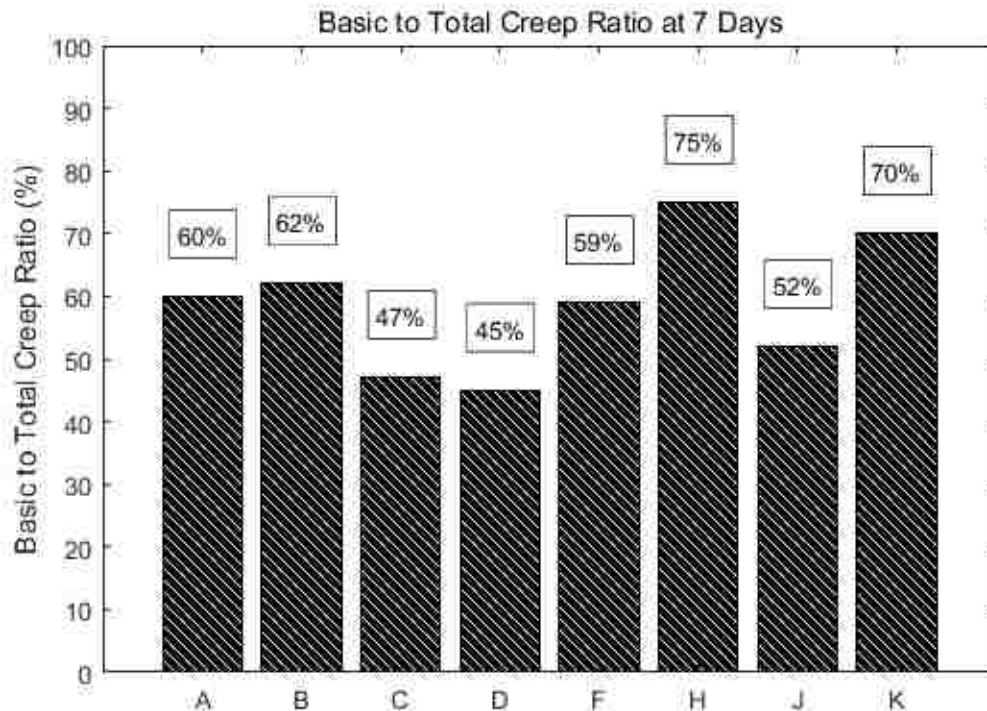
Figure 7.1 Contribution of Basic Creep at 7 Days

The ratios at 7 days ranged from 45-75%. As discussed before there is reason to believe that the sealed cylinder for Specimen H was not sealed properly and that might be skewing the results for that specimen. If H is excluded, the contribution of the basic creep ranged from 45-70%.

Figure 7.2 shows this ratio for all specimens with constant loading histories at 100 days after loading. For Specimen J, the ratio is shown for 79 days, because this specimen had not yet reached an age of 100 days at the time of writing.

For all specimens except for C, the contribution of the basic creep has increased from 7 days to 100 days. As discussed in Chapter 4, the measured basic creep strains for Specimen C are unreliable, because two of the three gages failed on the sealed creep cylinder. The measurement indicate that the drying creep happened mostly during early ages after loading, and as time passed, the basic creep became a larger proportion of the total creep. At 100 days the basic creep in the sealed cylinder of Specimen H has actually surpassed the total creep of the unsealed cylinder by 2%, which reinforces the notion that something was wrong with the sealing of that cylinder.
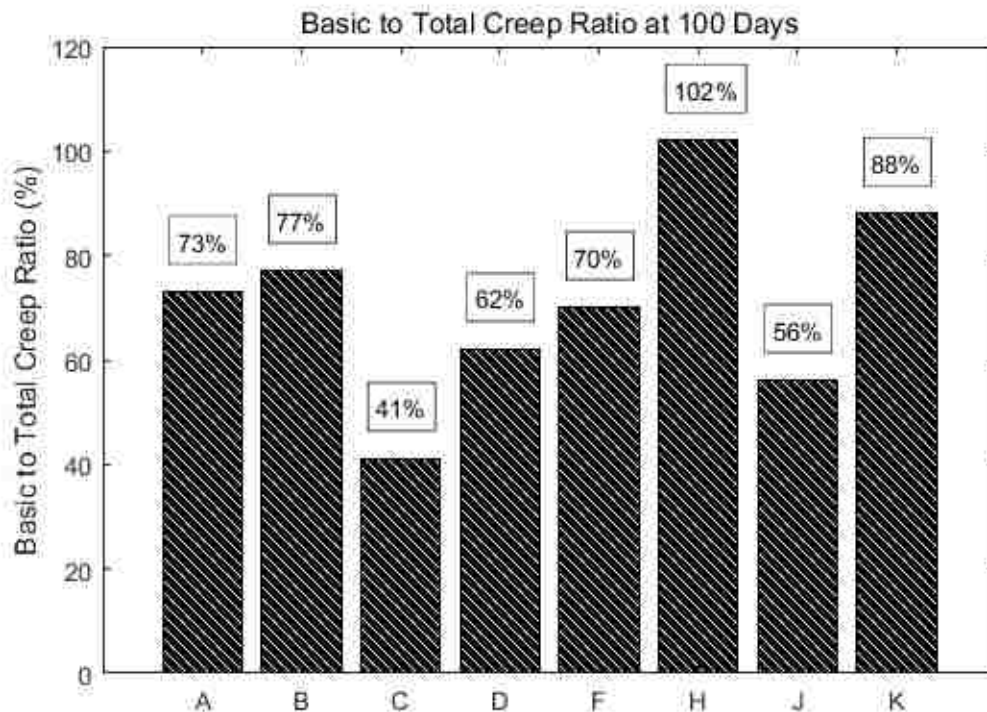
Figure 7.2 Contribution of Basic Creep at 100 Days

7.2 Effects of Curing

Three specimens with three different curing regimes (hot, weekend and ambient) were loaded at early ages and compared to evaluate the effect of curing on creep. All three of the specimens were loaded to a stress of 2.7 ksi. Specimen A (hot cured) was loaded at 0.7 days, Specimen B (weekend cured) was loaded at 2.8 days, and Specimen C (ambient cured) was loaded at 3.8 days. Figure 7.3 shows total creep strain data for the three specimens.
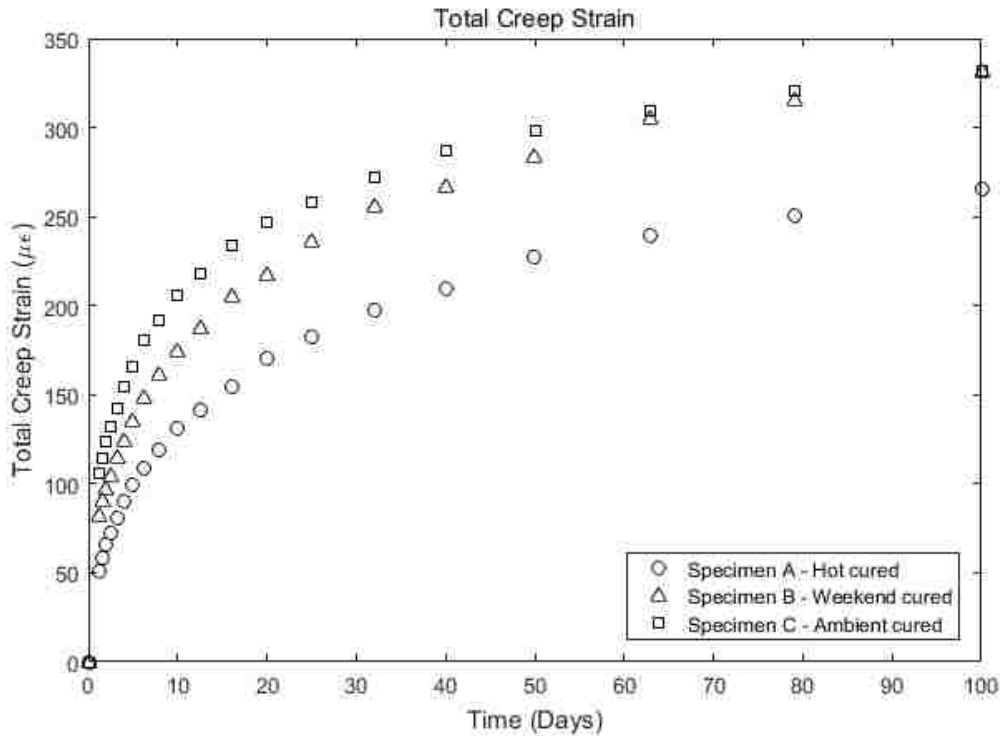
Figure 7.3 Effect of Curing Regimes on Total Creep Strain

At 100 days, the weekend- and ambient-cured specimen had crept by approximately the same amount, but at early ages the ambient-cured specimen creeps a little more than the weekend-cured one. For the entire 100-day period, the total creep of the hot-cured concrete were less than the total creep of the other two specimens.

To account for differences in concrete strength, the total creep strains were normalized by the initial elastic strain to produce curves of the creep coefficient. Figure 7.4 shows creep coefficients for the unsealed cylinders for the three specimens.
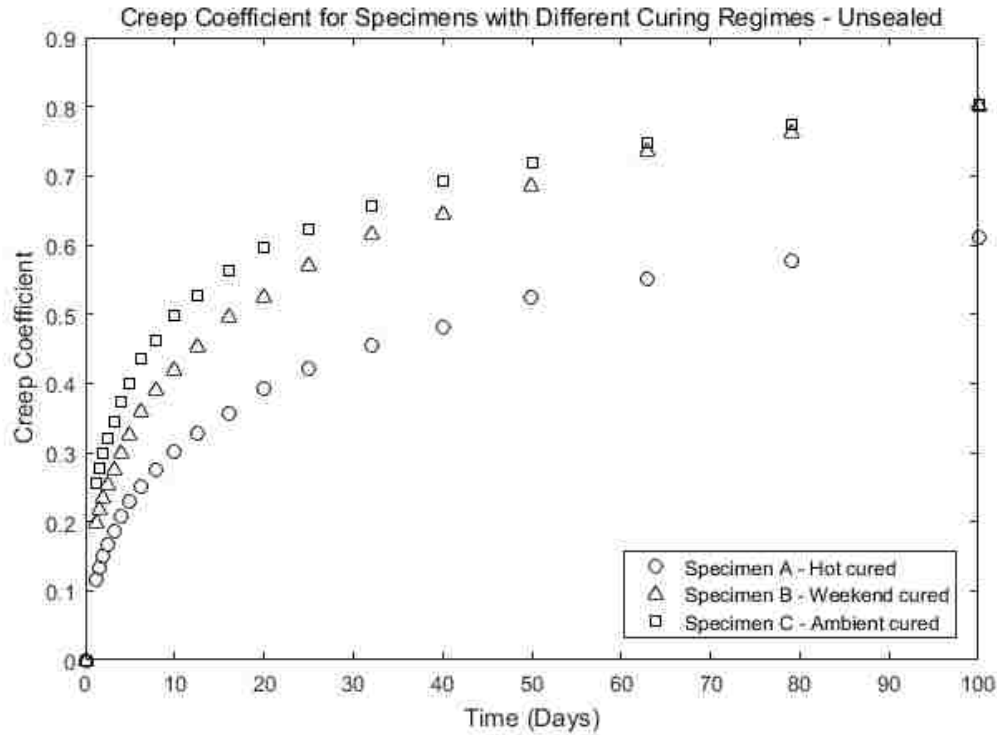
Figure 7.4 Creep Coefficient for Specimens with Different Curing Regimes - Unsealed

The creep coefficient tells almost exactly the same story as the absolute creep strain values do. At 100 days the creep coefficient was approximately equal for the weekend- and the ambient-cured concrete at 0.8 and the creep coefficient for the hot-cured concrete is considerably lower at 0.6.

Figure 7.5 shows basic creep strain data for the three specimens. Data from the sealed cylinder of Specimen C cannot tell us anything reliably, since two out of the three gages on that cylinder failed, but it is shown for the sake of completeness. The same information is shown in Figure 7.6 in terms of the creep coefficient.
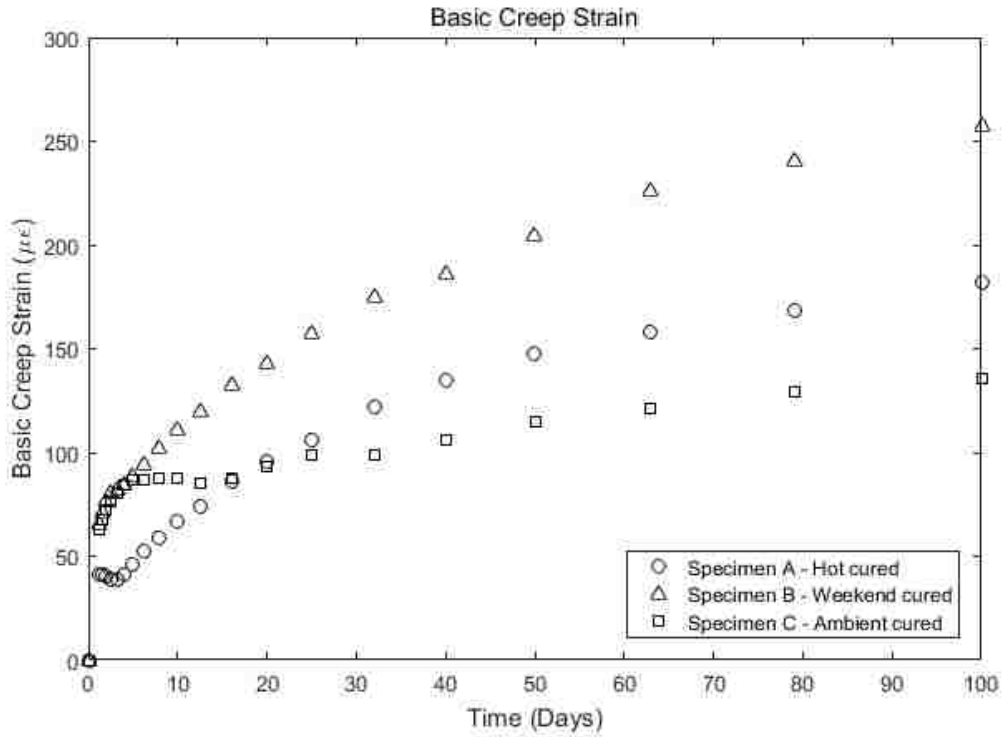
Figure 7.5 Effect of Curing Regimes on Basic Creep Strain

Before the gage failure occurred in Specimen C the basic strains for the weekend-cured and ambient-cured concretes seem to be almost identical. Similar to what was observed for the total strain, the basic strain of the hot-cured specimen is considerably lower than that of the other two specimen for the entire 100-day period.
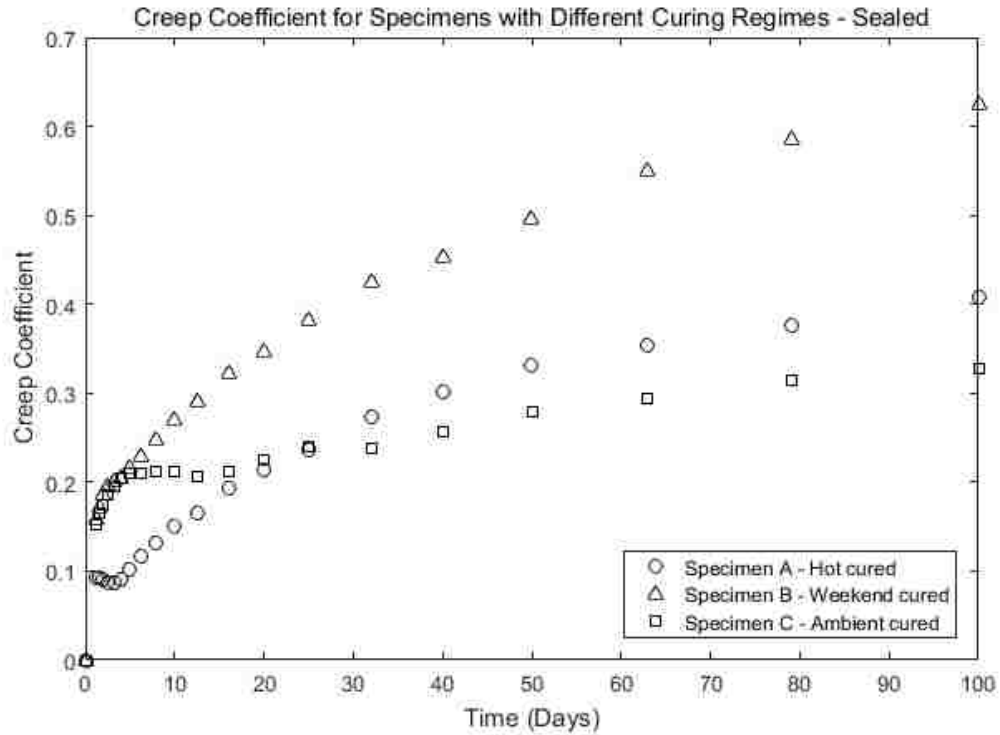
Figure 7.6 Creep Coefficient for Specimens with Different Curing Regimes - Sealed

As with the unsealed cylinders the creep coefficient tells the same story as the absolute creep strain values.

Figure 7.7 shows drying creep strain data for the three specimens. Again, data from Specimen C was compromised by gage failures in the sealed cylinders. The drying creep strains for the weekend- and hot-cured specimens are almost identical for the entire 100-day period.
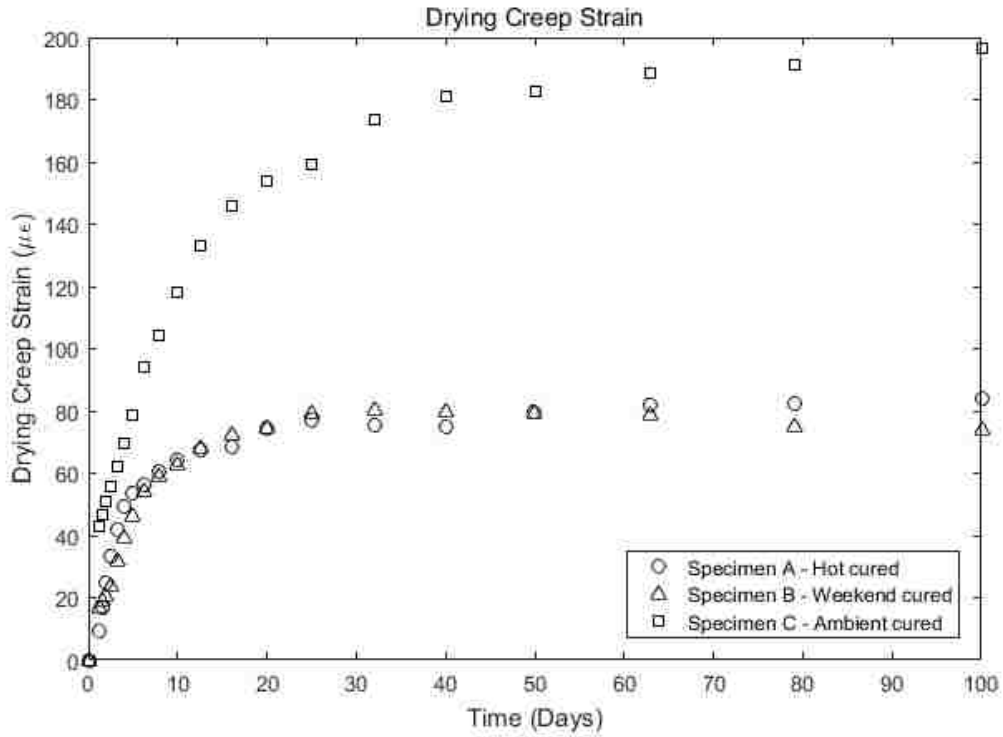
Figure 7.7 Effect of Curing Regimes on Drying Creep Strain

7.3   Effects of Time of Loading

Figure 7.8 shows total creep strains versus time since loading from the unsealed cylinders of specimen A, D, F, H and J, which were loaded at 0.7, 3.8, 7.8, 12.7 and 57.7 days, respectively.
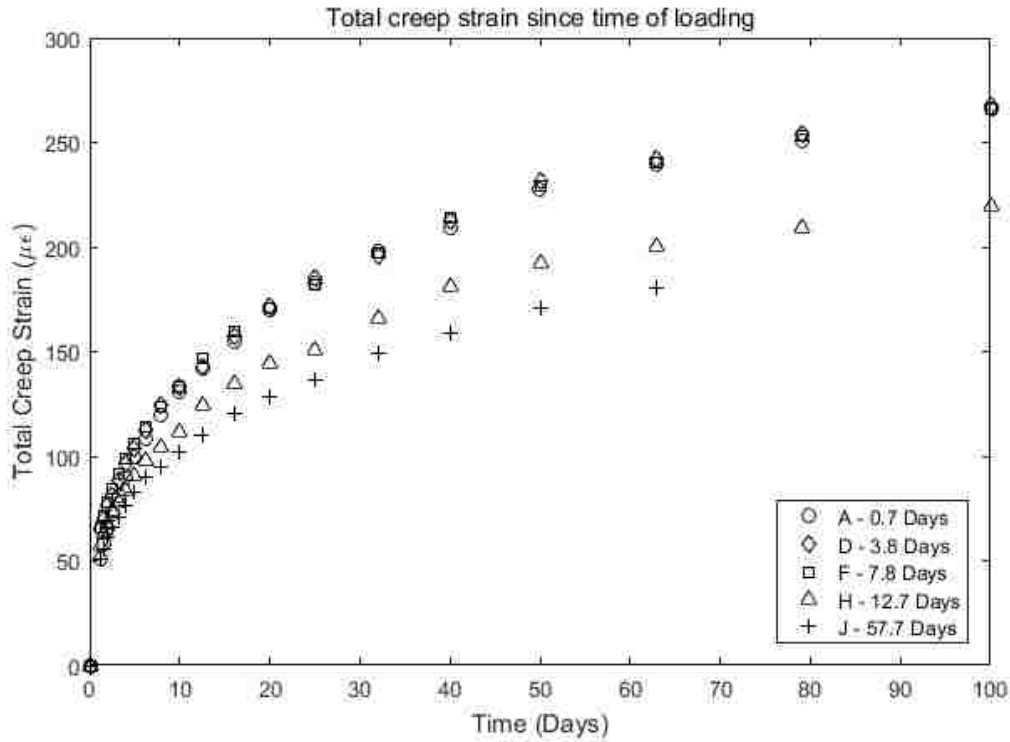
Figure 7.8 Effect of Time of Loading on Total Creep Strain

Specimen A, D and F seem to yield identical results with regard to creep. This result is surprising, because it suggests that the age of loading does not influence creep for the first week after the concrete is cast. This is contrary to predictions made by most models in use today. The age of loading does seem to have an effect on the creep for loading ages higher than 7 days as specimen H loaded at 12.8 days creeps less than A, D and F and specimen J loaded at 57.7 days creeps even less than specimen H.

To account for the increase in concrete strength, Figure 7.9 shows the same data in terms of the creep coefficient.
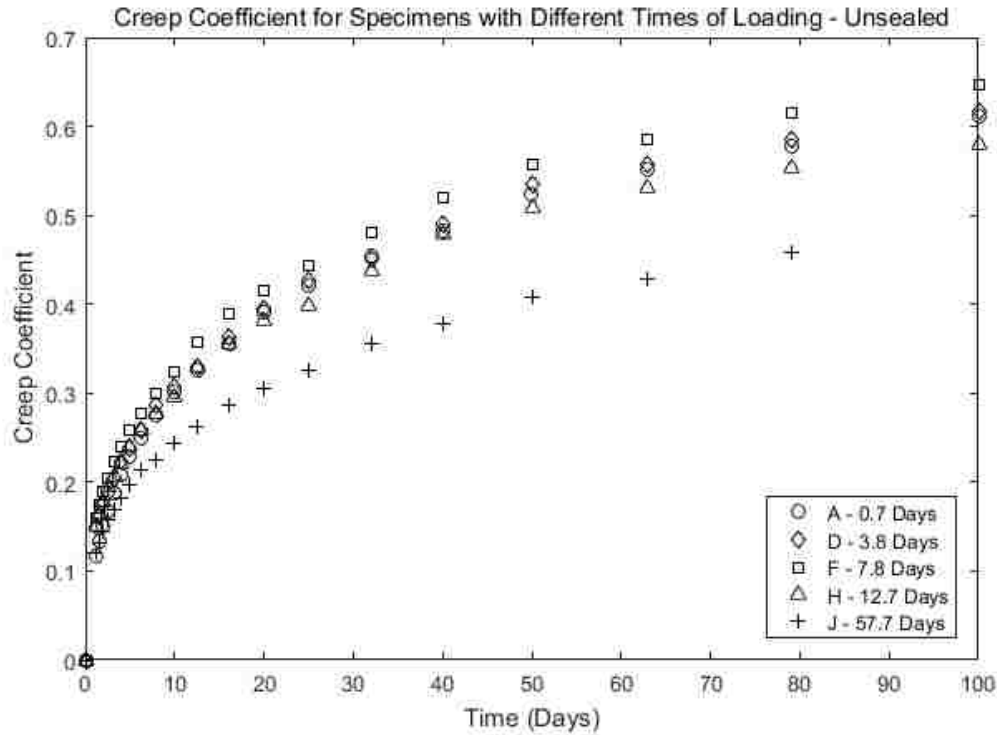
Figure 7.9 Creep Coefficient for Specimens with Different Times of Loading - Unsealed

At 100 days the creep coefficients for specimens A and D are approximately the same (just over 0.6), but the creep coefficient of Specimen F was surprisingly slightly higher. The creep coefficient for Specimen H is, as was the case with the absolute creep strain, slightly lower than A, D and F, and the creep coefficient for Specimen J is considerably lower than the other four at 80 days.

Figure 7.10 shows basic creep strains versus time since loading from the sealed cylinders of specimen A, D, F, H, and J. Because so many gages on the sealed cylinders failed after a certain amount of time, not much meaning can be derived from Figure 7.10.
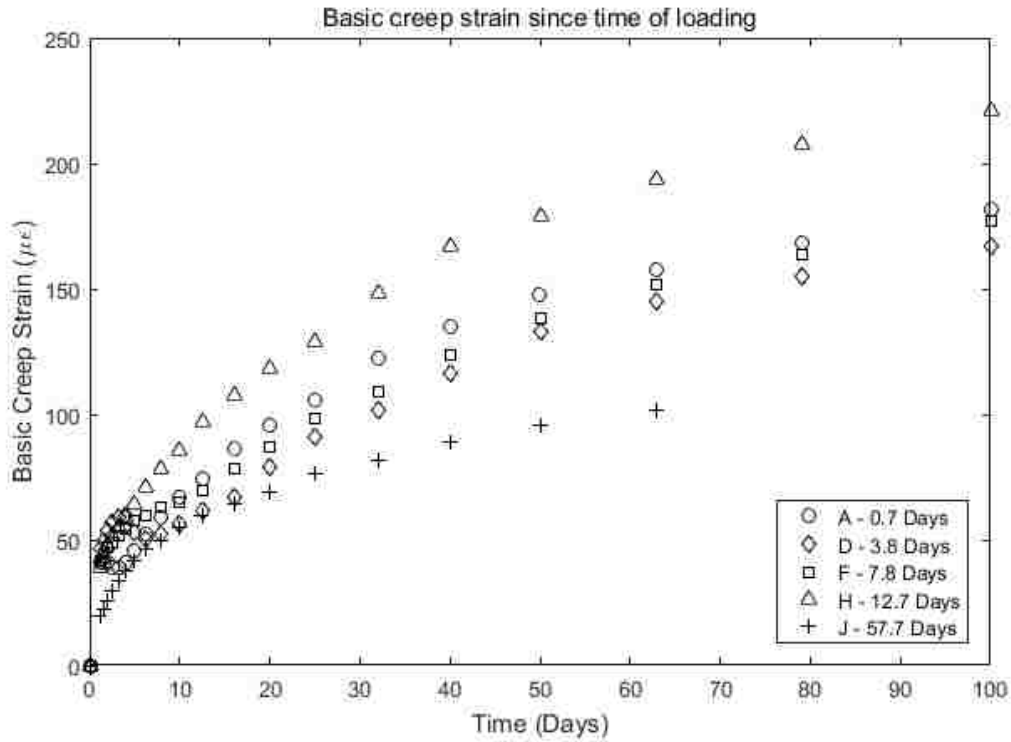
Figure 7.10 Effect of Time of Loading on Basic Creep Strain

To account for the increase in concrete strength, Figure 7.11 shows the same data in terms of the creep coefficient. Because so many gages on the sealed cylinders failed after a certain amount of time, not much meaning can be derived from Figure 7.11.
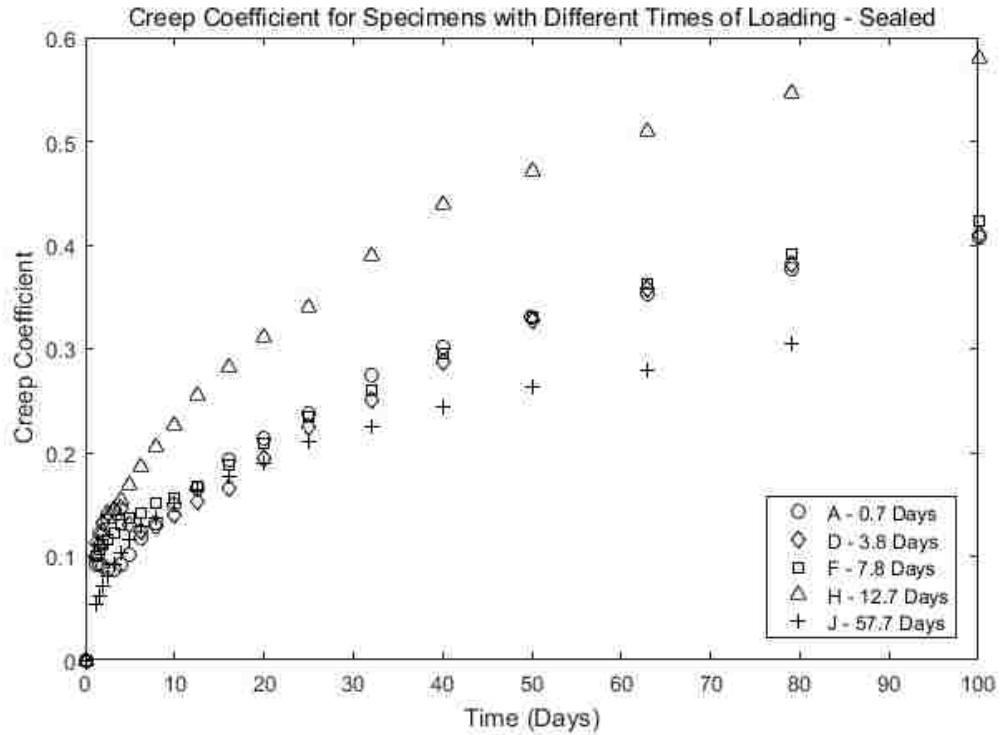
Figure 7.11 Creep Coefficient for Specimens with Different Times of Loading - Sealed

Figure 7.12 shows drying creep strains versus time since loading from the sealed cylinders of specimen A, D, F, H, and J. Since these data were obtained by subtracting the basic creep strains from the total creep strains not much meaning can be derived from Figure 7.12 due to the malfunctioning gages in many of the sealed cylinders.
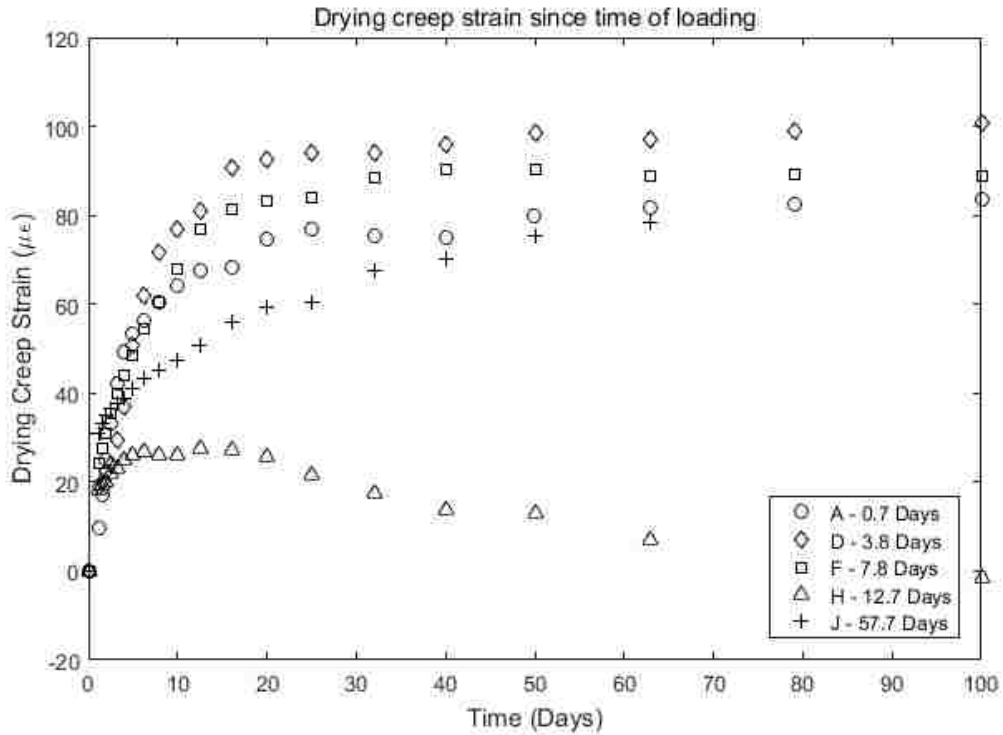
Figure 7.12 Effect of Times of Loading on Drying Creep Strain

7.4 Residual Creep

Since three of the specimens were unloaded at various times, it was possible to evaluate the proportion of creep strains that were recoverable upon unloading. Figure 7.13 shows a comparison between strains for the unsealed and sealed cylinders of Specimen E loaded at 0.7 days and unloaded at 3.8 days. The unsealed cylinder creep considerably more than the sealed one in the time between the loading and the unloading but then seems to recover less of the creep after the unloading than the sealed cylinder.
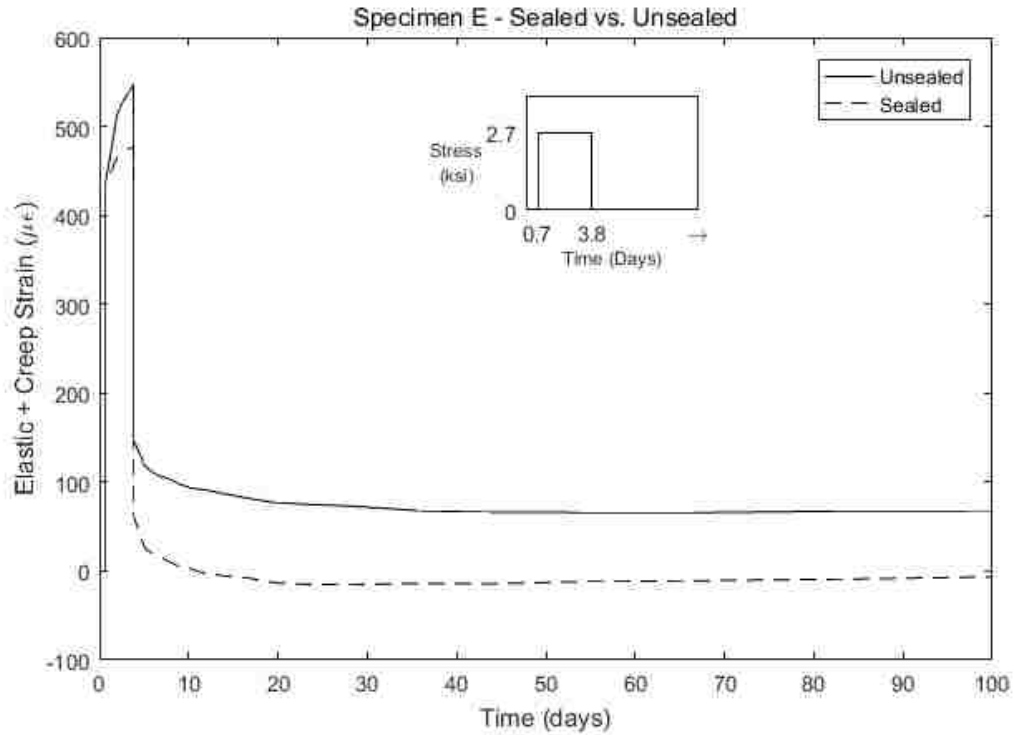
Figure 7.13 Residual Creep in Specimen E

Figure 7.14 compares strains for the unsealed and the sealed cylinders for Specimen G, which was loaded at 0.7 days and unloaded at 7.8 days. A gage failure in the sealed cylinder shortly after loading tarnishes these results, but again, there are signs of more creep recovery in the sealed cylinder than the unsealed one.
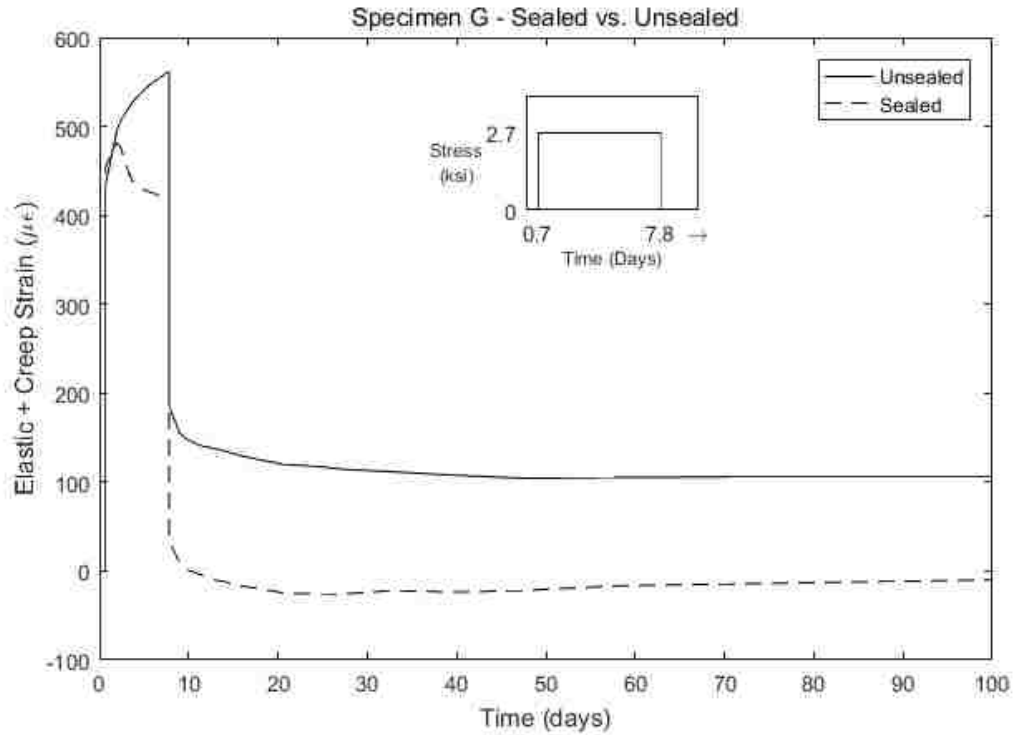
Figure 7.14 Residual Creep in Specimen G

Figure 7.15 compares the strains for the unsealed and the sealed cylinder for Specimen I loaded at 0.8 days, unloaded to 2/3 of the original value at 3.8 days, unloaded to 1/3 of the original value at 7.8 days and unloaded completely at 14.8 days. Again, the sealed cylinder seems to have recovered almost all of its creep, whereas the unsealed cylinder did not.
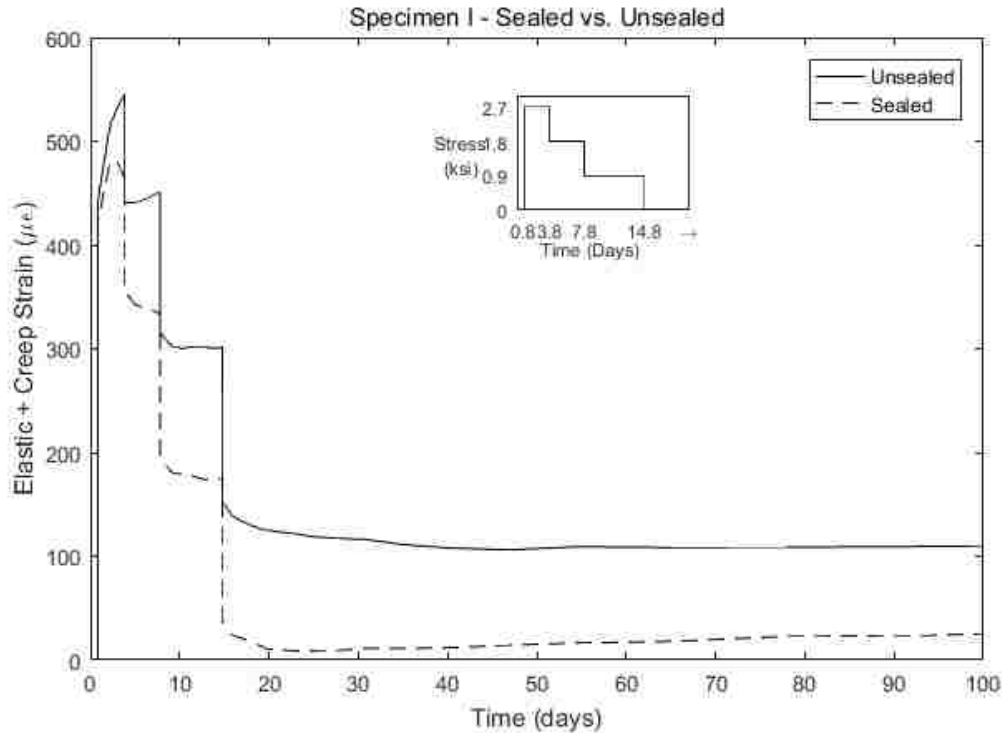
Figure 7.15 Residual Creep in Specimen I

In all three cases, the creep in the sealed cylinders was completely recovered shortly after unloading whereas there was substantial residual creep in the unsealed cylinders. This suggests that basic creep is recoverable when the concrete is unloaded, but drying creep is not fully recoverable.

7.5   Parametrization of Creep Data

Processed data for the basic, drying and total creeps from all 11 specimens was fitted with the same time-dependent curve that was used for shrinkage in Chapter 6. Plots of the data along with the curve fits can be found in Appendix C for each of the specimens.

Table 7.1 shows the parameters yielded by doing a least-squares fit to the data for the 8 specimens subjected to a constant load.

Table 7.1 Curve Fit Parameters for Drying, Basic and Total Creep

	Total Creep			Basic Creep			Drying Creep		
	$\varepsilon(28)$	a	n	$\varepsilon(28)$	a	n	$\varepsilon(28)$	a	n
A	189	2.30	0.56	124	858.69	0.37	76	1.04	1.49
B	242	2.45	0.49	163	267962.35	0.35	76	1.05	1.50
C	265	1.76	0.50	105	1.72	0.33	165	1.35	0.89
D	190	3.18	0.45	70	190.15	0.58	95	1.07	1.53
F	187	1.72	1.09	116	14725.85	0.35	85	1.13	1.06
H	159	3.02	0.43	141	8.02	0.46	19	1.00	1.34
J	143	4.08	0.40	79	2.33	0.57	64	3.85	0.32
K	337	2.45	0.56	270	281.43	0.38	57	1.00	5.86

- The least squares fit converged to a solution in all cases

- The parameter a represents the ratio between the strain at infinite time and the strain at 28 days. For the specimens subjected to constant loads, the values of this parameter for total creep ranged from 1.72 to 4.08.

- The values of a varied much more for basic creep. After 100 days, the strains measured in the sealed cylinders were still increasing, so it is difficult to estimate the ultimate shrinkage. The large a values are explained by the fact that the time window for the dataset is not sufficiently long enough to converge to plausible solution.

- For total creep, the value of n was approximately equal to 0.5 for all specimens, except Specimen F. For basic creep, the value of n ranged from 0.33 to 0.58.

- The parameters see randomly scattered across curing regimes, times of loading and stress histories. No major trends can be derived from these results.

Table 7.2 shows the predicted ultimate strain and t_{50} values for the 8 specimens subjected to constant load.

Table 7.2 Predicted Ultimate Strain and t_{50} Values for Drying, Basic and Total Creep

	Total Creep		Basic Creep		Drying Creep		Basic + Drying
	ε_{ult}	t_{50} (days)	ε_{ult}	t_{50} (days)	ε_{ult}	t_{50} (days)	ε_{ult}
A	435	45	104334	2.2E09	80	3	104414
B	594	60	3.8E06	8.2E16	80	4	3.8E06
C	466	16	181	10	222	8	403
D	604	158	13218	252041	101	5	13319
F	322	21	1.1E06	2.1E13	96	4	1.1E06
H	481	141	1129	2018	19	0	1148
J	583	475	185	46	247	763	432
K	827	55	75489	8.6E07	57	3	75546

- Specimen A, B, C, D, F, H and J which were all loaded to 2700 psi, all have ultimate total creep ranging from 300-600$\mu\varepsilon$ with no apparent trend even though they have different curing regimes, time of loading etc.

- Specimen K which was loaded to 4500 psi, has ultimate total creep of 827$\mu\varepsilon$.

- Many of the ultimate strains and t_{50} values predicted for the basic creep seem implausible, most likely because of the short time of monitoring.

- All monotonic specimens, excluding J, had t_{50} values of less than 10 days for drying creep. This suggests that most of the drying creep occurred early after loading.

Table 7.3 shows the parameters yielded by doing a least squares fit to the data for the 3 specimens subjected to variable loading. One fit was produced for data following each stress change.

Table 7.3 Curve Fit Parameters for Drying, Basic and Total Creep – Variable Loading

	Total Creep			Basic Creep			Drying Creep		
	$\varepsilon(28)$	a	n	$\varepsilon(28)$	a	n	$\varepsilon(28)$	a	n
E1	309	369.41	0.47	111	369.53	0.46	195	369.47	0.49
E2	-75	1.19	0.81	-71	1.05	1.11	-2	71.36	1.70
G1	171	1.24	0.76	N/A	N/A	N/A	178	1.01	2.13
G2	-73	1.23	0.72	-53	1.01	1.50	-18	2.48	1.39
I1	180	1.18	0.80	67	16076.94	0.28	3761	7.58	1.92
I2	138	1.13	2.38	-47	8.31	0.46	131	3.29	0.88
I3	-14	1.00	2.91	-20	1.02	1.13	28	5.30	1.37
I4	-41	1.14	0.94	-21	1.00	2.38	-20	1.85	1.51

- The least squares fit converged to a solution in all cases, except for the basic creep of Specimen G before unloading (G1). This lack of convergence is likely caused by a combination of the dataset time window being very short, only 7 days, and more importantly, a malfunction in that time period in one of the gages on the sealed cylinder for that specimen.

- The fits for E2, G2 and I2-4 all represent unloadings which explains the negative $\varepsilon(28)$ values. The I2 value is positive because even though the stress was reduced it was still sufficient so that the specimen kept creeping instead of recovering creep.

- The parameter a represents the ratio between the strain at infinite time and the strain at 28 days. The values of a were near 1.1 for all specimens except E1, which had an implausible value of 369. The exception for Specimen E before unloading (E1) is likely caused by the fact that those data points only cover about 4 days and the slope does not change sufficiently in that time for the fit to converge to a sensible solution.

Table 7.4 shows the predicted ultimate strain and t_{50} values for the three specimens that had variable load.

Table 7.4 Predicted Ultimate Strain and t_{50} Values for Drying, Basic and Total Creep – Variable Loading

	Total Creep		Basic Creep		Drying Creep		Basic + Drying
	ε_{ult}	t_{50} (days)	ε_{ult}	t_{50} (days)	ε_{ult}	t_{50} (days)	ε_{ult}
E1	114254	8.4E06	41090	9.5E06	72105	4.8E06	113195
E2	-89	4	-75	2	-127	340	-202
G1	212	4	N/A	N/A	179	3	N/A
G2	-90	4	-54	2	-45	37	-99
I1	212	3	169840	4.1E16	28527	75	198367
I2	156	12	-389	2176	430	72	41
I3	-14	1	-21	1	150	81	129
I4	-47	3	-21	1	-37	25	-58

- Specimen E1 and I1 yield largely implausible results as they were only loaded for 3 days which is not a sufficiently long time period to yield useful results.
- In all cases of complete removal of load (E2, G2 and I4) the t_{50} value is 3-4 days. This suggests that most of the creep recovery happens a few days after the load is removed.

CHAPTER 8 SUPERPOSITION OF CREEP MEASUREMENTS

Nearly all of the creep data available for concrete available in the literature was derived from tests in which the load was constant. ACI 208 suggests that more complex load histories can be analyzed by superimposing the effects of each load increment. (ACI Committee 209, 2008). The test plan, with its various times of loading and unloading and different loading values, was in large part designed to test the validity of the principle of superposition for the concrete used in this project.

The validity of superposition can be investigated through the use of data from the loaded and unloaded specimens. If two specimens are loaded at time t_1, and at time t_2 one of them is partially or completely unloaded and a third is loaded, the difference between the two continuously loaded specimens should give the same result as the one that is loaded at time t_1 and then unloaded at time t_2, if superposition is valid.

8.1 Effect of Load Level

If superposition is applicable, the effects of loading need to be proportional to the level of loading. To test this hypothesis, Specimen A was loaded at 0.7 days to 2.7 ksi, and specimen K was loaded at the same time to a stress of 4.5 ksi. If superposition is valid, creep strains observed in Specimen A should be $2.7/4.5 = 60\%$ of the creep strains observed in specimen K.

Figure 8.1 shows elastic and creep strain versus time after loading for the unsealed cylinders of specimen A and specimen K multiplied by a factor of 0.6. The stress histories for those specimens are also shown within Figure 8.1. There is a slight difference between the two curves, but at 100 days, the two strains differ by only 8.1%.

Figure 8.2 shows the ratio between the measured strains for specimens A and K with time. The ratio is nearly constant, with an average value is 0.555 which is 92.5% of the expected value of 0.6.
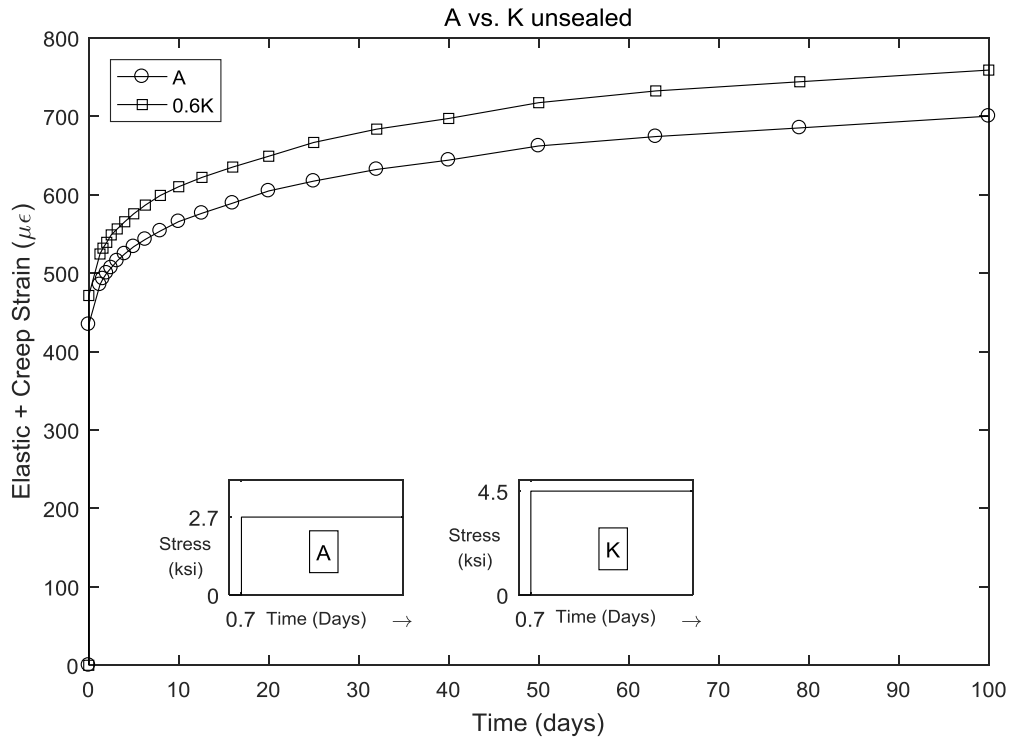
Figure 8.1 Comparison between Specimens A and K - Unsealed
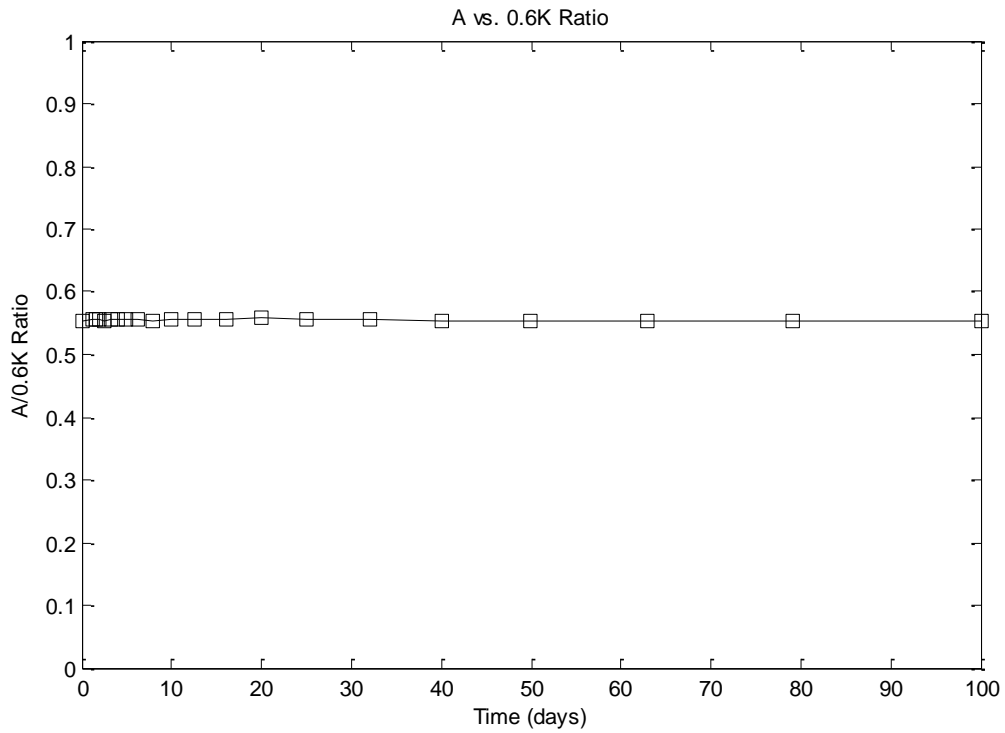
Figure 8.2 Ratio between Creep Strains for Specimens A and K - Unsealed

Similarly, Figure 8.3 shows elastic and creep strains versus time after loading for the sealed cylinders of specimen A and specimen K multiplied by 0.6. Again, there is a slight difference between the two. Figure 8.4 shows the ratio between A and K with time. If the anomalous skip in the early data, presumably due to a gage fault, is ignored, the ratio is again reasonably stable and the average value is 0.535 which is 89.2% of the expected value of 0.6.

Figure 8.3 Comparison between Basic Creep Strains for Specimens A and K – Sealed
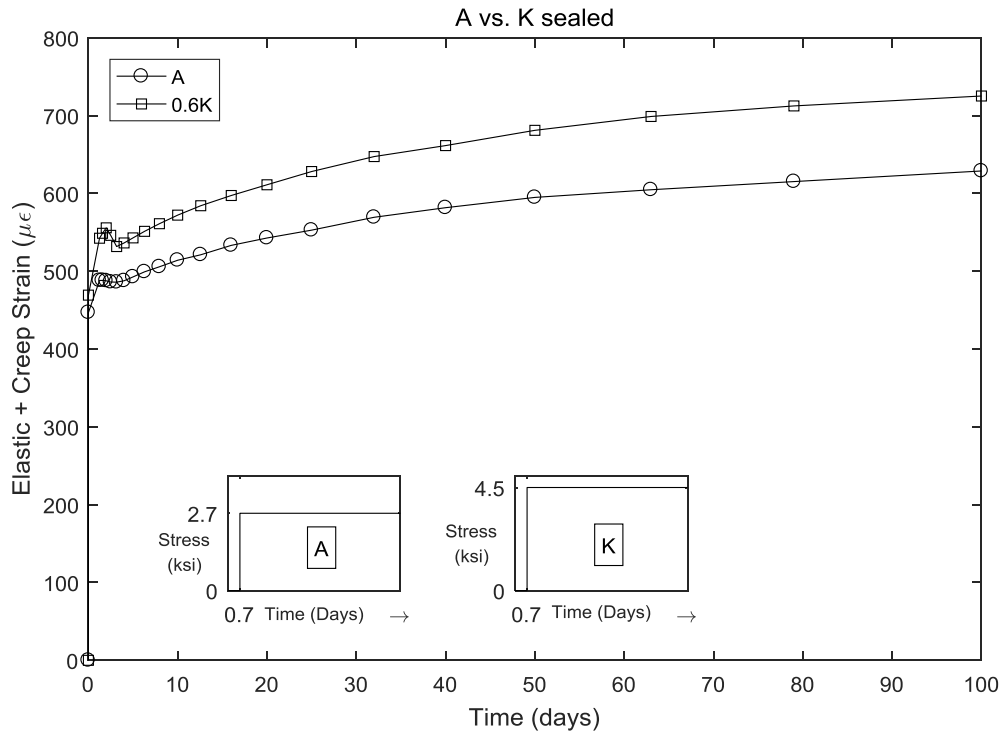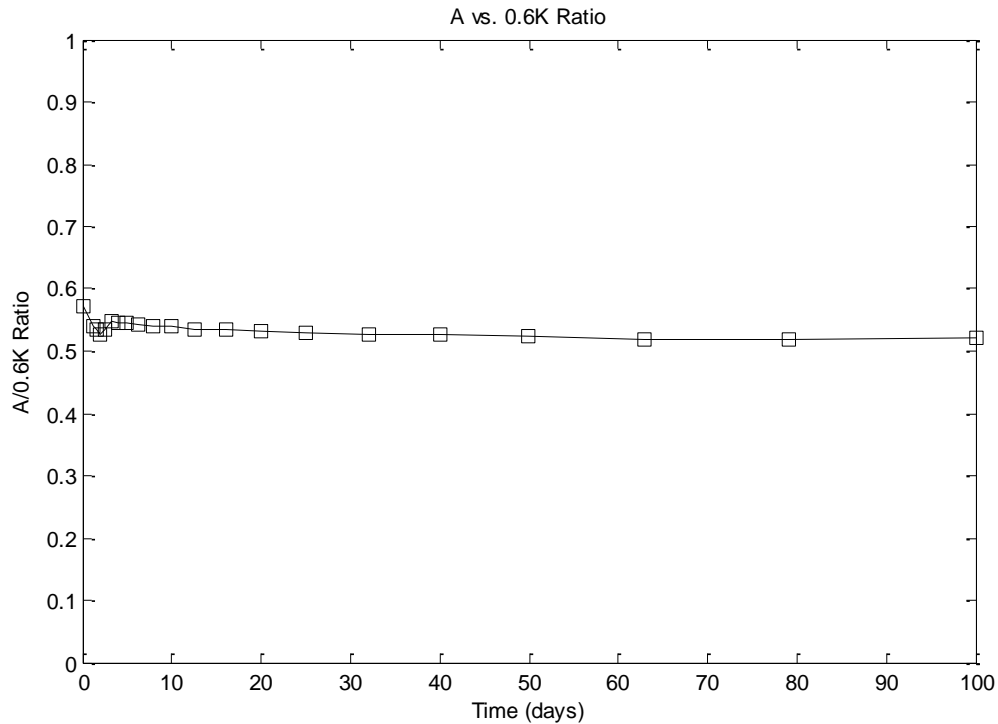
Figure 8.4 Ratio between Specimens A and K - Sealed

Both the sealed and the unsealed cylinders yield results close to expectations. However they both had slightly greater strain values for 0.6K than expected. The implication is that, at the higher stress (4.5 ksi on Specimen K) creep strain is a slightly non-linear function of stress. At the time of loading, the strength of the concrete was around 10,000 psi, so specimen K was loaded to 45% of its strength. This is just over the normally accepted limit for linear behavior, which is 40% of the strength of the concrete. (Wight 2016).

8.2   Load Superposition for Loading/Unloading at 3.8 Days

Specimens A and E were both loaded to a stress of 2.7 ksi at 0.7 days, and E was later unloaded at 3.8 days, whereas specimen D was loaded for the first time to a stress of 2.7 ksi at 3.8 days. The stress histories for those specimens are shown within Figure 8.5.

Figure 8.5 compares the differences between measured elastic and creep strains for the unsealed cylinders for A-D and E. Similarly, Figure 8.6 shows the comparison for the creep strains after each loading/unloading. The creep strains were obtained by subtracting subsequent strain values from elastic strain values from each loading/unloading event. The elastic strain values from the loading were subtracted from the strain values available in between the loading and the unloading to obtain the first

79

part of the curve and the elastic strain values from the unloading were subtracted from the strain values available after the unloading to obtain the second part of the curve.

The two creep curves look similar. There is an unexplained higher early creep in specimen E than in specimen A, A and E were loaded to the same level at the same age so they are expected to yield identical strains. However, this difference is irrelevant to the issue of superposition, since Specimen D was not loaded until 3.8 days. The creep recovery curves look similar but there is a faster "recovery" in the A-D curve which might suggest that stress history plays a role in creep and creep recovery.

Figure 8.7 compares the elastic strain values for the two curves for each stress change event. The percentage on top of each group of bars indicates the relative difference between the two values. If superposition was perfectly valid and perfect data could be obtained these values would in all cases be identical. The elastic values for the initial loading of specimens A and E are within 1% of each other, and the values for the unloading which really are the elastic strain for the initial loading of Specimen D and the elastic strain for the unloading of Specimen E are within 10% of each other.

Figure 8.5 Superposition Comparison A-D = E – Unsealed

Figure 8.6 Superposition Comparison A-D = E – Unsealed – Creep Strains

Figure 8.7 Superposition Comparison A-D = E – Unsealed – Elastic Strains

Figure 8.8 compares the elastic and creep strains between the sealed cylinders for A-D and E. Figure 8.9 shows the comparison for the creep strains after each loading/unloading. These results are greatly affected by a gage failure in specimen D, which happened about 3 days after loading. The initial creep before the unloading is fairly similar for the two curves and before the gage failure the more rapid "recovery" in the A-D curve is again observed.

Figure 8.10 compares the elastic strain values for the two curves for each stress change event. The elastic values for both the loading and the unloading are within 3% of each other.
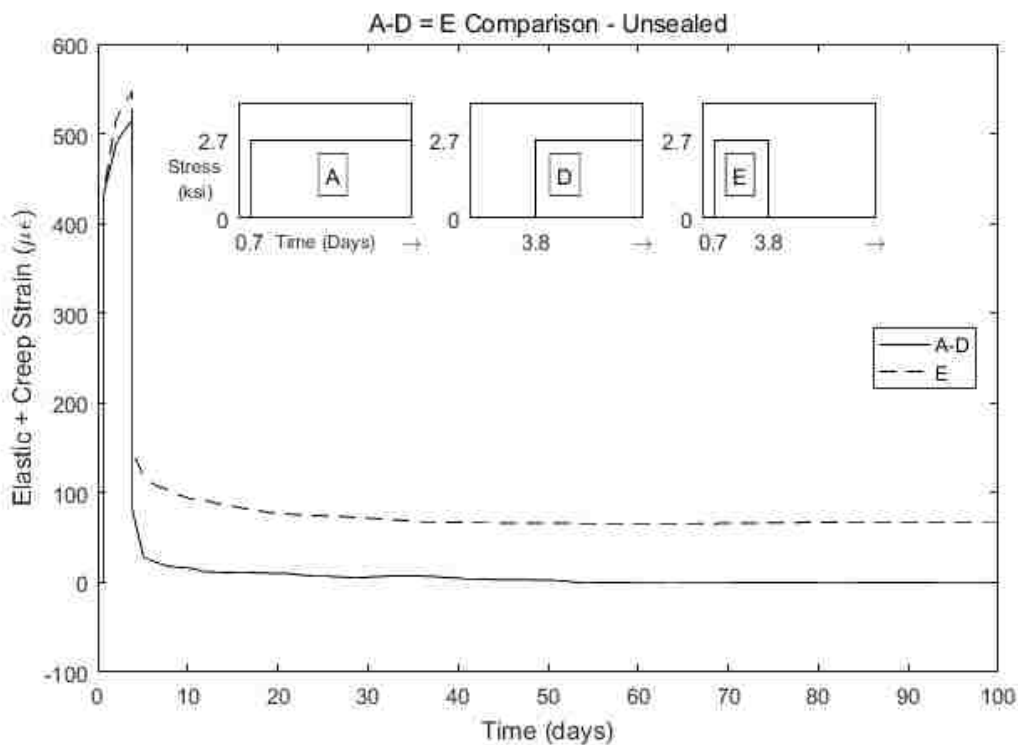
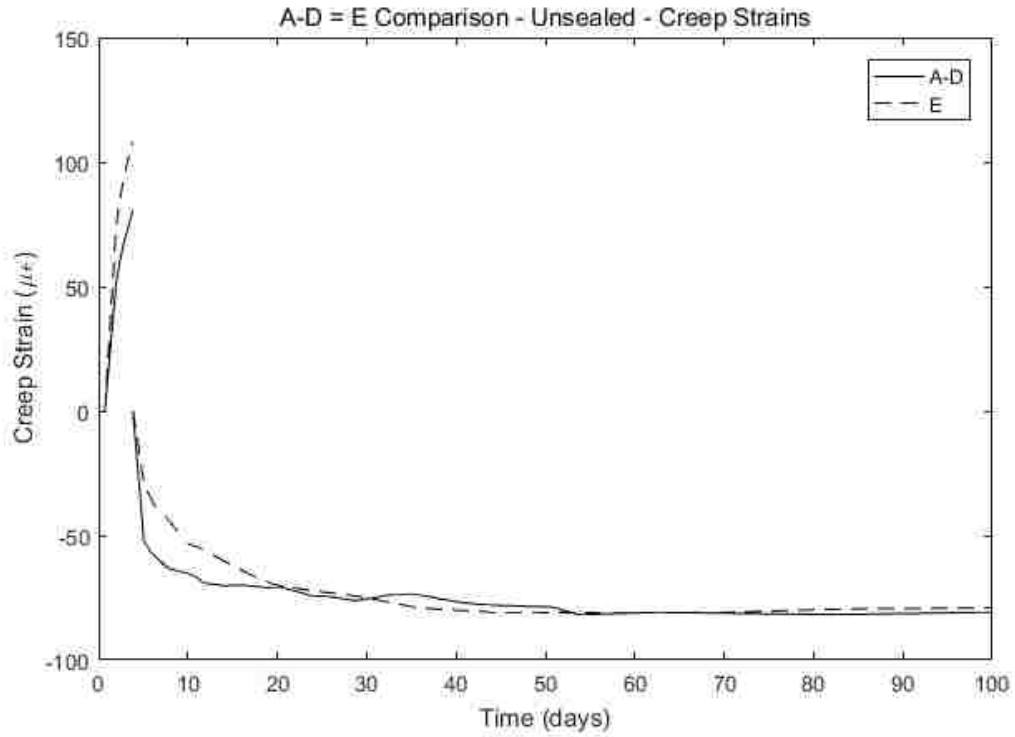

Figure 8.8 Superposition Comparison A-D = E – Sealed

Figure 8.9 Superposition Comparison A-D = E – Sealed – Creep Strains

Figure 8.10 Superposition Comparison A-D = E – Sealed – Elastic Strains

8.3   Load Superposition for Loading/Unloading at 7.8 Days

The second case of this type of comparison involves specimen A and G which were both loaded at 0.7 days and G was later unloaded at 7.8 days while specimen F was loaded at 7.8 days. The stress histories for those specimens are shown within Figure 8.11. Figure 8.11 compares the unsealed cylinders elastic and creep strains for A-F and G. Figure 8.12 shows the comparison for the creep strains after each loading/unloading. This comparison seems to yield similar results as the one before, a slight difference in early creep between A and G and then a bit more early creep „recovery" from A-F than from G.

Figure 8.13 compares the elastic strain values for the two curves for each stress change event. The percentage on top of each group of bars indicates the relative difference between the two values. If superposition was perfectly valid and perfect data could be obtained, these values would in all cases be identical. These results are similar to those found for superposition for loading at 3.8 days (A-D = E), the initial loading elastic strains are within 1% of each other and the unloading elastic strains are within 10% of each other.

Figure 8.11 Superposition Comparison A-F = G – Unsealed

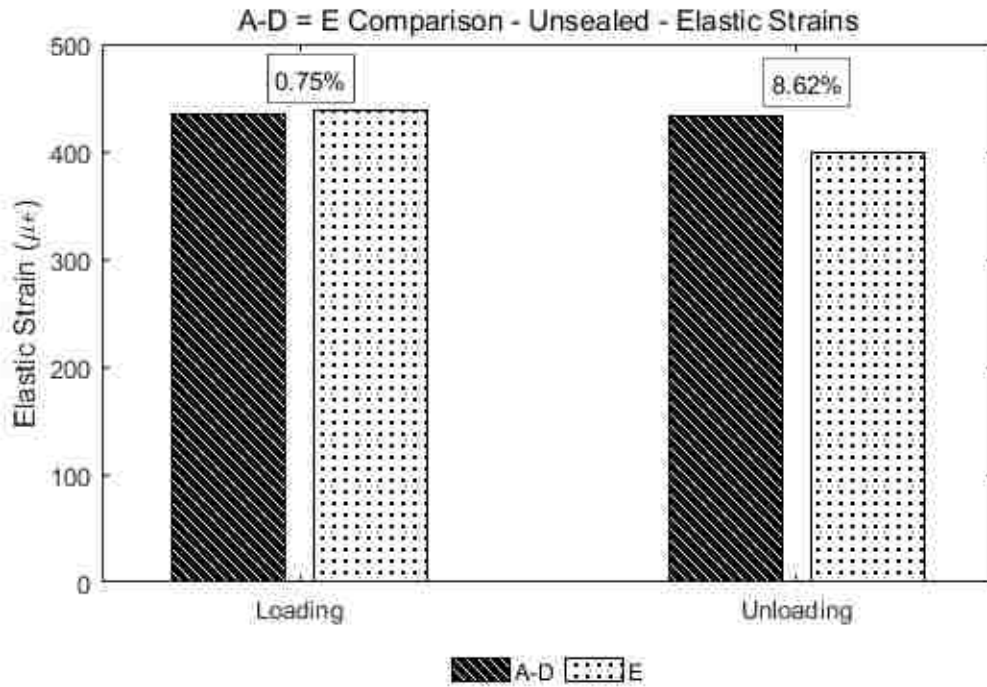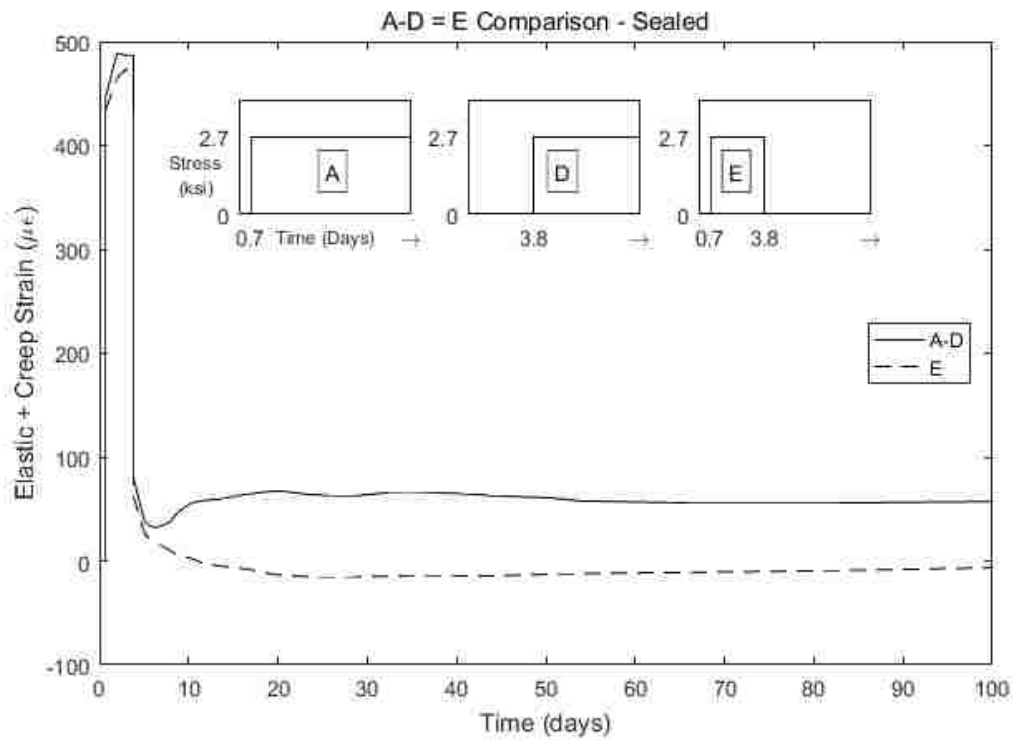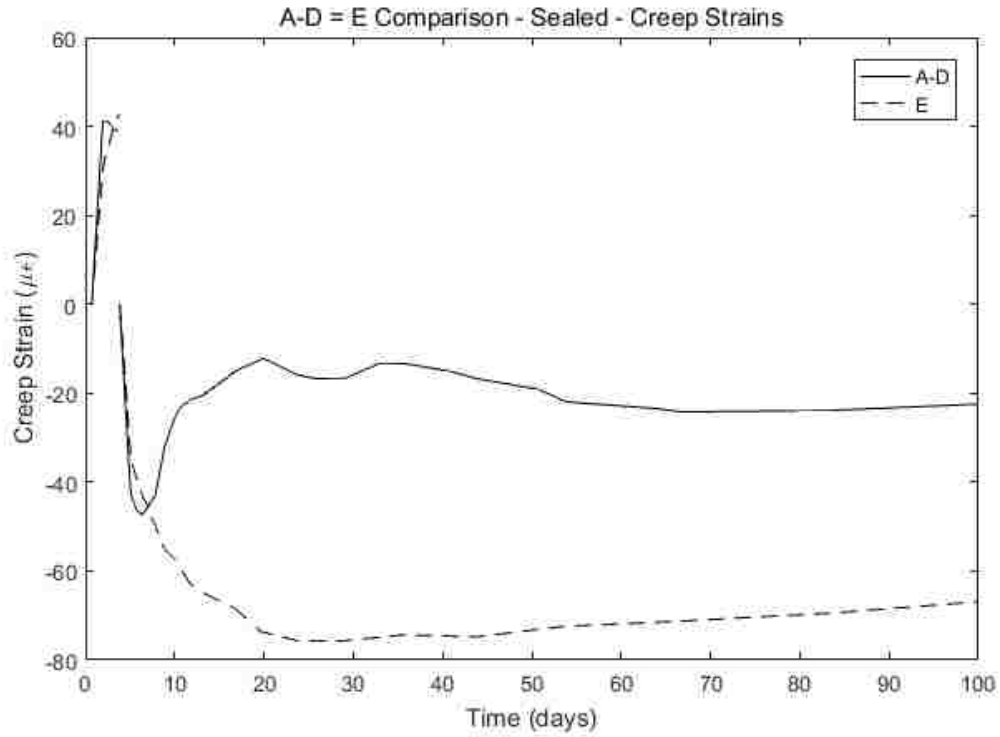**Figure 8.12 Superposition Comparison A-F = G – Unsealed – Creep Strains**

Figure 8.13 Superposition Comparison A-F = G – Unsealed – Elastic Strains

85

Figure 8.14 shows the comparison between the sealed cylinders for A-F and G and Figure 8.15 shows the comparison for the creep strains after each loading/unloading. Again, gage failures, especially those between 1 and 7 days, prevent meaningful interpretation of these results. There is however a hint of the previously observed quicker recovery of strains for A-F than for G.

Figure 8.16 shows the comparison between elastic strain values for the two curves for each stress change event. The percentage on top of each group of bars indicates the relative difference between the two values. If superposition was perfectly valid and perfect data could be obtained these values would in all cases be identical. Again, a similar result as seen before is observed. The elastic strains from the initial loading are within 2% of each other and the unloading elastic strains are within 10% of each other.

Figure 8.14 Superposition Comparison A-F = G – Sealed

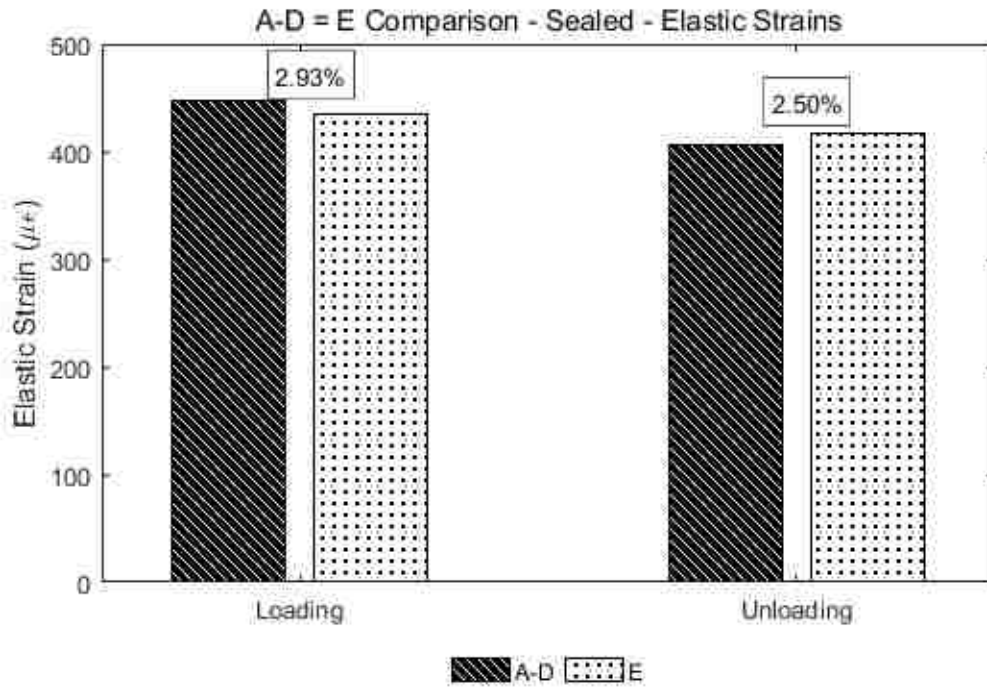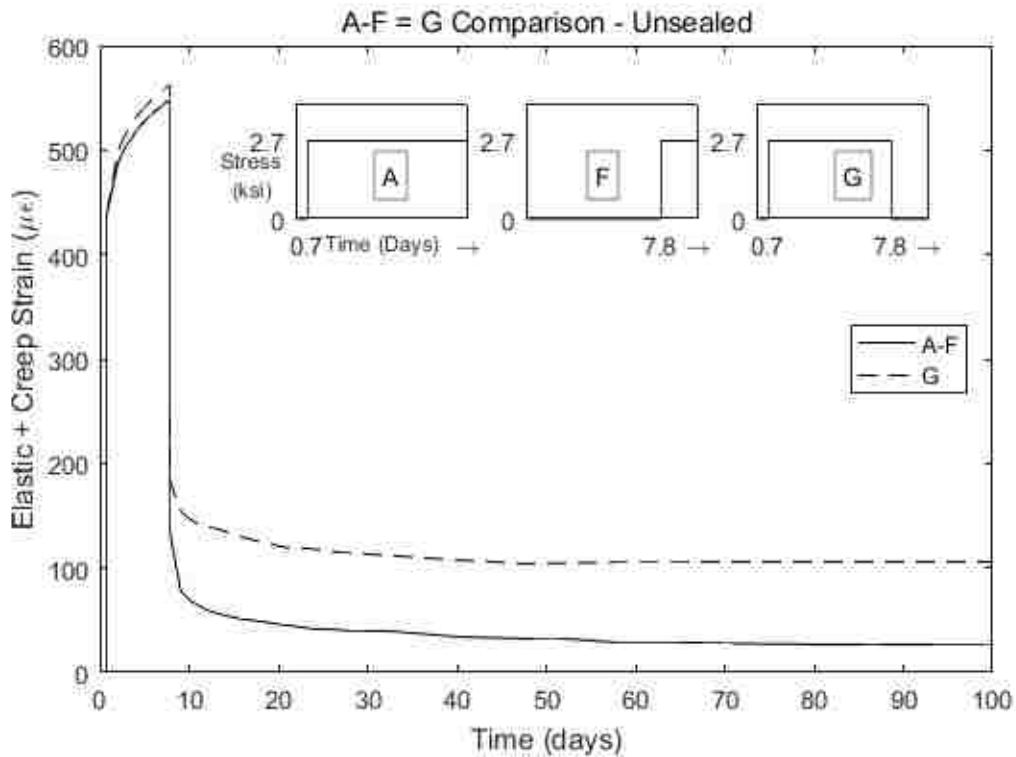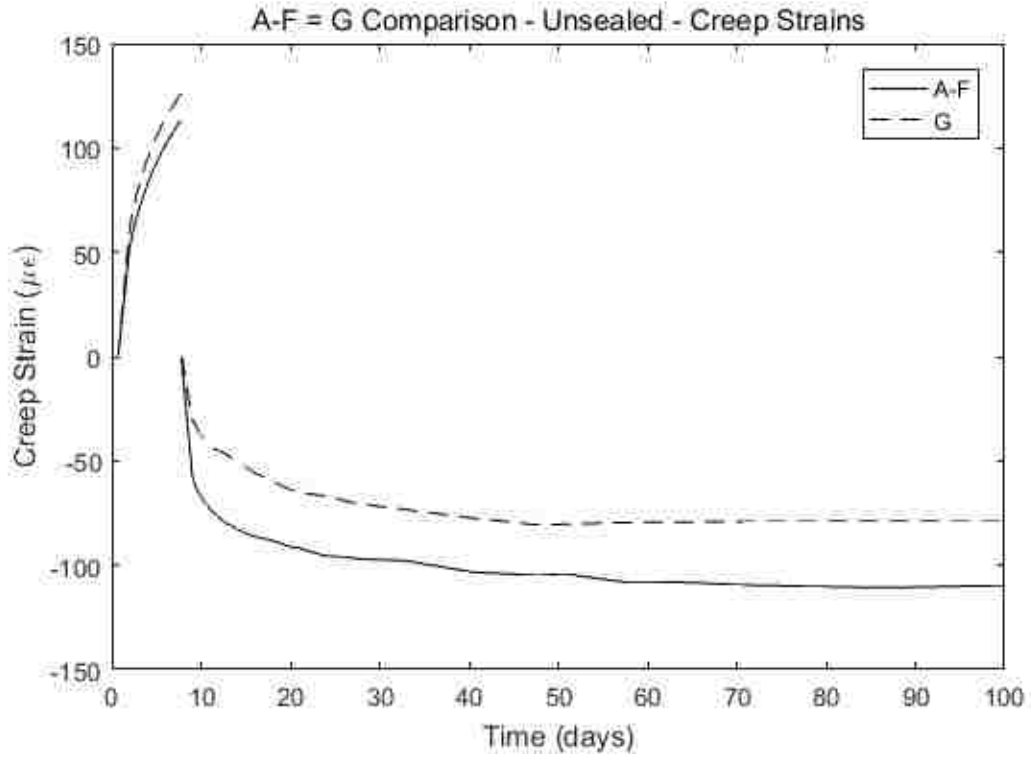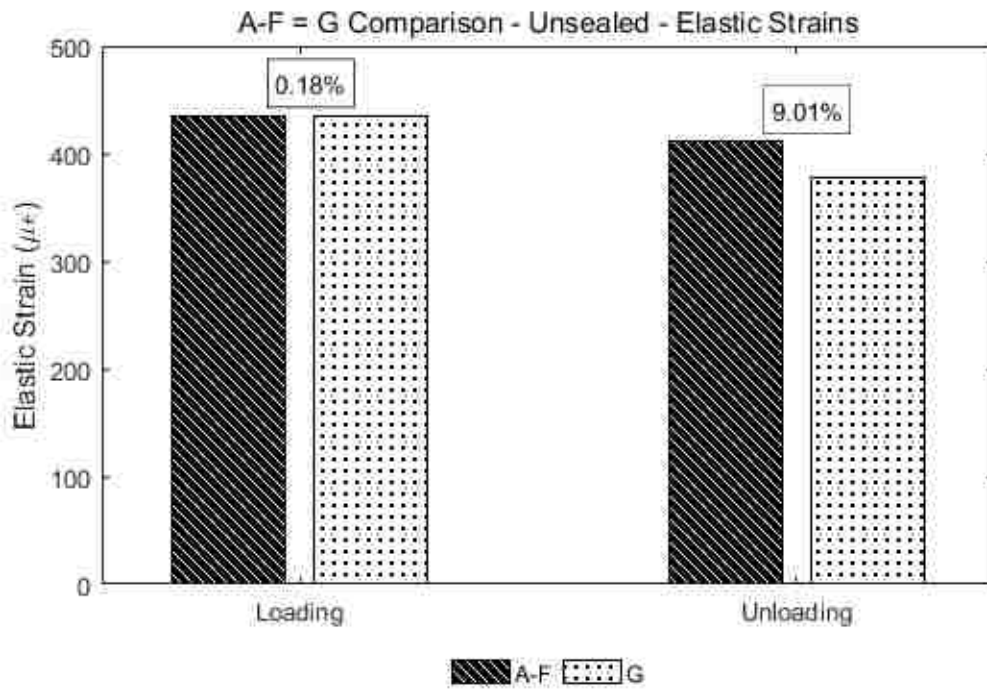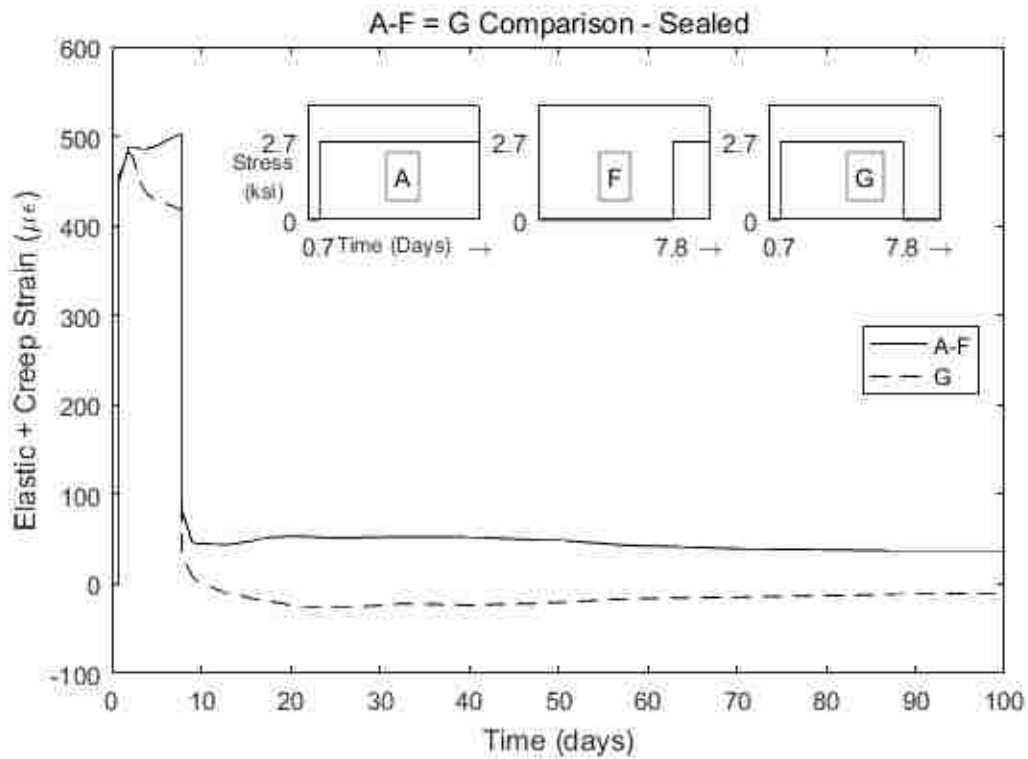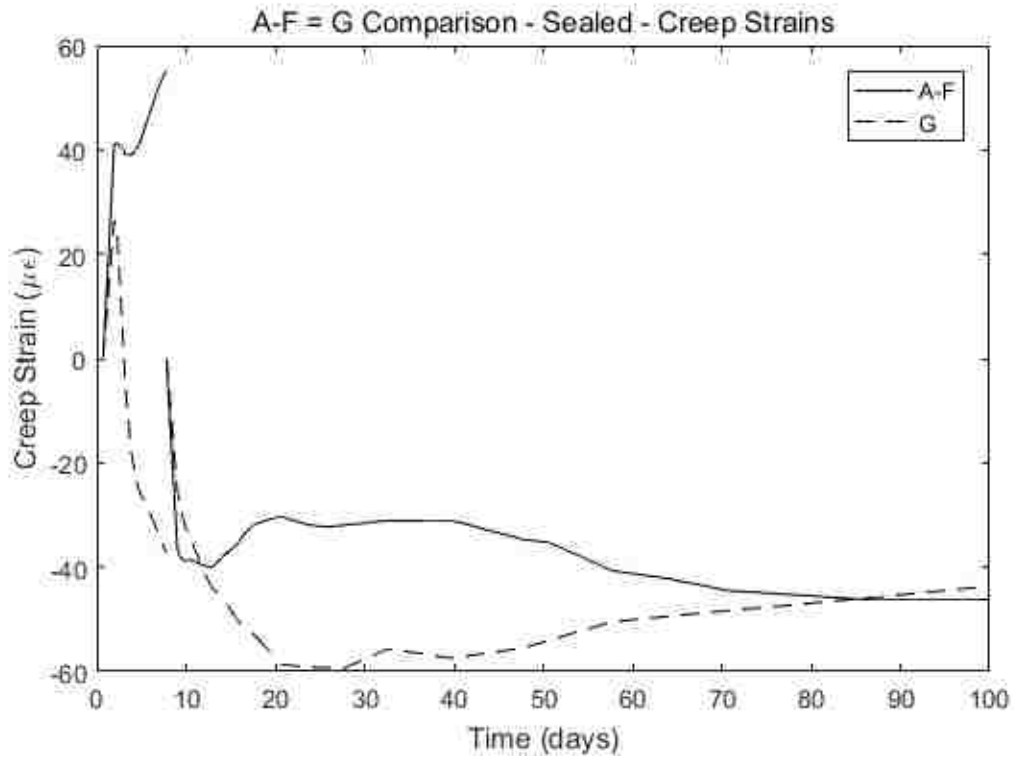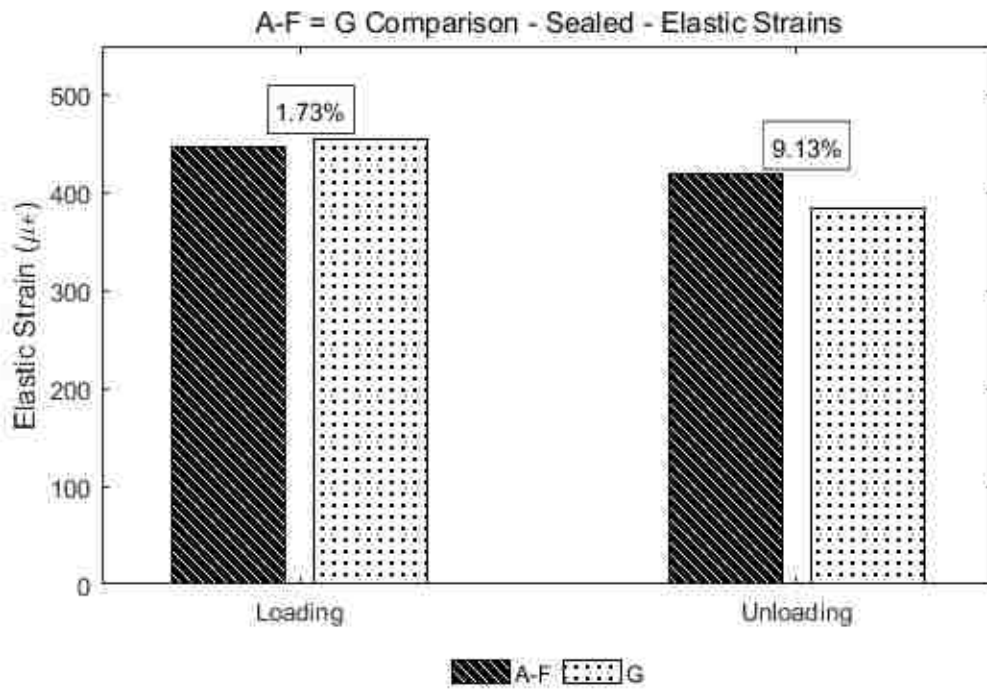**Figure 8.15 Superposition Comparison A-F = G – Sealed – Creep Strains**

Figure 8.16 Superposition Comparison A-F = G – Sealed – Elastic Strains

The foregoing results constitute a very severe test of the experimental procedure and material consistency, and some of the difficulties in interpretation are likely caused by small physical variations rather than failures of the concrete model being used to describe the behavior. For example, the creep strains at this age are only a small proportion of the total strain, so a small error in estimating or measuring the elastic strain leads to a large relative error in the derived creep strain. Also, slight differences in the concretes used in cylinders A, F and G will be amplified by taking the differences between their strains.

8.4   Superposition for Partial Unloading

Similar comparisons can be made for the difference between Specimen I and specimens A, D and F. The stress histories for those cylinders are shown within Figure 8.17. All four specimens were loaded to 2.7 ksi at different ages, and I partially unloaded as the stress history diagram explains. The intention was to compare strains from Specimen I up until its second unloading with the strains from Specimen A with a third of the strains from Specimen D (A-0.33D) subtracted up until the same time and to compare strains from Specimen I up until its final unloading with the strains from Specimen A with a third of the strains from Specimen D and F (A-0.33D-0.33F) subtracted up until the same time.

Specimens A and I were loaded at 0.7 days and 0.8 days respectively, and the load on I was then reduced to 2/3 of its original value at 3.8 days, whereas specimen D was loaded at 3.8 days. The idea was that subtracting a third of the D curve from A should yield a curve identical to I from the start until the second unloading described below. Ideally specimen A and I would have been loaded at the exact same moment but for practical reasons, there was a slight gap between the two loadings.

Figure 8.17 compares the measured elastic and creep strains for the unsealed cylinders for A-0.33D and I. Figure 8.18 shows the corresponding comparison for the creep strains after each loading/unloading. These results agree in large part with the previously observed cases in that there is an unexplained slight difference between early creep in I and A and that there is slightly more rapid creep recovery in the curve than would be expected from the principle of superposition. For the part of the curve between 1 and 4 days, Specimen I, which was loaded slightly later than Specimen A, should show a lower strain but the opposite is true. This suggests that either the concrete or the actual loading was slightly different for these two specimens.

Figure 8.19 shows the comparison between elastic strain values for the two curves for each stress change event. The percentage on top of each group of bars indicates the relative difference between the two values. If superposition was perfectly valid and perfect data could be obtained these values would in all cases be identical. Similar to previously observed results, the elastic strains for the initial loading are within 2% of each other. For the partial unloading however, the elastic strains differ by 37%. The

88

unloading stress change is only a third of the loading stress change and thus it takes a smaller absolute error to yield a large relative error than for the loading event.

Figure 8.17 Superposition Comparison A-0.33D = I – Unsealed

Figure 8.18 Superposition Comparison A-0.33D = I – Unsealed – Creep Strains

Figure 8.19 Superposition Comparison A-0.33D = I – Unsealed – Elastic Strains

Figure 8.20 shows the comparison between the sealed cylinders for A-0.33D and I and Figure 8.21 shows the comparison for the creep strains after each loading/unloading. The faulty gage in specimen D must be remembered while interpreting these results. However the two curves are close to each other and considering the gage malfunction there is nothing here to undermine the validity of superposition.

Figure 8.22 shows the comparison between elastic strain values for the two curves for each stress change event. The percentage on top of each group of bars indicates the relative difference between the two values. If superposition was perfectly valid and perfect data could be obtained these values would in all cases be identical. Similar to previously observed results, the elastic strains for the initial loading are within 6% of each other. For the partial unloading however, the elastic strains differ by 22%. The unloading stress change is only a third of the loading stress change and thus it takes a smaller absolute error to yield a large relative error than for the loading event.
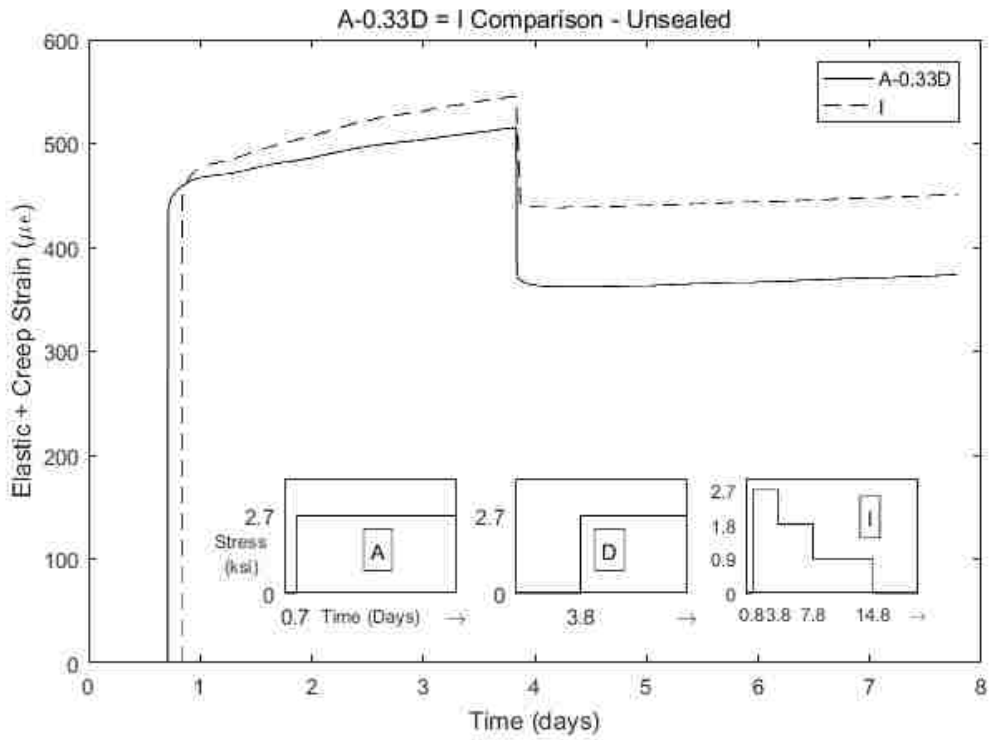

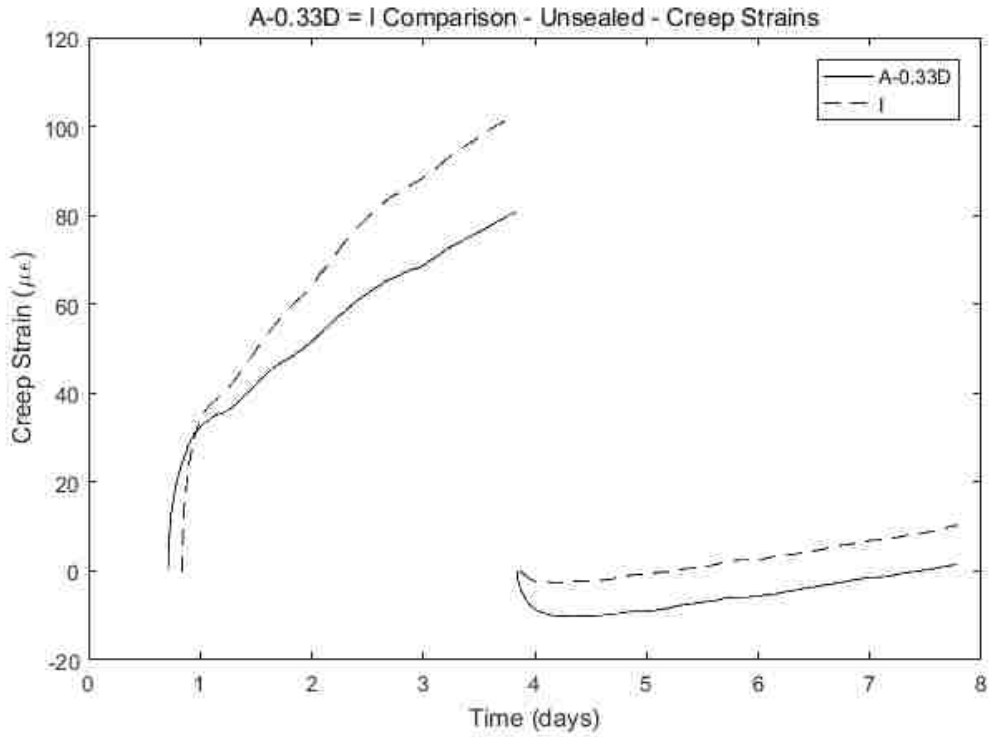**Figure 8.20 Superposition Comparison A-0.33D = I – Sealed**

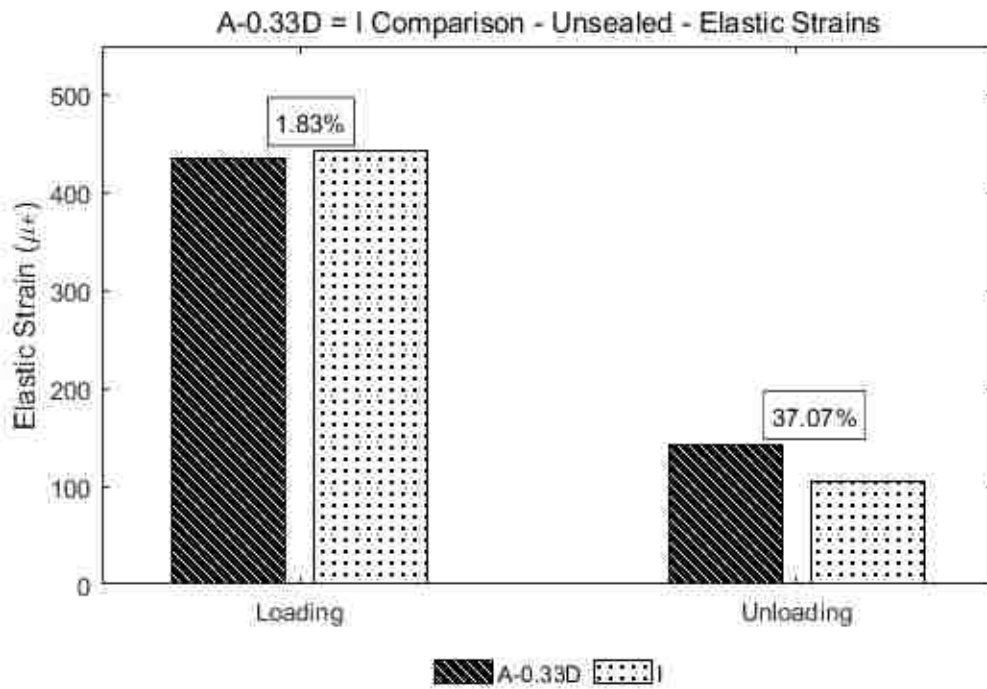**Figure 8.21 Superposition Comparison A-0.33D = I – Sealed – Creep Strains**

Figure 8.22 Superposition Comparison A-0.33D = I – Sealed – Elastic Strains

8.5   Superposition for Stepped Unloading

Figure 8.23 shows the comparison between the unsealed cylinders for A-0.33D-0.33F and I and Figure 8.24 shows the comparison for the creep strains after each loading/unloading. These results are in agreement with the previous cases and do not seem to add anything else to the discussion other than reinforcement of the points previously made.

Figure 8.25 shows the comparison between elastic strain values for the two curves for each stress change event. The percentage on top of each group of bars indicates the relative difference between the two values. If superposition was perfectly valid and perfect data could be obtained these values would in all cases be identical. The first two comparisons are the same as for the A-0.33D = I comparison and have already been discussed. The elastic strain values for the second unloading differ only by 0.33%, which is impressive, because for such a small stress change is only takes a small absolute error for the relative error to become large.
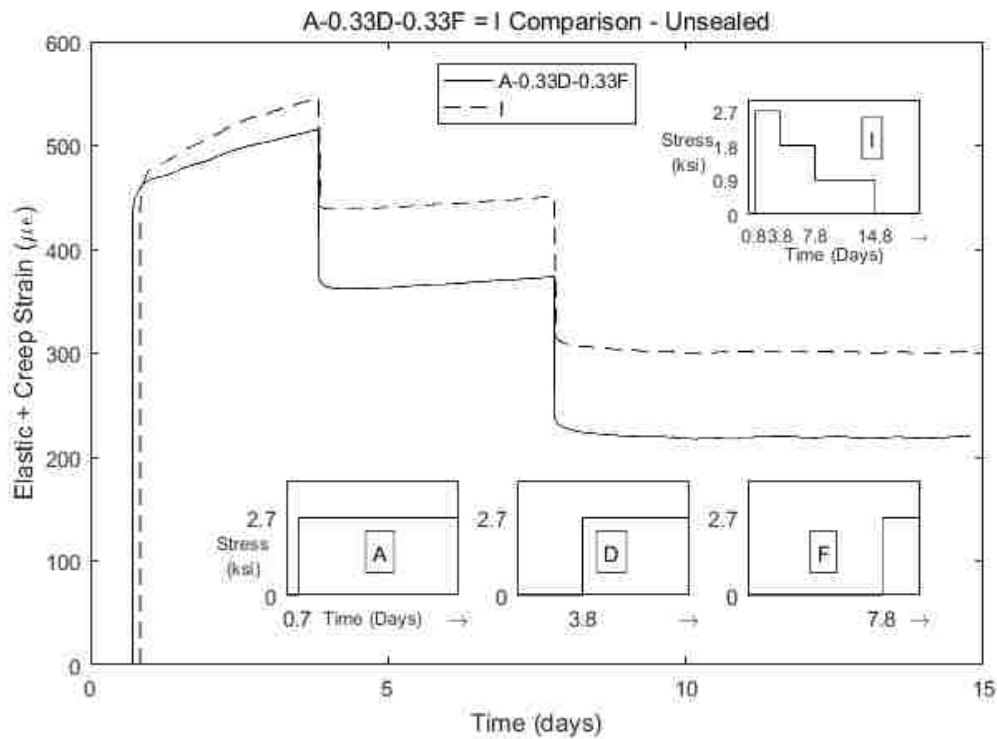
Figure 8.23 Superposition Comparison A-0.33D-0.33F = I – Unsealed
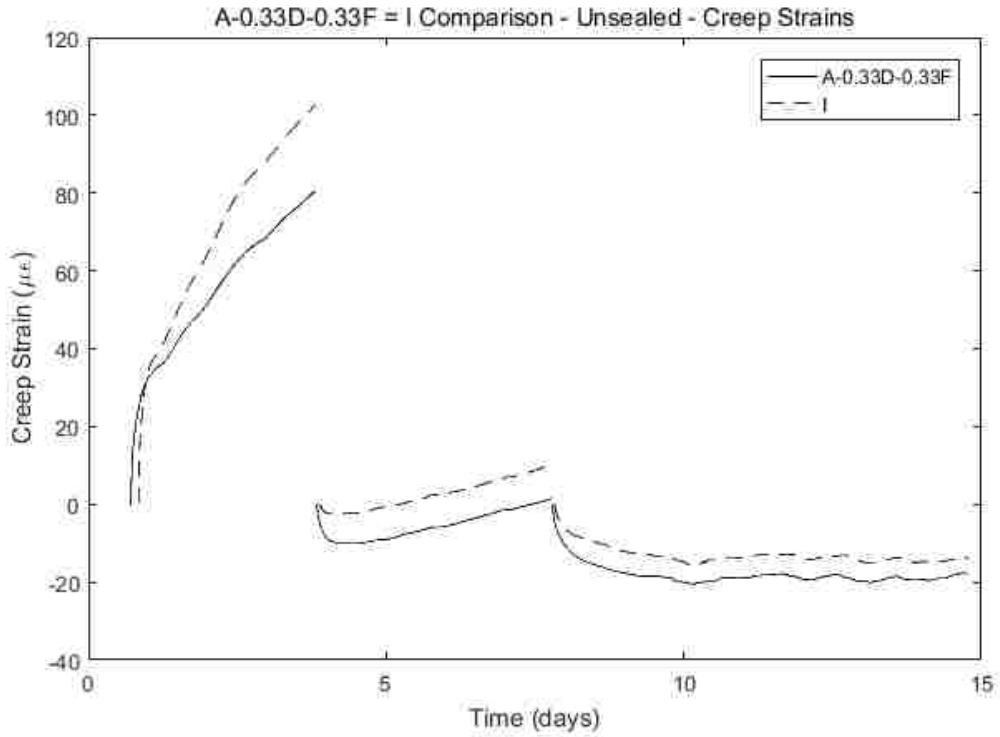
Figure 8.24 Superposition Comparison A-0.33D-0.33F = I – Unsealed – Creep Strains
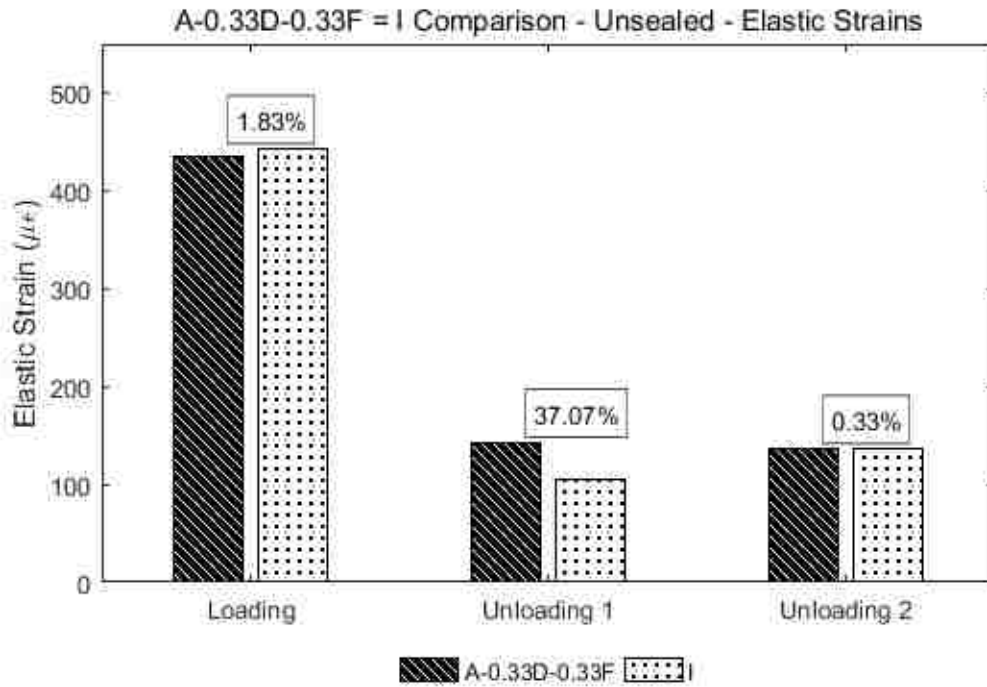
Figure 8.25 Superposition Comparison A-0.33D-0.33F = I – Unsealed – Elastic Strains

Figure 8.26 shows the comparison between the sealed cylinders for A-0.33D-0.33F and I and Figure 8.27 shows the comparison for the creep strains after each loading/unloading. Again, these results must be taken with a grain of salt due to gage failures. A weird pattern is apparent in these two partial unloading cases where the superposition curve rises after both partial unloadings but the I curve falls. This might be explained by the faulty gages present in these specimen.

Figure 8.28 shows the comparison between elastic strain values for the two curves for each stress change event. The percentage on top of each group of bars indicates the relative difference between the two values. If superposition was perfectly valid and perfect data could be obtained these values would in all cases be identical.
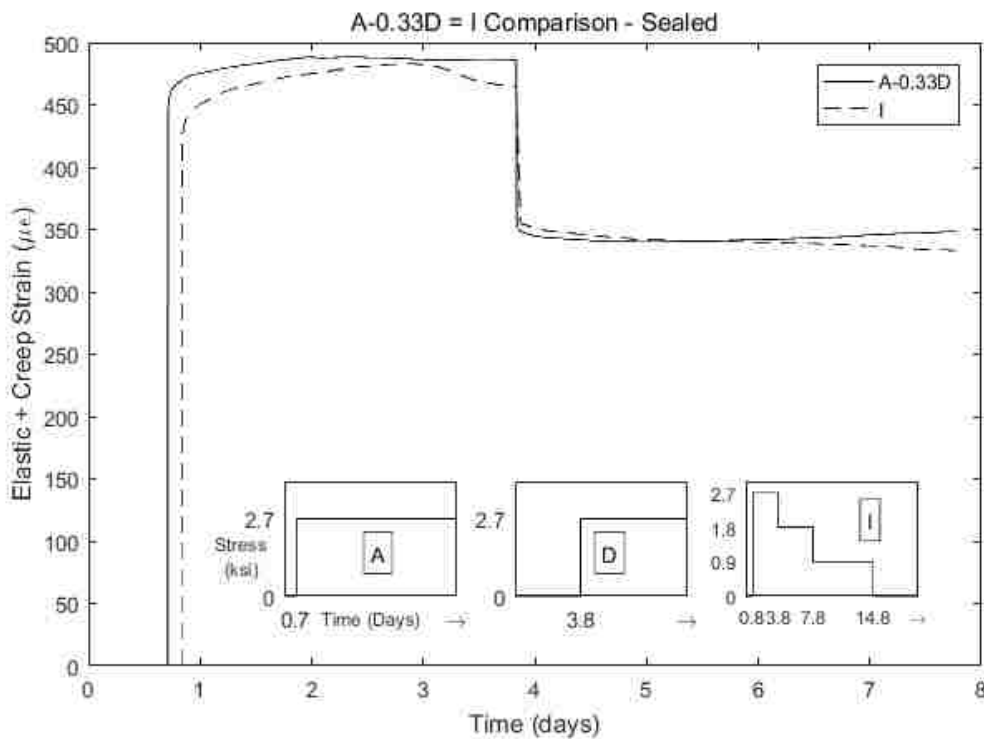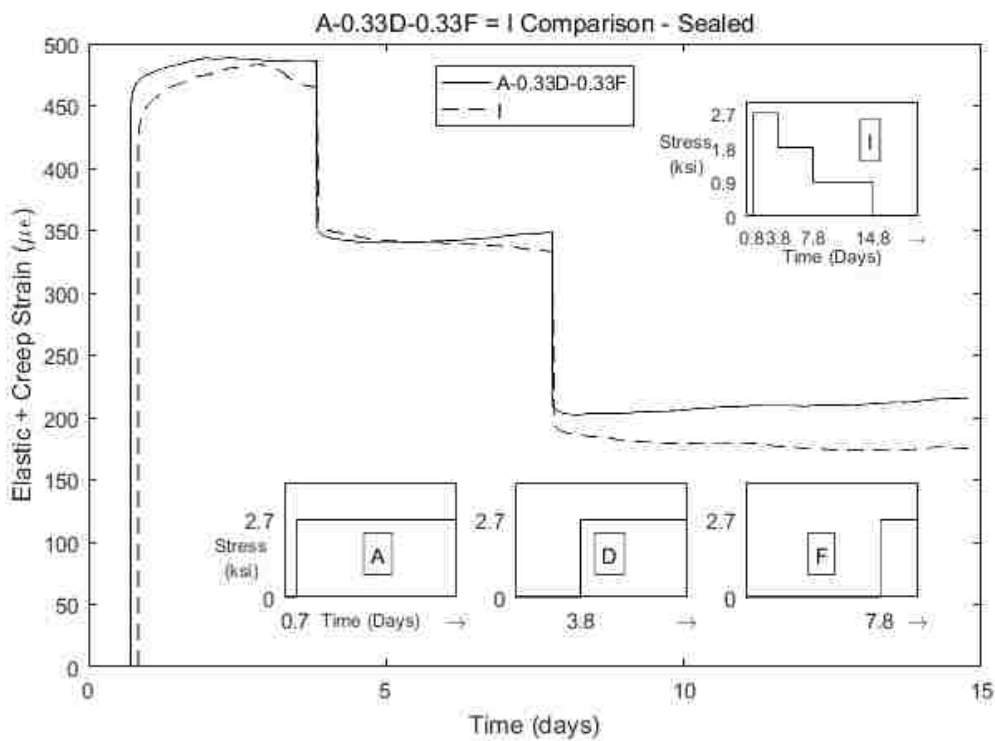

Figure 8.26 Superposition Comparison A-0.33D-0.33F = I – Sealed
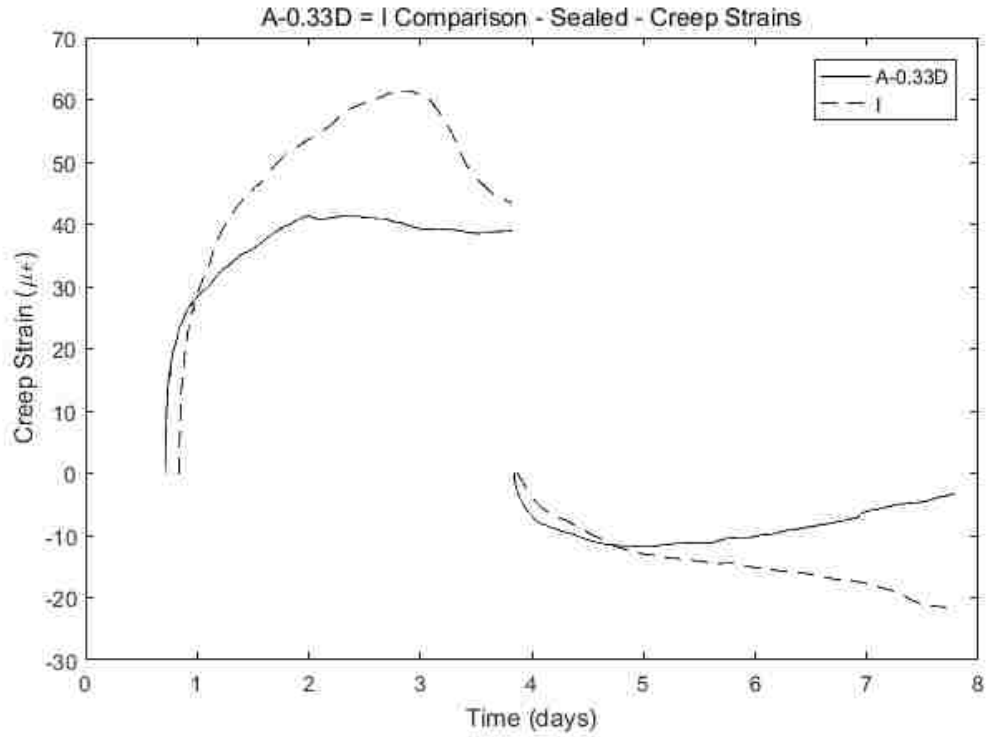
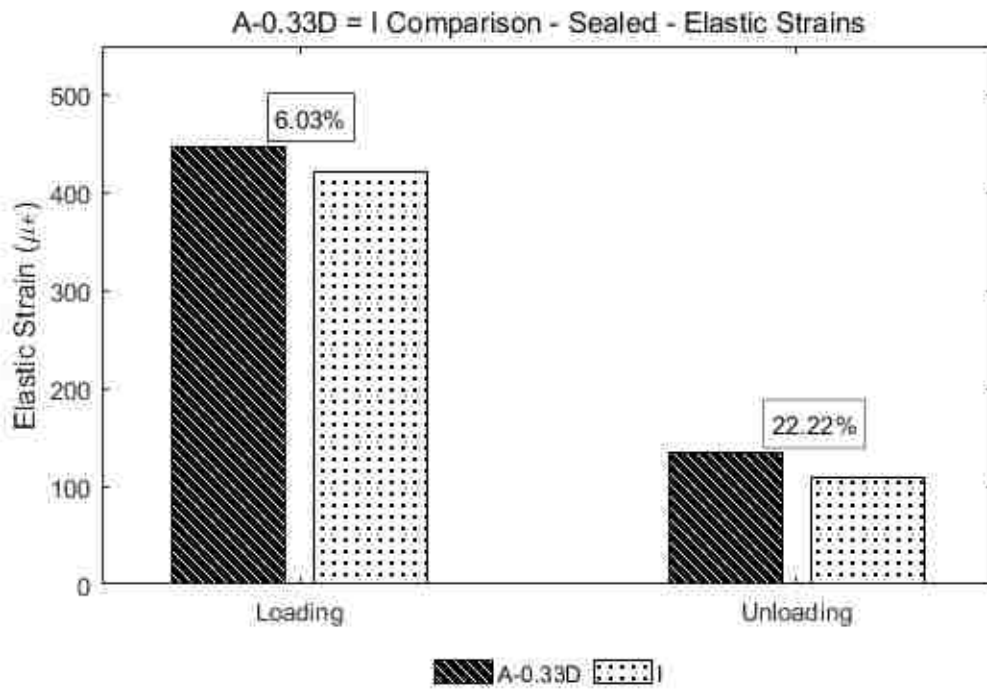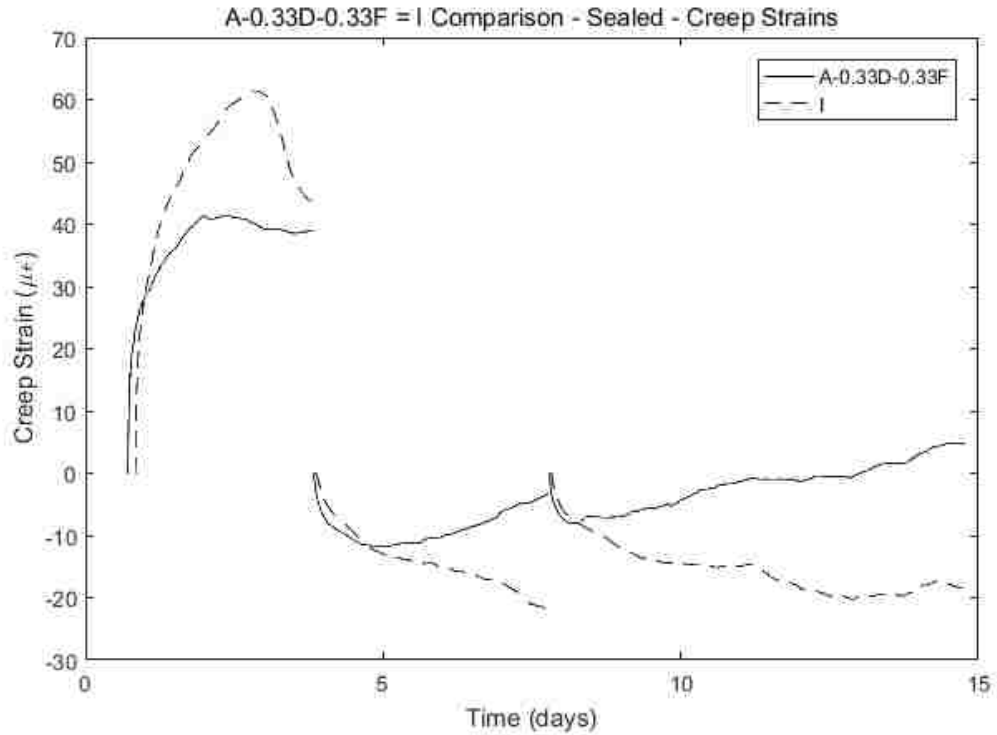**Figure 8.27 Superposition Comparison A-0.33D-0.33F = I – Sealed – Creep Strains**
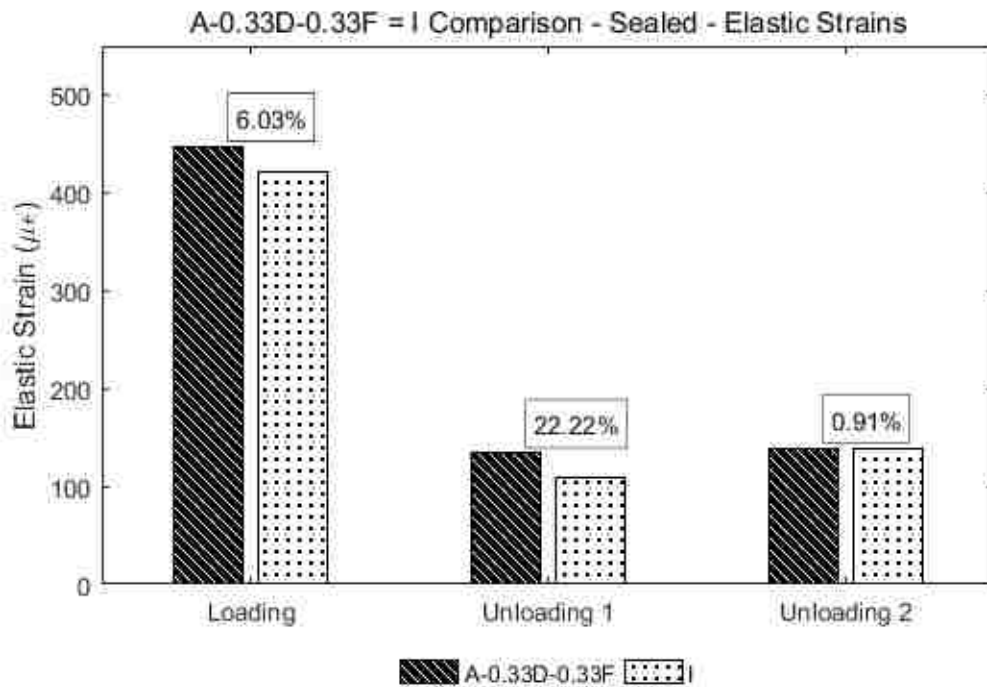
Figure 8.28 Superposition Comparison A-0.33D-0.33F = I – Sealed – Elastic Strains

The first two comparisons are the same as for the A-0.33D = I comparison and have already been discussed. The elastic strain values for the second unloading differ only by 0.91% which is impressive because for such a small stress change is only takes a small absolute error for the relative error to become large.

Overall, these results seem to suggest that while the principle of superposition is not likely to be entirely accurate given the complexity of the chemical processes that take place within in the concrete over time, it is close enough as an approximation to have value as a practical design method. There is however an apparent trend throughout these results that creep recovery by superposition, obtained by subtracting creep of a previously unloaded specimen happens more quickly than actual creep recovery of a previously loaded specimen that is being unloaded.

CHAPTER 9 MODEL DESCRIPTION

The new model, put forth in this chapter, is a one-dimensional rate-type model based on visco-elastic behavior. It is intended to provide a functional form sufficiently versatile that it can replicate a variety of measured results, and to satisfy the principles of thermodynamics. It was originally developed for use in a program to predict prestress loss and camber in precast, prestressed, concrete bridge girders. The model can also be used for other applications in which creep needs to be modeled. It may be formulated for either stress as a function of known strain (such as in a relaxation test) or strain as a function of known stress (such as in a creep test, like the one described in this thesis).

9.1 Detailed Description of the Model

The model is shown schematically in Figure 9.1. It consists of a chain of Kelvin elements, to the end of which is attached a pure elastic spring element. A Kelvin element consists of a linear spring in parallel with a linear dashpot, in which the resistance is proportional to the strain rate, $d\varepsilon/dt$. The figure shows three Kelvin elements, but as many as desired can be used. All of the material parameters, such as the springs in the Kelvin units, have properties that can vary with time. Kelvin chains have been proposed before, but it is the time-varying element properties that make the model novel. For example, the time-dependence of the elastic spring constant allows for changes in the elastic modulus, E_c, over time.

The variations in element properties are chosen so that they represent, at each time step, the addition of a new unstressed element in parallel with the existing ones. For example, at the start of the second time step, the spring stiffness of each of the Kelvin springs is increased to represent the two springs in parallel. A reduction in stiffness is not allowed, because it would represent removal of a stressed spring element. This choice represents a physical system that could be built in practice, and is therefore thermodynamically valid; energy is neither created nor destroyed by the change in properties.
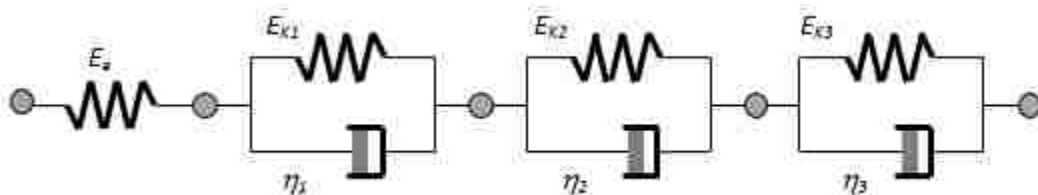
Figure 9.1 Diagram of the New Model

9.2 Time Variation of Concrete Properties

The model form for a single Kelvin element is derived first, and it is then incorporated into the chain. In each case the parameters are assigned time-varying properties.

The way in which the properties change with time can be chosen to fit any particular measured data, but it is useful to choose a single form, with user-selectable parameters, to achieve that goal. For the purposes of this project, the elastic spring properties were taken as the elastic modulus of the concrete, and thus, their time-dependent behavior is outlined in Eq. 5.6. The values for c, n_w, and n_f in Eq. 5.6 are taken from the first column of Table 5.5. The time-dependent behavior of the Kelvin element parameters (if they are chosen to vary with time) is explained in Eq. 9.1. The symbol E_k used in Eq. 9.1 represents the modulus of elasticity of the spring but the time-dependent behavior of the dashpot viscosity, η, has the same form.

$$E_k(t) = \kappa(t)^{0.4} * E_k(28)$$ 9.1

where $\kappa(t)$ is taken from Eq. 5.5. In order to reduce the number of free parameters in the model, t_0 was taken as 0 for all Kelvin element properties and they were therefore assumed to start changing right after the mixing of the concrete. The exponent 0.4 was taken so that the Kelvin element properties changed in a way that is directly comparable to the concrete strength gain.

9.3 Governing Equations for the Creep Model

The general constitutive equation for a Kelvin element, which may or may not have time-dependent properties, in incremental form is

$$\Delta\sigma = E_k\Delta\varepsilon + \Delta(\eta\dot{\varepsilon})$$ 9.2

This can also be written as

$$\Delta\sigma = \left[E_k\frac{\Delta\varepsilon}{\Delta t} + \frac{\Delta(\eta\dot{\varepsilon})}{\Delta t}\right]\Delta t$$ 9.3

If we take the limit as Δt approaches 0

$$\lim_{\Delta t \to 0}\frac{\Delta\sigma}{\Delta t} = \lim_{\Delta t \to 0}\left[E_k\frac{\Delta\varepsilon}{\Delta t} + \frac{\Delta(\eta\dot{\varepsilon})}{\Delta t}\right]$$ 9.4

we end up with

$$\frac{d\sigma}{dt} = \frac{E_k d\varepsilon}{dt} + \frac{d(\eta\dot{\varepsilon})}{dt} = \dot{\varepsilon}(E_k + \dot{\eta}) + \eta\ddot{\varepsilon}$$ 9.5

or

$$\dot{\sigma} = \dot{\varepsilon}E_{eff} + \eta\ddot{\varepsilon}$$ 9.6

where

E_{eff} = the effective Kelvin modulus, given by $E_K + \dot{\eta}$

and the dot implies differentiation with respect to time.

9.4   Solution Procedures

The nature of the solution for the Kelvin elements depends on whether stress or strain is known. In a creep test, the stress is known and the strain is sought, whereas in a girder camber problem, it is likely that, at each cross-section and at each time step, it will be necessary to find the curvature iteratively by trial and error. For each trial curvature, the strain in each concrete element will be known and the stress will be sought. The solution for strain under a known stress regime (i.e. a creep test) is considered here.

9.4.1   Solution for Strain as a Function of Stress

Because the Kelvin element is in general nonlinear, a numerical solution procedure was first considered. A Kelvin chain element resembles a viscously damped dynamic system, albeit one with no mass, so Newmark's procedure was selected and implemented. For a system with constant properties, the procedure gave good results, but only under restricted circumstances. The primary restriction occurred with sudden loading, such as might be expected at the start of a creep test or at release of prestress in a girder. Then, it was found that, unless the time step directly after the completion of loading had exactly the same value as the time steps during the loading, the predicted strains were seriously in error. Perhaps surprisingly, the length of the time steps proved to be unimportant, either in the absolute or relative to the intrinsic time constant of the element, $\tau = \eta/E_K$. This behavior was attributed to the absence of mass in the system, which in turn implies that the strain is a continuous function of time but the strain rate is not. Newmark's method is based on a Taylor series expansion, which is strictly valid only if the dependent variable (here, strain) is continuous and differentiable. The consequence was that that approach was abandoned on the basis that such restrictions on the time step were unacceptable for general use.

Instead, the properties were treated as being constant (taken as the average of the start and end values of each time step), and the stress was allowed to vary linearly, within any time step. Then an exact, closed-form, solution within the time step is possible, and the strains from each time strep can be added in an incremental analysis. For a Kelvin element, the exact solution to Eq. 9.6 at time, t, if conditions at time 0.0 are given, is then

$$\varepsilon_K(t) = \varepsilon_K(0) + \dot{\varepsilon}_K(0)\tau\left[1 - e^{-t/\tau}\right] + \frac{\dot{\sigma}}{E_{eff}}\left[t - \tau\left(1 - e^{-t/\tau}\right)\right]$$

9.7

$$\dot{\varepsilon}_K(t) = \dot{\varepsilon}_K(0)e^{-t/\tau} + \frac{\dot{\sigma}}{E_{eff}(t)}\left(1 - e^{-t/\tau}\right)$$

9.8

$$\ddot{\varepsilon}_K(t) = -\dot{\varepsilon}_K(0)\frac{e^{-t/\tau}}{\tau} + \frac{\dot{\sigma}}{E_{eff}}\left(\frac{e^{-t/\tau}}{\tau}\right)$$

9.9

where

$\tau = \eta/E_{eff}$ = the intrinsic decay time of the unit

$\dot{\sigma}$ = the rate of change of stress with time

$\dot{\varepsilon}_K(0)$ = strain rate at the start of the time interval

Note that, if the properties are constant during a time step, $\dot{\eta} = 0$ and $E_{eff} = E_k$.

Eqs. (9.7-9.9) provide the solutions for strain within a Kelvin element. By setting $t = \varDelta t$, the step size, and writing the equation in incremental form, the strain increment during the time step is

$$\Delta\varepsilon_K = \dot{\varepsilon}_K(t)\left[1 - e^{-\Delta t/\tau}\right]\tau + \frac{\Delta\sigma}{E_{eff}}\left[1 - \frac{\tau}{\Delta t}\left(1 - e^{-\Delta t/\tau}\right)\right]$$

9.10

In the elastic element, the strain change is calculated using the same assumption of constant properties during the time step and is

$$\Delta\varepsilon_e = \frac{\dot{\sigma}\Delta t}{E_e\left(1 + 0.5 * \Delta E_e/E_e\right)}$$

9.11

The error in the elastic strain introduced by the assumption of constant properties within the time step is small, as can be seen by comparing with the exact solution for the case when the modulus changes linearly with time during the interval. In that case

$$\Delta \varepsilon_e = \frac{\dot{\sigma} \Delta t}{\Delta E_e} \ln\left(1 + \Delta E_e / E_e\right)$$

9.12

The ratio of the two strain increments (constant/average) is

$$ratio = \frac{\delta}{\left(1 + \frac{1}{2}\delta\right)\ln(1+\delta)}$$

9.13

where $\delta = \Delta E_e / E_e$

This ratio converges to $1 / \left(1 - \frac{\delta^2}{4}\right)$ for $\delta \ll 1.0$. If, in the interests of consistency with the Kelvin element calculations, the elastic strain increment is computed assuming constant average properties, the step size (and hence, δ) can be selected so as to make the error in the solution as small as desired.

The total strain increment is obtained by computing the increments in the individual elements (elastic and Kelvin) and adding them. This procedure is valid for multiple Kelvin elements.

9.5 Relationship between Model Parameters and Conventional Material Constants

To predict creep behavior, numerical values are needed for the model parameters. However, even ultimate creep values vary significantly from one concrete to another, and variations with time also depend on environmental parameters such as relative humidity and V/S ratio. For example, Brooks (2005), in a 30-year creep study, found ultimate creep coefficients varying from 1.2 to 9.6. Thus, the most accurate approach is to conduct material-specific tests and calibrate the model to the results, as is done in this study.

The most commonly used material constants to describe concrete deformations are $E_{c,28}$ and C_{cu}. ACI 318-14 (ACI 2014) also gives a table of time-dependent long-term deflection multipliers that can be taken as indicators of creep rate effects. It would be useful to be able to map these constants to the parameters of the proposed model, so that values can be estimated simply. This is done below. The important relationships are derived for Kelvin elements with fixed parameters; then a more general procedure is suggested for elements with time-varying parameters.

Elastic modulus, E_c, of the concrete. This maps directly to E_e, the stiffness of the elastic spring element. This should be set equal to the elastic modulus, E_c, for the concrete in question. If that is not known, the

generalized relationship given in Eq. 5.6 in Chapter 5 with constants from Table 5.5 in Chapter 5 should be used. That relationship expresses E_c in terms of f_c so, if the time variation of strength is known, it can be used to generate values for n, t_0 and a in Eq. 5.5, and the modulus can be computed from strength. In the absence of better information, provisional values for steam cured, high strength concrete (such as is used in pretensioned products), and for medium strength cast-in-place concrete, can be found in Table 5.3 in Chapter 5.

Ultimate creep coefficient, C_{cu}. This is generally taken to be the ratio of the creep strain at infinite time to the initial elastic strain, assuming constant stress. To calculate the elastic strain, the E_{el} value at the time of loading is needed, and this may not be available. However, in practice, the initial elastic strain is often computed using $E_{c,28}$, instead. If both E_e and the model parameters are treated as constant over time, C_{cu} is related to the model parameters by

$$C_{cu} = \frac{E_e}{E_k}$$
9.14

Eq. 9.14 allows E_k to be computed if C_{cu} and E_e are known. This procedure is unique only for Kelvin elements with constant parameters. If more than one Kelvin element is used in the model, E_k in Eq. 9.14 should be replaced by $E_{k,eq}$, defined by

$$E_{k,eq} = \left[\sum_{j=1}^{N} \frac{1}{E_{k,j}} \right]^{-1}$$
9.15

In that case, even if the value of C_{cu} is known, the values of the various $E_{k,j}$ stiffnesses are not uniquely defined, and further information is needed to choose them.

Dashpot stiffness, η. This is related to the intrinsic time constant, τ, for the system by

$$\tau = \frac{\eta}{E_{eff}}$$
9.16

For a system with parameters that do not vary with time, in which case E_{eff} is simply E_k, τ represents the time needed to complete 63.2%, i.e. (1-1/e), of the ultimate creep deformation. Results from a previous project on HPC bridge girders (Barr 2000) suggest that, for such members, τ should be on the order of 3 months.

If the model parameters are chosen to be functions of time, the relationships between the conventional constants and the model parameters depend on the functional form of the time variation of those parameters. It is then necessary to conduct trials, guided by the foregoing results for fixed parameters, to

achieve a model that replicates the desired combination of conventional parameters. Unique, one-to-one relationships such as those given above, do not exist.

CHAPTER 10 MODEL CALIBRATION

10.1 Calibration Overview

The data from the nine hot-cured specimens were used to calibrate the numerical model described in Chapter 9. These nine specimens had a variety of stress histories and times of loading, as outlined in Chapter 3. One goal of this research was to obtain a single set of material parameters for hot-cured concrete that would be independent of loading values and times of loading.

As outlined in Chapter 9 the model is made up of a single elastic spring and an arbitrary number of Kelvin elements in series, having either constant or changing spring and dashpot parameters. In this chapter, four configurations of the model are calibrated against the test data. They are the following:

- Single Kelvin element with constant parameters
- Single Kelvin element with time-dependent parameters
- Two Kelvin elements with constant parameters
- Two Kelvin elements, one with constant parameters and one with time-dependent parameters

10.2 Calibration Methodology

The datasets for each of the specimens were obtained, as explained in Chapter 4.3, by taking the average strain measurement from the unsealed cylinder of each specimen and subtracting from it the average strain measurement from the corresponding unsealed shrinkage cylinder. The dataset was then reduced by taking only data points at even intervals of 0.1 in log time (days), plus a single measurement at each side of a stress change event. When the loading changed on the specimen at any time after the initial loading, as was the case for three of the specimen, the sampling at equal intervals of 0.1 in log time „resets" and so data points were taken at $10^{0.1}$, $10^{0.2}$ days and so on after that stress change event. This left a set of data points for each specimen with more data points closer in time to any stress change event than further away, as that is when a large part of the creep was expected to take place.

The elastic strain induced by a change in stress was modeled with the single elastic spring in the model. The elastic modulus of that spring was taken as the elastic modulus of the concrete itself. The calibration of a time-dependent function for the elastic modulus of the concrete was described in Chapter 5. This was used to model the elastic spring. The only input parameters required to model this spring were the unit weight and the mean 28-day compressive strength of the concrete.

The creep strain was modeled by the Kelvin elements and was taken as the processed data minus the elastic strains. These data points are used for the calibration. The time-dependency of any of the Kelvin element parameters (i.e. the springs and dashpots) was assumed to be given as the 28-day value multiplied by the function given by Eq. 9.1. If constant parameters are desired, a was simply set to 1.0 and the function defaulted to 1.0 at all times.

For elements with time-varying properties, the values of E_K and η were linked because the ratio η/E_K represents the intrinsic time constant, τ, of the element. Because E_K and τ represent physical entities that can be expected to lie within bounds that can be envisioned, it is more useful to use them as the free variables and to compute η from them. In the interests of simplicity, it was decided to keep τ constant within an element even as E_K changed over time, so the parameters a and n were constrained to be equal for the spring and the dashpot of the same Kelvin element.

For every Kelvin element, $E_{K,28}$ and τ_{28} must be obtained by calibration. In addition, for elements with time-dependent properties, a and an n must also be calibrated, resulting in 4 parameters per Kelvin element.

An objective function was used to identify the optimal set of parameters across all nine specimens. The function had the following form:

$$f\left(\varepsilon_p, \varepsilon_m, n_d, n_s\right) = \frac{\sum_{j=1}^{n_s} \frac{\sqrt{\sum_{i=1}^{n_d}\left(\varepsilon_m - \varepsilon_p\right)^2}}{n_{d,j}}}{n_s} \qquad 10.1$$

where

ε_p – Strain calculated with model (microstrain)

ε_m – Strain measurement (microstrain)

$n_{d,j}$ – Number of data points for specimen j

n_s – Number of specimens (nine)

For every specimen, the sum of the squares of the errors between measured and predicted values was calculated, the square root of that number was computed, and then that result was divided by the number of data points for that specimen. These resulting values were then summed up for all specimens and divided by the number of specimens.

The calculations were done in Excel, and the optimal value was identified using the Solver function. The results of this calibration for four different configurations of the model are provided in the following sections for each type of model.

10.3 One Kelvin Element – Constant Parameters

The simplest possible configuration of the model is an elastic spring connected to a single Kelvin element with constant parameters. Its simplicity makes it unlikely to provide the best fit to the data, but the parameters will, at the least, serve as a guide for values in the more complex models calibrated later. A second drawback of constant-parameter models is that the constant parameters will always lead to all creep being fully recovered upon the removal of load. As was shown in Section 7.4 on residual creep this does not seem to be the case.

The only two parameters calibrated in this configuration are the 28 day value for the spring's modulus of elasticity, $E_{k,28}$, and value for the intrinsic time constant, τ. Table 10.1 shows the calibrated values for the two parameters, as well as the optimal value of the objective function.

Table 10.1 Calibrated Parameter Values for Configuration 1

$E_{k,28}$ (ksi)	12000
τ (days)	10
Objective function value	6.09

Figure 10.1 shows the individual objective function values for each specimen. This comparison can shed some light on whether or not any specimen is getting a much worse fit by the model than any other specimen. The horizontal line represents the average value for the objective function.
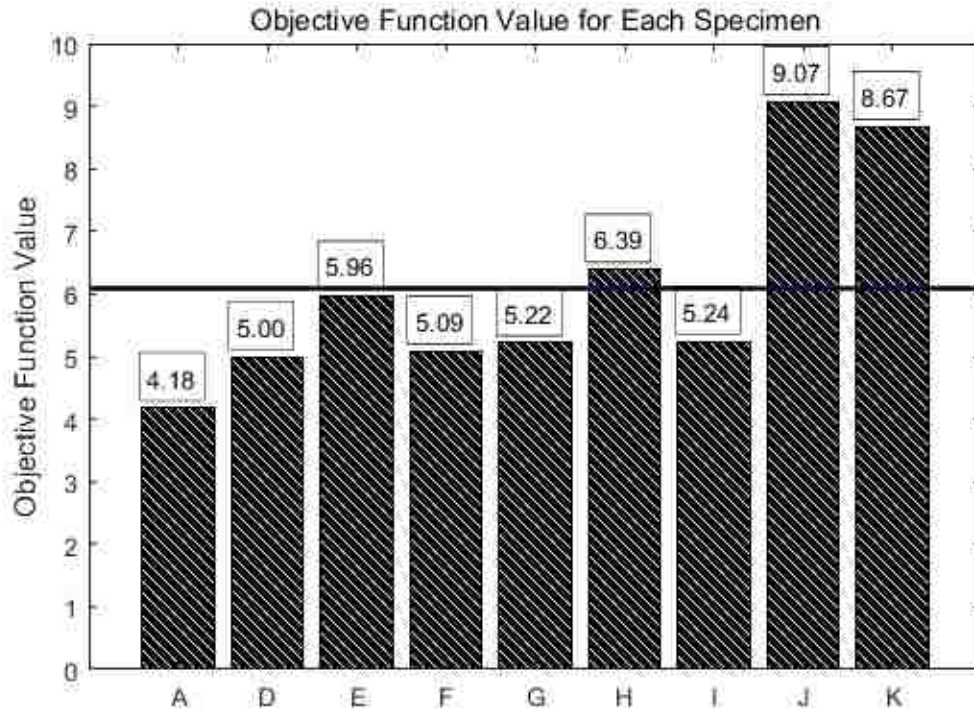
Figure 10.1 Objective Function Values for All Specimen – Configuration 1

The greatest contributors to the objective function value were specimens J and K. J was loaded late (57 days), so it is not surprising that a constant value model did not match the measured strains well for that specimen. Specimen K was loaded to a high level of stress (4500 psi) than the other specimens.

10.4 One Kelvin Element – Time-Dependent Parameters

With time-dependent parameters, the fit should be expected to be as good as, or better than, the constant-parameter model. This version of the model has the additional feature that it can replicate incomplete recovery of creep upon removal of load. There are four parameters to be calibrated in this configuration: $E_{K,28}$, τ, a and n. Table 10.2 shows the optimal values for the four parameters and the minimum value of the objective function.

Table 10.2 Calibrated Parameter Values for Configuration 2

$E_{k,28}$ (ksi)	14000
τ (days)	11.4
a	1.56
n	0.78
Objective function value	4.44

The minimum value of the objective function has decreased significantly from the value computed for the constant-parameter model. The E_k and τ_{28} values are similar, but not identical, to the values obtained for the constant parameter fit. The a and n values also seem reasonable.

Figure 10.2 shows the individual objective function values for each specimen.
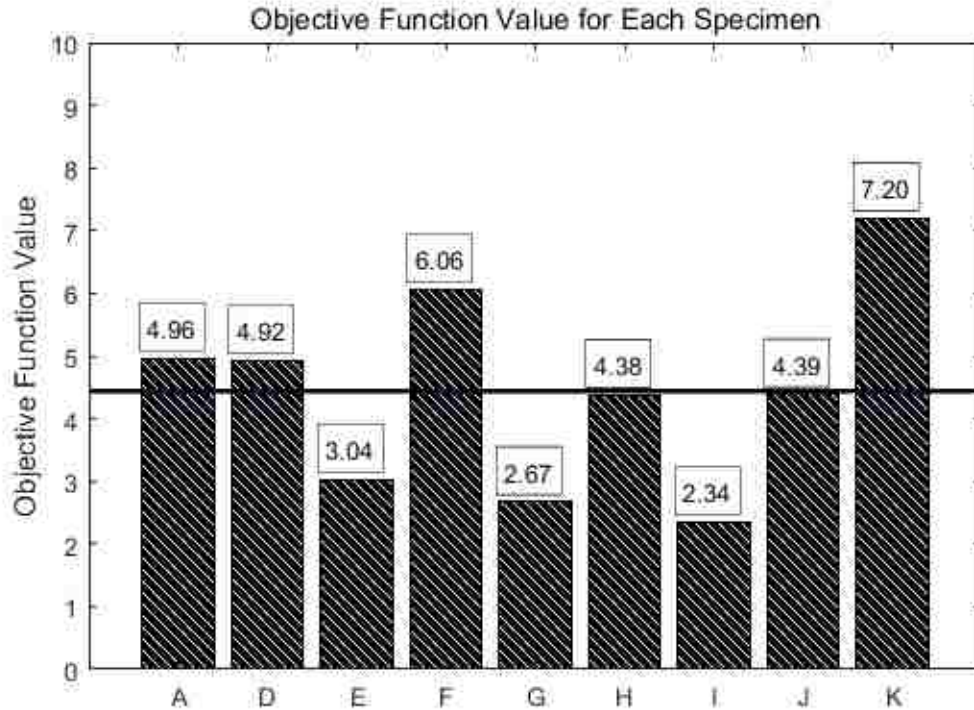

Figure 10.2 Objective Function Values for All Specimen – Configuration 2

The contributions from each specimen are little more evenly spread for this configuration, although Specimen K still makes the largest contribution (7.20). As expected, the contribution of the late-loaded specimen (Specimen J) is greatly reduced. In addition, notice how much better this fit is for the three specimens that were unloaded, namely E, G and I. This suggests that having time-dependent parameters more accurately models concrete with a variable stress history. The fact that Specimen K provided the worst fit in both calibrations suggests that either the model is less able to predict creep for specimens loaded to high stresses, or that the quality of the data for Specimen K might be poorer than the other data.

10.5 Two Kelvin Elements – Constant Parameters

As mentioned in Section 10.3, a strong case can be made against the usage of constant parameter elements, because they are unable to predict anything but complete creep recovery upon removal of load. When the fit was performed using two Kelvin elements with constant parameters it lead to the solver making one of the elements so stiff that it provided effectively no strain and thus yielding almost exactly the same parameters for the other element as using only one constant element (Section 10.3). Therefore the usage of this configuration of the model was ruled out. Providing results for this fit in any more detail would be redundant.

10.6 Two Kelvin Elements – One Constant, One Time-Dependent

A final configuration, with one Kelvin element with constant parameters and one with time-dependent parameters, was calibrated. In Section 7.4 on residual creep, the creep in the sealed cylinders was completely recovered in all three cases, whereas the creep in the unsealed cylinders was not. This suggests that a part of the creep of hot-cured concrete might be recoverable but not all of it. A Kelvin element with constant parameters can therefore represent recoverable creep and a Kelvin element with time-dependent parameters could represent non- or partially-recoverable creep. In this configuration there are six different parameters to be calibrated. They are a set of the two parameters calibrated in Chapter 10.3 and the four parameters calibrated in Chapter 10.4. Table 10.3 shows the calibrated values for the six parameters and the minimized value of the objective function. The superscript signifies which Kelvin element the parameter corresponds to, Kelvin element 1 is the one with time-dependent parameters and Kelvin element 2 is the one with constant parameters.

Table 10.3 Calibrated Parameter Values for Configuration 3

Time-Dependent Parameters (Element 1)	$E^1_{k,28}$ (ksi)	15500
	τ^1 (days)	32.3
	a^1	1.1
	n^1	1.48
Constant Parameters (Element 2)	$E^2_{k,28}$ (ksi)	33000
	τ^2 (days)	3.0
	Objective function value	3.26

The minimized value of the objective function was lower for this configuration than the two others previously tested, suggesting that this configuration provides a better overall fit than both the other configurations. Figure 10.3 shows the individual objective function values for each specimen.
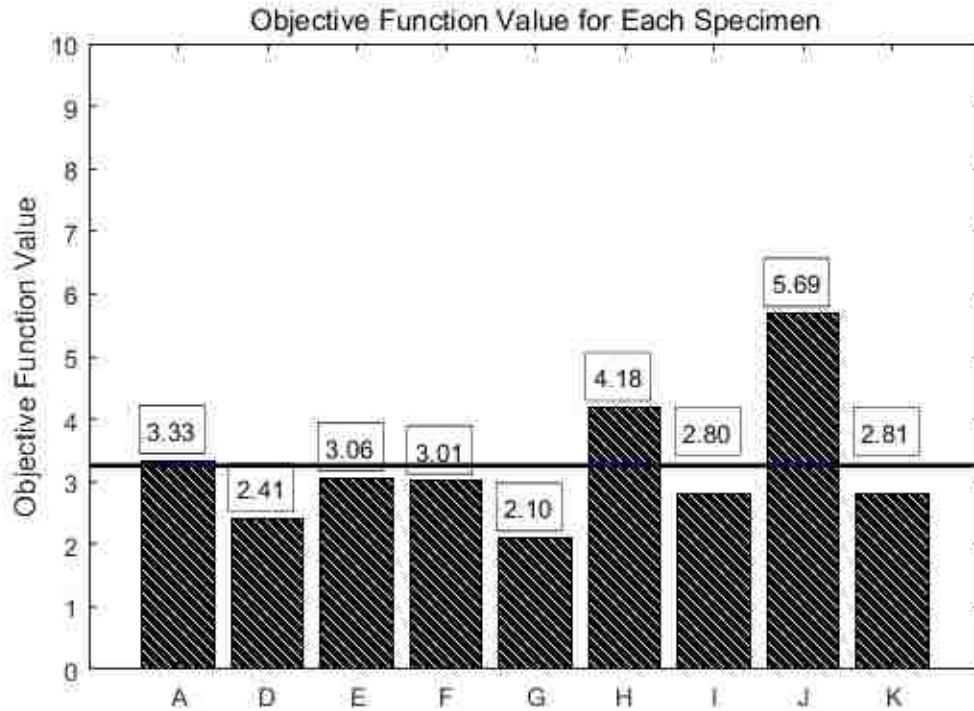
Figure 10.3 Objective Function Values for All Specimen – Configuration 3

For this configuration, Specimen J contributed by far the most to the overall value of the objective function (5.69). The rest of the specimens had similar contributions.

10.7 Comparison of Model Performance

To provide a visual representation of how well these three configurations fit the data, Figure 10.4 shows data for a specimen with monotonic loading (A), along with the calculated values for the three optimized models from section 10.3, 10.4 and 10.5. For this specimen, the average RMS error was 4.18 for the one-element, constant-value model, 4.96 for the one-element time-dependent models and 3.33 for the two element, time-dependent model. The two-element model provided the best fit to the data for this specimen.

Similarly, Figure 10.5, compares the model fits for a specimen with a variable stress history (E). For this specimen, the model fits were similar for the one-element and two element models with time-dependent parameters.

Figure 10.6 shows data for a specimen loaded late (J). In this case, the best fit was provided by the one-element, time-dependent model. Similar plots for all nine specimens can be found in Appendix D.
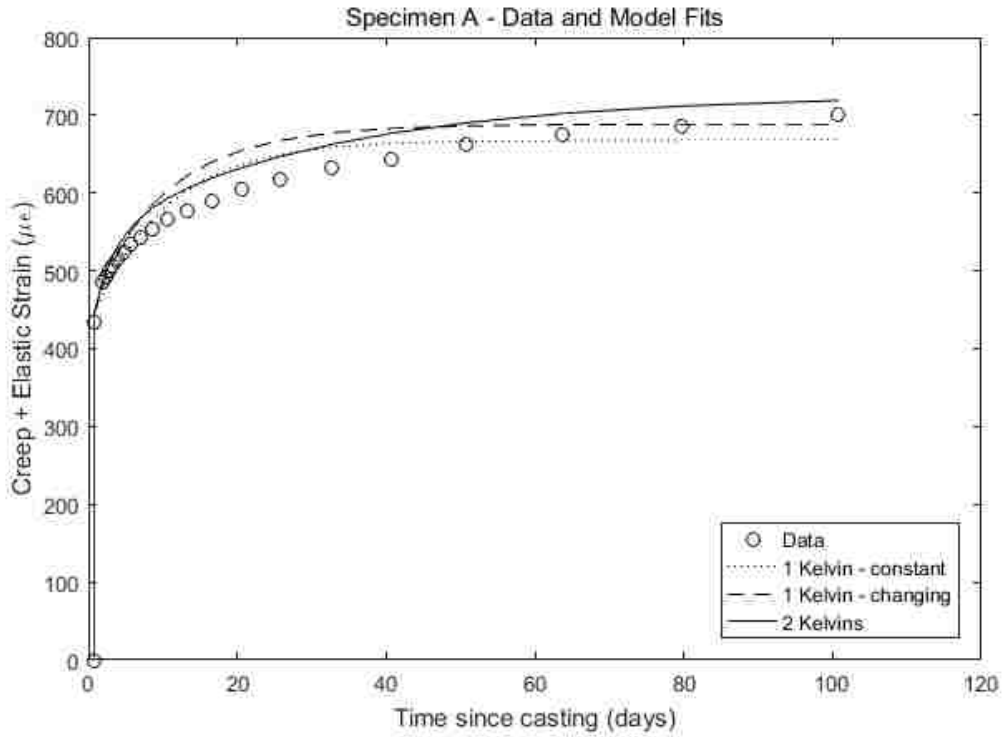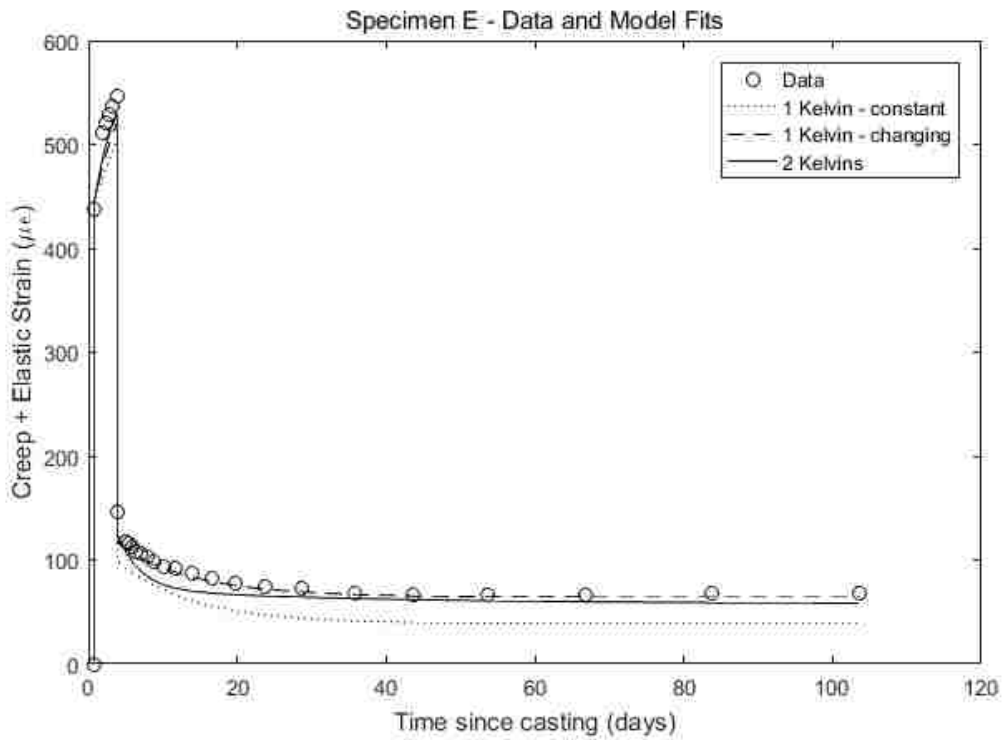
Figure 10.4 Model Fits to Specimen A

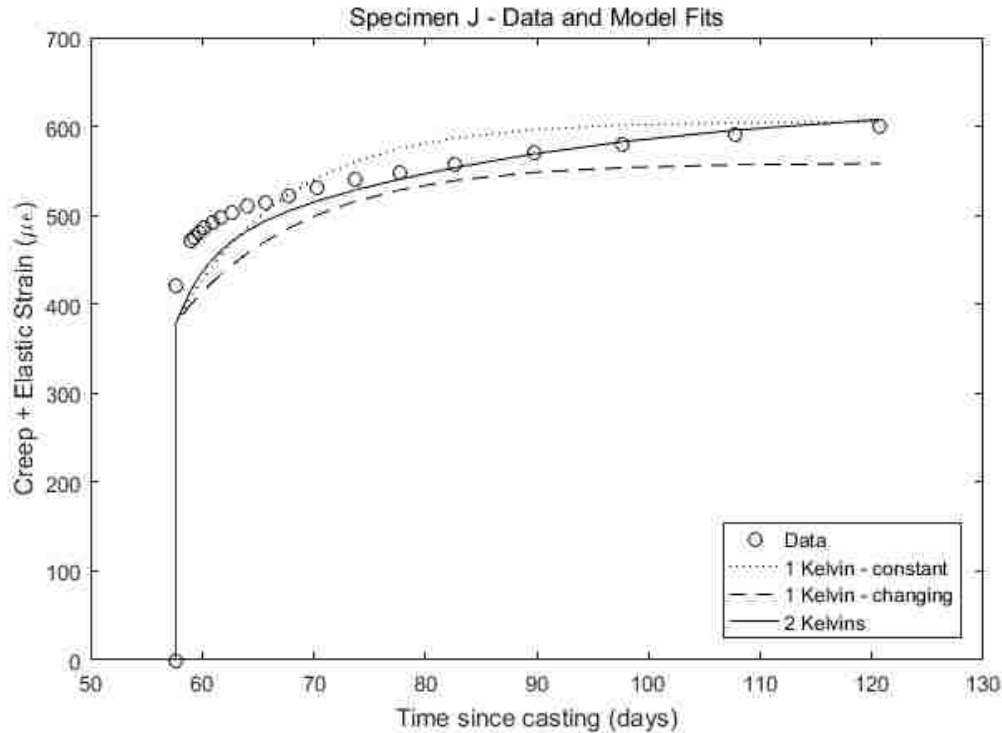**Figure 10.5 Model Fits to Specimen E**

111

Figure 10.6 Model Fits to Specimen J

As the values of the minimized objective function suggests, the best overall fit was provided by having 2 Kelvin elements, one with constant parameters and one with time-dependent parameters. It is possible that a model configuration not considered here could provide an even better fit. It is also possible that a calibration with a larger and more versatile dataset can provide a different result. Using a model with two Kelvin elements as described above can still be useful, as a good fit is obtained across all specimen using that configuration. It is especially impressive to look at the fit achieved to the specimens with variable stress history. Being able to model creep of concrete with variable stress histories was one of the objectives of this thesis and this configuration of the model does a good job at that.

10.8 Fits for Single Specimens

Since fits in all configurations tested in this project were done to the dataset as a whole as opposed to fitting to each curve individually, the model does not do a perfect job of predicting any single curve. This was done so that a single set of parameters could be obtained for a specific curing regime, hot-curing in this case, independent of loading value, time of loading or loading history. The model is, however, capable of fitting any single creep curve much closer if it is calibrated to that curve only. To demonstrate this, the 2 Kelvin element configuration from Chapter 10.6 was fitted to specimens A, E and J individually. The fit to the curve from Specimen A is shown in Figure 10.7.
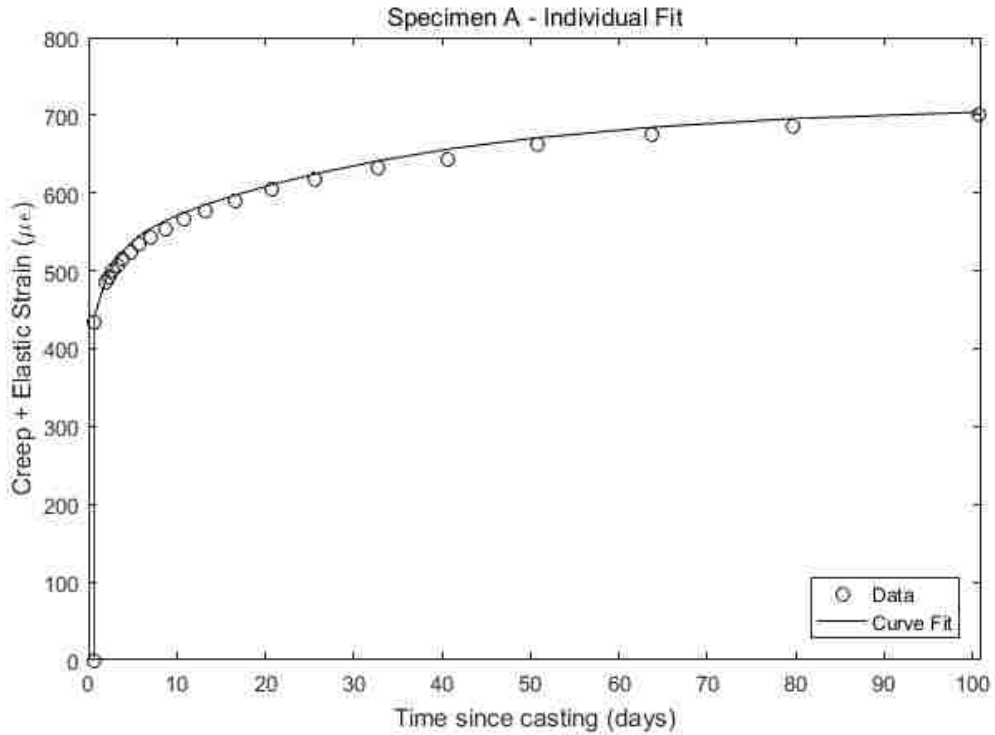
112

Figure 10.7 Individual Fit to Specimen A

An improvement to the fit can clearly be seen, despite the fact that the model still over predicts the strain very slightly for most of the 100 days. The parameters from the individual fit to Specimen A are given in Table 10.4. The value of the objective function for Specimen A was 0.59, whereas it was 3.33 for the model configuration that was calibrated to fit all nine datasets.
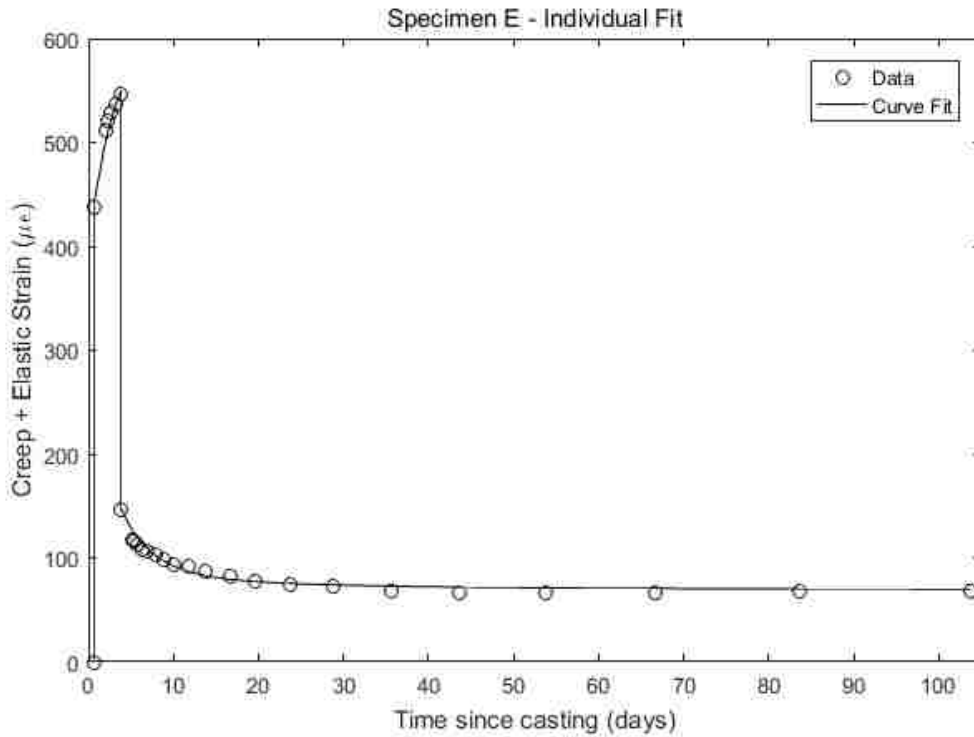
Table 10.4 Calibrated Parameter Values for Specimen A

$E^1_{k,28}$ (ksi)	14596
τ^1 (days)	34.3
a^1	1.013
n^1	1.50
$E^2_{k,28}$ (ksi)	34000
τ^2 (days)	2.2
Objective function value	0.59

The fit to the curve from Specimen E is shown in Figure 10.8. A great fit is achieved throughout the test period. The parameters from the individual fit to Specimen E are given in Table 10.5. The value of the

113

objective function for Specimen E was 1.20, whereas it was 3.06 for the model configuration that was calibrated to fit all nine datasets.
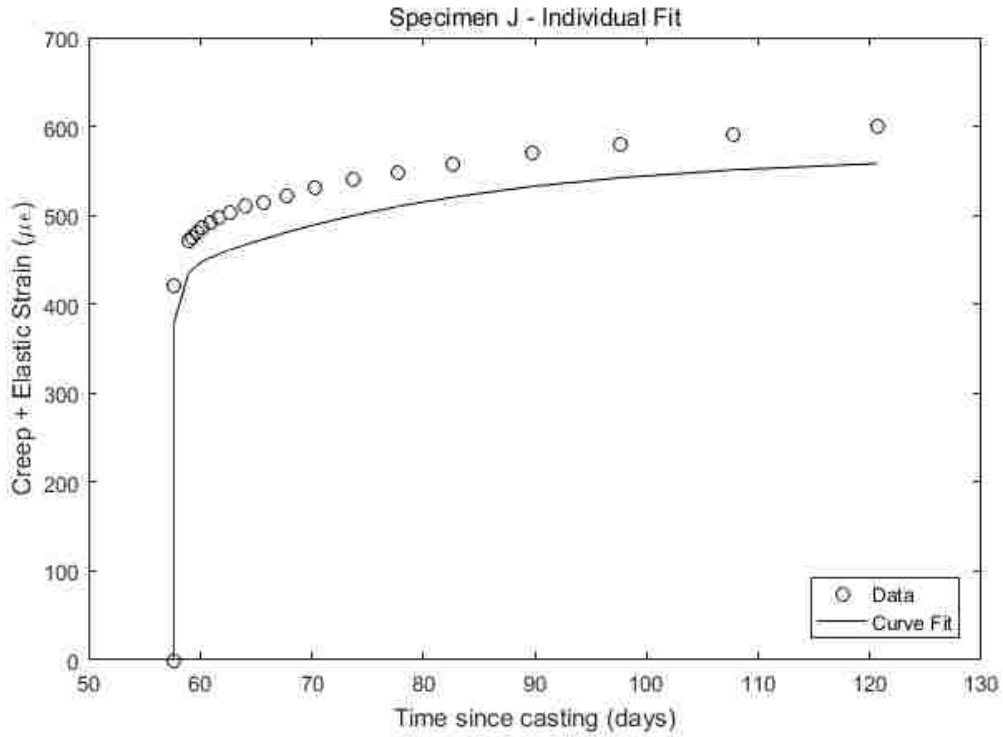

Figure 10.8 Individual Fit to Specimen E

Table 10.5 Calibrated Parameter Values for Specimen E

$E^1_{k,28}$ (ksi)	24500
τ^1 (days)	20.4
a^1	1.33
n^1	1.50
$E^2_{k,28}$ (ksi)	26000
τ^2 (days)	3.65
Objective function value	1.20

The fit to the curve from Specimen J is shown in Figure 10.9. At first sight, this fit does not look very good. This can be explained by the fact that the elastic value measured for the unsealed cylinder of Specimen J was higher than expected and anomalous to the rest of the elastic strain data. The elastic spring, therefore, predicts a lower elastic strain value than was observed in the specimen. Figure 10.9 shows the curve fit to the creep strain only. The value of the objective function for Specimen J was 0.47, whereas it was 5.69 for the model configuration that was calibrated to fit all nine datasets.

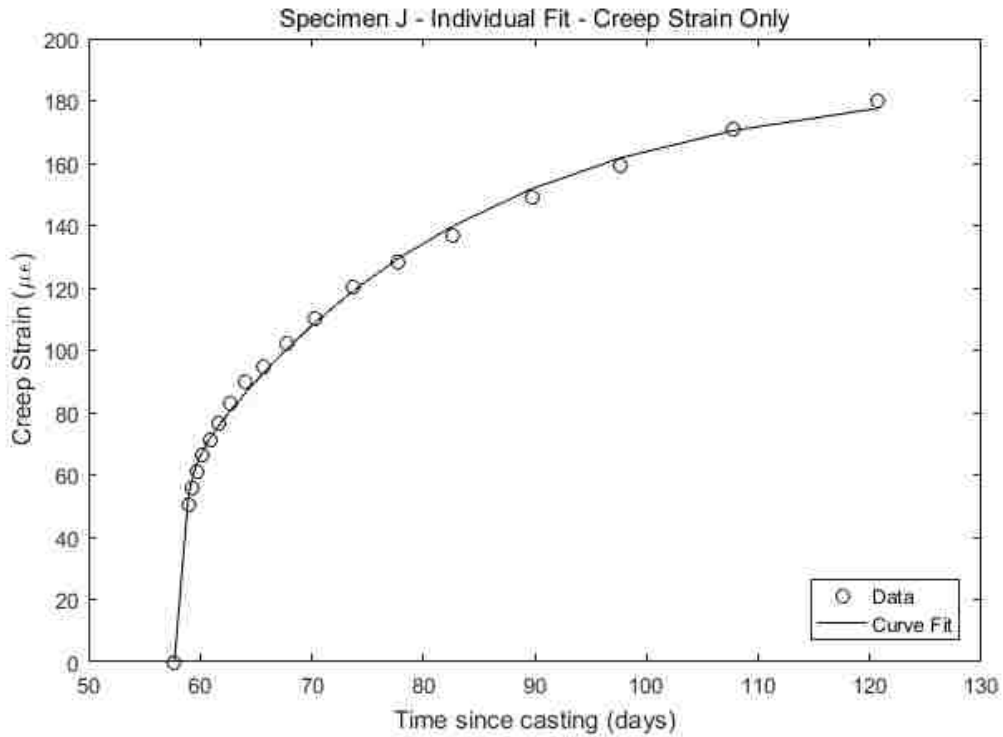**Figure 10.9 Individual Fit to Specimen J**

Figure 10.10 Individual Fit to Specimen J – Creep Only

115

Figure 10.10 shows that the curve fits well to the creep data. The parameters from the individual fit to Specimen E are given in Table 10.6.

Table 10.6 Calibrated Parameter Values for Specimen J

$E^1_{k,28}$ (ksi)	20000
τ^1 (days)	25.0
a^1	1.23
n^1	0.41
$E^2_{k,28}$ (ksi)	47700
τ^2 (days)	0.71
Objective function value	0.47

CHAPTER 11 DISCUSSION

This chapter discusses some of the key findings of this research.

11.1 Test Setup

The testing procedures provided consistent and reliable long-term data on the elastic, shrinkage and creep strains for hot-cured concrete. The confidence in the measurements stems is attributable to the consistency of the measurements.

- The measured elastic strains in the sealed an unsealed cylinders were consistent. For a total of set of 16 measurements of elastic behavior (11 specimens loadings and 5 unloadings), the ratio of the elastic strains measured in the sealed and unsealed cylinders had an average value of 0.99 with a coefficient of variation of 4.8%.

- Each of 12 shrinkage cylinders (six sealed and unsealed) cylinders were monitored with two strain gages each. All of the gages on the unsealed cylinders appeared to perform well, but three of the sealed-cylinder gages malfunctioned (Appendix B.12). For the 6 pairs of gages for the unsealed cylinders, the average absolute difference between the measurements from the two gages at 100 days was 38$\mu\varepsilon$. For the three remaining pairs of sealed cylinders, the corresponding average absolute difference was 25$\mu\varepsilon$.

- It was difficult to determine the consistency of the creep measurements, because the three gages did not provide any redundancy for strain measurements resulting from an eccentric load.

- None of the 33 gages on the unsealed cylinders appeared to fail. In contrast, 8 of the 33 gages on the sealed cylinders appeared to malfunction.

11.2 Material Behavior

The time-dependent function chosen to fit the compressive strength data fit well to data from both hot-cured and ambient-cured concrete. The hot-cured concrete gained strength faster at early ages and this was represented in the curve fits as the parameter n was higher for the hot-cured fit than for the ambient-cured one. The higher this parameter is the faster early strength gain is predicted by the time dependent function. The parameter t_0, which is a time offset that offsets the time of the start of strength gain from 0, was assumed to be 5 hours. This assumption was based on backing out an intercept to the x-axis when the strength data was plotted against time.

The elastic modulus for the hot-cured concrete was also higher at early ages than for the ambient-cured concrete but then dropped a little before resuming a steady increase with time. This was surprising as both strength and elastic modulus are usually assumed to be always increasing with time. This trend has,

117

however, been observed before at CTC (Chapman, 2016). The elastic modulus fit well to the compressive strength at all ages. The parameters yielded by the fit fell between the values given by ACI and AASHTO. Elastic modulus values derived by dividing the stress in the creep rigs by the measured values of elastic strain in the specimens agreed well with measured elastic modulus values, apart from values derived from partial unloadings. The cause of this is believed to be the fact that the unloading procedure was rather crude and our ability to retain exactly the desired amount of stress after the partial unloading was limited. Another factor is that the stress change in each partial unloading was only a third of the initial loading, and if it is assumed that the same potential error in the load is the same every time, it will be a higher proportion of the total stress change in the partial unloading. It is, therefore, likely that the assumed stress change value from the partial unloading events contains some error.

Shrinkage measurements for the two hot-cured batches of concrete were in good agreement which is testament to the good quality of the data and the good performance of the VW gages. Hot-cured concrete shrank more than weekend-cured concrete which in turn shrank more than ambient-cured concrete. Sealed cylinders shrank less than unsealed ones across all specimens which is an indication that the sealing of the concrete was successful. Drying shrinkage seemed to mostly take place within the first 30-40 days while the autogenous shrinkage seemed to operate on a longer timescale. This seems a little unusual and might be a function of the low V/S ratio of the cylinders.

Sealed cylinders crept less than unsealed ones across the whole dataset, which is an indication that the sealing of the concrete was successful. An exception to this would be Specimen H where the sealed cylinder curve was lower than the unsealed one early one but caught up with it at around 100 days. This might be explained by a bad sealing job done on this particular specimen. Basic to total creep ratios, excluding Specimen H, ranged from 45-70% 7 days after loading and from 41-88% 100 days after loading. These ratios would most likely be different for different V/S ratios.

By comparing creep strains from specimens with different curing regimes it was observed that the hot-cured concrete crept the least, followed by the weekend-cured concrete and the ambient-cured concrete crept the most. This is surprising, as the shrinkage results told exactly the opposite story. Since shrinkage and creep are believed to be dependent on the same material properties it would make sense that curing regimes would have the same effect on shrinkage and creep. This was not found to be the case and an explanation for why this is so was not found.

The time of loading of the hot-cured concrete, rather oddly, did not seem to have an effect on the total creep for ages of loading ranging from 1-8 days. Hot-cured concrete loaded at 12.7 days crept less than the three specimens loaded within 8 days and hot-cured concrete loaded at 57.7 days crept considerably

less than the one loaded at 12.7 days. The time of loading does therefore seem to have an effect on the total creep in the sense that the older the concrete is when it is loaded, the less it creeps. This effect was however expected to also be observed with concretes loaded within 1-8 days, which did not turn out to be the case.

Similar to behavior observed in shrinkage, the drying creep seemed mostly to take place within the first 30-40 days while the basic creep seemed to operate on a longer timescale. This seems a little unusual and might be a function of the low V/S ratio of the cylinders.

Specimens that underwent unloading at any time in the test period provided data on creep recovery. These three specimens all seemed to indicate that basic creep is recoverable while drying creep is not, since almost all creep was recovered in the sealed cylinders of these three specimens whereas the unsealed cylinders all had some residual creep. Branson (1977) claims that this is in fact the case.

Results of the chapter on superposition seem to suggest that while the principle of superposition is not likely to be entirely accurate, given the complexity of the chemical processes that take place within in the concrete over time, it is close enough as an approximation to have value as a practical design method. There is however an apparent trend throughout these results that creep recovery predicted by superposition, obtained by subtracting creep of a previously unloaded specimen happens more quickly than actual creep recovery of a previously loaded specimen that is being unloaded.

11.3 Proposed Model

The model outlined in Chapter 9 was able to fit the data well in the 2 Kelvin element configuration using one element with constant parameters and one with changing parameters. The fit was good when the optimization was done across all specimens at once and thus, a single set of parameters was obtained, independent of the time of loading, the loading value and the loading history. It was also demonstrated that the model is able to fit to the data even more closely if the optimization is done on a single specimen at a time. Doing this, however, would mean that one set of parameters would be obtained for each of the specimens which would not be applicable to any other type of loading history or time.

This particular model configuration was able to fit the data well out to 100 days but when data have been collected over a longer period of time, a re-calibration should be done. It is quite possible that one or more Kelvin elements would have to be added to predict behavior that happens further out than 100 days from the time of loading. This is due to the fact that each Kelvin element has asymptotic behavior towards a certain value and if creep strains in the concrete are continuing to increase after 100 days, these 2 Kelvin

elements will not be able to predict that. A third Kelvin element with a large time constant would be needed to model that potential behavior more closely.

Time constants for the Kelvin elements ranged from 3-33 days. These values are lower than suggested by Barr (2000). In his thesis he found that the majority of the creep and shrinkage occurred in the first 100 days. However, Barr did his tests on girders, not cylinders and the girders had a different V/S ratio than the cylinders used in this study. Again, a re-calibration with data that cover a longer time period might shed some more light on this subject.

CHAPTER 12 SUMMARY, CONCLUSIONS AND RECOMMENDATIONS

12.1 Summary

The first objective of this thesis was to design and conduct an experiment to measure the elastic, shrinkage and creep strains of hot-cured, high-strength concrete used in precast prestressed bridge girders. As discussed in Chapter 3, eleven specimens were tested with different times of loading, levels of loading and loading histories. For the sake of comparison, two of the eleven specimens had alternate curing regimes: weekend- and ambient-curing. Each specimen consisted of one sealed and one unsealed cylinder stacked on top of each other and loaded in a creep rig, as well as a set of unloaded, sealed and unsealed cylinders to measure shrinkage. Specimens from the same batch and with the same curing regime shared shrinkage cylinders in order to minimize the amount of concrete and the number of gages needed. Strains were measured using vibrating wire gages glued to the cylinders and connected to a data acquisition system, which recorded data every four minutes for the entire test period. This approach yielded a lot of data, so the dataset was reduced, as described in Chapter 4.

Concrete from a different but nominally identical batch to the concrete used for those 11 specimens was measured for strength and elastic modulus by Concrete Technology Corporation for a period of 56 days. These measurements were performed on hot-cured and ambient-cured concrete. A time-dependent function was designed for the strength gain of the concrete and a least-squares fit to the data was used to calibrate the parameters of the function. For the relationship between strength and modulus of elasticity, a generalized form of the time-dependent function used by ACI and AASHTO was fitted to the data.

Processed data for both shrinkage and creep was obtained and curves were fitted to the data in an attempt to detect any patterns from the parameters yielded from the fit. The effects of loading history, time of loading and curing regimes were inspected by considering the measured elastic strains (Chapter 5), shrinkage strains (Chapter 6) and creep strains (Chapter 7). Data from specimens that were loaded and then unloaded were inspected in order to see whether creep was fully, partially or non-recoverable. The validity of the principle of superposition for creep strains was evaluated in Chapter 8.

A one-dimensional rate-type model based on visco-elastic behavior was developed to predict creep strains for hot-cured high strength concrete with a variable stress history (Chapter 9). The model consists of a single elastic spring in series with any number of Kelvin elements which themselves consist of a linear spring in series with a linear dashpot. All the springs and dashpots may have time-dependent properties. This feature allows the model to follow the time variations in the elastic modulus of the concrete and to model non-recoverable creep. The model may be formulated for either stress as a function of given strain

(such as in a relaxation test) or strain as a function of given stress (such as in a creep test, like the one described in this thesis).

The model was calibrated in four different configurations. In all cases, the elastic spring was made to represent the elastic modulus of the concrete and the modulus of elasticity of the spring with time was taken as the best-fit curve to the elastic modulus data created in Chapter 5. The Kelvin elements, representing the creep, were calibrated in the following configurations:

- One Kelvin element with constant parameters
- One Kelvin element with time-dependent parameters
- Two Kelvin elements with constant parameters
- Two Kelvin elements, one with constant parameters and a second one with time-dependent parameters

12.2 Conclusions

The test and analysis program led to conclusions about the test procedures, the measured material behavior and the proposed numerical model.

12.2.1 Test Setup

The high quality of the measured data suggests that the VW gages work well for measuring long-term shrinkage and creep strains (Section 11.1). The use of automatic VW gages connected to a datalogger made it possible to eliminate the measurement errors of using more traditional manual Whittemore gages. The consistency of the measured data between gages in a particular test, and between tests, suggests that the data are of high quality. However, some problems were experienced with malfunctioning gages on some of the sealed cylinders, and the data only covers 100 days.

12.2.2 Material Behavior

- Elastic moduli derived from measured elastic strains from loaded specimens in the creep rigs were nearly identical for the sealed and unsealed cylinders. The inferred elastic moduli from the creep-rig elastic deformation were consistent with the elastic modulus values independently measured by CTC. The data could be approximated with the following equation:
  - $E_c(t) = 0.012w^{1.89}\bar{f}_c(t)^{0.4}$

    where w = unit weight of the concrete (pcf)

    $\bar{f}_c(t)$ = compressive strength with time (psi)

122

- Contrary to expectations, the hot-cured specimens shrank more that both the ambient- and weekend-cured specimens.

- The ratio of the basic to total creep ratios for all specimens (except for H, for which there was reason to believe that the sealing of the sealed cylinder was unsuccessful), ranged from 45-70% at 7 days after loading. This ratio ranged from 41-88% at 100 days after loading.

- Drying creep seems to have occurred over a shorter time period than basic creep with the 4"x8" cylinders used here. Across all specimens, most of the 100-day drying creep happened within the first 20 days and the drying creep was approximately constant from 30-40 days onwards. This might be due to a low volume to surface ratio, or it might be a property of hot-cured concrete, or both.

- The age at loading had almost no effect on total creep strains for loading ages up to 7 days. After 100 days, concrete loaded at age 7 days had crept almost exactly the same amount as concrete loaded after 0.7 days or 3.8 days. However, concrete loaded at 12.7 days had considerably less creep at 100 days and concrete loaded at 57.7 days had considerably less creep than earlier loaded concretes, 63 days after loading.

- Early loaded ambient- and weekend cured concretes had similar levels of total creep after 100 days, but early loaded hot-cured concrete had crept considerably less after 100 days. This finding is the reverse of that for shrinkage.

- Data from the unloaded specimens suggests that basic creep is fully recoverable while drying creep is not.

- Results suggest that, while the principle of superposition is not likely to be entirely accurate given the complexity of the chemical processes that take place within in the concrete over time, it is a close enough approximation to have value as a practical way of predicting response to time-varying stress histories.

12.2.3 Proposed Model

- The combination of an elastic element and a series of Kelvin elements provides a versatile way of modeling the elastic and creep behavior of concrete. Of the model configurations tested in this project, the one with two Kelvin elements, one with constant parameters and one with changing parameters, yielded the best results, on average. The model was able to fit the entire dataset, including the specimens with partial or complete unloading, with an rms. error of only 3.26 microstrain, and a worst rms. error (in Specimen J) of 5.69 microstrain. When the parameters were optimized against data from a single specimen, the fit was much closer. A convenient

feature of this configuration is that the element with constant parameters can account for recoverable creep while the one with changing parameters can account for non-recoverable creep.

12.3 Recommendations for Further Research

- More data over a longer time period is needed for more thorough calibration of the model. In its current state the model can only be said to do a good job of predicting creep strains out to 100 days.
- The effect of the volume-to-surface ratio should be investigated by using bigger cylinders. This model can work as a module for creep predictions into the camber program developed by Davison (2013).
- A more thorough study of recoverable vs. non-recoverable creep should be conducted.
- The creep and shrinkage of weekend- and ambient-cured concretes should be studied in more detail. Data from those studies would be relevant to makers of precast bridge girders just like the data presented in this thesis.
- The creep and shrinkage of self-consolidating concrete (SCC) should be studied. The industry is moving towards using SCC in place of traditional reinforced concrete.
- A configuration of the model using two Kelvin elements, one with constant parameters and one with changing parameters is suggested for use in models for predicting camber in girders. A caveat should follow, however, as re-calibration with a longer dataset might yield different results for the model parameters. The model should be incorporated into a camber program such as Davison's (2013) and the predictions should be checked against actual measured camber histories.

Notation

a = Ratio between ultimate value and 28-day value in new time-dependent function

a = Strength gain constant for concrete in the ACI 209R-92 model

A = Cross sectional area

b = Strength gain constant for concrete in the ACI 209R-92 model

c = Multiplication constant for the equation predicting elastic modulus with time

C_{cu} = Creep coefficient

E = Modulus of elasticity

E_c = Modulus of elasticity of concrete

E_e = Modulus of elasticity of elastic spring

E_{eff} = Effective modulus of elasticity

E_k = Modulus of elasticity of Kelvin-element spring

$\bar{f}_c$ = Compressive strength of concrete

L = Length

n = Exponent in new time-dependent function

$n_{d,j}$ = Number of data points for Specimen j

n_f = Compressive strength exponent

n_s = Number of specimens

n_w = Unit weight exponent

r = Ratio of strengths at t_N days and 28 days

s = Strength gain constant for concrete in the GL2000 model

t = time

t_N = Time in days from which the ratio r is defined

t_0 = Time offset from zero in new time-dependent function

t_1 = Time in days when $\beta = 1$

t_{50} = Time it takes to reach 50% of ultimate strain value

w = Unit weight of concrete

β = Time-dependent function for concrete strength in the GL2000 model

δ = Relative incremental change in Elastic modulus

Δt = Time increment

$\Delta\varepsilon$ = Strain increment

$\Delta\sigma$ = Stress increment

ε = Strain

$\dot{\varepsilon}$ = Strain rate

$\ddot{\varepsilon}$ = Second derivative of strain with respect to time

ε_{el} = Elastic strain

ε_k = Strain in Kelvin-element

$\dot{\varepsilon}_k$ = Strain rate in Kelvin-element

$\ddot{\varepsilon}_k$ = Second derivative of strain in Kelvin-element with respect to time

ε_m = Measured strain from dataset

ε_p = Predicted strain from model

ε_{ult} = Ultimate strain

κ = Time-dependent function for concrete strength in the Kelvin-element model

η = Dashpot viscosity

σ = Stress

$\dot{\sigma}$ = Stress rate

τ = Intrinsic time constant of Kelvin-element

References

American Concrete Institute (ACI), 2014, *Building Code Requirements for Structural Concrete (ACI 318-14).* Farmington Hills, Michigan.

ACI Committee 209, 2008, *Guide for Modeling and Calculating Shrinkage and Creep in Hardened Concrete (ACI 209.2R-08),* Farmington Hills, MI: American Concrete Institute.

American Association of State Highway and Transportation Officials (AASHTO), 2014. *LRFD Bridge Design Specifications*, 7th edition, Washington, D.C.

Barr, P. J., 2000, "Consistent Crudeness in Prestressed Concrete Girder Design," *Doctoral Dissertation,* Seattle, WA: University of Washington.

Bazant, Z. P., and Panula, L., 1978, "Practical Prediction of Time Dependent Deformations of Concrete, Parts I-IV," Materials and Structures, V. 11, pp. 307-316, 317-378, 425- 434; V. 12, pp. 169-183.

Branson, D. E., 1963, "Instantaneous and Time-Dependent Deflections of Simple and Continuous Reinforced Concrete Beams," *Report* No. 7, Part I, Alabama Highway Research Department, Bureau of Public Roads, Aug., pp. 1-78.

Branson, D. E., 1964, "Time-Dependent Effects in Composite Concrete Beams," ACI Journal, *Proceedings* V. 61, No. 2, Feb., pp. 213-230.

Branson, D. E., 1968, "Design Procedures for Computing Deflections," ACI Journal, *Proceedings* V. 65, No. 9, Sept., pp. 730-742.

Branson, D.E., 1977, *Deformation of Concrete Structures*, McGraw Hill Book Co., New York.

Branson, D. E., and Chen, C. I., 1972, "Design Procedures for Predicting and Evaluating the Time-Dependent Deformation of Reinforced, Partially Prestressed and Fully Prestressed Structures of Different Weight Concrete," *Research Report*, Civil Engineering Department, University of Iowa, Iowa City, IA, Aug.

Branson, D. E., and Christianson, M. L., 1971, "Time Dependent Concrete Properties Related to Design—Strength and Elastic Properties, Creep and Shrinkage," *Creep, Shrinkage and Temperature Effects,* SP-27, American Concrete Institute, Farmington Hills, MI, pp. 257-277.

Branson, D. E., and Kripanarayanan, K. M., 1971, "Loss of Prestress, Camber and Deflection of Noncomposite and Composite Prestressed Concrete Structures," PCI Journal, V. 16, No. 5, Sept.-Oct., pp. 22-52.

Branson, D. E.; Meyers, B. L.; and Kripanarayanan. K. M., 1970, "Loss of Prestress, Camber, and Deflection of Noncomposite and Composite Structures Using Different Weight Concretes," *Final Report* No. 70-6, Iowa Highway Commission, Aug., pp. 1-229.

Branson, D. E., and Ozell, A. M., 1961, "Camber in Prestressed Concrete Beams," ACI Journal, *Proceedings* V. 57, No. 12, June, pp. 1549-1574.

Brooks, J. J., 2005, "30-year Creep and Shrinkage of Concrete," *Magazine of Concrete Research,* V. 57, No. 9, Nov., pp. 545-556.

Brown, A. O., 2005, "An Experimental Investigation into Superposition of Creep Strains for Concrete," *Masters Thesis*, Ottawa, Canada: University of Ottawa.

CEB, 1999, "Structural Concrete—Textbook on Behaviour, Design and Performance. Updated Knowledge of the CEB/FIP Model Code 1990", *fib Bulletin* 2, V. 2, Federation Internationle du Beton, Lausanne, Switzerland, pp. 37-52.

Chapman, D., 2016. Personal Communication. Concrete Technology Corporation (CTC).

Davison, B., 2013, "Prediction of Time-Dependent Stresses and Deflections in Prestressed, Concrete Girders: From Start of Fabrication to End of Service Life", *Masters Thesis,* Seattle, WA: University of Washington.

Gardner, N. J., 2004, "Comparison of Prediction Provisions for Drying Shrinkage and Creep of Normal Strength Concretes", *Canadian Journal for Civil Engineering*, V. 31, No. 5, Sept.-Oct., pp. 767-775.

Gardner, N. J., and Lockman, M. J., 2001, "Design Provisions for Drying Shrinkage and Creep of Normal Strength Concrete," *ACI Materials Journal*, V. 98, No. 2, Mar.-Apr., pp. 159-167.

Gardner, N. J., and Tsuruta, H., 2004, "Is Superposition of Creep Strains Valid for Concretes Subjected to Drying Creep?" *ACI Materials Journal*, V. 101, No. 5, Sept-Oct., pp. 409-415.

Geokon, 2016, *Instruction Manual Model 4000 (and 4050) Vibrating Wire Strain Gage,* Lebanon, NH: Geokon Inc.

Hillsdorf, H. K., and Carreira, D. J., 1980, "ACI-CEB Conclusions of the Hubert Rusch Workshop on Creep of Concrete," Concrete International, V. 2, No. II, Nov., p. 77.

Kuttner, C. H., 1997, "Creep and Shrinkage for Windows: the Program for the RILEM Databank," Karlsruhe University, Version 1.0, Weimar, Berlin and Karlsruhe, Germany.

McDonald, D. B., 1990, "Selected Topics on Drying Shrinkage, Wetting Expansion, and Creep of Concrete," PhD thesis, School of Civil and Mining Engineering, Sydney University, Australia.

McDonald, D. B., and Roper, H., 1993, "Accuracy of Prediction Models for Shrinkage of Concrete," *ACI Materials Journal*, V. 90, No.3, May-June, pp. 265-271.

McHenry, D., 1943. "A New Aspect of Creep in Concrete and its Application to Design," Proceedings, ASTM, V. 43, pp. 1069-1084

Meyers, B. L.; Branson, D. E.; Schumann, C. G., and Christianson, M. L., 1970, "The Prediction of Creep and Shrinkage Properties of Concrete," *Final Report* No. 70-5, Iowa Highway Commission, Aug., pp. 1-140.

Muller, H. S.; Bazant, Z. P.; and Kuttner, C. H., 1999, "Data Base on Creep and Shrinkage Tests," Rilem Subcommittee 5 Repon RILEM TC 107-CSP, RILEM, Paris, 81 pp.

Muller, H. S., and Hilsdorf, H. K., 1990, „General Task Group 9, "CEB *Comité Euro-International du Béton,* Paris, France, 201 pp.

Pan, Z.; Lü, Z, and Fu, C. C., 2011, "Experimental Study on Creep and Shrinkage of High-Strength Plain Concrete and Reinforced Concrete," *Advances in Structural Engineering,* V. 14, No. II, Apr., pp. 235-248.

Robertson, I. N., 2000, "Correlation of Creep and Shrinkage Models with Field Observations," *The Adam Neville Symposium: Creep and Shrinkage-Structural Design Effects*, SP-194, A. AI-Manaseer, ed., American Concrete Institute, Farmington Hills, MI, pp. 261-282.

Wight, J.K., 2016. *Reinforced Concrete. Mechanics and Design,* 7th Ed, Pearson Prentice Hall, Upper Saddle River, NJ, pp. 79.

Appendix A Preliminary Work

Before any data could be collected, a considerable effort had to be put in to getting the creep rigs ready to go. Aside from the brute force labor required to disassemble the rigs, move them to the room where the experiments took place and assemble them there it was necessary to test the equipment in a variety of ways so as to gain as much control over the experiment conditions as possible. This appendix describes these tests and the conclusions drawn from them.

A.1 Rig Capacity

The capacity of the rig can be varied by changing the size and number of springs put in. We had two sizes of springs to choose from. The bigger one had an outer diameter of 8 inches, the diameter of the coil was 1.5 inches and it's free standing height was 8 inches. The smaller one had an outer diameter of 4.5 inches, a coil diameter of 1 inch and a free standing height of 7.8 inches. A load-deflection test was performed on both of the springs to determine their stiffness. Figure A.1 shows the results for the big spring and Figure A.2 shows the results for the small spring.
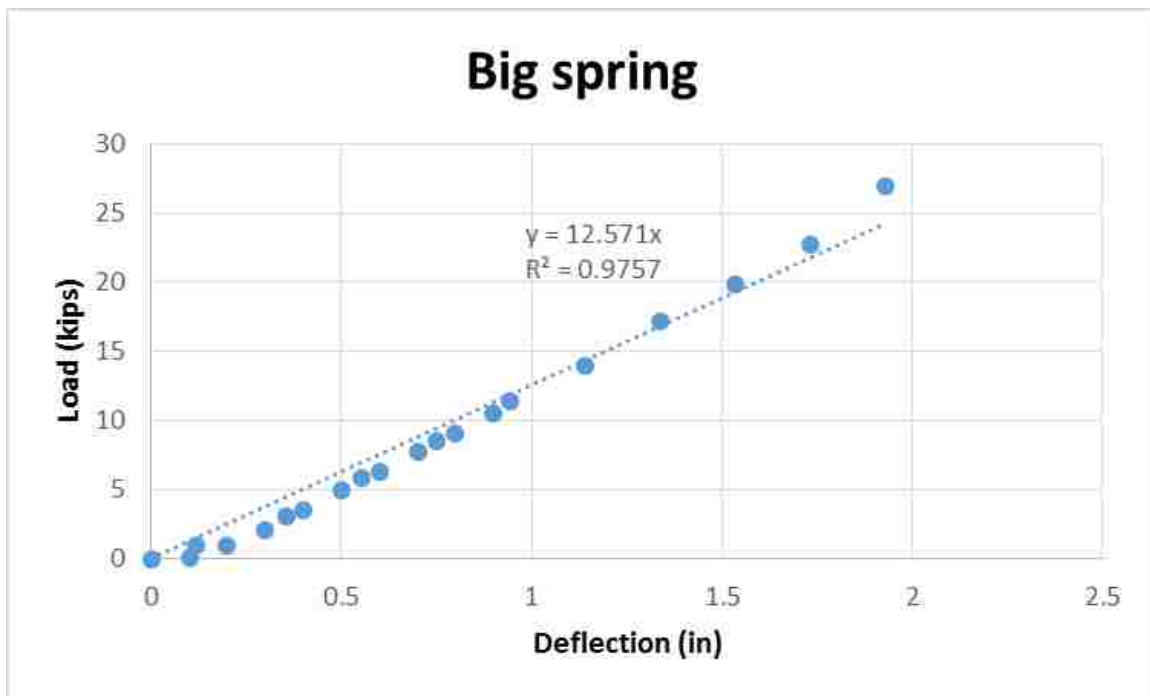
Figure A.1 Load-deflection Results for the Outer Spring in the Creep Rig
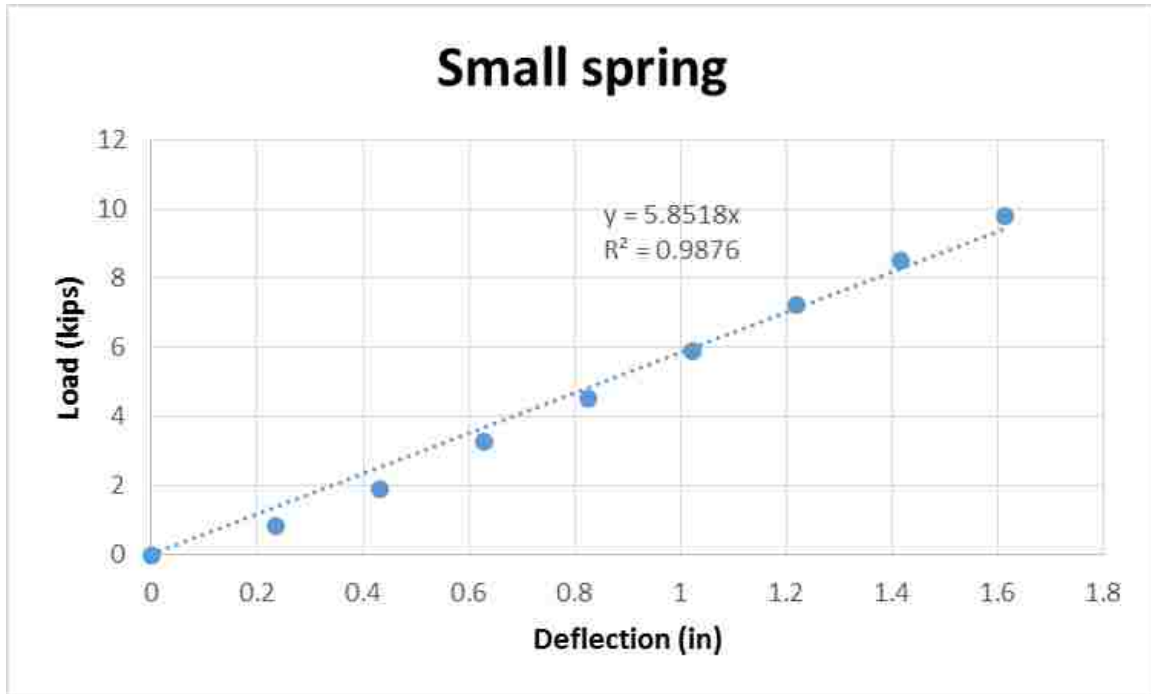
Figure A.2 Load-deflection Results for the Inner Spring in the Creep Rig

In the rig the springs are set up in sets which consist of a small spring inside a big one. If we combine the stiffness of the two springs we get a stiffness of 18.42 kips/in for each set. This is not entirely accurate as the free height of the springs varies a little so they don't start compressing at the same time. The true load deflection curve for a set of springs is therefore bi-linear. The big spring will deflect 0.2 inches before the smaller one comes into contact and the maximum deflection of the set is 2 inches. We can therefore assume that the capacity of each set is:

$$P_{max} = 12.571 \; ^{kips}/_{in} * 0.2in + 18.423 \; ^{kips}/_{in} * 1.8in = 35.676 \; kips$$

It is desirable that the rig can be used with as many different concrete strengths as possible and both with 6x12 cylinders and 4x8 cylinders. We assume an upper value of required capacity of loading a 6x12 cylinder with an $\bar{f}_c$ of 12500 psi to 40% of its strength. Thus

$$P = 0.4\bar{f}_c * A_{6x12} = 0.4 * 12.5ksi * 9\pi = 141.4 \; kips$$

With 4 sets of springs we get

$$P_{max} = 4 * 35.676 \; kips = 142.7 \; kips$$

With this check in mind it was decided to put 4 sets of springs in each rig.

A.2 Number of Gages

One of the things we had to decide on was how many gages we should put on each cylinder. It needed to be a compromise between technical and budgetary restrictions and the guarantee of getting reliable data. From a practical perspective it is virtually impossible to get completely rid of any eccentricity of load in the rigs. If the load was purely axial as would be ideal, only one gage would be needed on each cylinder. An experiment was carried out where six gages were stuck on a cylinder which was loaded in a rig. Two-, three- and four-gage averages were calculated and the coefficient of variance was calculated for all of the data. The cylinder was loaded twice for just over an hour each time to get data for elastic strains plus a little bit of creep. For the first loading the 3 gage averages showed the least variance by far. However for the second loading the 3 gage averages came off worse than both the 2 gage and 4 gage averages. In both cases the 2 gage averages showed the greatest variance and were therefore deemed an unfeasible solution. Having 4 gages on each cylinder would have been beneficial but it would have meant maxing out the multiplexers available and this would have reduced the number of specimens that could have been monitored simultaneously. As data from 3 gage averages was really in the same ballpark as data from 4 gage averages we decided to go with 3 gages per cylinder instead of investing in more expensive equipment. As the shrinkage cylinders are unloaded the eccentricity problem is not present and so 2 gages per cylinder was deemed sufficient for them.

A.3 Epoxy vs. Superglue

One of the problems we faced was how we should stick the strain gages on to the concrete. Two methods were proposed, a two part epoxy and superglue. After testing out both methods, it was apparent that the epoxy took much longer to mix and harden and was harder to apply. It was also observed to creep a little bit for the first hour of loading. The superglue however took under a minute to settle and didn't creep at all. When the actual tests were being set up a lot of things were happening in a short amount of time and having a quick and easy way to apply strain gages to the cylinders was of utmost importance. Therefore it was decided to go with the superglue.

A.4 Ram Calibration

A hydraulic ram connected to a hand pump was used to apply load to the rigs. In order to know how much load was being applied we had to calibrate the ram. A pressure gage on the line between the pump and the ram displayed the pressure in bars. Figure A.3 displays the relationship between the value read on the pressure gage and the ram force, as recorded in a calibrated test machine, converted to stress on a 4" diameter cylinder.
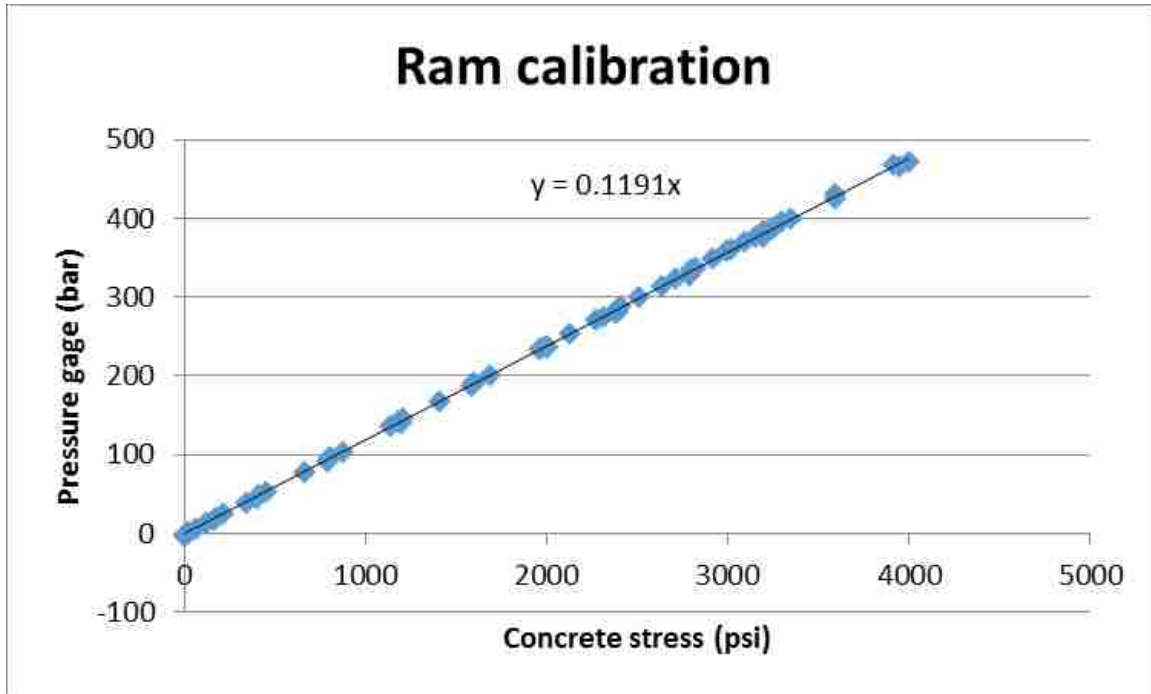
Figure A.3 Relationship between Value on Pressure Gage and Concrete Stress

A.5 Temperature Test

There were some concerns over whether temperature would greatly affect the gages. The gages are claimed to be temperature-independent, because the body of the gage and the vibrating wire are made from the same material. Thus, for a given temperature increase, both will expand by the same amount and the stress in the wire will remain the same. A test was conducted where a gage was hooked up to a handheld readout box and stuck in an oven. Changes in the oven temperature and strain reading of the gage were monitored in a temperature range from 25°C to 40°C and the strain reading range was about 20 με. That gives us a thermal coefficient of

$$\alpha = \frac{20\mu\varepsilon}{15°K} = 1.33 \,^{\mu\varepsilon}/_{°K}$$

This is about an order of magnitude smaller than the coefficient of thermal expansion for stainless steel, so it was concluded that the self-compensation was working satisfactorily. The temperature was expected to change by no more than 2°C, so the corresponding strain error was expected to be less than 3με. This was considered small enough to ignore.

A.6 Temperature and Relative Humidity in Test Room

For part of the test period the temperature and relative humidity in the room where the creep rigs were placed were recorded once per day. Readings were taken from a simple hygrometer with a digital thermometer. Data from these recordings is displayed in Figure A.4.

Figure A.4 Temperature and Relative Humidity in the Lab

A.7 Gage Factor Experiments

The vibrating wire gages come from the factory with a so called gage factor which is applied to the data to correct the values read by the gages. Geokon, the manufacturer of the gages suggests a factor of 0.96 to compensate for the fact that the method of wire clamping effectively shortens the vibrating wire slightly causing the strain to be over-registered. (Geokon 2016). However, elastic strains observed in prior experiments had been slightly lower than what was expected from stress over elastic modulus calculations. This made us think there were more factors at work than just this wire clamping error and we set out to find a gage factor that would get us close to the actual strains. The first experiment conducted was one where, instead of measuring strains in a concrete cylinder, an aluminum tube was stuck in one of the rigs with both the vibrating wire gages and some electric resistance (ERS) gages. These are applied straight onto the material being measured and not mounted on blocks that are glued on

it. If the shear resistance in the glue is a considerable factor then this experiment should pick up a difference in strains between the ERS gages and the vibrating wire gages. However, data from this experiment was so out of tune with what was expected and raised more questions than it answered that it was eventually abandoned (it appeared as the bending flexibility of the tube wall might have allowed the mounting blocks to rotate slightly, causing less shortening in the gages than the tube). Instead, a tension test on an aluminum rod was conducted with both ERS and vibrating wire gages. The idea behind the experiment was that by putting the aluminum rod under pure axial tension we could determine how far from the correct strain value the gages were since we assumed that we knew the elastic modulus of the aluminum pretty well. The rod was put twice under a 2.15 kip tension force and results from the tests can be seen in Table A.1.

Table A.1 Results from Tension Test

Test 1					
ERS 1	492	με	VW 1	410	με
ERS 2	600	με	VW 2	650	με
Average	546	με	Average	530	με
Ratio	**1.03**				
Test 2					
ERS 1	452	με	VW 1	440	με
ERS 2	509	με	VW 2	490	με
Average	480.5	με	Average	465	με
Ratio	**1.03**				

From these results it can be seen that some moment was existent in the experiment. The strains are also a bit bigger than expected since the cross-sectional area of the rod was only 0.5 in^2 and thus:

$$\varepsilon_{calc} = \frac{\sigma}{E} = \frac{P}{AE} = \frac{2.15 \; kips}{0.5 in^2 * 10000 ksi} = 430 \mu\varepsilon$$

It was therefore decided that these tests were not conclusive enough to start the actual tests. Instead we decided to do a standard elastic modulus test on two of the dummy cylinders we had been using for earlier tests and load them in a rig. This way, we would know the E of the concrete in question and the gages would be tested in the exact environment in which they would actually be operating in the real tests. The elastic modulus test yielded elastic moduli of 4786.5 ksi and 4943.4 ksi for the two cylinders. These two were stacked in a rig along with a third cylinder to make up the height and gaged with three gages each. The stack was loaded to 119.8 bar on the pressure gage on the pump which corresponds to about 1.006 ksi. The expected elastic strain was calculated for each cylinder from the known elastic moduli and these

values were compared with the measured ones. The geometric mean of the two ratios was taken and made to be exactly 1 by changing the gage factor via the goal seek function in Excel. This procedure yielded a gage factor of 1.125 as opposed to the 0.96 value recommended by Geokon. This result was plausible, because it suggested that the glue used to attach the blocks had some flexibility and caused the gage to strain less than the specimen. It was suspected that Geokon had calibrated their gage factor by loading the gages directly, rather than by using the mounting blocks, but the company was unable to confirm this. In the end, however, none of these results were deemed conclusive enough to use a different gage factor than the one recommended by Geokon. All of the data was therefore obtained by using a gage factor of 0.96.

A.8 Standardization of Loading Procedure

After the first set of loading had taken place, data from some of the specimen proved to be inconsistent with expectations. After some pondering, an inconsistency in the way the rigs were loaded was deemed the culprit. The bottom plates of the rigs were not all at the same distance from the springs and to compensate for that difference, a stack of steel plates had been used. This resulted in the fact that for some of the rigs, the piston of the ram would be extended very far and the piston may therefore have tilted slightly, leading to partial binding and friction against the cylinder wall. As a result of this only a part of the load observed on the pressure gage was transferred into the rig. To fix this problem we got rid of the steel plate stack all together and fixed the bottom plates of all the rigs to a distance of 7.5 inches from the bottom of the plate on which the springs sit. This distance is just enough to get the ram in between the plates and so the piston doesn't have to extend far out to start pushing against the plate. All data on elastic strains observed after this change was reasonably close to expected values.

Appendix B Raw Data

B.1 Specimen A
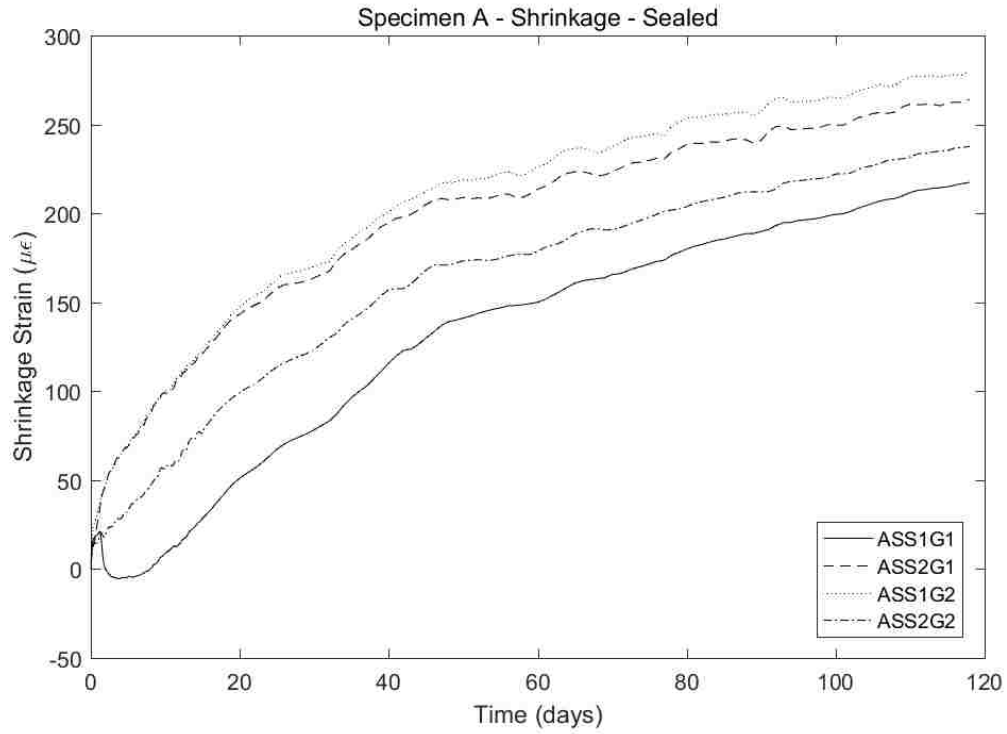
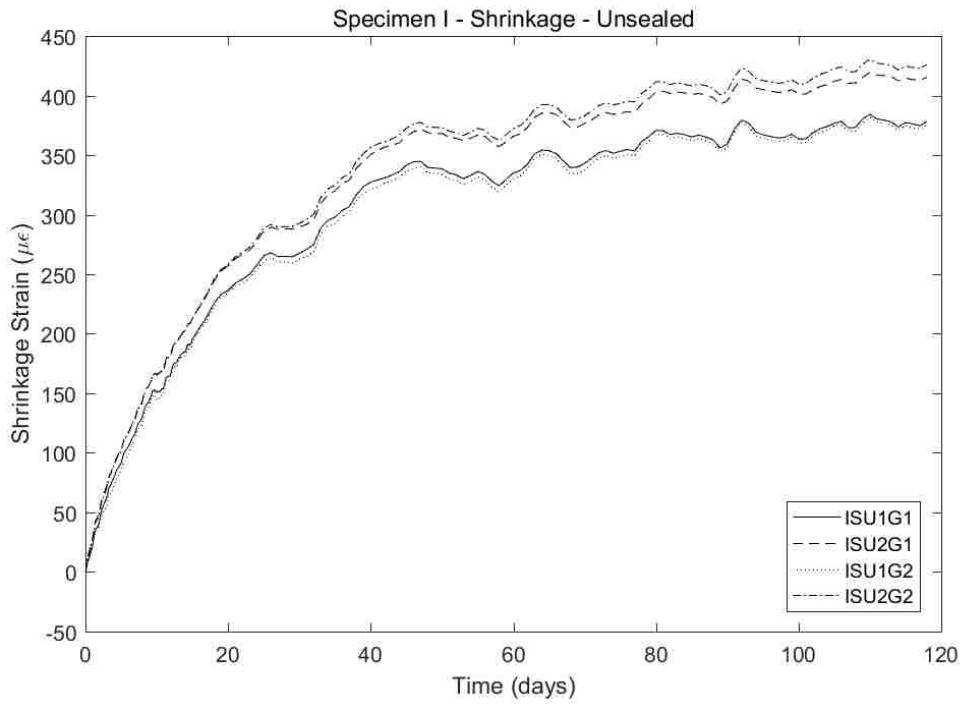**Figure B.1 Specimen A – Sealed Shrinkage Cylinder**
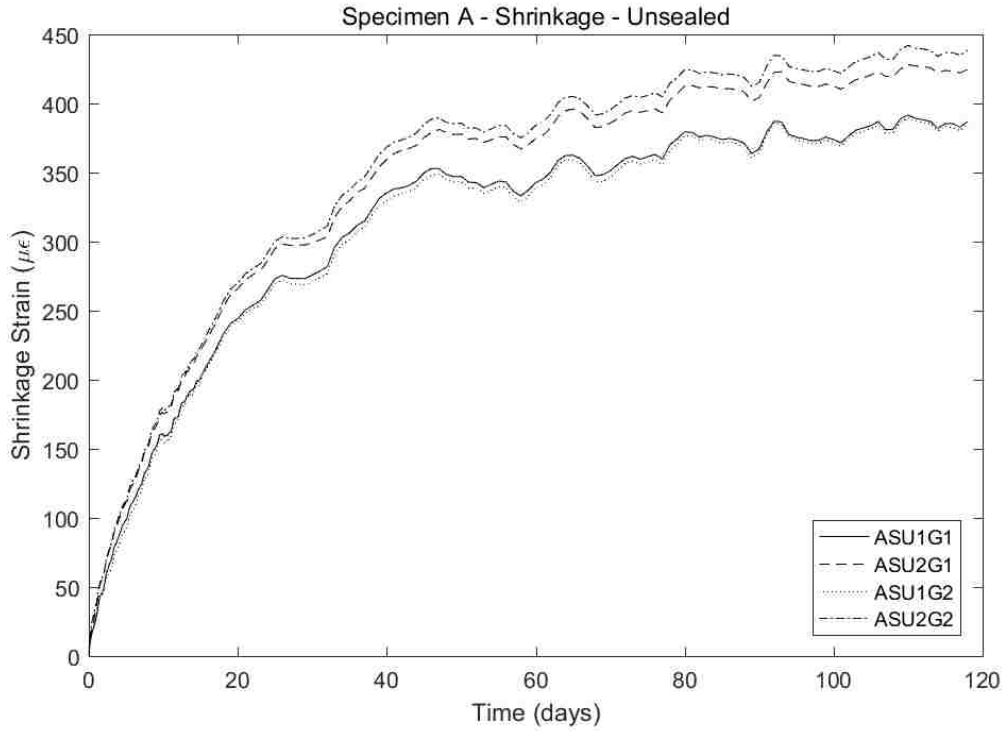
Figure B.2 Specimen A – Sealed Shrinkage Cylinder
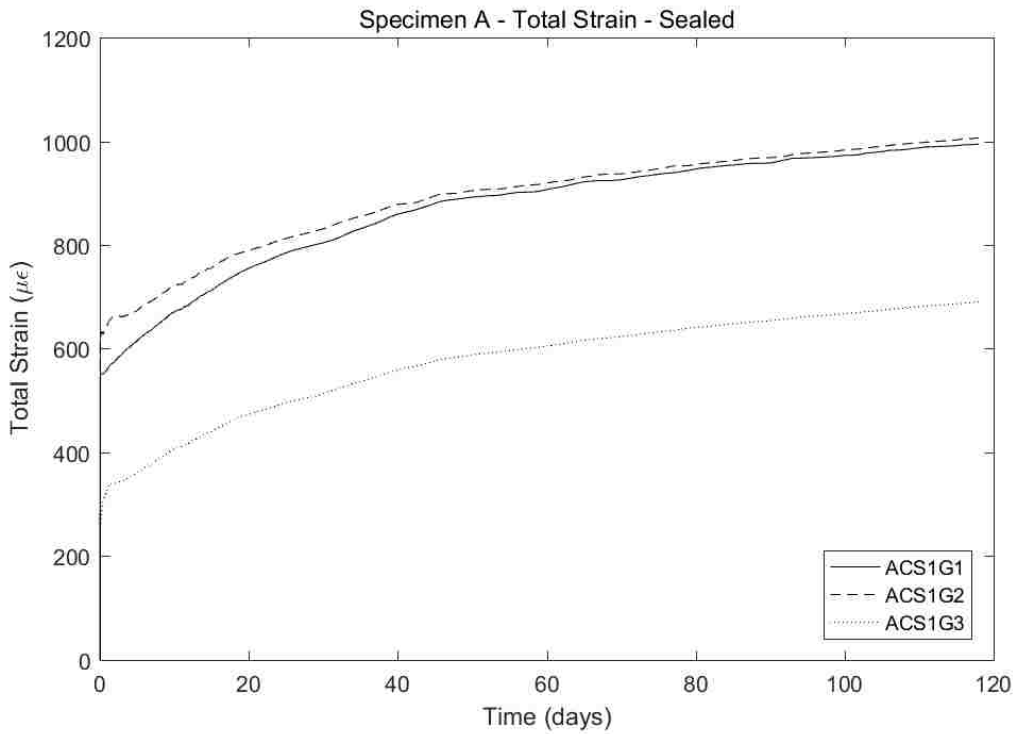
Figure B.3 Specimen A – Sealed Creep Cylinder
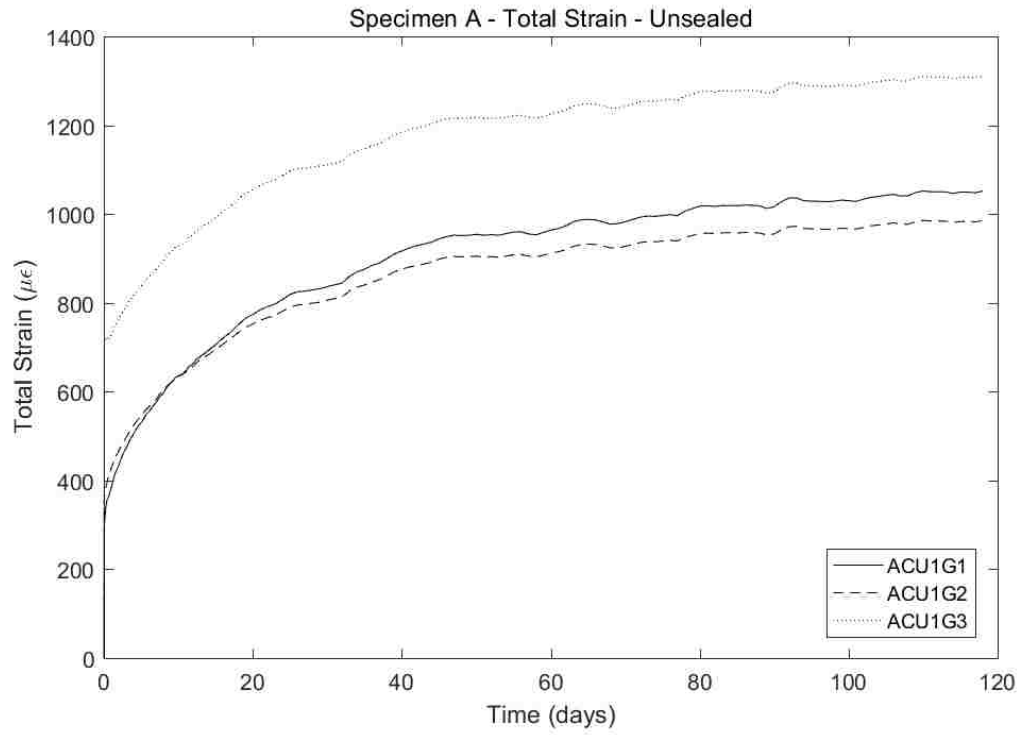
Figure B.4 Specimen A – Unsealed Creep Cylinder
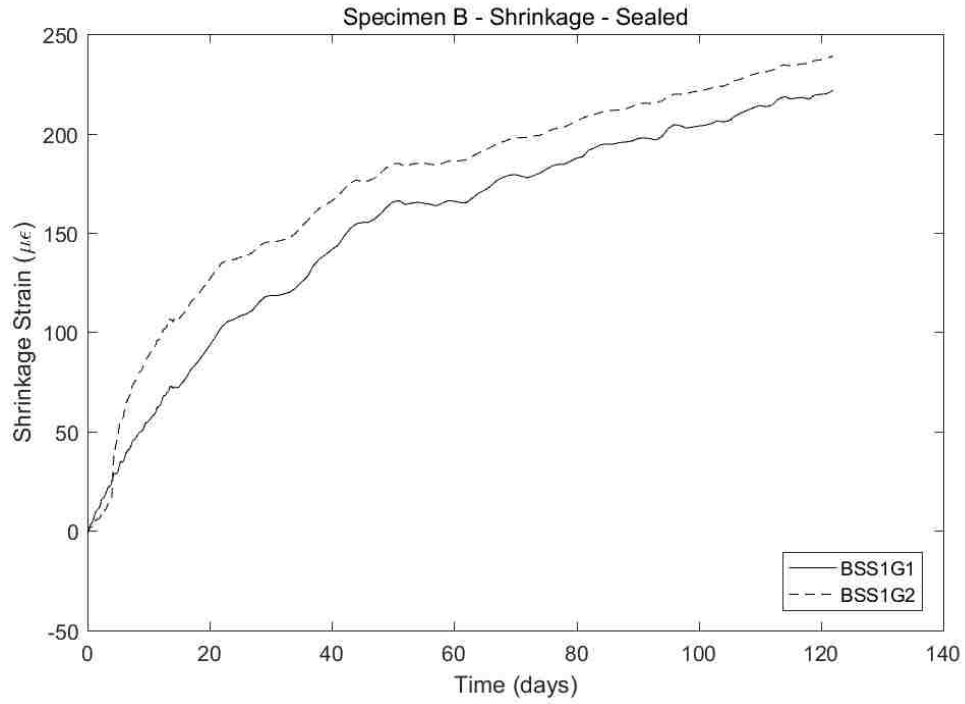
Figure B.5 Specimen B – Sealed Shrinkage Cylinder
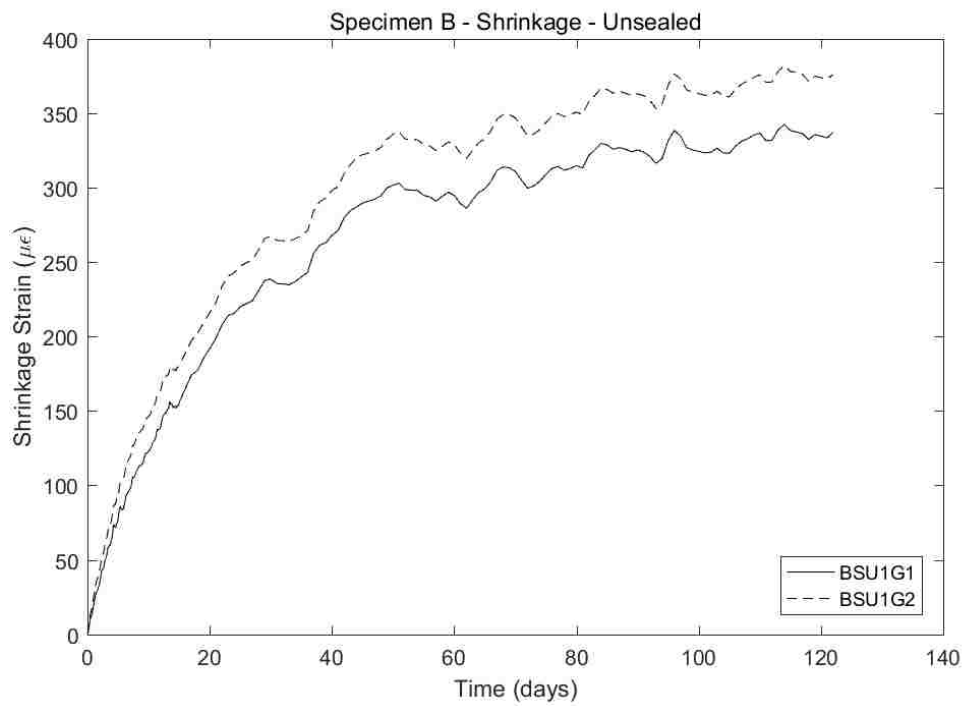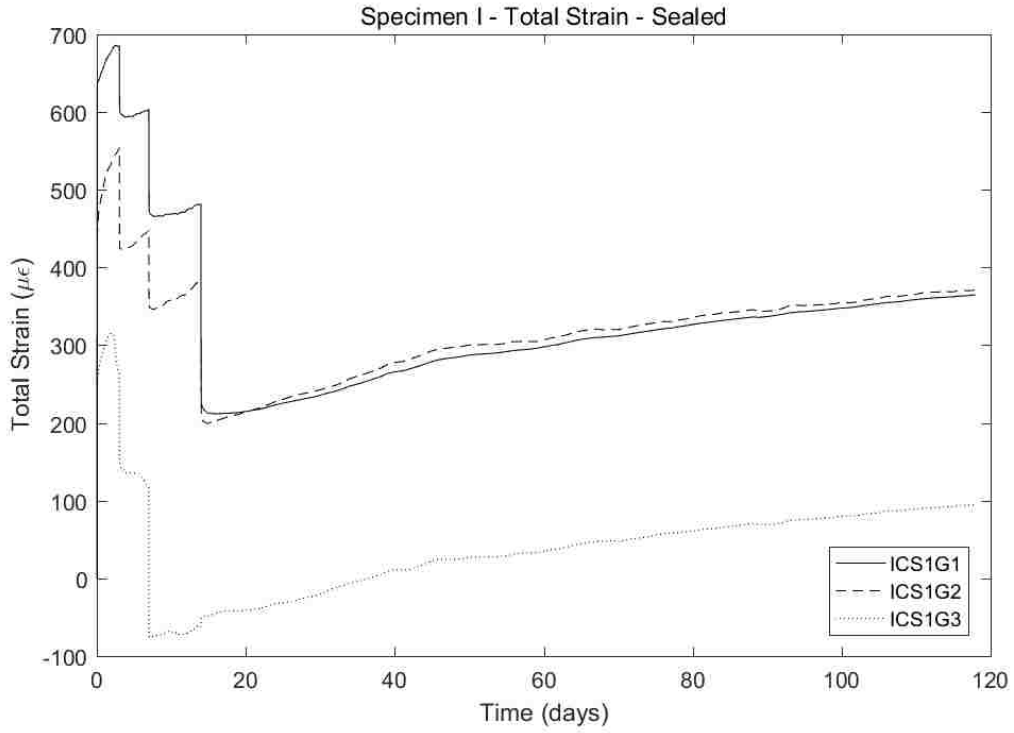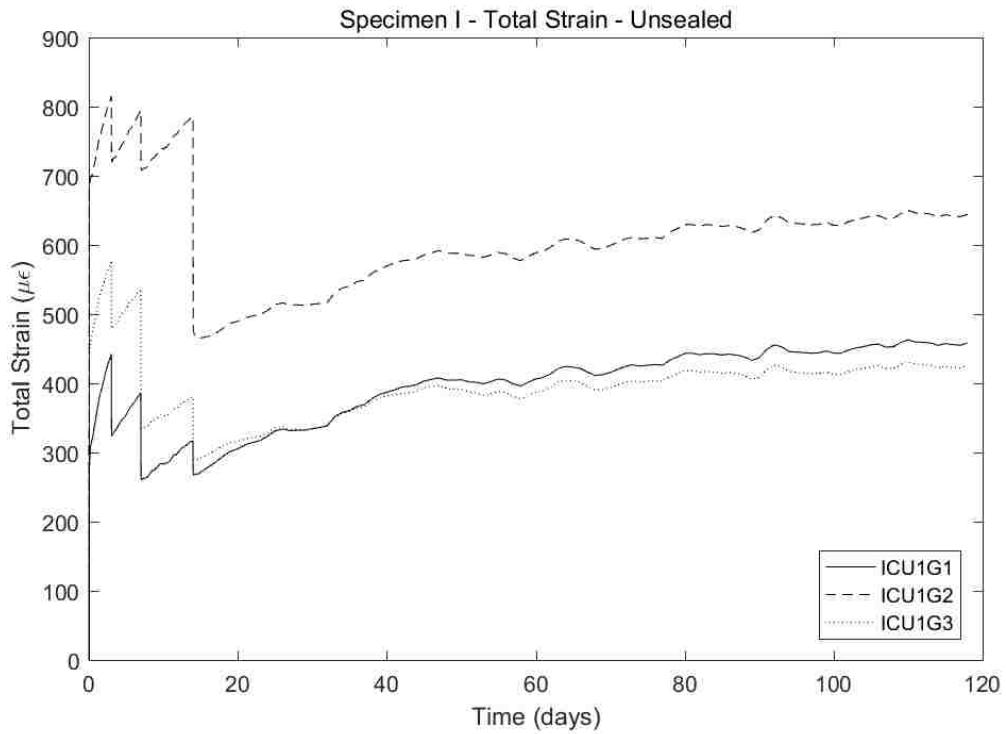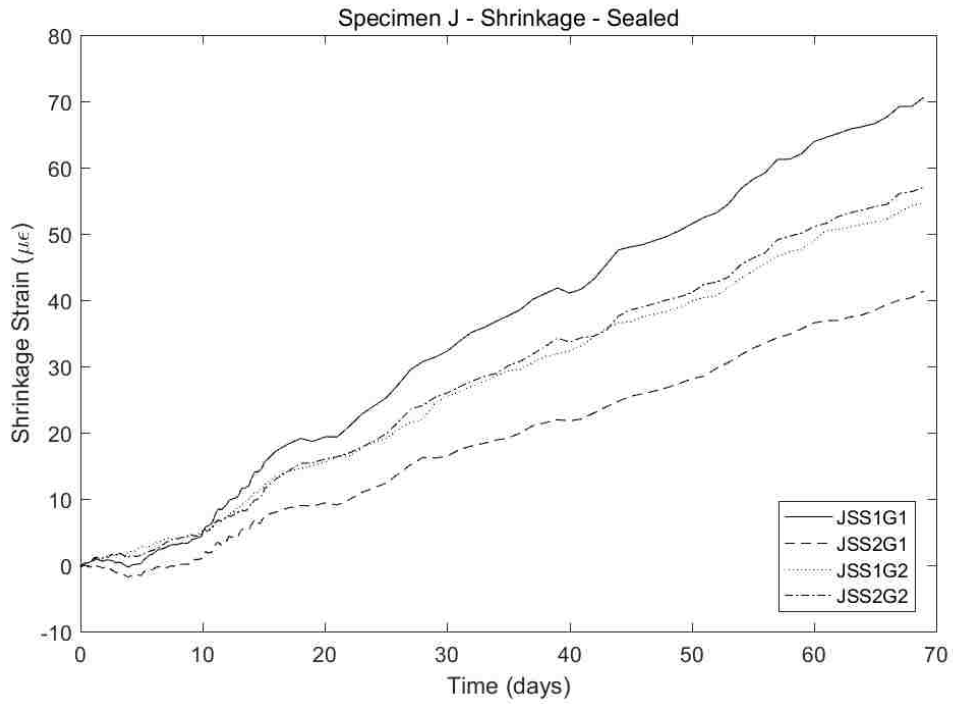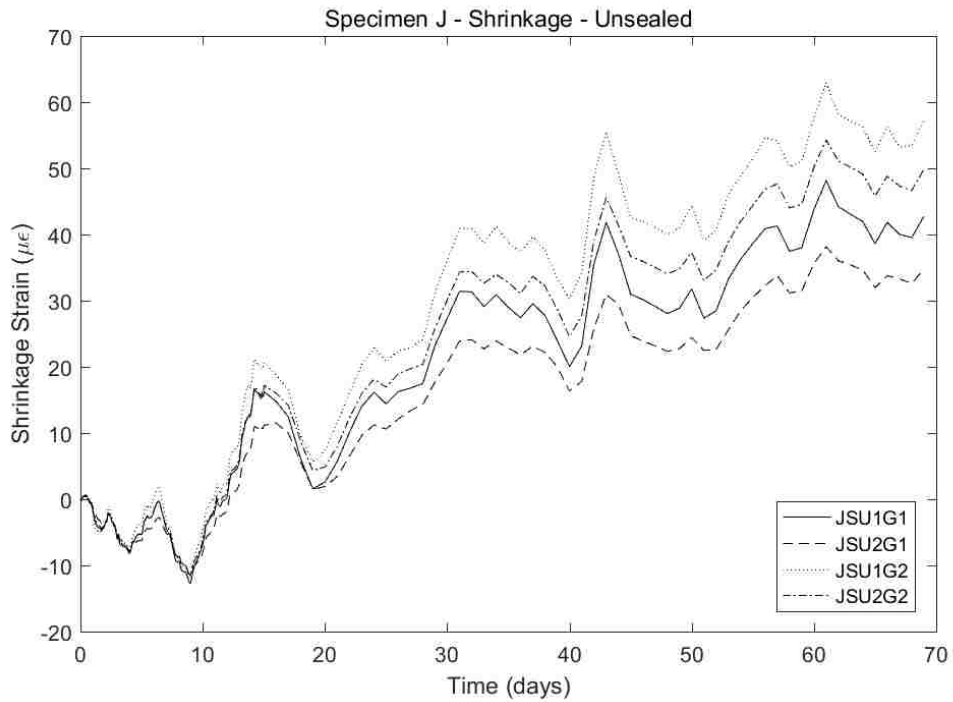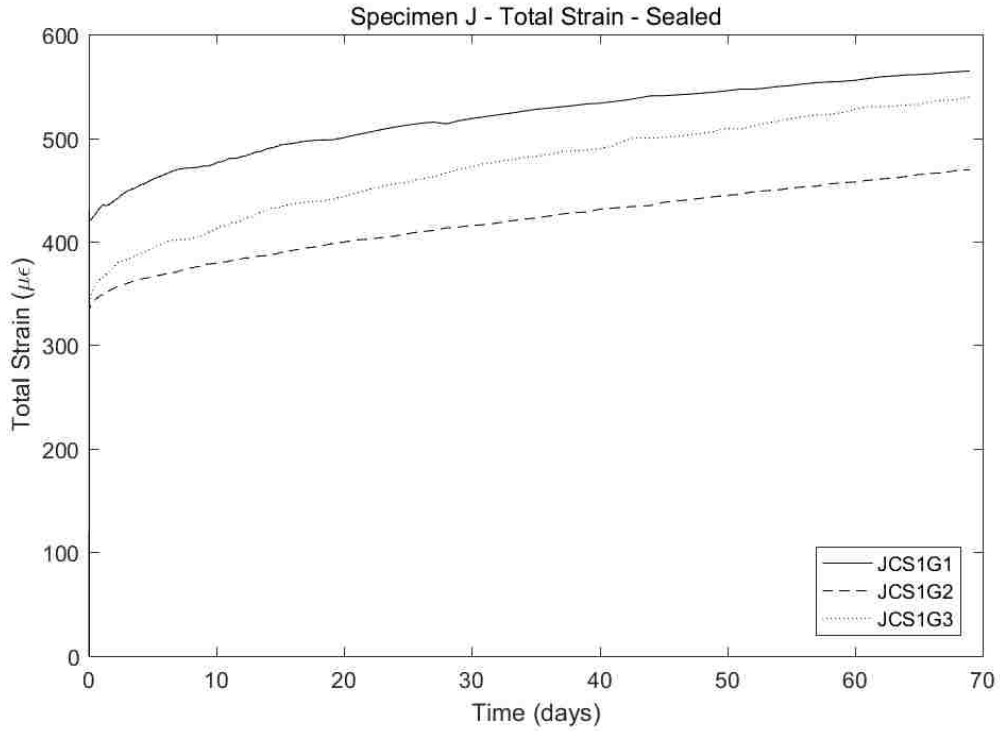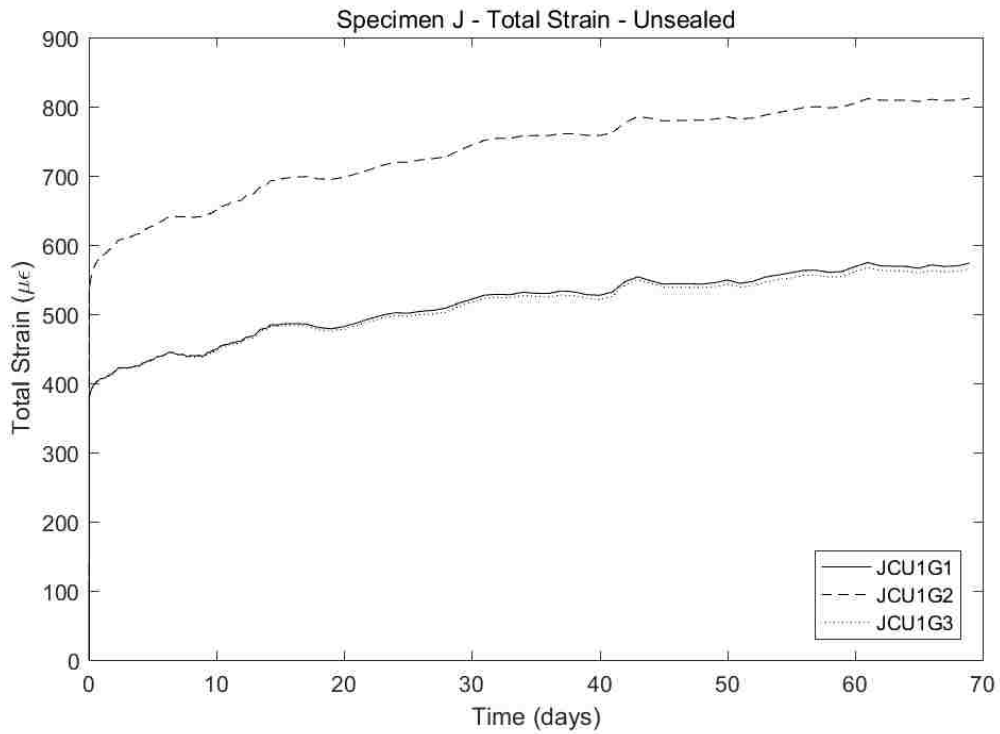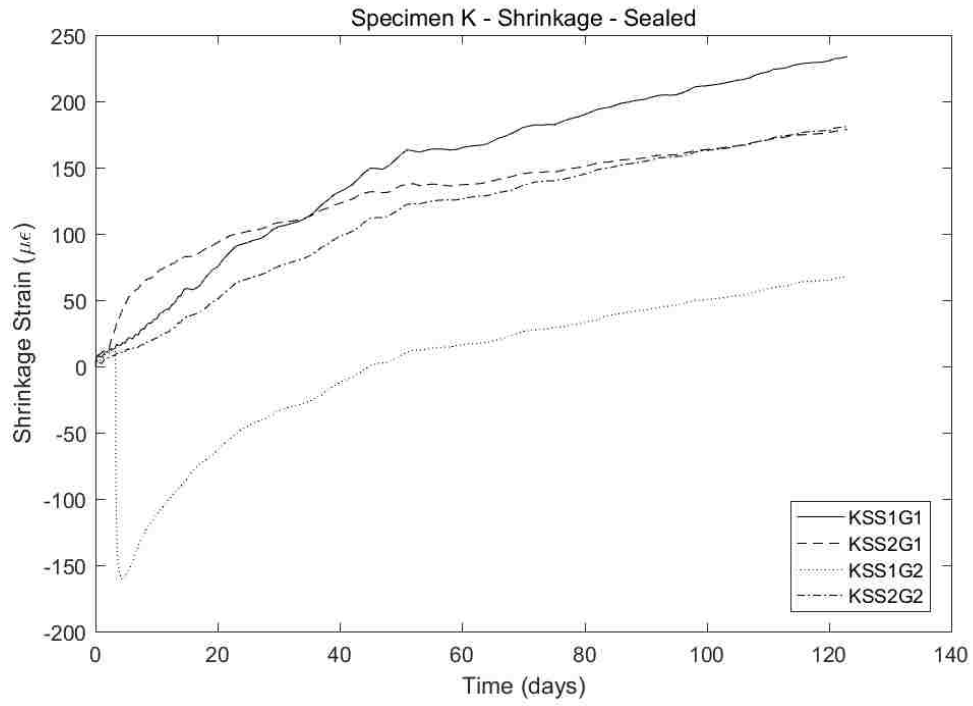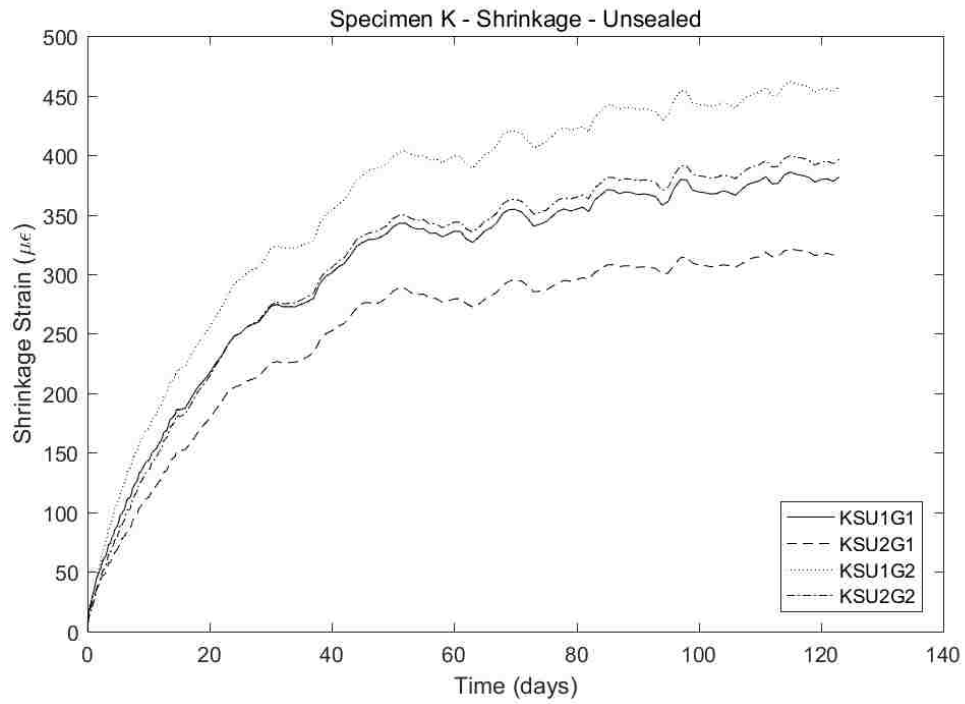

Figure B.6 Specimen B – Unsealed Shrinkage Cylinder
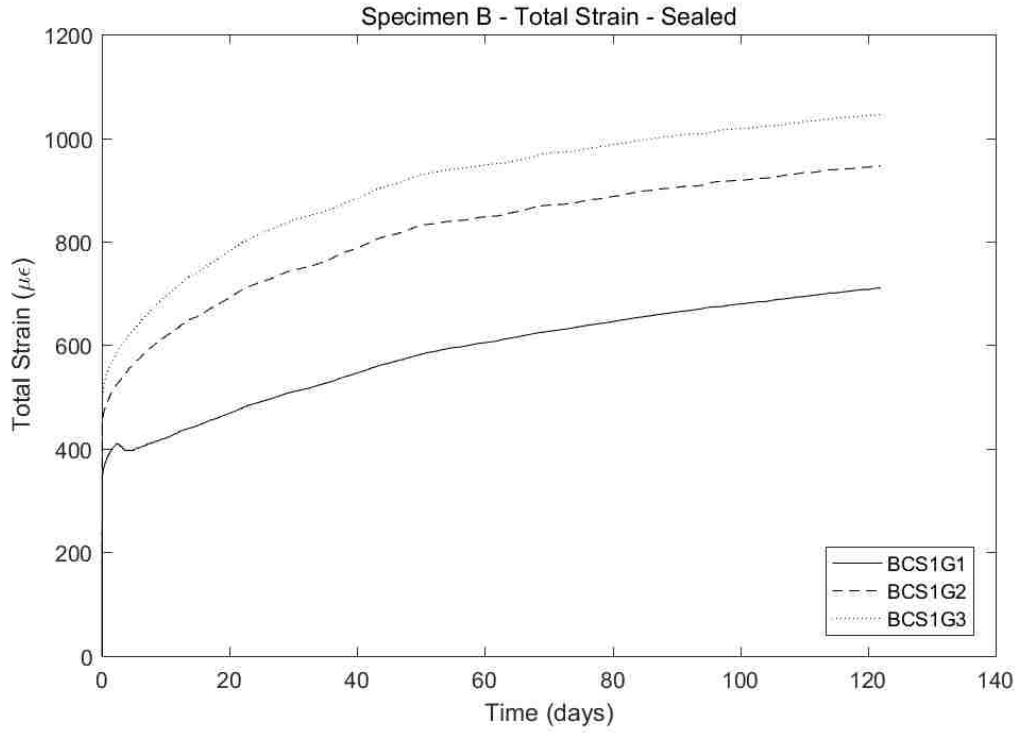
Figure B.7 Specimen B – Sealed Creep Cylinder
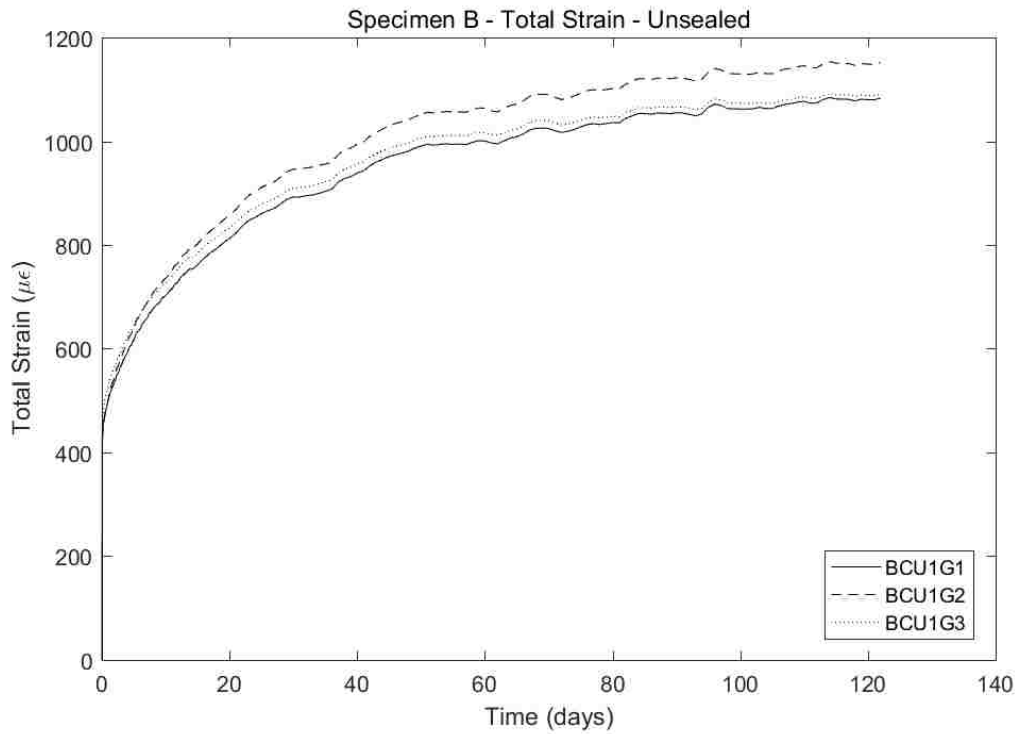
Figure B.8 Specimen B – Unsealed Creep Cylinder

141
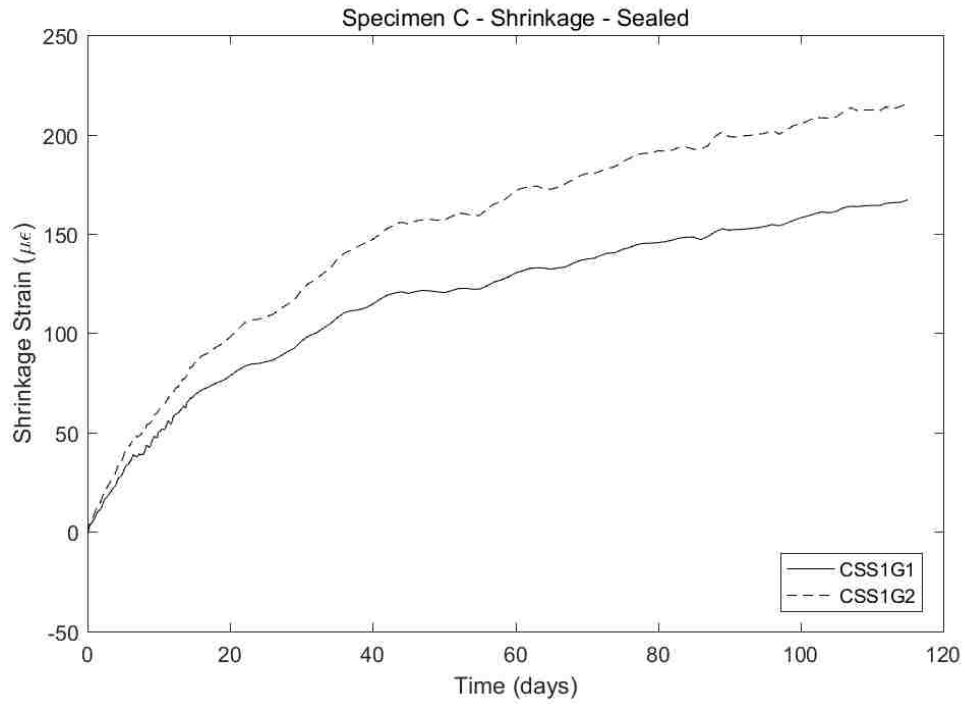
B.3 Specimen C

Figure B.9 Specimen C – Sealed Shrinkage Cylinder
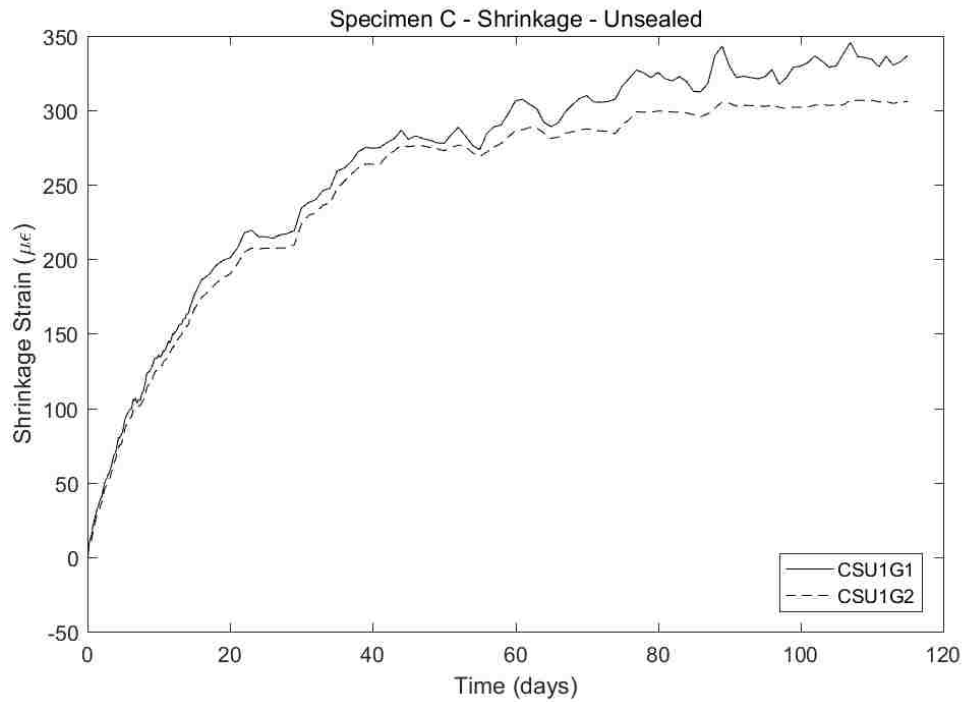
Figure B.10 Specimen C – Unsealed Shrinkage Cylinder
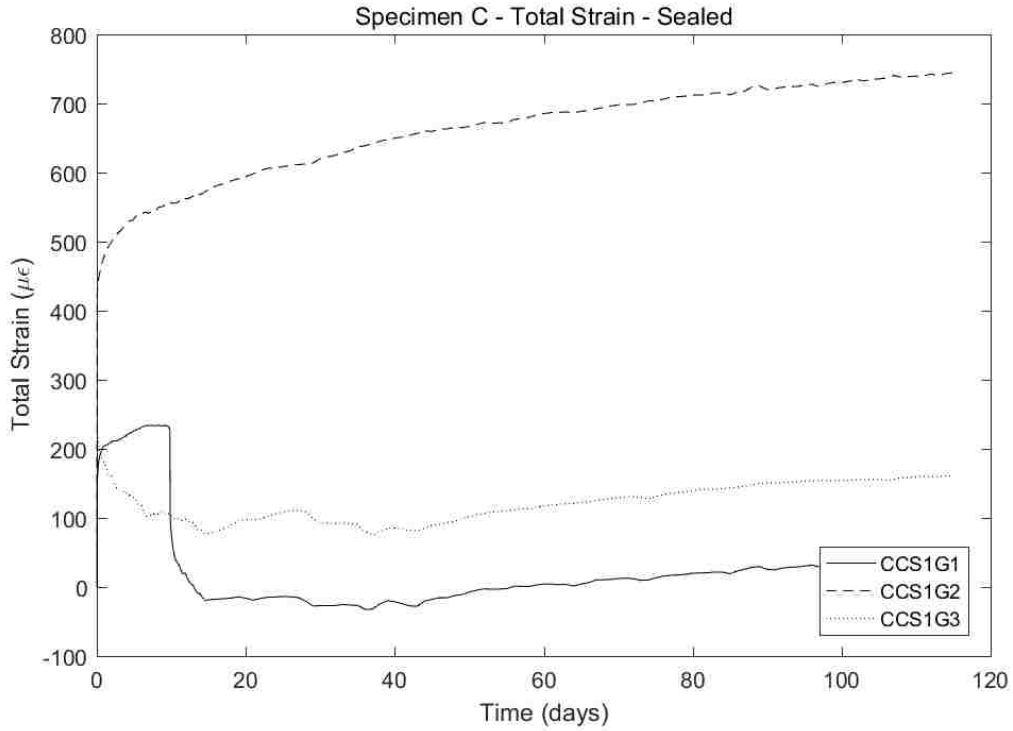
Figure B.11 Specimen C – Sealed Creep Cylinder
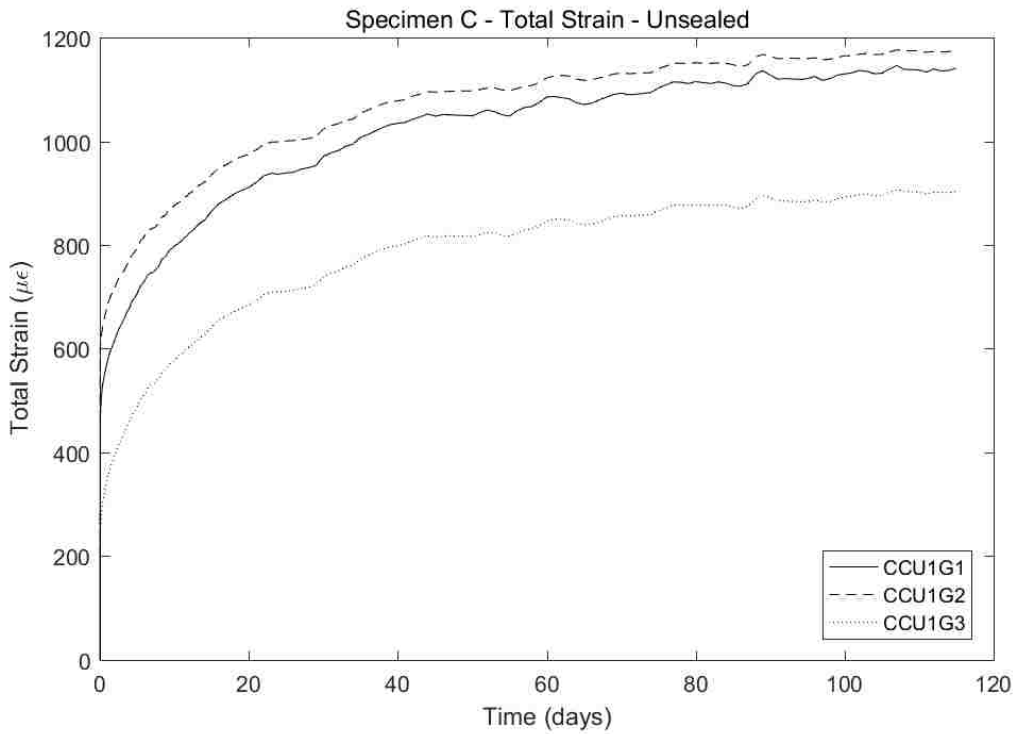
Figure B.12 Specimen C – Unsealed Creep Cylinder

143
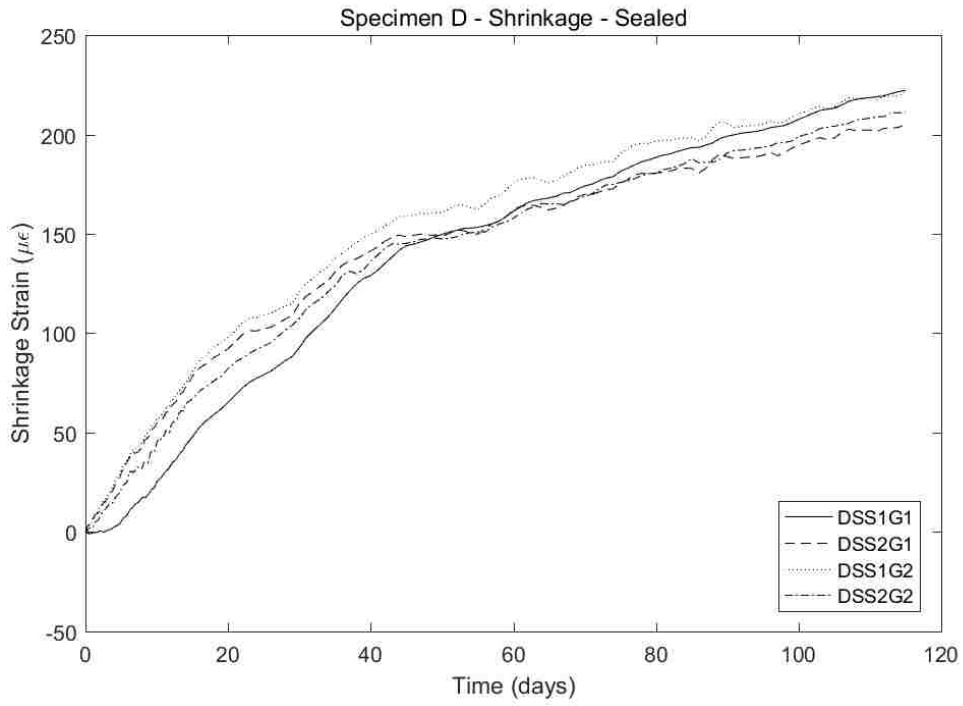
B.4 Specimen D

Figure B.13 Specimen D – Sealed Shrinkage Cylinder
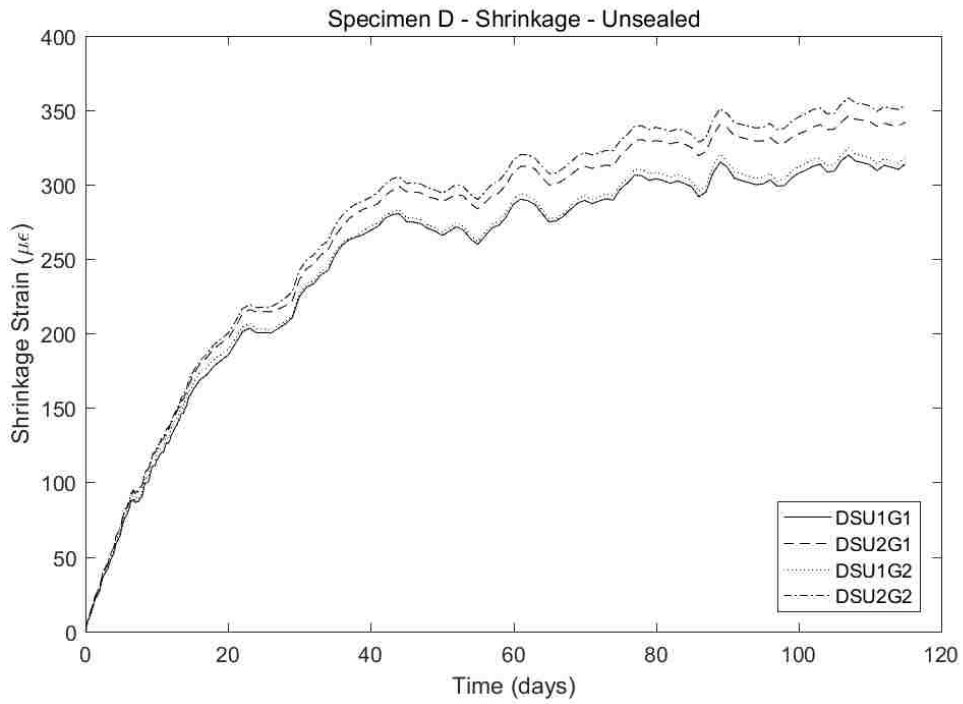
Figure B.14 Specimen D – Unsealed Shrinkage Cylinder
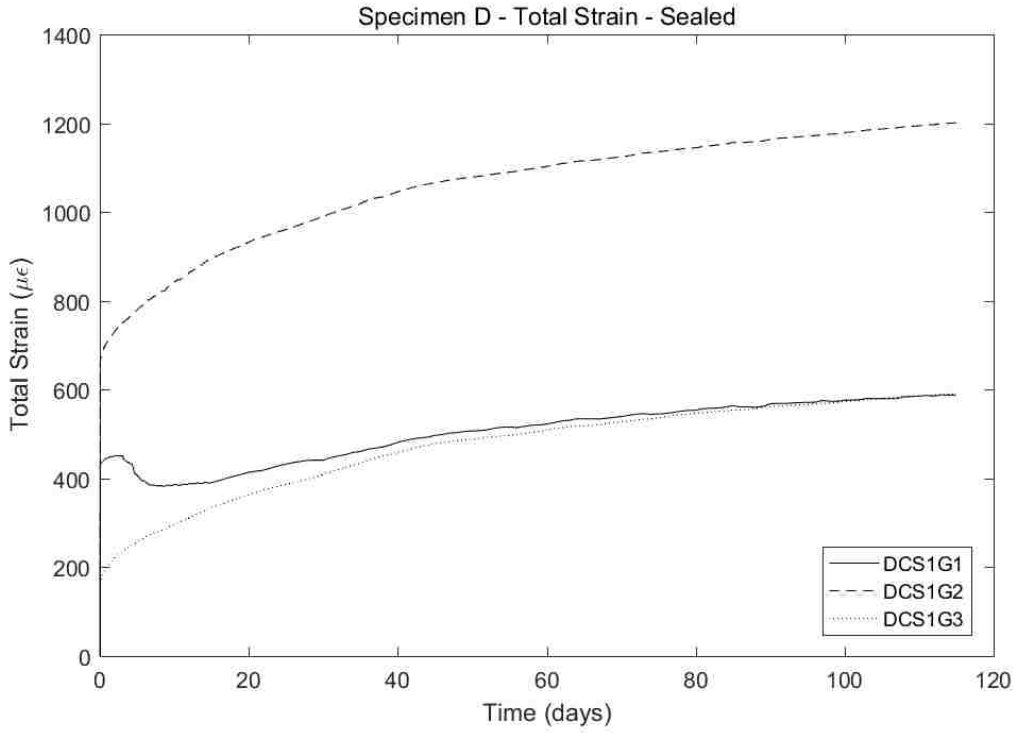
Figure B.15 Specimen D – Sealed Creep Cylinder
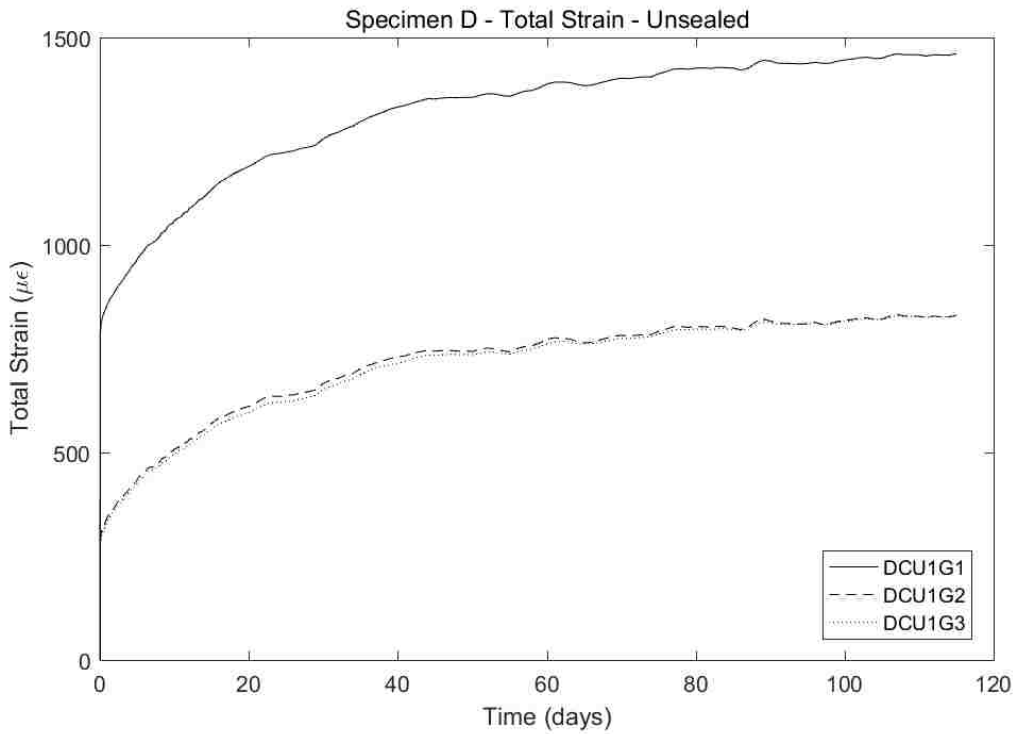
Figure B.16 Specimen D – Unsealed Creep Cylinder

B.5 Specimen E
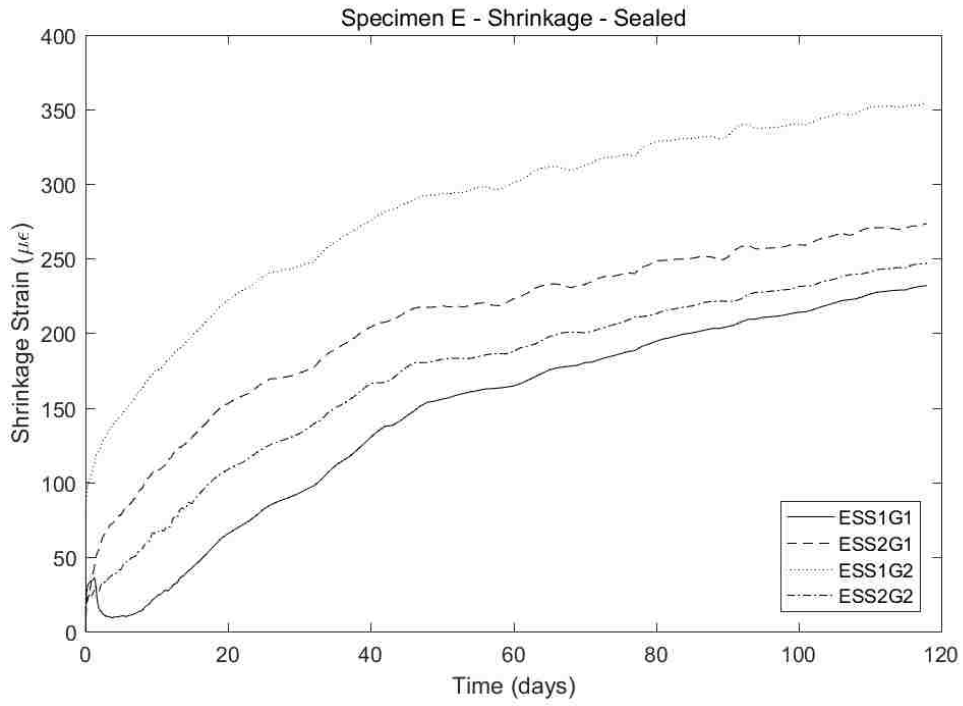
Figure B.17 Specimen E – Sealed Shrinkage Cylinder
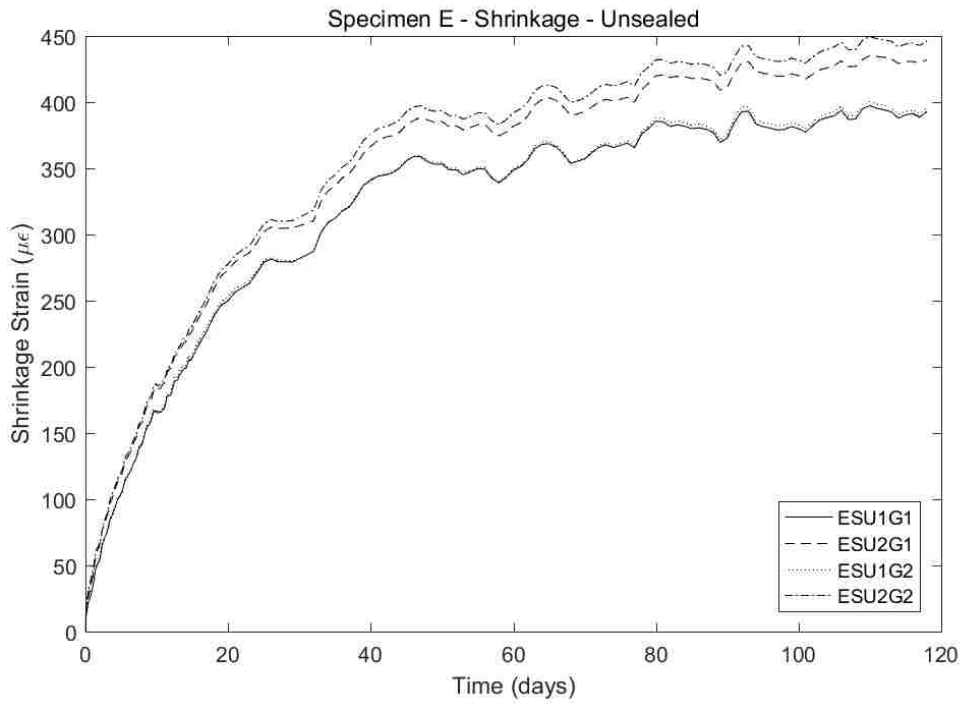
Figure B.18 Specimen E – Unsealed Shrinkage Cylinder
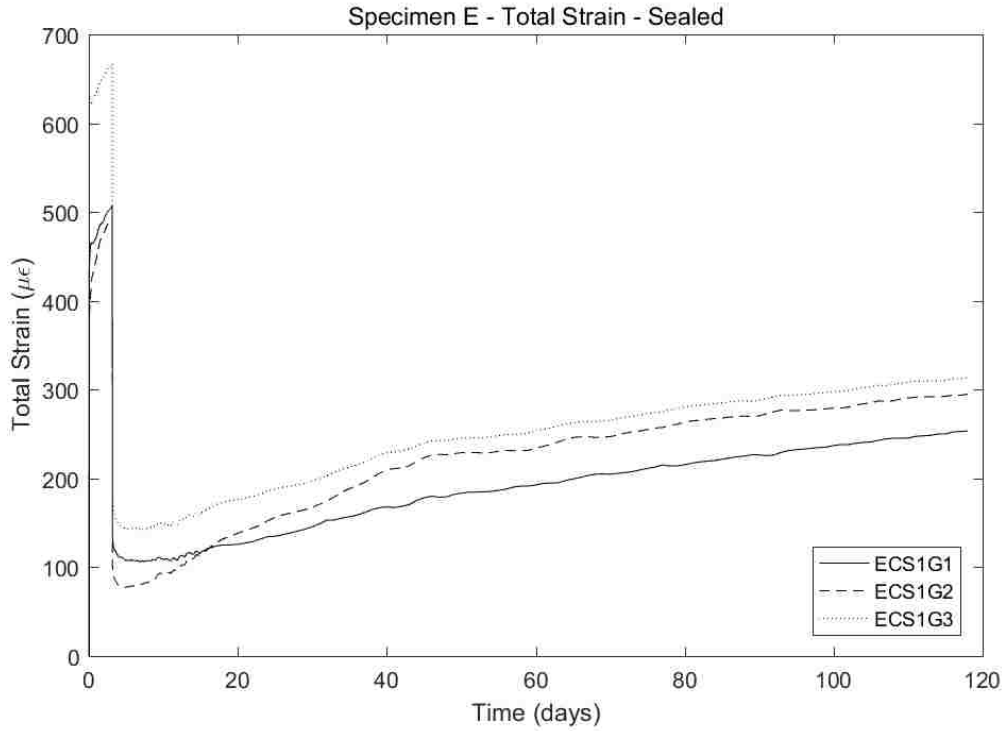
Figure B.19 Specimen E – Sealed Creep Cylinder
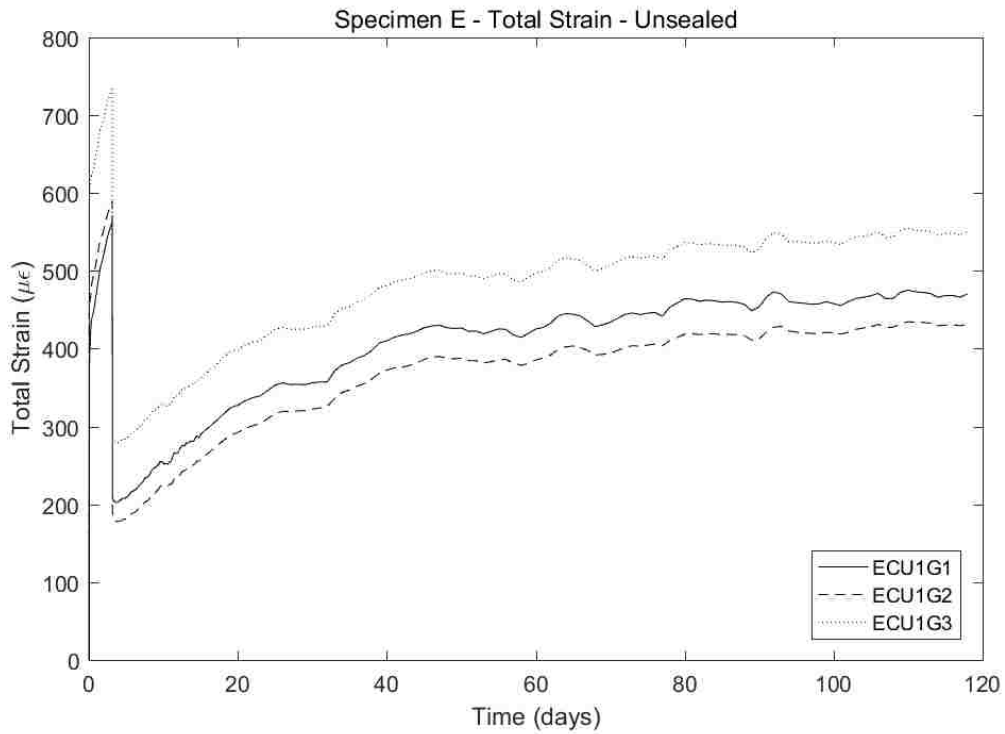
Figure B.20 Specimen E – Unsealed Creep Cylinder

147
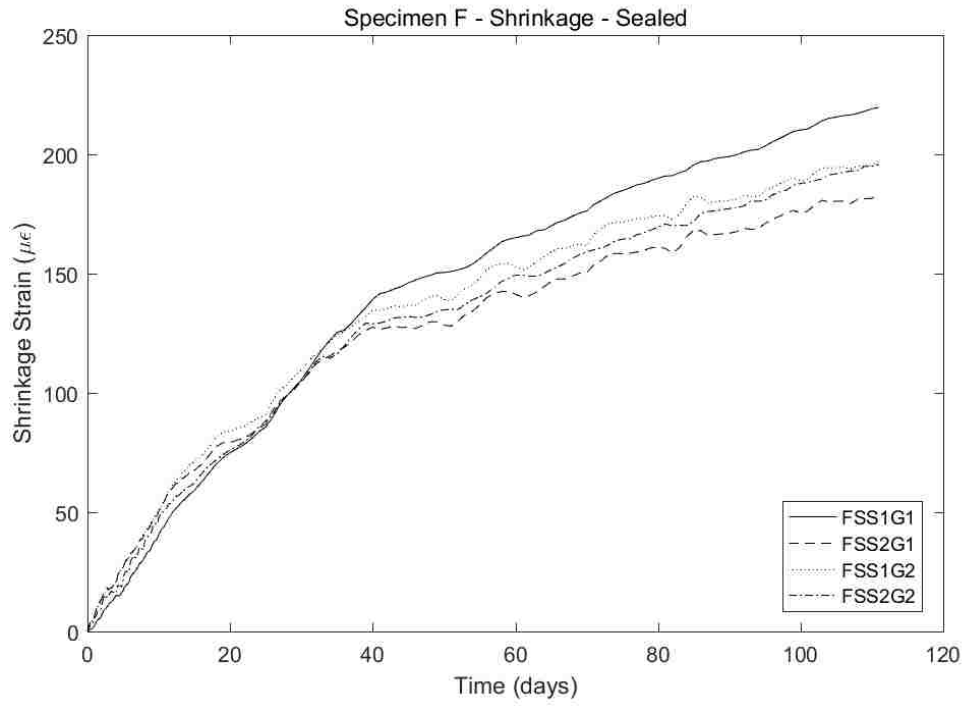
Figure B.21 Specimen F – Sealed Shrinkage Cylinder
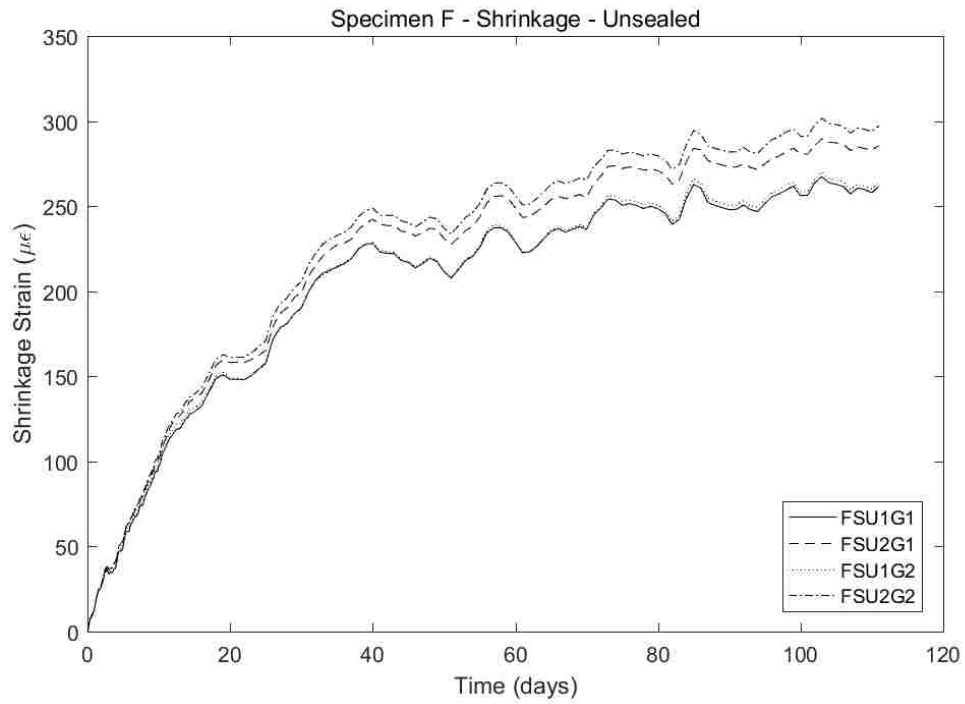
Figure B.22 Specimen F – Unsealed Shrinkage Cylinder
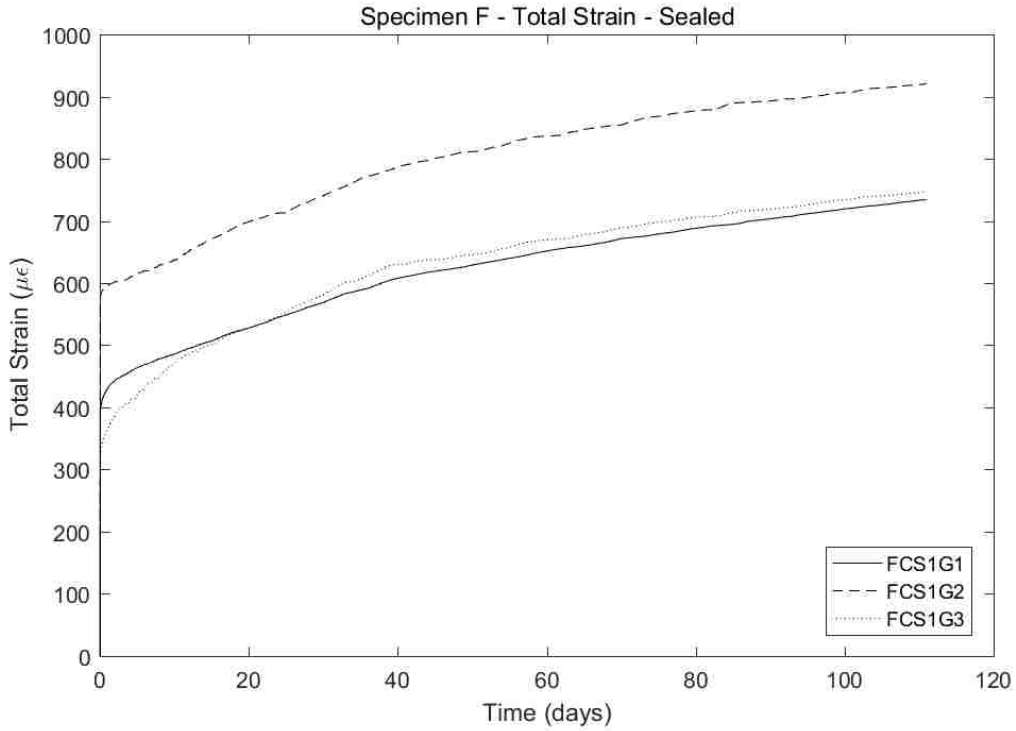
Figure B.23 Specimen F – Sealed Creep Cylinder
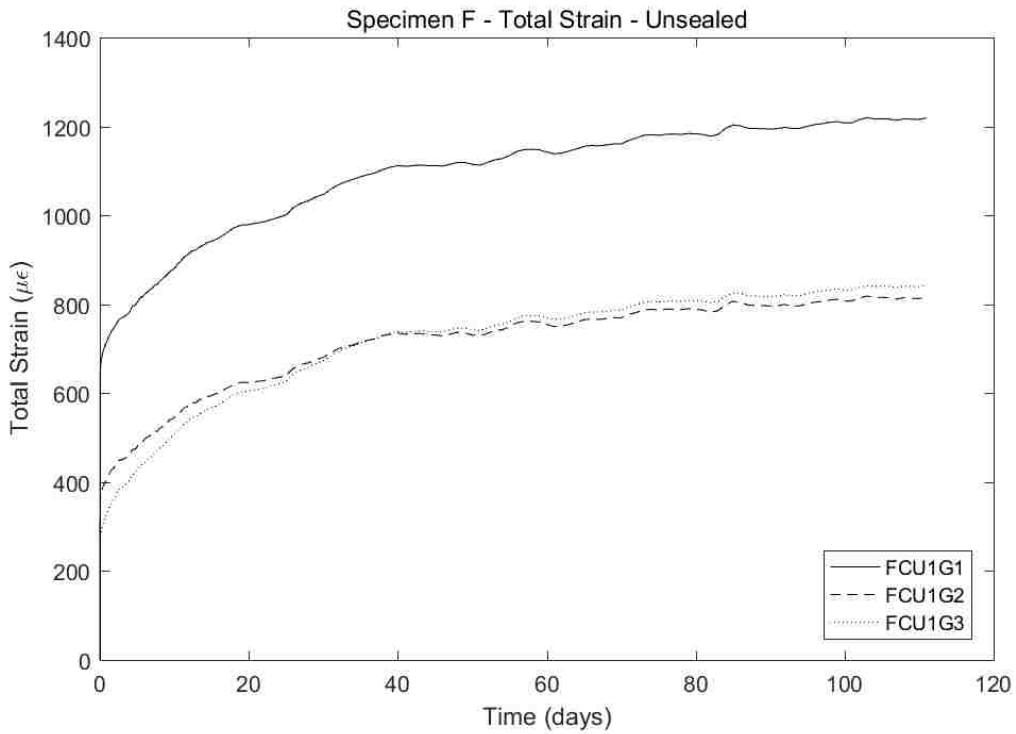
Figure B.24 Specimen F – Unsealed Creep Cylinder

149
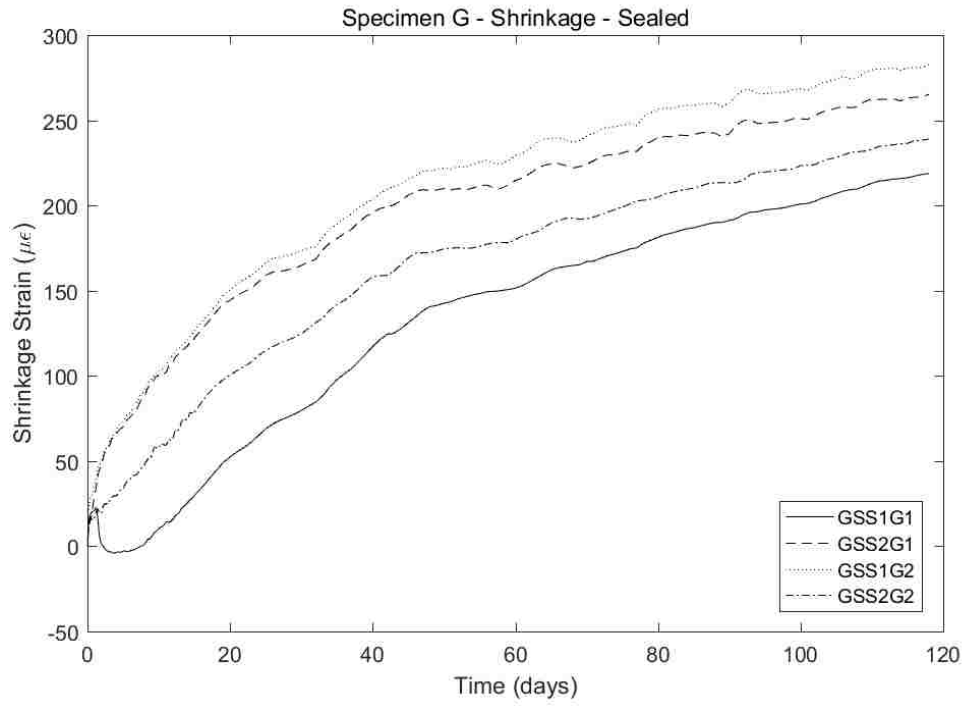
B.7 Specimen G

Figure B.25 Specimen G – Sealed Shrinkage Cylinder
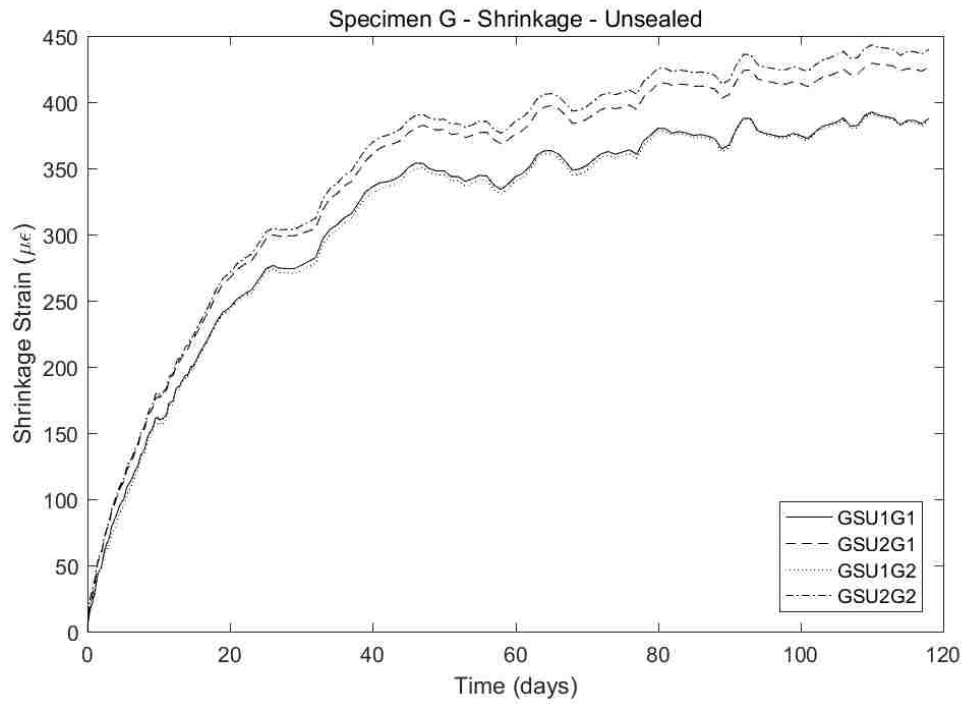
Figure B.26 Specimen G – Unsealed Shrinkage Cylinder

150
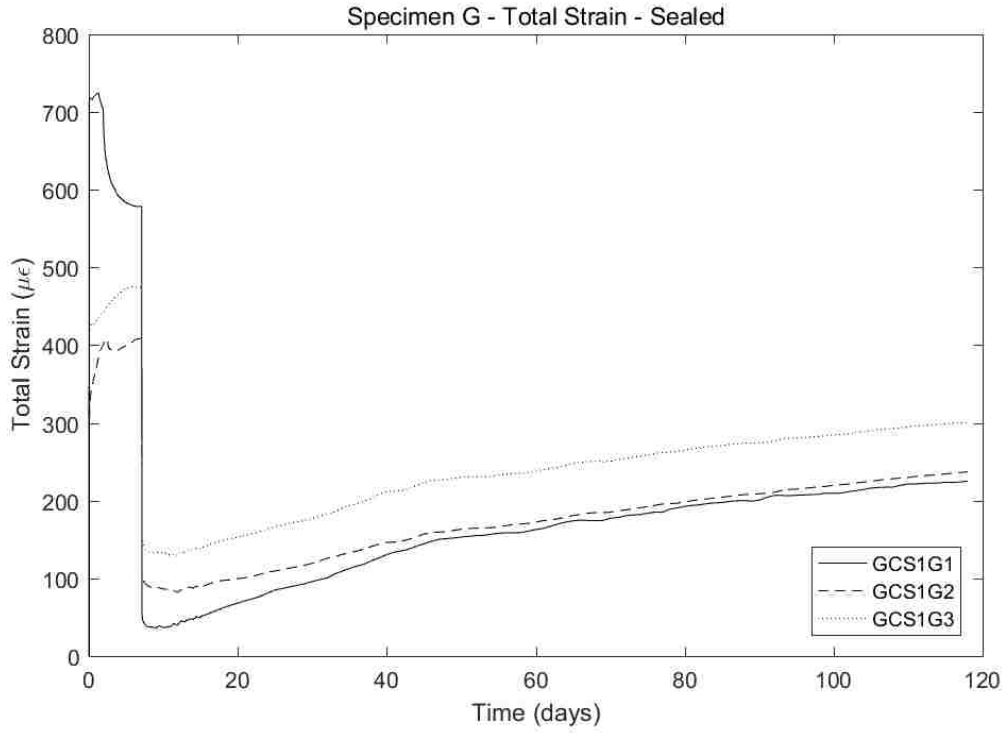
Figure B.27 Specimen G – Sealed Creep Cylinder
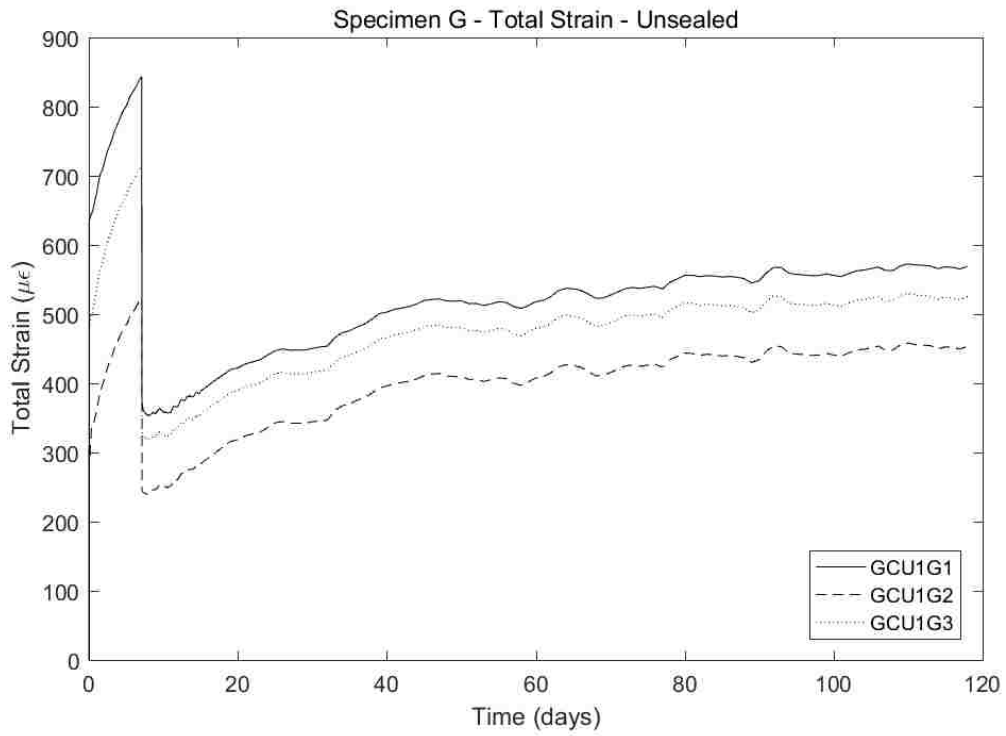
Figure B.28 Specimen G – Unsealed Creep Cylinder

151
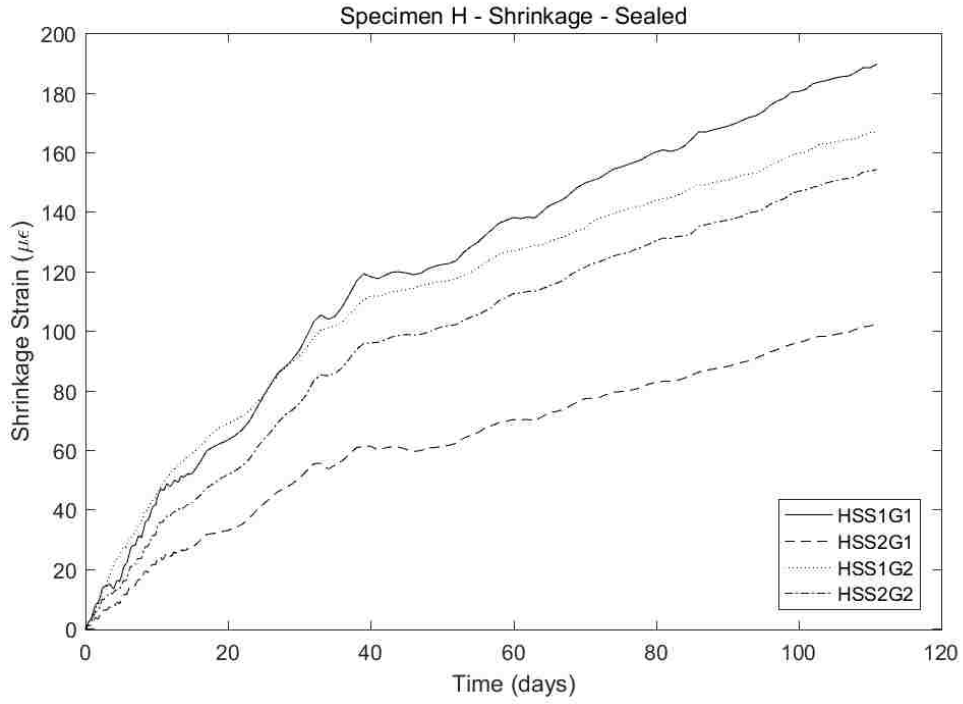
Figure B.29 Specimen H – Sealed Shrinkage Cylinder
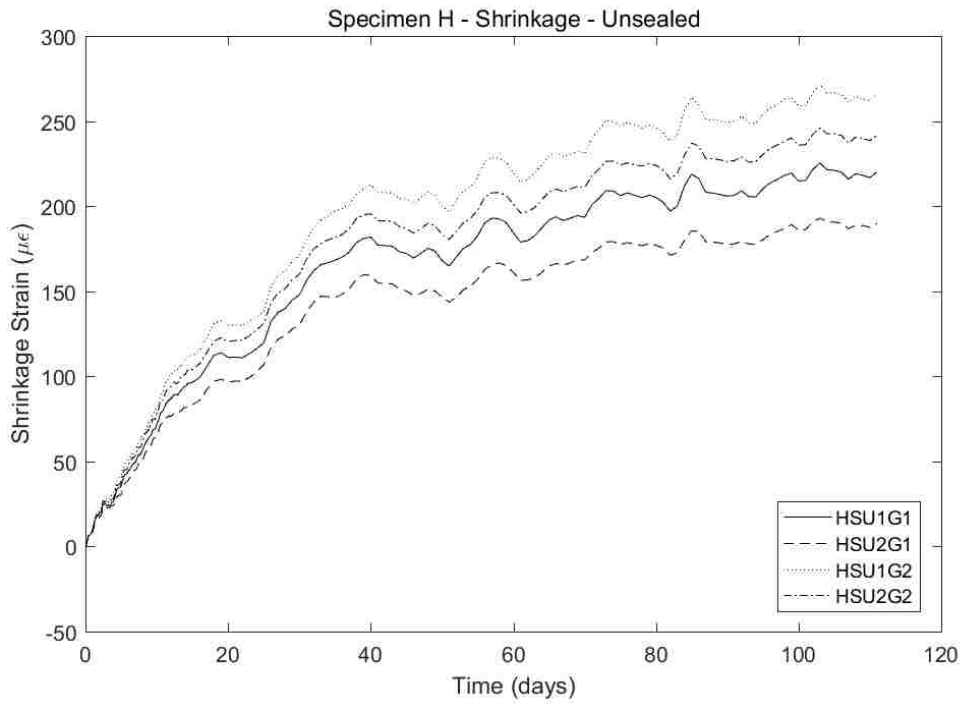
Figure B.30 Specimen H – Unsealed Shrinkage Cylinder
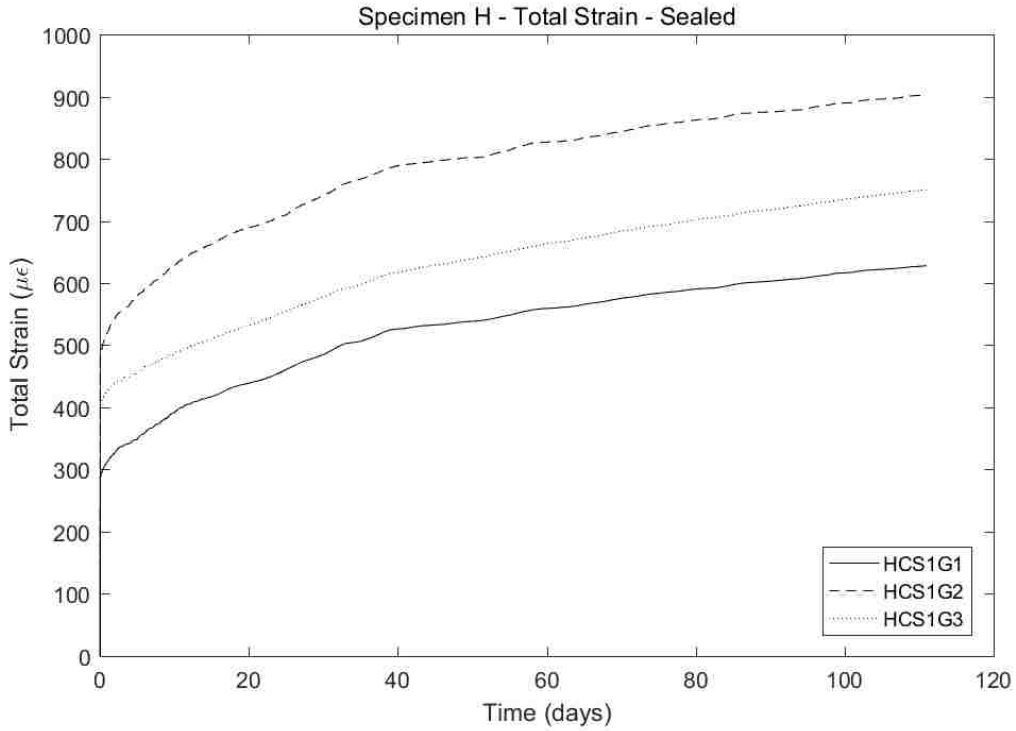
Figure B.31 Specimen H – Sealed Creep Cylinder
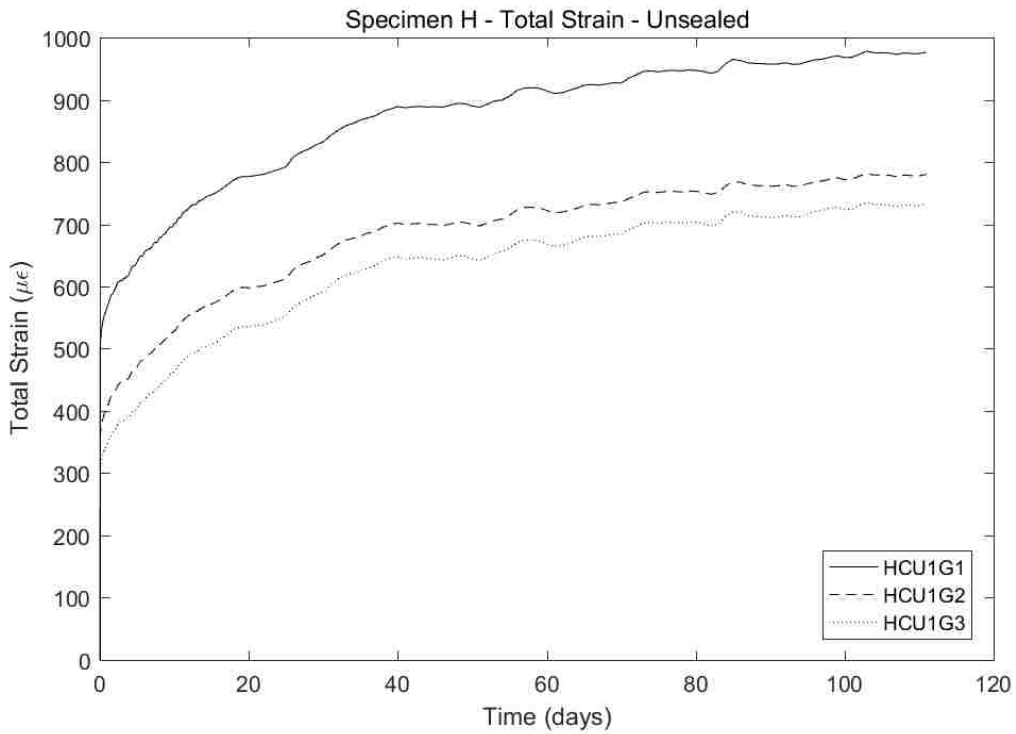
Figure B.32 Specimen H – Unsealed Creep Cylinder
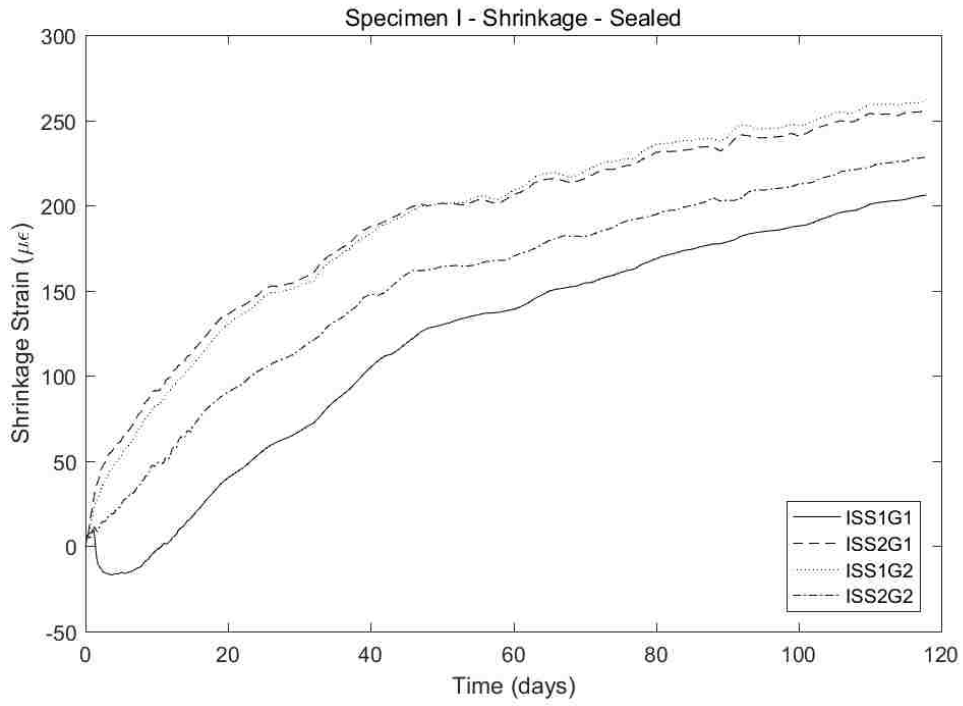
Figure B.33 Specimen I – Sealed Shrinkage Cylinder

Figure B.34 Specimen I – Unsealed Shrinkage Cylinder

Figure B.35 Specimen I – Sealed Creep Cylinder

Figure B.36 Specimen I – Unsealed Creep Cylinder

155

Figure B.37 Specimen J – Sealed Shrinkage Cylinder

Figure B.38 Specimen J – Unsealed Shrinkage Cylinder

Figure B.39 Specimen J – Sealed Creep Cylinder

Figure B.40 Specimen J – Unsealed Creep Cylinder

157

Figure B.41 Specimen K – Sealed Shrinkage Cylinder

Figure B.42 Specimen K – Unsealed Shrinkage Cylinder
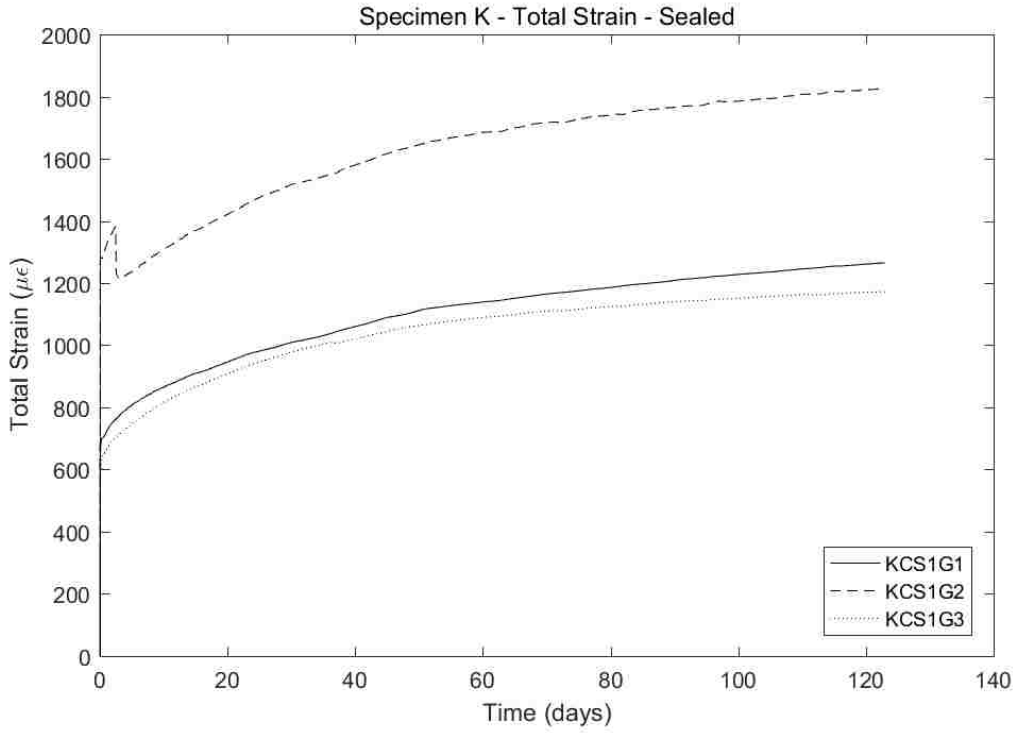
Figure B.43 Specimen K – Sealed Creep Cylinder
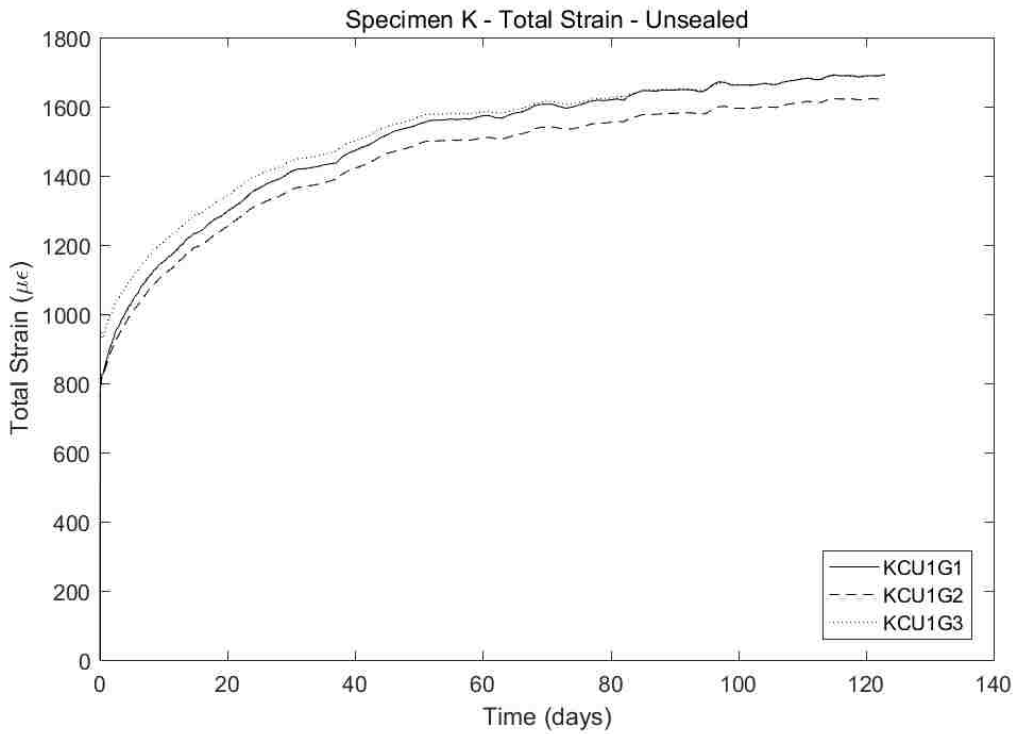
Figure B.44 Specimen K – Unsealed Creep Cylinder

159

B.12 Overview of Gage Failures

Table B.1 shows an overview of all the gages that had any kind of malfunction during the test period, and whether or not it was kept in the dataset or scrapped.

Table B.1 List of Malfunctioning Gages

Gage ID	Cylinder Type	Fate
ASS1G1/ESS1G1/GSS1G1/ISS1G1	Shrinkage	Scrapped
BSS1G2	Shrinkage	Scrapped
BCS1G1	Creep	Kept
CCS1G1	Creep	Scrapped
CCS1G3	Creep	Scrapped
DCS1G1	Creep	Kept
GCS1G1	Creep	Kept
GCS1G2	Creep	Kept
ICS1G3	Creep	Kept
KSS1G2	Shrinkage	Scrapped
KCS1G2	Creep	Kept

Appendix C Creep Strains

This Appendix contains total, basic and drying creep strain data for all 11 specimens plotted with their respective curve fits obtained by the parametrization outlined in Chapter 7.5.
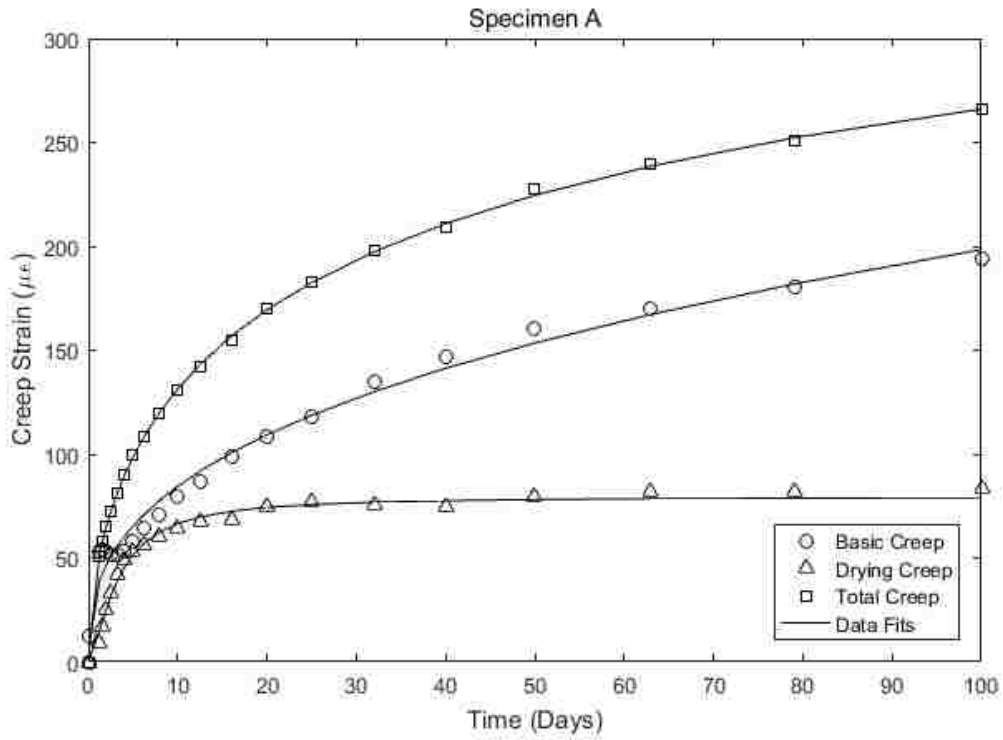
Figure C.1 Creep Strain Data and Curve Fits – Specimen A
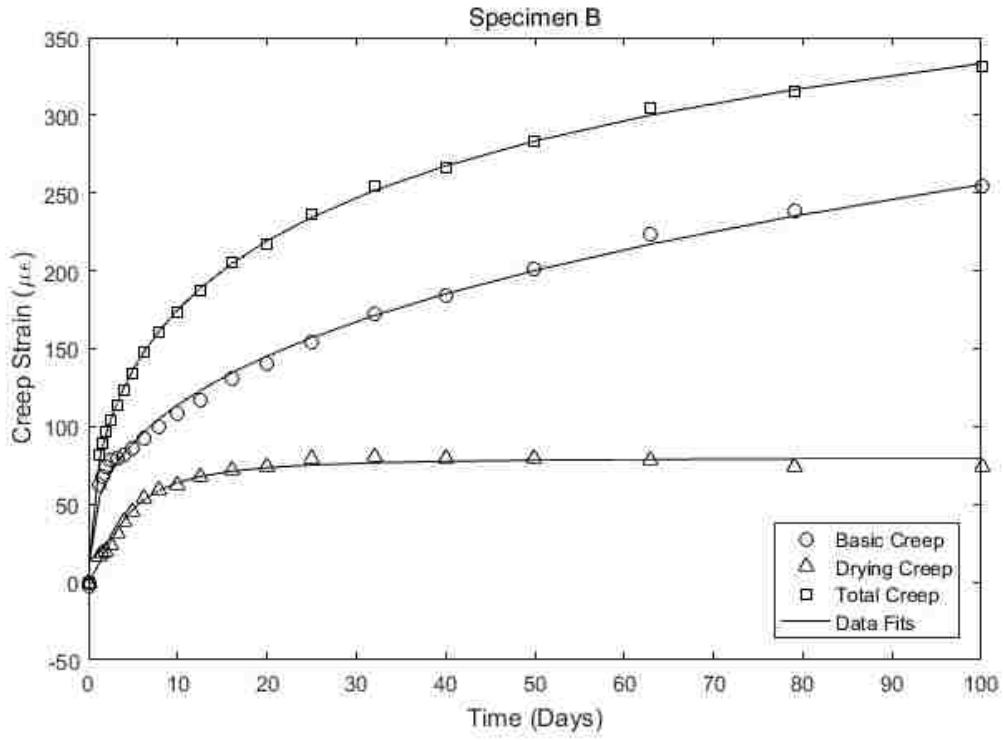
Figure C.2 Creep Strain Data and Curve Fits – Specimen B
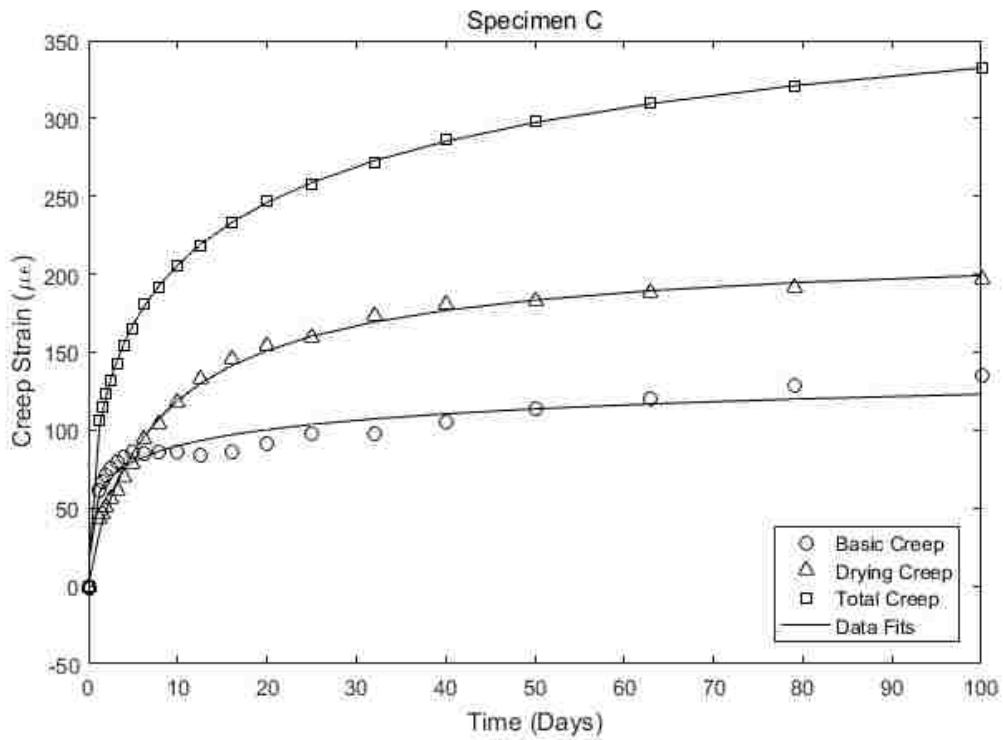
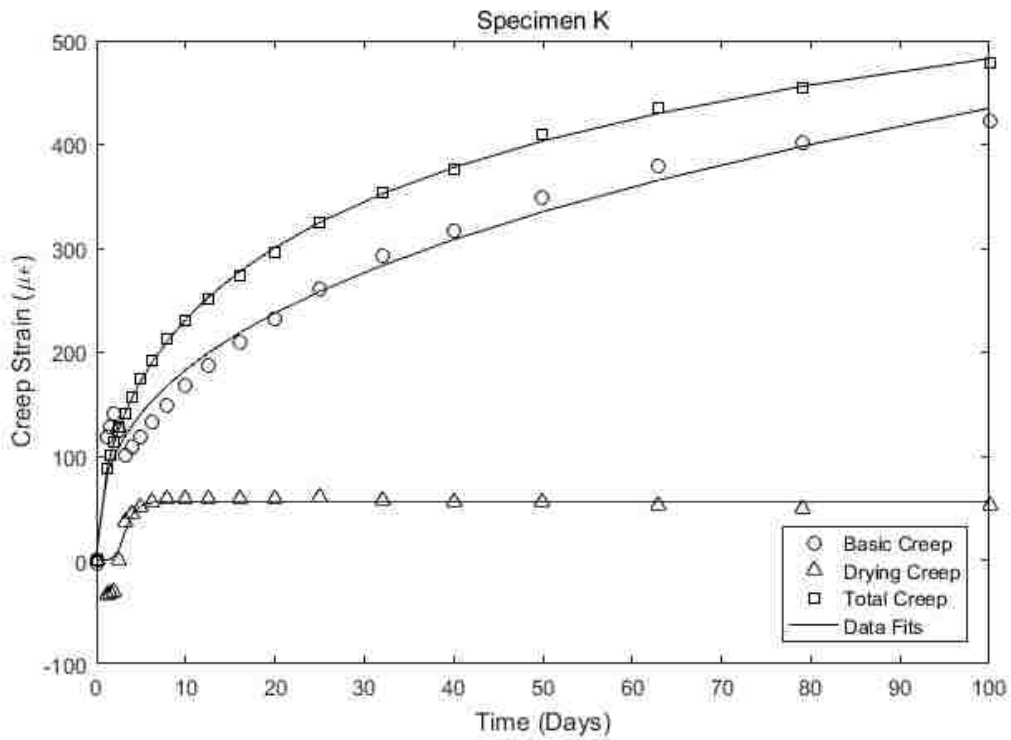**Figure C.3 Creep Strain Data and Curve Fits – Specimen C**
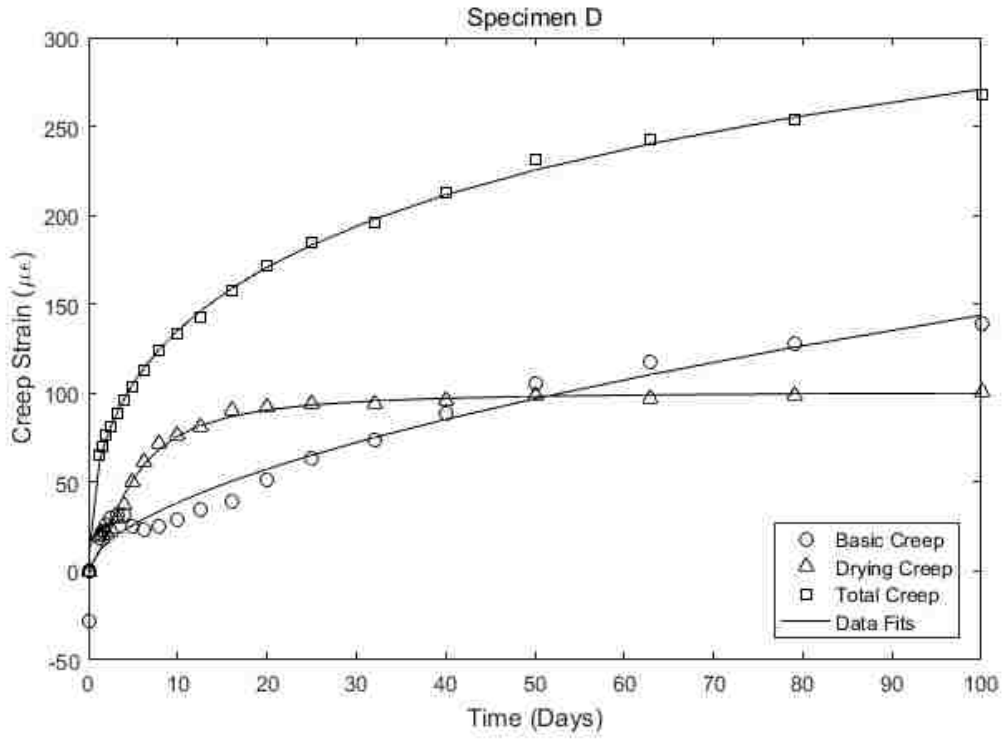
Figure C.4 Creep Strain Data and Curve Fits – Specimen D
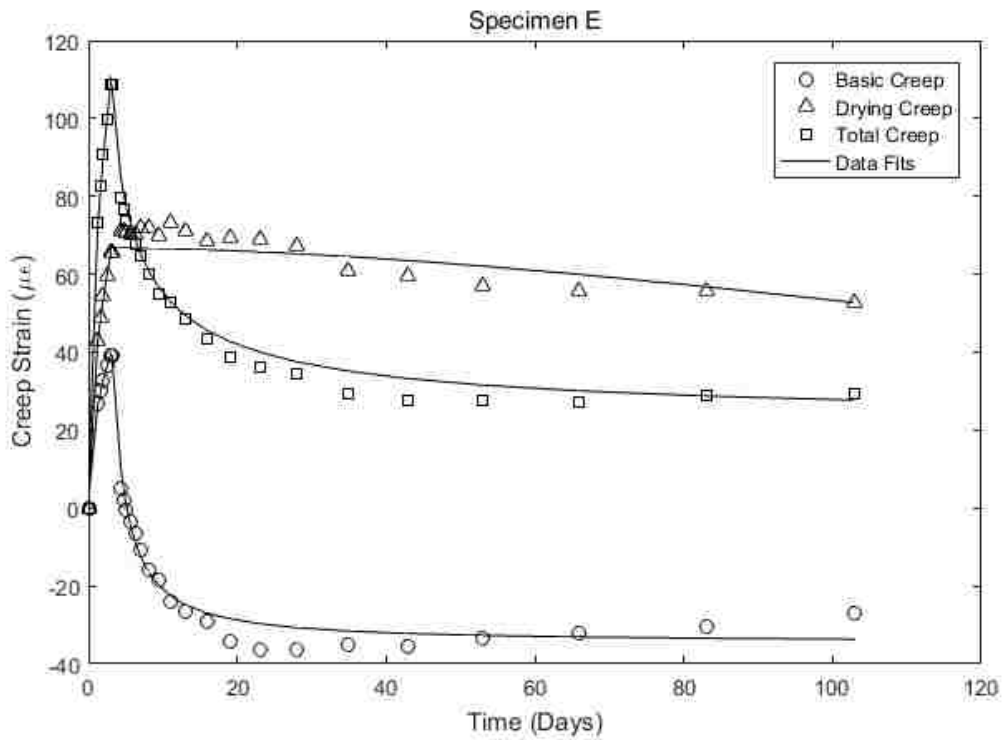
Figure C.5 Creep Strain Data and Curve Fits – Specimen E

163
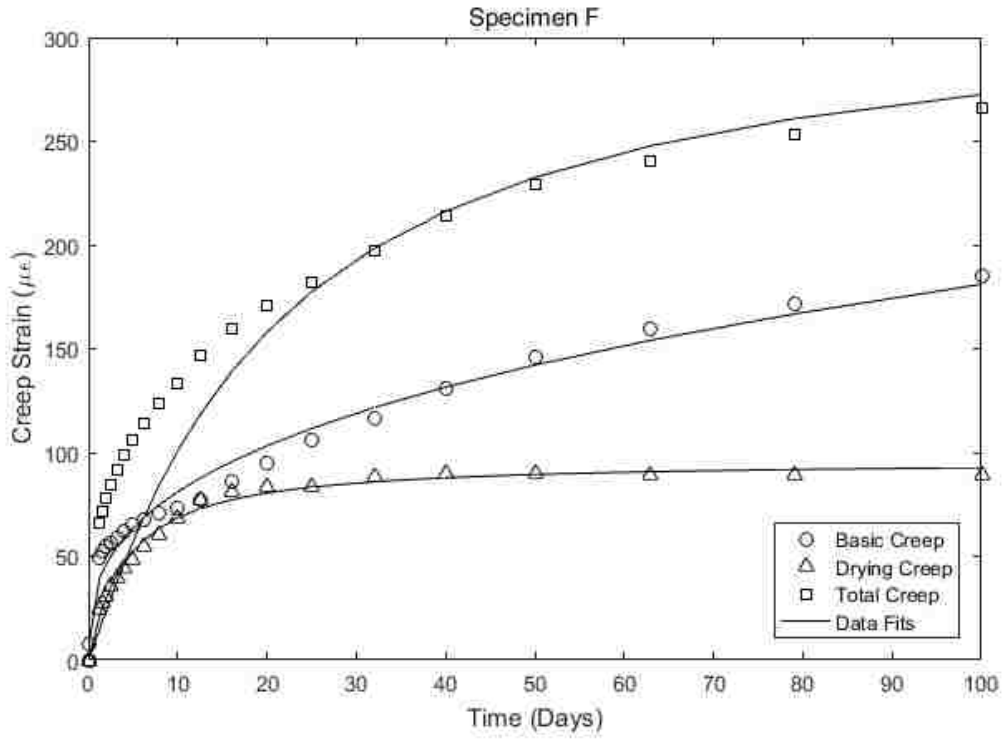
Figure C.6 Creep Strain Data and Curve Fits – Specimen F
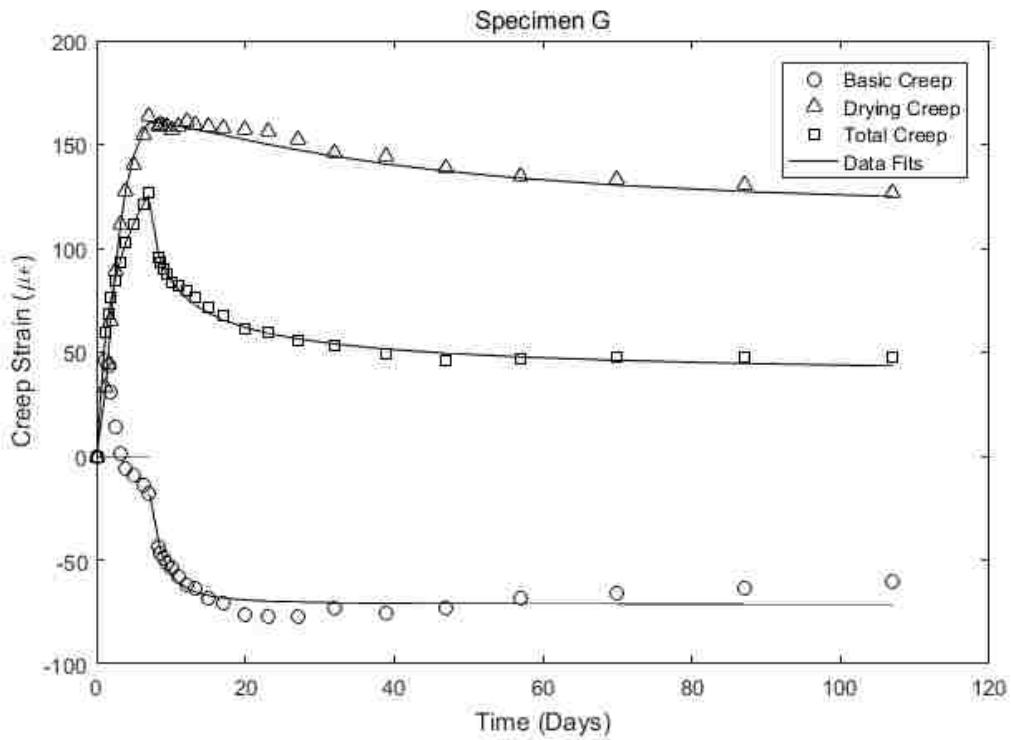
Figure C.7 Creep Strain Data and Curve Fits – Specimen G

164
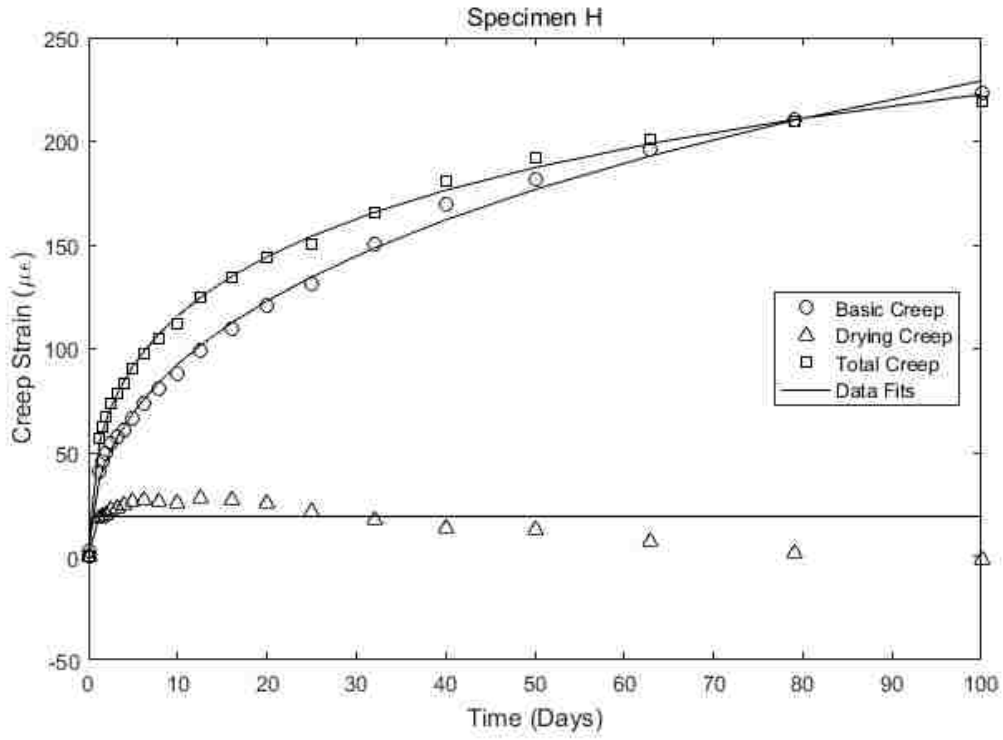
Figure C.8 Creep Strain Data and Curve Fits – Specimen H
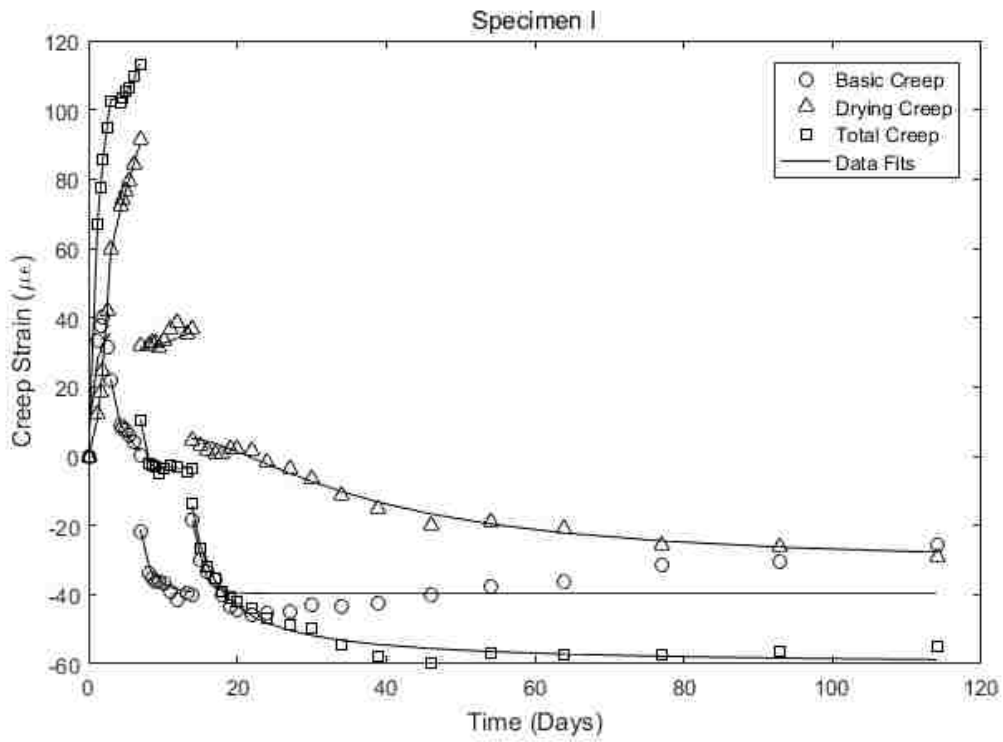
Figure C.9 Creep Strain Data and Curve Fits – Specimen I

165
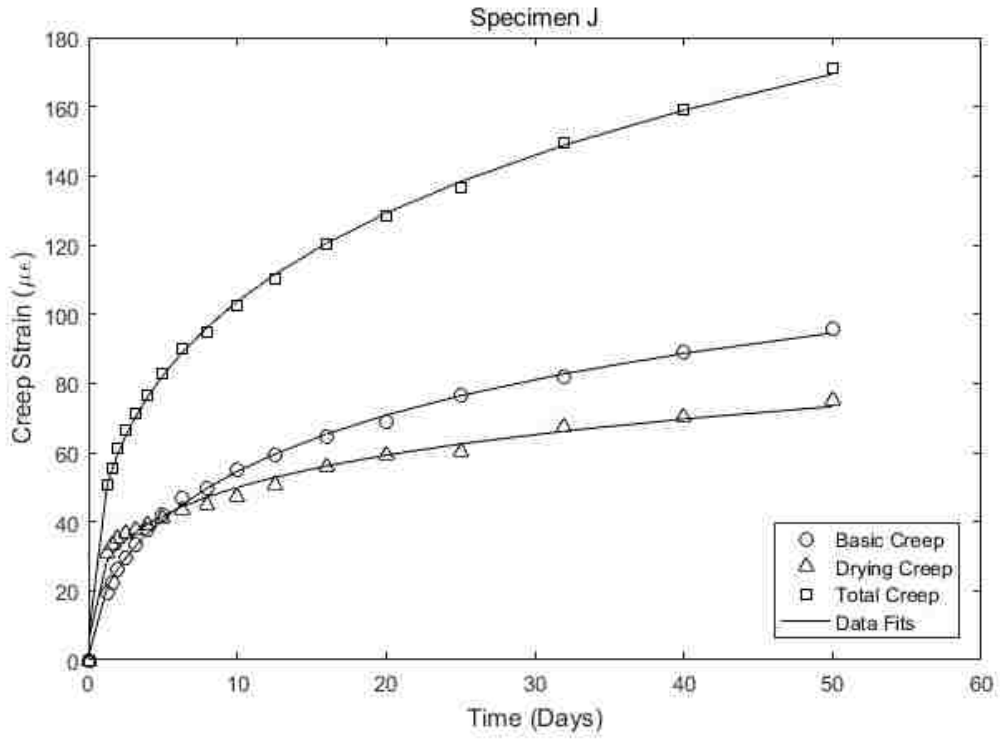
Figure C.10 Creep Strain Data and Curve Fits – Specimen J

Figure C.11 Creep Strain Data and Curve Fits – Specimen K
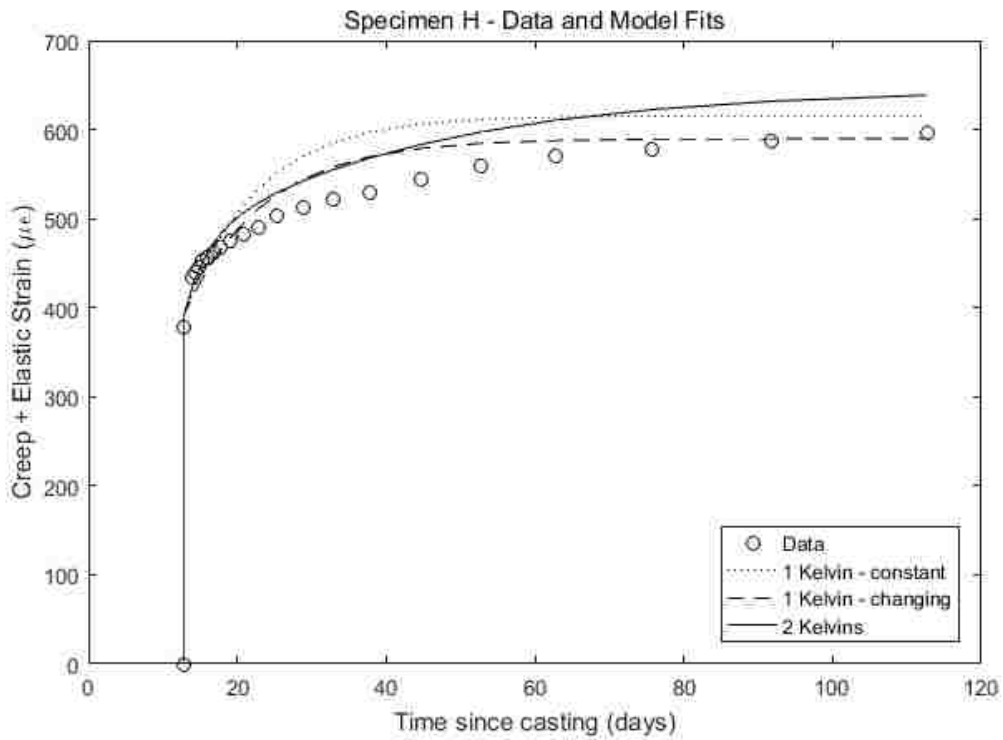
166

Appendix D Model Fits
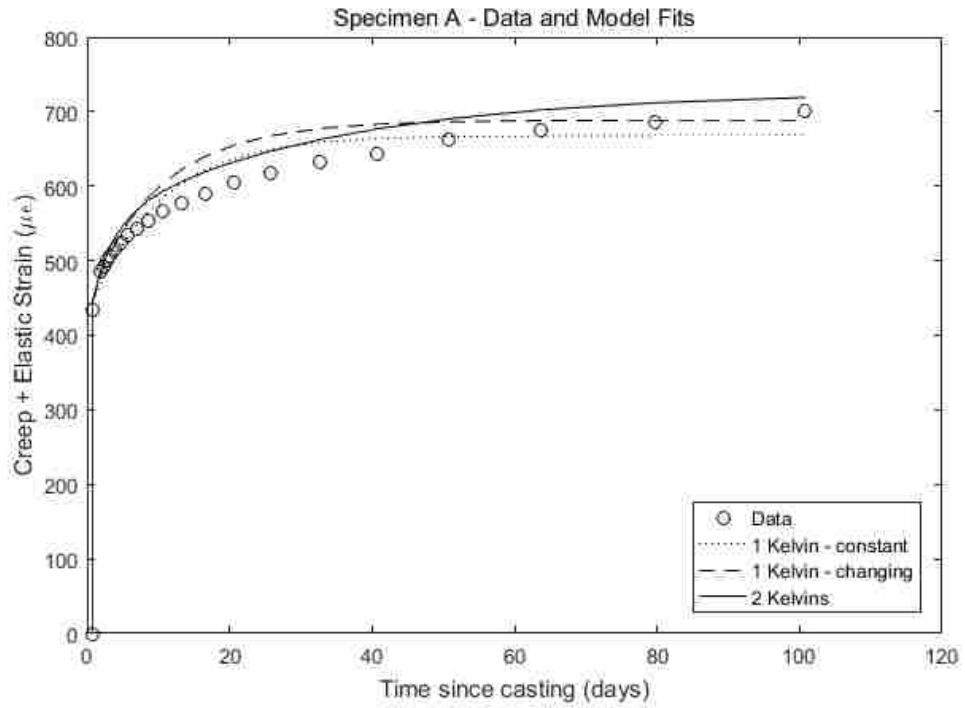
Figure D.1 Model Fits to Specimen A
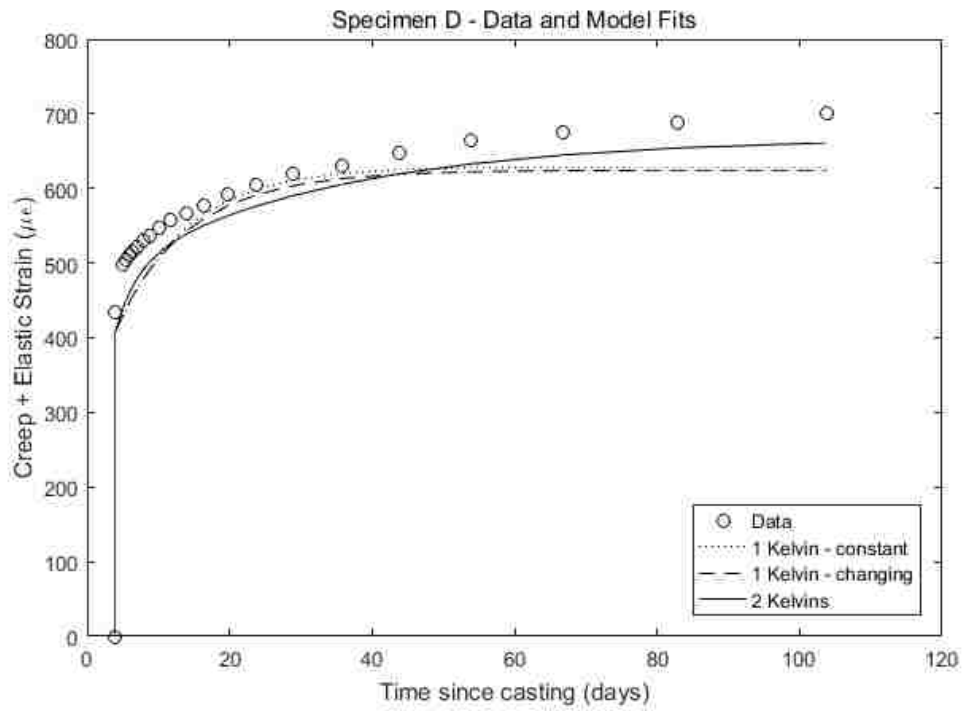
Figure D.2 Model Fits to Specimen D

167
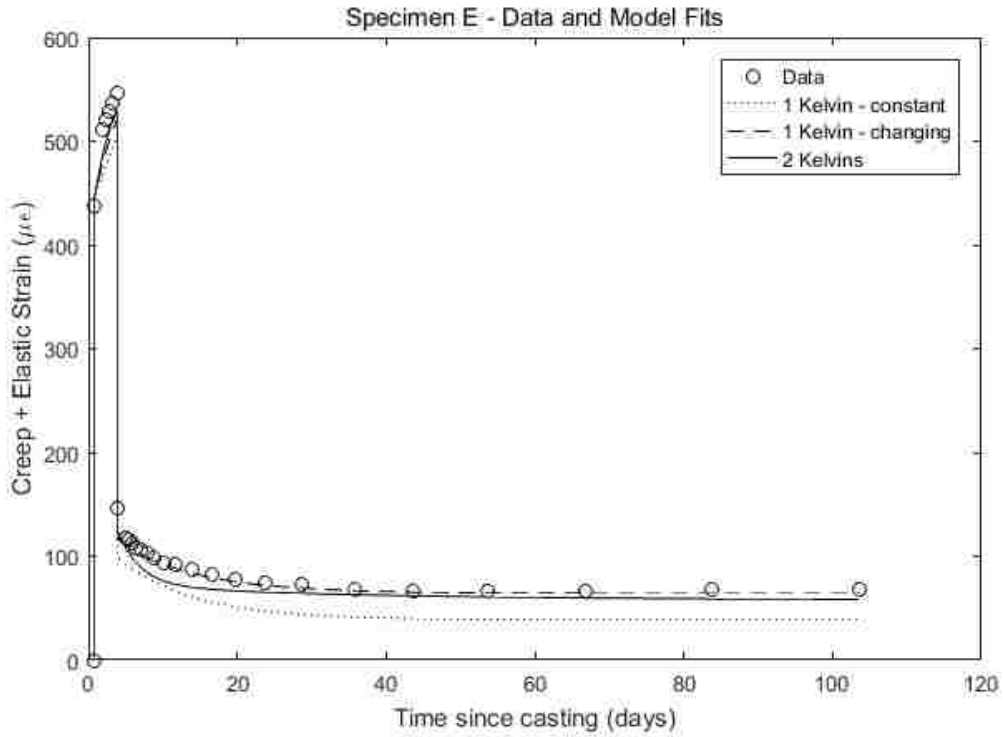
Figure D.3 Model Fits to Specimen E
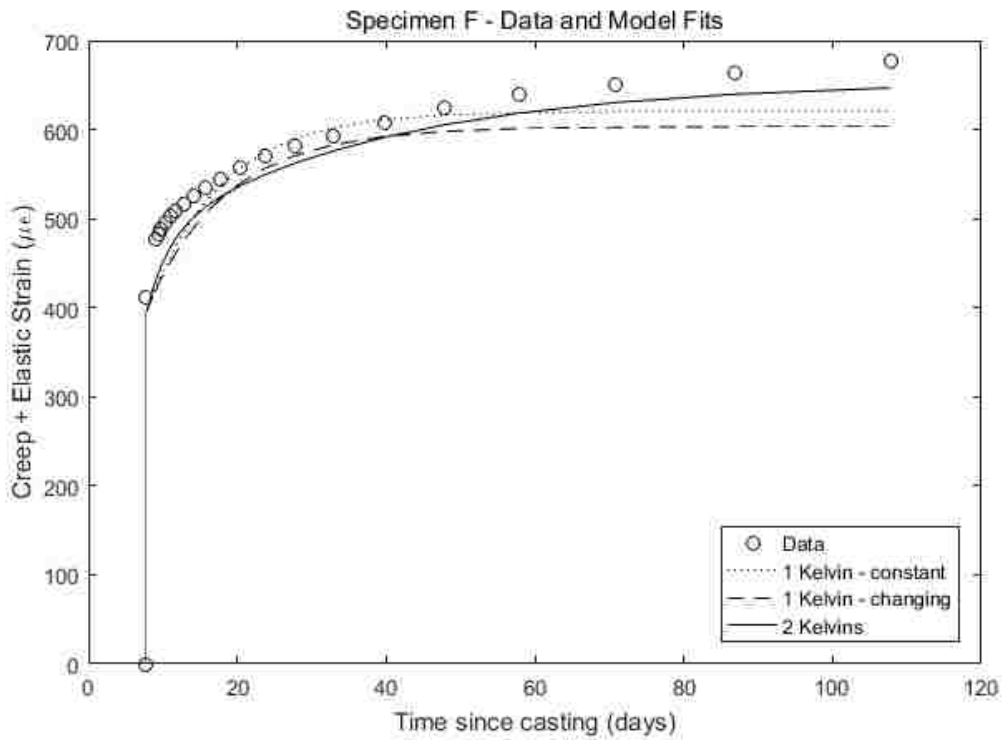
Figure D.4 Model Fits to Specimen F

168
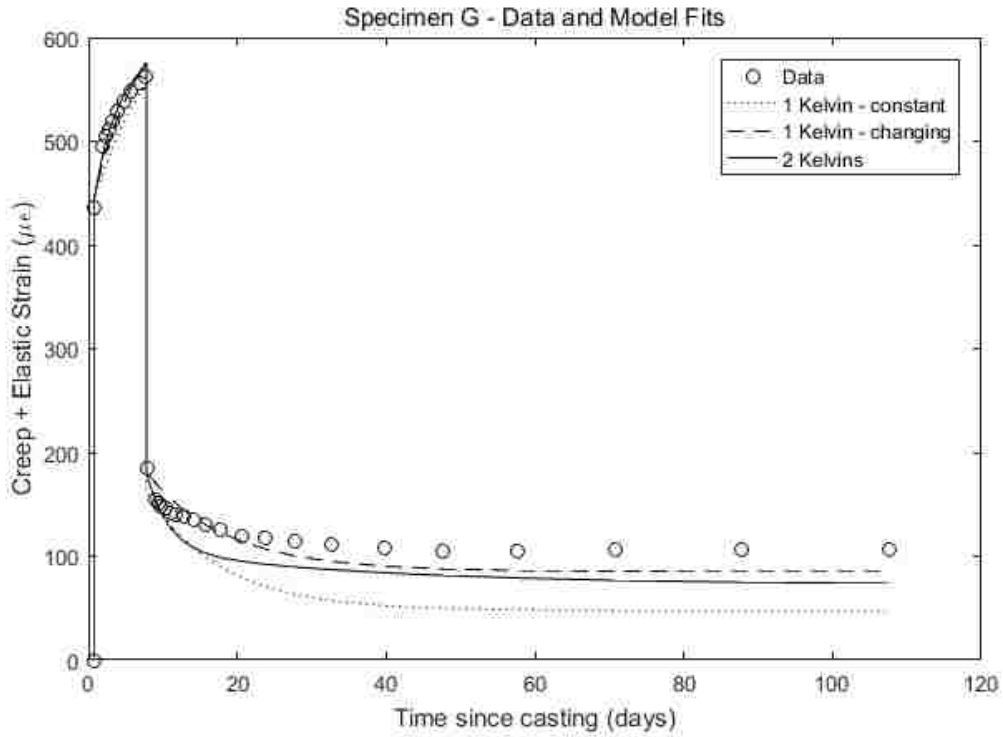
Figure D.5 Model Fits to Specimen G

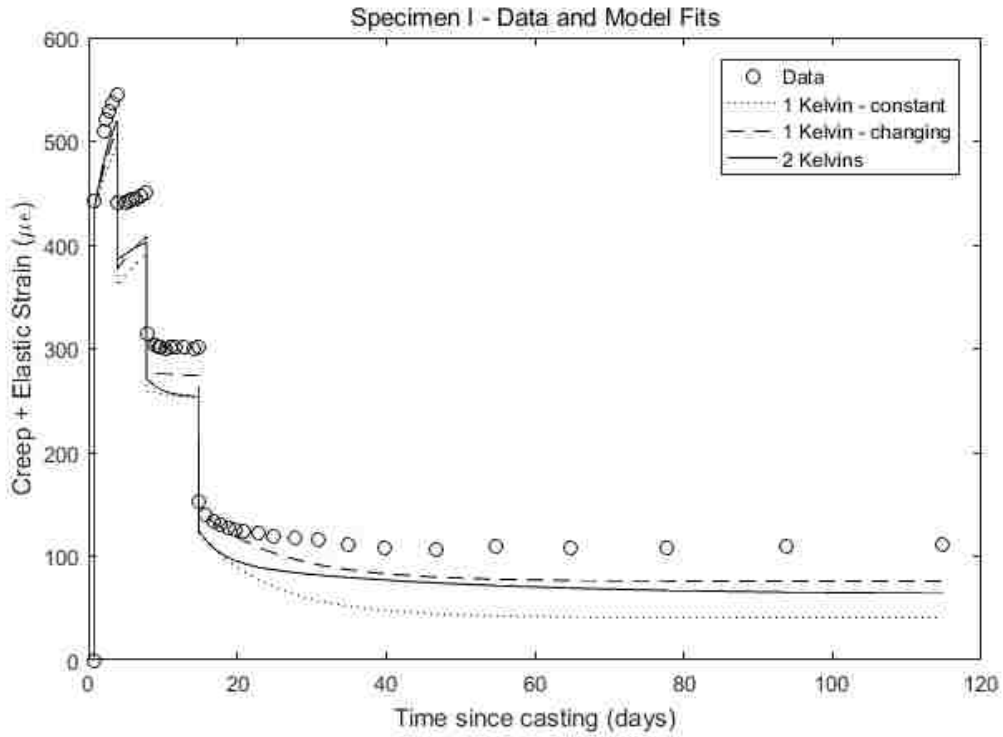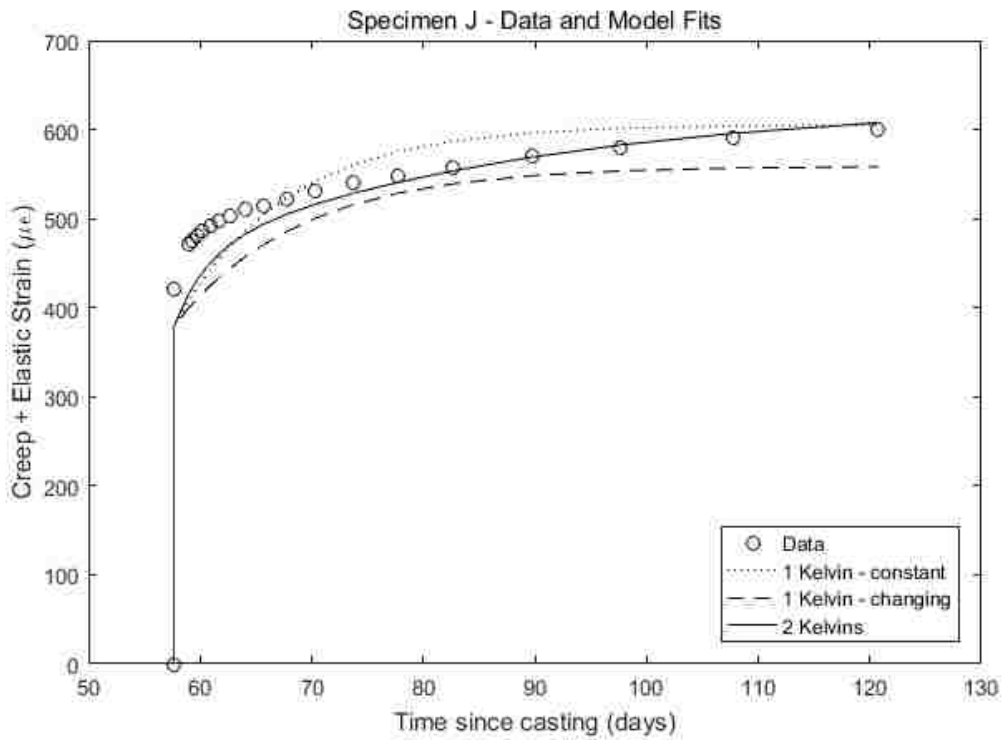**Figure D.6 Model Fits to Specimen H**
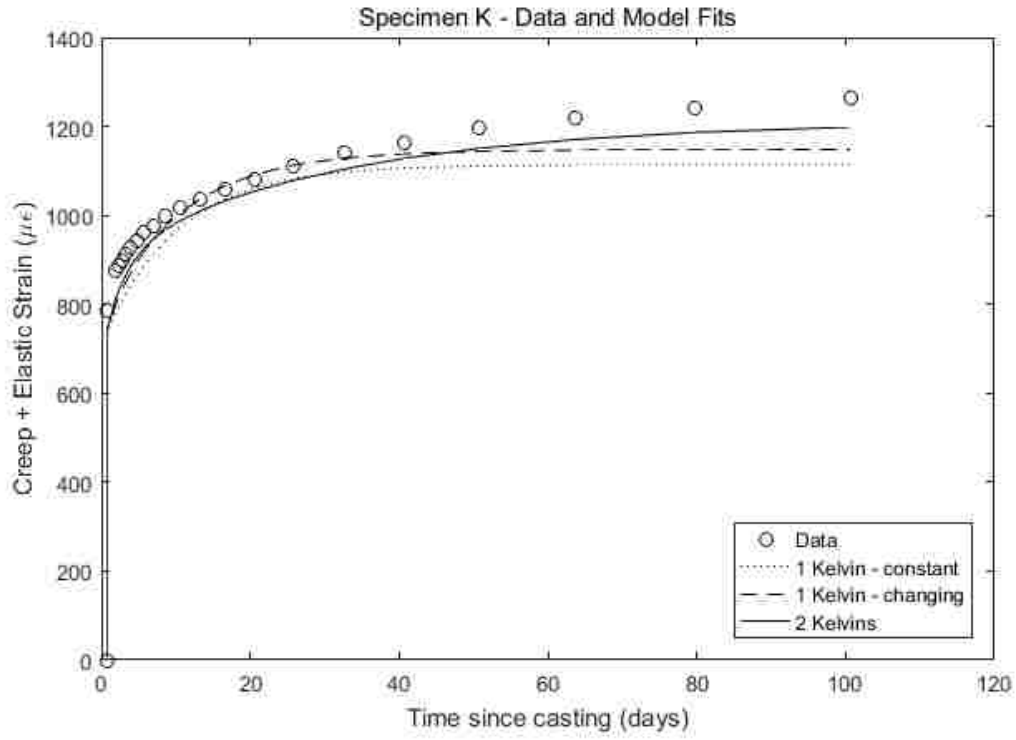
Figure D.7 Model Fits to Specimen I

Figure D.8 Model Fits to Specimen J

170

Figure D.9 Model Fits to Specimen K